

Investigation on CO₂ Geological Sequestration in the Deccan Volcanic Province through Multiphase Flow and Reactive Transport Simulations

THESIS

Submitted in partial fulfillment
of the requirements for the degree of

DOCTOR OF PHILOSOPHY

by

PUNNAM PRADEEP REDDY

ID. No. 2018PHXF0042H

Under the Supervision of

Prof. VIKRANT KUMAR SURASANI

&

Under the Co-Supervision of

Prof. BALAJI KRISHNAMURTHY



BITS Pilani
Pilani | Dubai | Goa | Hyderabad

BIRLA INSTITUTE OF TECHNOLOGY & SCIENCE, PILANI

2023

CERTIFICATE

This is to certify that the thesis entitled “**Investigation on CO₂ Geological Sequestration in the Deccan Volcanic Province through Multiphase Flow and Reactive Transport Simulations**” was submitted by **PUNNAM PRADEEP REDDY**, ID. No. **2018PHXF0042H** for an award of PhD of the institute embodies original work done by him under my supervision.

Signature of the Supervisor:

Name in capital letters:

Prof. VIKRANTH KUMAR SURASANI

Designation:

Associate Professor, Chemical Engineering Department

Date:

Signature of the Co-Supervisors:

Name in capital letters:

Prof. BALAJI KRISHNAMURTHY

Designation:

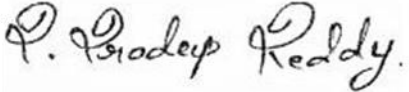
Associate Professor, Chemical Engineering Department

Date:

BIRLA INSTITUTE OF TECHNOLOGY AND SCIENCE, PILANI

Declaration

I, **Punnam Pradeep Reddy**, bearing ID number **2018PHXF0042H**, hereby declare that the research work presented in this thesis, entitled "*Investigation on CO₂ Geological Sequestration in the Deccan Volcanic Province through Multiphase Flow and Reactive Transport Simulations,*" has been conducted by me under the guidance of Prof. Vikranth Kumar Surasani and Prof. Balaji Krishnamurthy at the Department of Chemical Engineering, BITS-Pilani Hyderabad Campus, India. The work is original and has not been submitted, in part or in full, for any degree at this or any other university.

Signature: 

Name: Punnam Pradeep Reddy

Date: 15th December 2023

Acknowledgement

I am immensely grateful to my supervisor, Prof. Vikranth Kumar Surasani, for his unwavering guidance, continuous support, and remarkable patience during my PhD study. His vast knowledge and extensive experience have been a constant source of encouragement throughout my academic research and daily life. His unwavering support has helped me address numerous challenges that have improved the acceptance of my papers, and I am truly grateful for his mentorship.

In addition to my supervisor, I express my heartfelt gratitude to my co-supervisor, Prof. Balaji Krishnamurthy, and my Doctoral Advisory Committee (DAC) members, Dr. Satyapaul Singh and Prof. Jagadeesh Anmala. Their guidance and insights have played a pivotal role in honing my research writing skills, and I am grateful for their endless support throughout my PhD. I would also like to thank Dr. Arnab Dutta for his encouragement and valuable suggestions in utilizing Artificial Neural Network (ANN) predictive analysis for CO₂ geological sequestration.

I conducted this research between August 2018 and June 2023 at the Birla Institute of Technology and Science - Pilani, Hyderabad Campus, Chemical Engineering Department. I am grateful to the department and the institute for awarding me the research scholarship that facilitated my study. I would also like to thank the Government of India's Science and Engineering Research Board (SERB) for their financial support through the Core Research Grant with File No. EMR/2017/02450.

I am pleased to acknowledge the assistance of Mr. D Vamsi Krishna and Mr. A Ramachandra Sarma, who made my access to research facilities and the Computer Center laboratory much more manageable. Their support has been invaluable in my research journey. I would also like to thank my friends and fellow research scholars at BITS, Pilani-Hyderabad Campus, whose companionship, late-night discussions, and shared experiences have been cherished memories.

I am ultimately thankful to my parents, partner, siblings, friends, and acquaintances, who have been unwavering in their prayers and support and have been instrumental in my success. Without them, I consider myself incomplete. Their unwavering moral support, encouragement, and inspiration have been invaluable in achieving my personal goals. I am incredibly grateful to my parents, pillars of my strength, for their unwavering financial support that has allowed me to pursue my PhD without hindrance.

Abstract

The utilizing of fossil fuels in power generation, cement production, fertilizer production, and other industrial sectors is one of the primary contributors to the significant amount of carbon dioxide emissions that are produced in India and the majority of other developing and developed nations. In order to bring down carbon dioxide emissions into the atmosphere, it is necessary to employ technologies like carbon capture and storage (CCS). In CCS methodologies, CO₂ geological sequestration (CGS) is the most effective method to dispose of CO₂ permanently in subsurface formations. These formations include abandoned oil reservoirs to assist in enhanced oil recovery (EOR) and geological sites rich in minerals suitable for mineral carbonation. First, CO₂ is captured at large emission sources, thus preventing CO₂ release into the atmosphere. Second, the captured carbon dioxide is transported to a geological storage location, and finally, it is injected into geological formations for permanent storage. According to the available lithological, petrophysical, and geochemical data, the Deccan Volcanic Province in India is one of the country's largest sinks for the geological sequestration of carbon dioxide. Approximately five million square kilometers of India are covered by Deccan basalt. This work presents the theoretical investigation of the feasibility of CO₂ geological sequestrations in the Deccan basalt.

The four trapping mechanisms determine the fate of injected CO₂ during the CO₂ Geological Sequestration (CGS) process. Once the CO₂ is injected into the geological subsurface formation domain, due to its lower density corresponding to the resident reservoir fluid, it tends to rise due to the buoyancy effect, and the formation's top impermeable caprock layer serves as the primary seal for the injected CO₂. This way of CO₂ trapping in the domain is known as the Structural trapping mechanism, which prevents the CO₂ from escaping to the Earth's surface and traps it in the subsurface. During CO₂ upward percolation through a porous formation, some quantity of CO₂

is trapped in the migration pathway or confined within the porous structure. This trapped quantity of CO₂ is classified as Residual trapped CO₂. Further, the confined CO₂ and structurally trapped CO₂ will dissolve in resident water to form weak carbonic acid; the process of CO₂ that underwent dissolution is classified as solubility trapping. Later, this weak carbonic acid will begin to react with mineral rocks, forming secondary carbonate minerals; this way, the mineral trapping mechanism will occur in the formation.

The present work looks into the possibility of implementing CO₂ geological sequestration in the Deccan Volcanic Province. The analysis is carried out by using the multiphase, multicomponent reactive transport modeling technique. The numerical simulation analysis is performed to investigate the effects of specific sequestration parameters, such as injection rate and injection point, as well as geological parameters, such as caprock morphology, petrophysical properties variation, and geological features, such as stairsteps traps and anticline, on CO₂ plume migration in the subsurface formation domain. The effect of these sequestration and geological parameter variations on the trapping mechanisms, sweeping efficiency, and structural integrity for the considered synthetic subsurface domain is investigated over a geological time scale. The results of this study provide insight into the potential implementation of CGS as well as a future estimate of CO₂ migration and entrapment of the considered geological formation domain. In addition, the impact of the fracture embedded in the caprock on the entrapment percentage and structural integrity are investigated on various morphological top surface domains. The impact of geological features on the cracked caprock is analyzed for structural integrity.

Additionally, the crack on the caprock, embedded with the stairsteps feature domain, is analyzed to study its influence on solubility trapping. In a subsequent portion of the results, the Machine Learning approach is used for the CGS analysis to evaluate its viability in reducing time

consumption and computational load. Future research will concentrate on caprock leakage analysis incorporating different types of cracks, leakage implications on various entrapment mechanisms, and machine learning approaches to predict entrapment percentage, leakage, and structural integrity over long geological time scales.

Keywords: *Carbon Capture and Storage, Deccan Volcanic Province, CO₂ Geological Sequestration, Reactive transport modeling, Structural trapping, Residual trapping, Solubility trapping, Mineral trapping, CO₂ leakage*

Table of Content

Abstract.....	v
1 Introduction.....	2
1.1 Perspective and Hypothesis.....	2
1.2 Overview of CO ₂ Geological Sequestration.....	3
1.3 Research Motivation	6
1.4 Research Gaps and Objectives	8
1.5 Contribution to the Scientific Research	10
1.6 Overview of Thesis	11
2 Literature Review	14
2.1 Introduction	14
2.2 CO ₂ Emissions.....	15
2.2.1 Country-wise CO ₂ Emissions	16
2.2.2 Industry-wise CO ₂ Emissions	17
2.3 Carbon Capture Utilization and Sequestration (CCUS).....	19
2.3.1 Carbon Capture and Utilization	19
2.3.2 Carbon Capture and Sequestration (CCS)	23
2.4 CO ₂ Geological Sequestration (CGS)	26
2.5 Trapping Mechanisms	28
2.5.1 Structural Trapping	29
2.5.2 Residual Trapping	31
2.5.3 Solubility Trapping	32
2.5.4 Mineral Trapping	34
2.5.5 Caprock Structural Integrity	36
2.5.6 Worldwide CGS Projects	38
2.6 Potentiality of CGS in India	44
2.6.1 Basalt Geological Formations.....	47

2.6.2	Deccan Volcanic Province	48
2.7	Numerical Study of Reactive Transport Modelling (RTM).....	50
2.8	Geological and Sequestration parametric studies.....	52
2.9	Utilization of Machine Learning in CO ₂ Geological Sequestration Analysis	55
2.10	Chapter Summary.....	57
3	Multiphase and Reactive Transport Modelling for CO₂ Geological Sequestration.....	61
3.1	Introduction	61
3.2	Reactive Transport Modeling for CGS	61
3.3	Multiphase Flow Equations.....	64
3.4	Brooks-Corey Relation.....	65
3.5	Reactive Transport Modelling.....	66
3.6	Estimation of trapping percentage.....	69
3.7	Modeling of Synthetic Domain: Methodology and Approaches	72
3.7.1	Synthetic geological domain for Structural- and Residual-trapping.....	72
3.7.2	Synthetic geological domain for Solubility- and Mineral-trapping	75
3.8	Simulation Methodology.....	77
4	Investigation of Trapping Mechanisms in Deccan Volcanic Province	81
4.1	Introduction	81
4.2	Investigation of Structural- and Residual Trapping Mechanisms in CGS.....	82
4.2.1	Base Case Scenario	84
4.2.2	Influence of Heterogeneity –Petrophysical properties.....	87
4.2.3	Influences of Injection Point Selection	90
4.2.4	Influences of Injection Rate	95
4.3	Investigation of Solubility Trapping Mechanism in CGS.....	96
4.3.1	Comparison between Primary and Solubility trapping mechanisms	98
4.3.2	Influence of Heterogeneity –Petrophysical properties.....	102

4.3.3	Influences of Injection Point Selection	105
4.4	Investigation of Mineral Trapping Mechanism in CGS.....	110
4.5	Summary	113
5	Investigating the Role of Caprock Morphology and Structural Integrity on the Solubility Trapping Mechanism	117
5.1	Introduction	117
5.2	Influence of caprock morphology on the solubility trapping.....	118
5.2.1	Modeling of synthetic geological domains	118
5.2.2	Base Case Scenario	119
5.2.3	Comparison study between two distinct caprock morphology	125
5.3	Influence of Structural Integrity Analysis on the Solubility Trapping	129
5.3.1	Modeling of synthetic geological domains.....	130
5.3.2	Impacts of caprock morphology on leaky caprock and CO ₂ entrapment	133
5.3.3	CO ₂ leakage in the stairsteps domain.....	138
5.4	Summary	141
6	Utilization of Machine Learning in the CO₂ Geological Sequestration Analysis.....	144
6.1	Introduction	144
6.2	Modeling of synthetic geological domains	145
6.3	Numerical Simulation Results.....	147
6.4	Utilization of Machine Learning: Time Series Neural Network Analysis.....	149
6.5	Summary	154
7	Conclusions.....	156
7.1	Realistic geological subsurface domain- Saurashtra, Gujarat, India.....	156
7.2	Structural- and Residual Trapping	157
7.3	Solubility Trapping	158
7.4	Mineral Trapping.....	159

7.5	Structural Integrity	161
7.6	Machine Learning Technique in CGS.....	162
7.7	Overall conclusions	163
7.8	Limitations of the Research.....	167
7.9	Future Research scope.....	168
References		170
Research Publications.....		195
Biography of Candidate		197
Biography of Supervisor.....		197
Biography of Co-Supervisor		197

List of Tables

<i>Table 2-1: Notable CCS projects worldwide for CO₂ geological storage. The asterisk next to the year indicates that the information is current as of that year [134].</i>	<i>40</i>
<i>Table 3-1: Multiphase flow and reactive transport model equations for CO₂ geological sequestration [22].</i>	<i>71</i>
<i>Table 3-2: Subsurface geochemical reactions of solubility and mineral trapping mechanisms [204].</i>	<i>77</i>
<i>Table 6-1: Comparison of R-squared and RMSE values of different training function algorithms for structural trapping [219].</i>	<i>153</i>
<i>Table 7-1: Illustration of major governing parameters influencing the corresponding trapping mechanisms [56], [58], [184]–[187], [204], [232], [63], [80], [109], [111], [180]–[183].</i>	<i>166</i>

List of Figures

- Figure 1.1: Descriptive illustration of various trapping mechanisms that occur in the subsurface formation and CO₂ leakage during CO₂ geological sequestration. 5**
- Figure 1.2: Illustration of the spread of Deccan flood Basalt in the Deccan Volcanic Province of India [33]..... 7**
- Figure 1.3: Illustrated flow chart of the research motivation and crucial aspects of the research. 8**
- Figure 2.1: Illustration of country-wise CO₂ emissions of China, the European Union (EU), India, and the United States of America (USA) (adapted from IEA 2021 Report [40]). .. 16**
- Figure 2.2: Illustration of (A) Percentage of coal usage and low-carbon technologies in energy production and (B) Usage of fossil fuels in the industrial sector and production of other essential products (adapted from IEA 2021 Report [40], [41])..... 18**
- Figure 2.3: Illustrates a flow chart of Carbon Capture Utilization and Sequestration classification. Only major categories are included in the flow chart..... 21**
- Figure 2.4: Schematic of Carbon Capture Storage (CCS), Illustrating the CO₂ capture point and geological injection grid. 28**
- Figure 2.5: Notable locations across India where carbon may be stored [161]..... 45**
- Figure 3.1: The figure illustrates different components: (A) Contour plots sourced from literature D. N. Murthy et al., [201], (B) Contour plot of the modeled geological domain, (C) Three-dimensional grid structure, and (D) The distribution of porosity and permeability within the domain, used for simulating Structural and Residual trapping [30], [111] 74**
- Figure 3.2: Figure shows (A) contour plots extracted from literature, D. N. Murthy et al., [201], (B) contour plot of the geological domain modeled, (C) three-dimensional grid**

<i>structure, and (D) distribution of porosity and permeability in the domain used for the Solubility trapping simulation.</i>	<i>76</i>
<i>Figure 4.1: Illustration of the categorization of structural trapping, residual trapping mechanisms, and movable plume in geological sequestration: (A-E) depicting the fate of CO₂ during and after injection into the geological formation [30]......</i>	<i>83</i>
<i>Figure 4.2: The fate of CO₂ through structural- and residual trapping phenomena across geological time is represented by the height of saturated CO₂ from the surface; the injection point is displayed by the letter I and (ii) CO₂ saturation in the 3D domain. A total of $7.227 \times 10^{10} \text{ m}^3$ of CO₂ was injected for the first 20 years [30]......</i>	<i>85</i>
<i>Figure 4.3: The percentage of CO₂ trapped in structural trapping, residual trapping, and movable plume is represented by a histogram. It was reported that the structural trapping and residual trapping contributions increased after injection [30].</i>	<i>87</i>
<i>Figure 4.4: A) Comparison of Sweeping efficiency for two distinct porosity and permeability ranges B) Comparison of Structural trapping, Residual trapping, and movable-plume percentages between the two petrophysical ranges [30]......</i>	<i>90</i>
<i>Figure 4.5: Dynamic evolution of Structural trapping, Residual trapping, and Movable plume when CO₂ is injected at A, B, C, D, E, and F injection points of the synthetic geological domain [30].</i>	<i>92</i>
<i>Figure 4.6: Geological topography has an impact on structural and residual entrapment. The diagram depicts the migration of CO₂ when it is introduced at various spots in the computation domain [30]......</i>	<i>94</i>
<i>Figure 4.7: Illustration of Structural trapping, Residual trapping, and Movable-plume at injection points B and C for varying injection rates $123.75 \times 10^5 \text{ m}^3/\text{day}$, $99 \times 10^5 \text{ m}^3/\text{day}$, $49.5 \times 10^5 \text{ m}^3/\text{day}$, $24.75 \times 10^5 \text{ m}^3/\text{day}$, and $12.375 \times 10^5 \text{ m}^3/\text{day}$ [30]......</i>	<i>96</i>
<i>Figure 4.8: (A) Comparison of CO₂ saturation for two simulation sets, (B) Structural-, Residual trapping and Movable plume percentage variation, and (C) Structural-,</i>	

<i>Residual-, Solubility trapping and Movable plume percentage variation over geological time scale [111].....</i>	<i>101</i>
<i>Figure 4.9: Comparison of CO₂ mole fraction in both simulation sets at 1500th and 3000th year. This result illustrates the solubility fingering phenomena observed in simulation set-2. In the 1500th year, the first sight of solubility fingers was observed in simulation set-2 [111].</i>	<i>102</i>
<i>Figure 4.10: (A) Illustration of the CO₂ liquid mole fraction migration and pH variation at the end of simulation time (3000th year), (B) Total CO₂ solubility trapping, (C) Reservoir pressure variation, and (D) Reservoir temperature variation for two simulation sets over geological time scale [111].....</i>	<i>104</i>
<i>Figure 4.11: Illustration of the CO₂ liquid mole fraction migration and pH variation at 1st, 1500th, and 3000th year. In the 1500th-year result, most of the injection points displayed solubility fingering [111].</i>	<i>107</i>
<i>Figure 4.12: (A) Total CO₂ solubility trapping and (B) Reservoir pressure variation for all injection points over a geological time scale [111].</i>	<i>109</i>
<i>Figure 4.13: Illustration of the CO₂ liquid mole fraction migration and pH variation in the 1st, 40th, and 2000th year.....</i>	<i>111</i>
<i>Figure 4.14: The figure illustrates the results of dynamic mineral volume fraction evolutions</i>	<i>113</i>
<i>Figure 5.1: Illustration of a schematic diagram of the three-dimensional grid structure of both the domains and petrophysical properties distribution [63].....</i>	<i>119</i>
<i>Figure 5.2: (A) Comparison of top view saturation of Structural- and Residual trapping only (Simulation set-1) and Structural-,Residual-, and Solubility trapping (simulation set-2) at 1st, 30th, and 3000th year (B) Structural- and Residual trapping variation (Without geochemical reactions), and (C) Structural-, Residual- and Solubility trapping (With geochemical reaction) variation over geological time scale [63].</i>	<i>121</i>

<i>Figure 5.3: Solubility fingering phenomenon during CO₂ geological sequestration and their evolution over geological time scale [63].</i>	<i>124</i>
<i>Figure 5.4: Illustration of CO₂ Mole Fraction and pH variation over geological time scale during CO₂ geological sequestration [63].</i>	<i>125</i>
<i>Figure 5.5: Influence of caprock morphology on (A) CO₂ Mole Fraction and (B) pH variation over a geological time scale [63].</i>	<i>127</i>
<i>Figure 5.6: Influence of caprock morphology on (A) Average reservoir pressure, (B) Average reservoir temperature, and (C) Aqueous and gaseous phase CO₂ quantity variation over geological time scale [63].</i>	<i>128</i>
<i>Figure 5.7: Illustrates a schematic diagram of the three-dimensional grid structure, the top view of the domain, and the distribution of petrophysical properties of three considered synthetic domains. In column two, the three-dimensional domain is made transparent in order to view the crack on the caprock from the top view.</i>	<i>132</i>
<i>Figure 5.8: Illustration of (A) CO₂ Mole Fraction and (B) pH variation over geological time scale during CO₂ geological sequestration.</i>	<i>134</i>
<i>Figure 5.9: Influence of caprock morphology on (A) Average reservoir pressure, (B) Average reservoir temperature, and (C) Solubility trapping of CO₂ variation over geological time scale.</i>	<i>137</i>
<i>Figure 5.10: Illustration of (A) CO₂ Mole Fraction and (B) pH variation over geological time scale during CO₂ geological sequestration.</i>	<i>139</i>
<i>Figure 5.11: Influence of caprock morphology on (A) Average reservoir pressure, (B) Average reservoir temperature, and (C) Solubility trapping of CO₂ variation over geological time scale.</i>	<i>140</i>
<i>Figure 6.1: (A) Three-dimensional grid structure with physical dimensions and computational cells; (B) Petrophysical properties distributions. The bold red letter I in the current figure is the injection point [219].</i>	<i>146</i>

Figure 6.2: (A) CO₂ plume migration in the geological domain, the results illustrated for 1, 30, 300, and 400 years, and (B) the number of CO₂ saturated cells variation over geological time scale [219]..... 148

Figure 6.3: (A) Average reservoir pressure and temperature variation; and (B) structural and residual trapping and movable plume variation over geological time scale [219]. 149

Figure 6.4: (A) Nonlinear Autoregressive Network with Exogenous Inputs (NARX) architecture; (B) Nonlinear Autoregressive Network (NAR) architecture. The figure illustrated the structural trapping as the target variable. In the case of NARX, if the residual trapping is selected as the target variable, then the structural trapping will be considered under the input variable [219]. 150

Figure 6.5: Comparison of different training function algorithms used with the NARX neural network. Levenberg-Marquardt has shown low deviation from simulation target data [219]..... 151

Figure 6.6: Comparisons of NAR-LM and NARX-LM with numerical results for (A) Structural trapping percentage variation and (B) Residual trapping percentage variation. NAR-LM has a very low deviation from target data at the same geological time scale [219]..... 152

Nomenclature

D	Phase Diffusivity Coefficient	[m ² s ⁻¹]
g	Gravity	[m s ⁻²]
H	Enthalpy	[kJ mol ⁻¹]
h	Vertical height	[m]
I	Reaction Rate	[mol lit ⁻¹ s ⁻¹]
<i>k</i>	Intrinsic permeability	[m ²]
<i>K_{eq}</i>	Equilibrium constant	[-]
<i>k_r</i>	Relative permeability	[-]
P	Pressure	[Pa]
<i>P_c</i>	Capillary pressure	[Pa]
<i>P_e</i>	Entry pressure	[Pa]
Q	Source or Sink terms	[kmol m ⁻³ s ⁻¹]
<i>Q_e</i>	Source or Sink term for energy	[-]
q	Darcy flux	[m s ⁻¹]
S	Saturation	[-]
<i>S_{e,l}</i>	Effective liquid saturation	[-]
<i>S_{e,g}</i>	Effective gas saturation	[-]
<i>S_{r,CO₂}</i>	Residual saturation of CO ₂	[-]
T	Temperature	[K]
U	Internal Energy	[kJ mol ⁻¹]
<i>V_r</i>	Volume of residual trapping grid cell	[m ³]
<i>V_s</i>	Volume of structural trapping grid cell	[m ³]

W	Formula Weight	[kg kmol ⁻¹]
X	Mole Fraction	[-]
z	Vertical Co-ordinate	[m]

Greek Letter

α	Empirical constants	[-]
ϕ	Porosity	[-]
κ	Thermal Conductivity	[W m ⁻¹ K ⁻¹]
ρ	Density	[kg m ⁻³]
τ	Tortuosity	[-]
μ	Viscosity	[Pa s]
ν	Co-efficient of reaction rate	[-]
η	Molar Density	[kmol m ⁻³]
ψ	Total concentration of species	[mol m ⁻³]
Ω	Total flux of species	[mol m ⁻² s ⁻¹]

Subscript/Superscript

p	Phase of specie
l	Liquid phase
g	Gas phase
w	Water
c	CO ₂
r	Rock
j	Primary species
m	Minerals

Abbreviation

ANN	Artificial Neural Network
ANN-GCS	Artificial Neural Network Geological CO ₂ Sequestration
BECCS	Bio-Energy with Carbon Capture and Storage
CBM	coalbed methane recovery
CCS	Carbon Capture and Sequestration
CCU	Carbon Capture and Utilization
CCUS	Carbon Capture Utilization and Sequestration
CO ₂ CRC	Cooperative Research Centre for Greenhouse Gas Technologies
ECMR	Enhanced coalbed methane recovery
EOR	Enhanced oil recovery
CGS	CO ₂ Geological Sequestration
GHG	greenhouse gas
IEA	International Energy Agency
IPCC	Intergovernmental Panel on Climate Change
MLP	Multilayer Perceptron
MLP-LM	Multilayer Perceptron - Levenberg-Marquardt
MRCSP	Midwest Regional Carbon Sequestration Partnership
MRST	MATLAB Reservoir Simulation Toolbox
NAR	Nonlinear Autoregressive Network
NARX	Nonlinear Autoregressive Network with Exogenous Inputs
PETSc	Portable Extension Toolkit for Scientific Computation

PSDM	Pre-Stacking and Depth Migration
PSTM	Pre-Stacking and Time Migration
RTI	Residual Trapping Index
RTM	Reactive Transport Modelling
SECARB	Southeast Regional Carbon Sequestration Partnership
STI	Structural Trapping Index
TTEI	Total Trapping Efficiency Index

CHAPTER 1: Introduction

1 Introduction

1.1 Perspective and Hypothesis

CO₂ Geological Sequestration (CGS), which involves injecting carbon dioxide into subsurface rock formations, is a promising strategy for mitigating the harmful impacts of CO₂ emissions into the atmosphere, such as climate change, global warming, etc. The Deccan Volcanic Province in India, with its extensive Deccan basalt formation, represents a potential target for CO₂ sequestration and countries' efforts to reach net zero carbon emissions, see **Figure 1.2** [1]–[9].

Research on CO₂ geological sequestration in India is minimal [10]. There is considerable uncertainty regarding the geological capacity for CO₂ sequestration in India. Certain studies suggest a potential CO₂ mitigation capacity of around 48 gigatons, while others indicate a much higher value of up to 572 gigatons [10]. This uncertainty is mainly because of the lack of proper research studies based on saline aquifers and basalt formation, which encompasses significant areas of Indian geology [10]. In the Indian scenario, the research trends are only towards the experimental evaluation of the behavior of geological formations towards reaction with supercritical CO₂ [8], [11]. However, success at the lab scale, field scale application, and risk analysis in geological time scales need a theoretical modeling approach. And modeling is the only way to understand the mineral rapping mechanism, where experiments have difficulty in implementation [12].

Multiphase flow and Reactive Transport Modeling (RTM) acts as a tool to elucidate the dynamics of geochemical and petrophysical behavior of geological formations to understand the response of sequestration. Thus, success largely depends on the virtual and augmented reality of field study as well as on risk analysis. In any geological sequestration project, modeling the behavior of geological formations towards injected carbon dioxide is an

important step. These modeling studies give a thorough understanding of the fate of injected CO₂ in geological time scales [13]. It is possible to model every aspect of geochemical sequestration, from the immediate effect of injection of CO₂ into a reservoir to the geochemical changes taking place over days to several decades of sequestration. Geological sequestration is an operation that has high-risk factors, so it is not advisable to implement a CCS project without adequately understanding the detailed effects and long-term impacts of sequestration in a geological formation [13]. Finally, reactive transport modeling (RTM) is an essential tool for better understanding CO₂ geological sequestration in the Deccan Volcanic Province. RTM can assist in informing choices concerning the feasibility and implementation of CO₂ sequestration projects in India by giving a complete and integrated perspective of the subsurface environment due to various trapping and subsurface geological phenomena [14]–[22].

1.2 Overview of CO₂ Geological Sequestration

CO₂ geological sequestration is a process in carbon capture and storage (CCS) that aims to store carbon dioxide (CO₂) in deep subsurface geological formations. This technique holds the potential for mitigating climate change by effectively trapping and isolating CO₂ in the geological subsurface over a long geological time. During CO₂ geological sequestration, various trapping mechanisms come into play to ensure that the CO₂ is trapped within the subsurface and prevent its escape into the atmosphere. The four trapping mechanisms are structural, residual, solubility, and mineral trapping [23]–[25]. **Figure 1.1** illustrates schematics of the CGS process and its associated trapping mechanism.

When CO₂ is injected into the targeted subsurface region, the first trapping mechanism that comes into effect is structural trapping, where the impermeable caprock layer primarily traps the injected CO₂. As the CO₂ plume migrates and percolates from the injection point towards the top impermeable layer, a portion of the CO₂ plume gets trapped in the pore spaces due to

capillary forces. This phenomenon is known as residual trapping. Over time, the CO₂ trapped by the combined effect of structural and residual trapping mechanisms (collectively known as primary mechanisms) comes into contact with resident water in the subsurface reservoir and undergoes a dissolution reaction. This trapping mechanism is called solubility trapping.

Furthermore, the dissolved CO₂ forms weak carbonic acids, decreasing pH in the subsurface formation region. The lowered pH conditions promote mineral dissolution and precipitation, leading to the formation of stable carbonate minerals that can permanently immobilize the CO₂ in the subsurface formation. The trapping of CO₂ through geochemical mineral interaction is categorized under the mineral trapping mechanism [23]–[25].

In any technology, there is always a possibility of failure, and in CGS technology, the leakage of CO₂ from the subsurface formation domain is a crucial concern. Several factors can contribute to leakage, and understanding and mitigating these risks are of utmost importance. One potential cause of leakage is the presence of pre-existing or induced fractures in the storage formation, which can provide pathways for CO₂ to escape to the surface. Another factor that can contribute to leakage is the potential failure or deterioration of the caprock, which is the impermeable layer that seals the storage formation. Suppose the caprock is compromised due to geological factors such as faulting, erosion, or human activities like drilling operations. In that case, it may establish a pathway for upward migration of CO₂, leading to its escape into the earth's surface. A detailed analysis must be carried out to analyze the impact of cracks or fractures on the caprock on CO₂ plume migration and safe storage during the pre-implementation phase of CGS projects [26], [27].

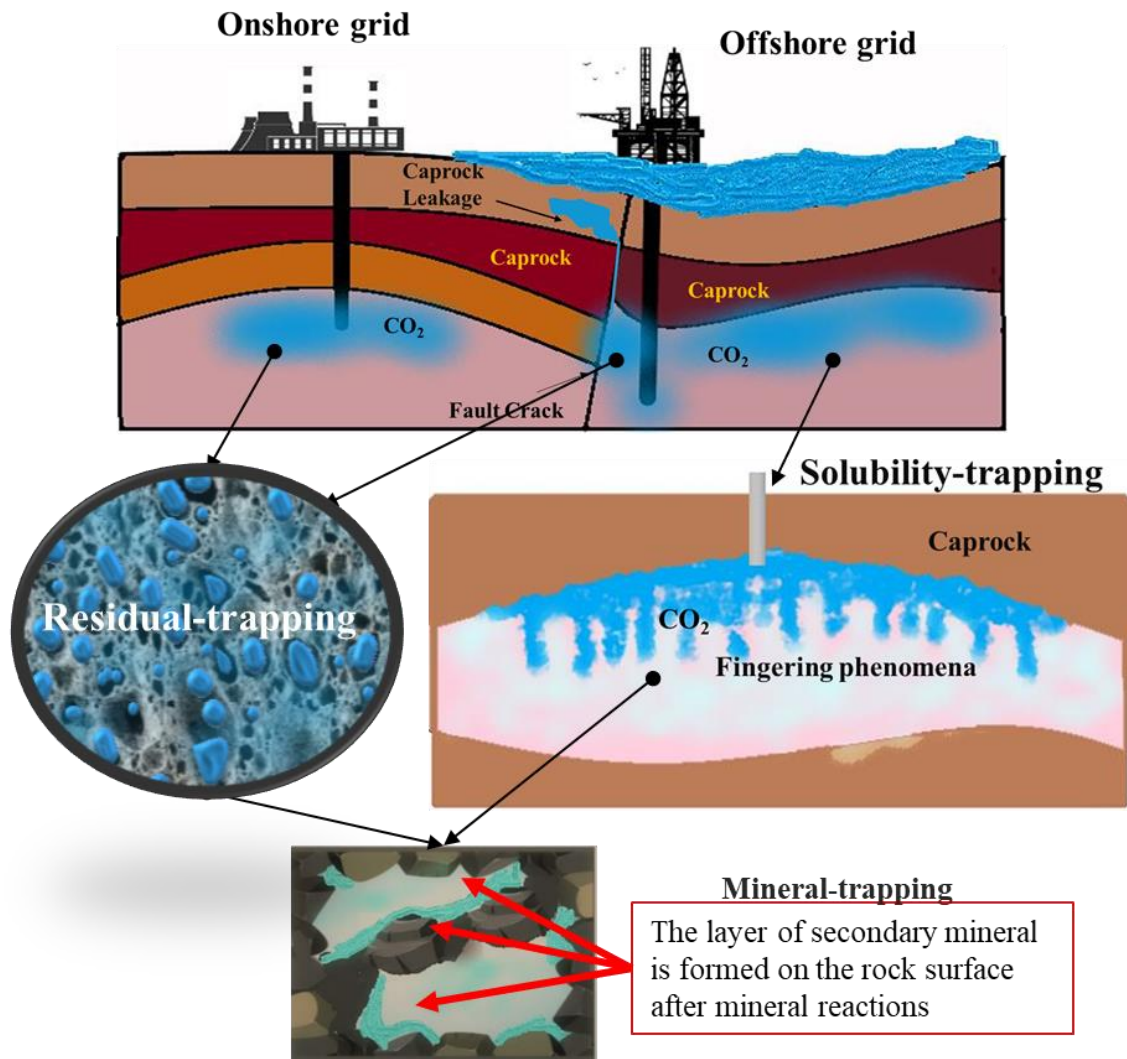


Figure 1.1: Descriptive illustration of various trapping mechanisms that occur in the subsurface formation and CO₂ leakage during CO₂ geological sequestration.

Conducting leakage analysis in parallel with the geological study provides valuable insights into the behavior of stored CO₂ and its potential interaction with the surrounding rock formations, caprock, and other geological features. It enables the detection and quantification of leakage pathways, which can inform the design of mitigation strategies and help in the development of more effective storage practices [26], [27].

Simulations are the preferred choice for conducting CO₂ geological sequestration analysis due to their ability to analyze geological processes over extended periods of time. Performing

experimental analysis of CO₂ geological sequestration presents several challenges and requires careful consideration. Conducting long-term experiments to assess the behavior of CO₂ in geological formations can be time-consuming and costly. The sequestration takes over extended periods, and studying the long-term effects requires continuous monitoring and observation. This necessitates dedicated research efforts, continuous funding, and patience to obtain meaningful data and insights. Additionally, the dynamic nature of geological systems and the potential for unexpected outcomes add further complexity to the analysis [26]–[29].

1.3 Research Motivation

The geological sequestration of CO₂ in the Deccan Volcanic Province is a viable strategy for lowering CO₂ emissions and minimizing the effects of climate change. Due to its vast storage capacity and advantageous geological properties, the Deccan Volcanic Province is an ideal region for CO₂ sequestration. The Deccan Volcanic Province has sequential layers of massive and vesicular basalts. The massive basalt can act as a cap rock that prevents CO₂ escape. The petrophysical properties and characteristics of vesicular basalt can act as a targeted region for the injection of captured CO₂ [30]. **Figure 1.2** illustrates the spread of Deccan flooded basalt in the Deccan Volcanic Province.

In addition, the Deccan Volcanic Province is situated in an area with significant CO₂ emissions, positioning it in a strategic location that can help India mitigate the consequences of climate change, see **Figure 1.2**. It is feasible to store CO₂ safely and effectively while simultaneously offering economic possibilities and contributing to energy security by adopting this technology. Because of its vast storage capacity and favorable geological properties, the Deccan Volcanic Province is an essential consideration for resolving the issue of growing atmospheric CO₂ levels [31], [32].

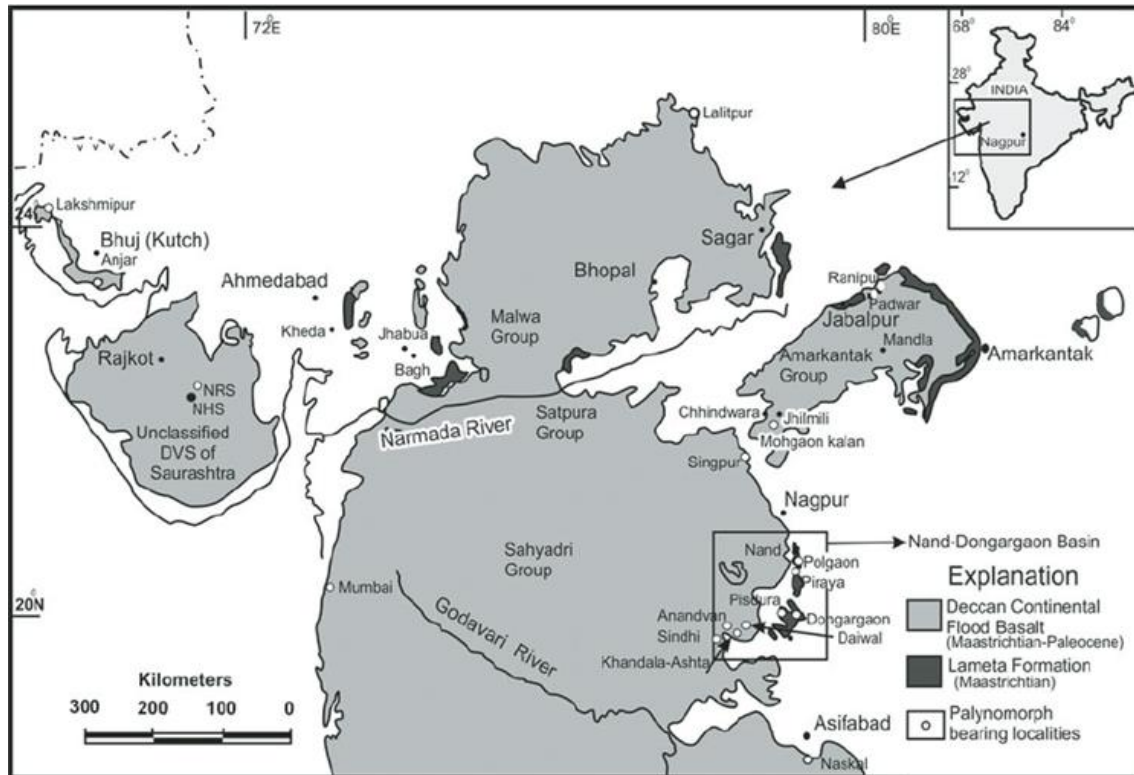


Figure 1.2: Illustration of the spread of Deccan flood Basalt in the Deccan Volcanic Province of India [33].

Numerical analysis using multiphase flow and reactive transport modeling for CO₂ geological sequestration investigation in the Deccan Volcanic Province aids in better understanding and prediction of CO₂ behavior in the subsurface, including interactions with rock and fluid systems, as well as the potential risks associated with its storage. Reactive transport modeling provides a precise evaluation of CO₂ storage stability in the subsurface and aids in identifying possible endangerments, such as CO₂ leakage, that may harm the surrounding environment.

Figure 1.3 illustrates the motivation for this numerical study of CO₂ geological sequestration in the Deccan Volcanic Province that contributes to the scientific understanding of subsurface CO₂ storage and to evaluate the feasibility of using this region as a potential site for CO₂ sequestration. Using numerical simulations, the aim is to investigate the geophysical and geochemical processes that govern CO₂ storage in this region and to predict the behavior of

CO₂ over time. This study has the potential to provide valuable intuitions into the technical and economic viability of CO₂ geological sequestration and to form decision-making for mitigating greenhouse gas emissions.

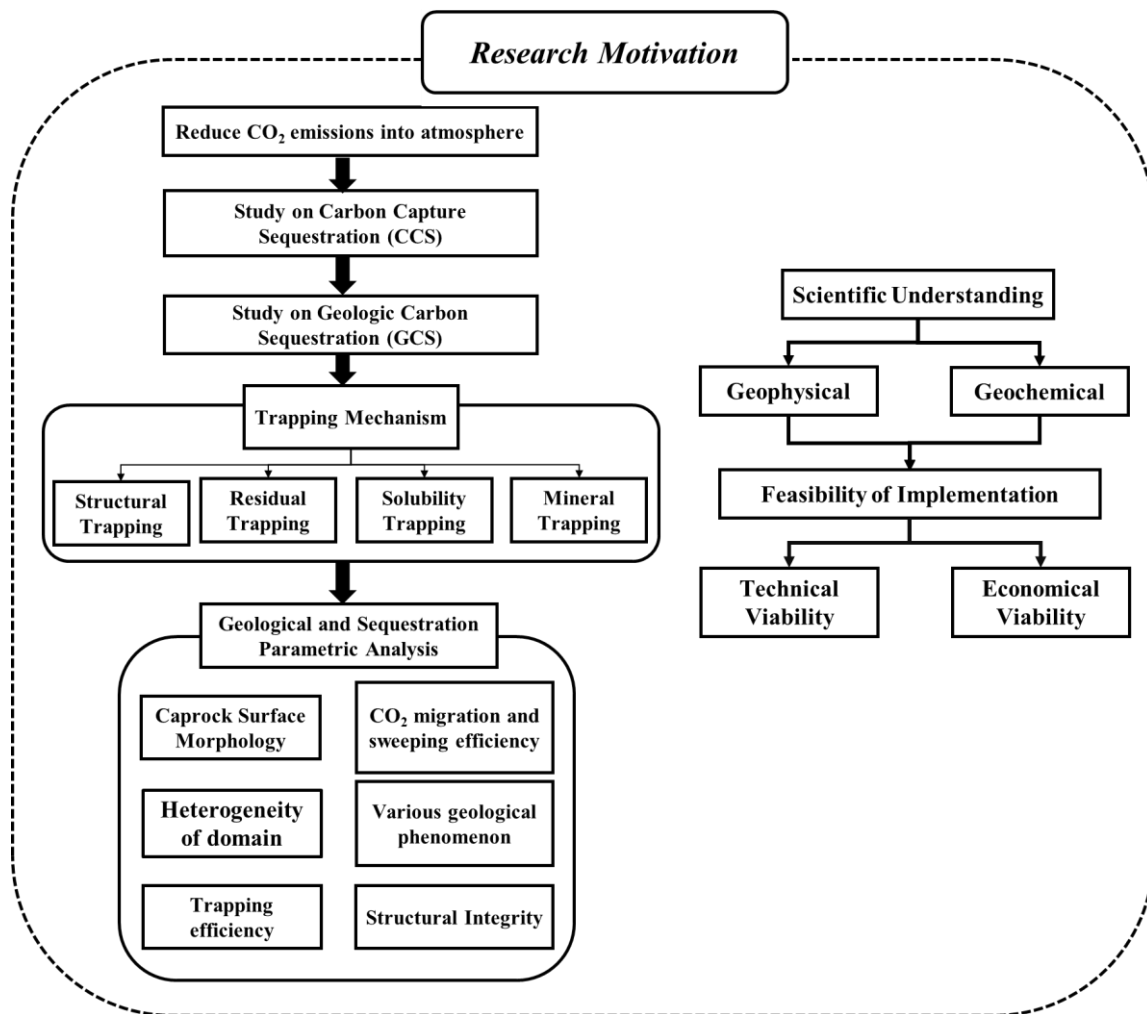


Figure 1.3: Illustrated flow chart of the research motivation and crucial aspects of the research.

1.4 Research Gaps and Objectives

Limited research has been conducted in India on CO₂ geological sequestration, mostly in the context of small-scale laboratory experiments [11]. There is no pilot scale-based geological sequestration exploration in the Deccan Volcanic Province of India. And there is no research on the definite range of CO₂ that can be stored in the Deccan trap region. Many researchers

have pointed out that the Deccan traps can be one of the most suitable regions for sequestration [10]. Still, plenty of exploration can be done at the appropriate depth range, or any desired caprock properties can be prescribed to safely guard the sequestered carbon dioxide. There is no research investigation on the integrity of the caprock and formation domain during CO₂ geological sequestration.

By adequately mapping layers and their respective thickness with their petrophysical properties in the domain, one can estimate the adequate amount of CO₂ stored in the formation domain. By carrying out the CO₂ sequestration simulation, the total safe storage CO₂ capacity can be evaluated over a geological time scale. The appropriate percentage of efficiency of different trapping mechanisms can be calculated in the simulation. The mineral trapping mechanism occurs in the subsurface formation domain, takes nearly hundreds of years, and the experiment setup can't be maintained for such long. The simulation analysis has the advantage of considering all the trapping mechanisms for analysis over a large geological time scale.

A lack of caprock leakage analysis is associated with the Deccan volcanic region of Indian origin. The simulation of caprock leakage analysis is expected to yield detailed measurements of deformation changes within the domain resulting from CO₂ injection. These studies can be helpful for the long-term storage of CO₂ and can be used to analyze the integrity of the storage capacity of the formation domain. It can also provide a range of stress developed in the domain during and after CO₂ injection. These studies can't be conducted efficiently with the help of experiments. The simulations have the advantage of performing numerical research over a vast domain volume and continuing it over a long geological time. The following are the objectives of the current research analysis included in this thesis.

1. Study the structural trapping of injected supercritical CO₂ into the geological formation of Deccan Volcanic Province.

2. Study the residual trapping of injected supercritical CO₂ into the geological formation of Deccan Volcanic Province.
3. Study the solubility trapping of Supercritical CO₂ into the formation liquid over the geological time scale at Deccan Volcanic Province.
4. Study the mineralization at Deccan Volcanic Province after the CO₂ sequestration in the geological formation domain for post-injection time scale.
5. Study the different types of trapping mechanisms in the CO₂ sequestration process with varying formation domain petrophysical properties over a geological time scale.
6. Leakage analyses of CO₂ sequestration into the geological formation of Deccan Volcanic Province.

1.5 Contribution to the Scientific Research

Performing numerical simulation and visualization of injected CO₂ plumes in the Deccan Traps, which are stairsteps that look like traps, is novel in current research. This study will provide critical information about the CO₂ plume migration in the domain after injection into the subsurface of the Deccan traps. Some crucial parameters are analyzed, such as influences on caprock morphology, petrophysical properties variation, reservoir pressure variation, and sweeping efficiency.

CO₂ sequestration knowledge: The study would increase knowledge about the potential of Deccan Volcanic Province as a suitable site for CO₂ sequestration, and it would also increase knowledge about how geological phenomena such as caprock morphology, petrophysical heterogeneity, and structural integrity impact the effectiveness of CO₂ sequestration.

Progress in Reactive Transport Modeling: The study would demonstrate the use of reactive transport modeling as a tool to understand the behavior of injected CO₂ in the subsurface and

how it interacts with the geological formations. This would be a considerable development in reactive transport modeling utilization with an unstructured grid structure, which approximately mimics the naturally formed geological subsurface formation domain.

Improved CO₂ Sequestration Techniques: The parametric study would provide insights into the various factors that influence the efficiency of CO₂ sequestration and could be used to optimize CO₂ sequestration techniques. These insights could be used in the selection of subsurface formation regions based on the assessment from the numerical analysis. This would advance the screening for the sequestration location for suitable implementation of CGS for the reduction of atmospheric carbon dioxide emissions.

Better Understanding of Geological Phenomena: The research would give a better understanding of geological phenomena such as CO₂ migration and movement with corresponding caprock morphology. It also helps analyze the CO₂ sweeping efficiency, caprock morphology, and petrophysical heterogeneity and how these factors influence CO₂ sequestration.

Overall, the study would contribute to the improvement of our knowledge and understanding of CO₂ geological sequestration, as well as provide vital information that might be used in the creation of CO₂ geological sequestration systems that are efficient and successful.

1.6 Overview of Thesis

The present thesis aims to provide a comprehensive overview of carbon dioxide (CO₂) geological sequestration in the Deccan Volcanic Province, covering various aspects across multiple chapters. **Chapter 1** introduces the research hypothesis, motivation, objectives, and contribution to scientific research. **Chapter 2** provides a comprehensive literature review that delves into various aspects related to CO₂ emissions. The review covers global CO₂ emissions, existing technologies for emissions reduction, and carbon capture and sequestration (CCS)

technology, along with associated trapping mechanisms. Additionally, the review explores the potential for CO₂ sequestration in the Deccan Volcanic Province of India as a study area. The chapter also discusses the utilization of multiphase flow and reactive transport modeling simulations and machine learning in this context. **Chapter 3** focuses on multiphase flow and reactive transport modeling (RTM) for CO₂ geological sequestration. **Chapter 4** delves into investigating the trapping mechanisms involved in the CGS in Deccan Volcanic Province and investigating the influence of geological and sequestration parameters.

Meanwhile, **Chapter 5** evaluates the significant influences of caprock morphology and structural integrity in the solubility trapping mechanism. The influences of caprock morphology study are carried out by modeling two distinct caprock morphology with integrating geological features. Structural integrity simulation analysis examines the impact of caprock morphology on leaky caprock and entrapment, as well as CO₂ leakage in the stairsteps domain. **Chapter 6** delves into the utilization of machine learning techniques in the analysis of CO₂ geological sequestration, exploring how machine learning can reduce computational time and effectively predict primary trapping mechanisms. Finally, in **Chapter 7**, the thesis concludes with discussions, conclusions, and suggestions for future research in the field of CO₂ geological sequestration. The overall contribution of the thesis lies in providing the feasibility of CO₂ geological sequestration, covering various aspects such as literature review, reactive transport modeling, and machine learning analysis by offering insights for further research in this area.

CHAPTER 2: Literature Review

2 Literature Review

2.1 Introduction

This chapter presents a comprehensive literature review on the topic of CO₂ geological sequestration. The chapter begins with an overview of CO₂ emissions and greenhouse gases in **Section 2.2**, which includes country-wise (**Section 2.2.1**) and industry-wise CO₂ emissions (**Section 2.2.2**). **Section 2.3** discusses the existing technology aimed at reduce CO₂ emissions into the atmosphere, i.e., the concept of carbon capture and sequestration (CCS). The special focus on the CO₂ storage method, CO₂ geological sequestration, is presented in **Section 2.4**. The detailed literature study on the different trapping mechanisms involved in CO₂ geological sequestration, such as structural trapping in **Section 2.5.1**, residual trapping in **Section 2.5.2**, solubility trapping in **Section 2.5.3**, and mineral trapping in **Section 2.5.4**, are comprehensively reviewed with the implication of caprock leakage in **Section 2.5.5**. The chapter further explores some notable projects worldwide on CO₂ geological sequestration in **Section 2.5.6**.

The feasibility and potential of CO₂ geological sequestration in India are explained in **Section 2.6**. The unique geological formations of basalt and the Deccan Volcanic Province, which hold promise for CO₂ geological sequestration, are also discussed in this **Section**. The modeling, simulation, and analysis of CGS, as well as the accompanying feasibility and achievements using reactive transport modeling (RTM), are briefly discussed in **Section 2.7**, and the importance of geological and sequestration parametric studies in understanding the effectiveness of CO₂ sequestration is highlighted in **Section 2.8**. Additionally, **Section 2.9** reviews the viability and benefit of the utilization of machine learning techniques for CO₂ geological sequestration analysis based on the existing literature. Through the comprehensive literature review, **Chapter 2** aims to provide a thorough understanding of various aspects

related to CO₂ geological sequestration, setting the foundation for the subsequent chapters that will delve into specific topics in greater depth.

2.2 CO₂ Emissions

Carbon dioxide is one of the most influential greenhouse gases (GHG) for global warming [34]. Greenhouse gases like CO₂, CH₄, N₂O, and fluorinated gases are accountable for the greenhouse gas effect, which absorbs the heat emitted by the Earth's surface; additionally, it acts as a shield by reflecting the heat radiation from the sun. However, excessive release of greenhouse gases leads to global warming. It allows the heat radiation from the sun into the Earth's atmosphere and restricts the heat escaping from the Earth's surface. So, the average temperature rises on the Earth's surface [35].

As per the Paris Agreement, most developed and developing countries have pledged to decrease global warming below 2 °C, preferably below 1.5 °C [36]. To reach this goal, the use of CCS technology is considered vital. There are many proposed methods and adaptive habits to minimize the effects of global warming, for example, enhancing tree plantation, reducing the usage of fossil fuels, reducing the usage of energy, relying on only green energy like wind energy and solar energy, an adaption of a particular lifestyle of using plastic less-products, etc. However, the implementation of these adaptive methods and the benefit from their effective impact can take a significant time. Even if implemented successfully, it will take significant time to achieve the reduction of CO₂ in the Earth's atmosphere. At present, the CO₂ percentage in the atmosphere has crossed alarming levels. Global warming might also be a reason for the increased occurrence of natural calamities and climate change within the last two decades.

Moreover, it is also recorded that during this period, the Earth's average temperature change rose by 0.8 °C from its previous 0.4 °C [37]. The primary reason behind sudden changes in temperature and natural calamities may be the increasing CO₂ in the Earth's atmosphere. Most

environmentalists blame the Industrial sector for the constant emissions of CO₂ into the atmosphere [38]. The energy and cement sectors, which rely heavily on fossil fuels, account for most CO₂ emissions [39].

2.2.1 Country-wise CO₂ Emissions

According to the latest survey, the top three countries for the most CO₂ emissions in the world are China, the United States of America, and India; see **Figure 2.1**. These countries are responsible for more than fifty percent of global emissions. The major culprit for this emission is the utilization of fossil fuels, mainly coal, for power production. According to the International Energy Agency (IEA) published report, China is leading in CO₂ emissions, followed by the United States of America (USA). However, it can be seen from **Figure 2.1** that China's and India's emissions are increasing. In contrast, the USA's and European Union's (EU) emissions have been reduced over the last two decades. It was also observed that during the year 2020 [40], global CO₂ emissions were dropping due to the pandemic; this trend was even observed for large emission countries like China and India; see **Figure 2.1** [40].

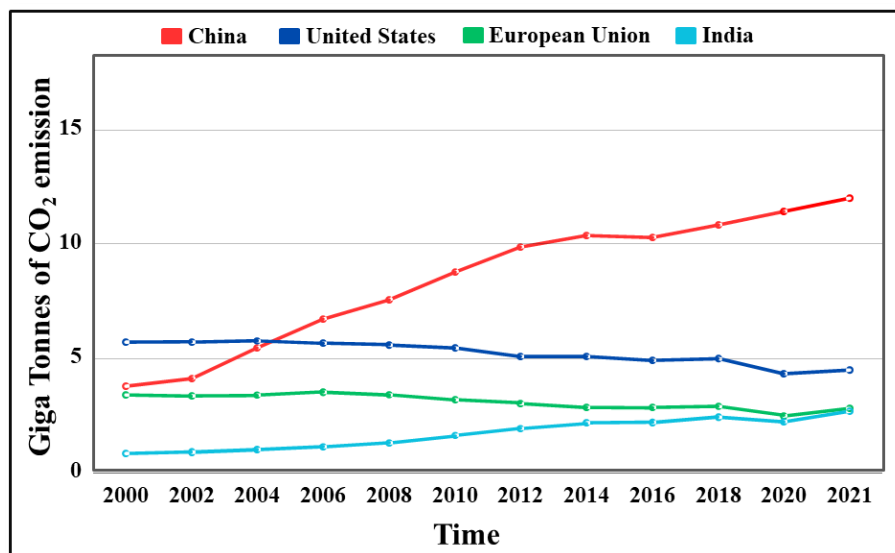


Figure 2.1: Illustration of country-wise CO₂ emissions of China, the European Union (EU), India, and the United States of America (USA) (adapted from IEA 2021 Report [40]).

Most of these emissions from developing and developed countries are from the energy production sector. Most of the high-emissions countries rely more on coal for energy production. The subsequent section illustrates the percentage of coal usage compared to other energy production technologies. It is challenging for high emission countries, especially developing countries, to reduce emissions without employing technologies like Carbon Capture Utilization and Sequestration (CCUS). The utilization of renewable energy sources alone proves insufficient to meet the energy requirements of developing nations; therefore, it is imperative for these countries to depend on conventional power plants and established technologies to fulfill their power demands while concurrently mitigating emissions adequately.[40].

2.2.2 Industry-wise CO₂ Emissions

Most of the industrial sector uses fossil fuels for power production. The countries rely mostly on coal for electricity production. According to the survey conducted, it was found that most of the coal utilization is in thermal power plants, followed by the metal industry, mainly the iron and steel industries, which uses the most coal and other fossil fuels after the thermal power plant. In the metal industry, fossil fuel is used in the boiler section for heat production [40].

Figure 2.2A illustrates the percentage of global energy production by utilizing coal and low-carbon technologies from the year 1971 [41]. For the past decade, low-carbon technologies have increased energy production, and it can also be observed that the reliance on coal has also decreased [41]. **Figure 2.2B** illustrates the utilization of various fossil fuels in the industrial sectors for various production processes. Compared to other fossil fuels, coal consumption is the most prevalent. Coal is primarily used in thermal power plants to generate electricity. After coal, oil and natural gas are the most commonly used fossil fuels in industrial sectors.

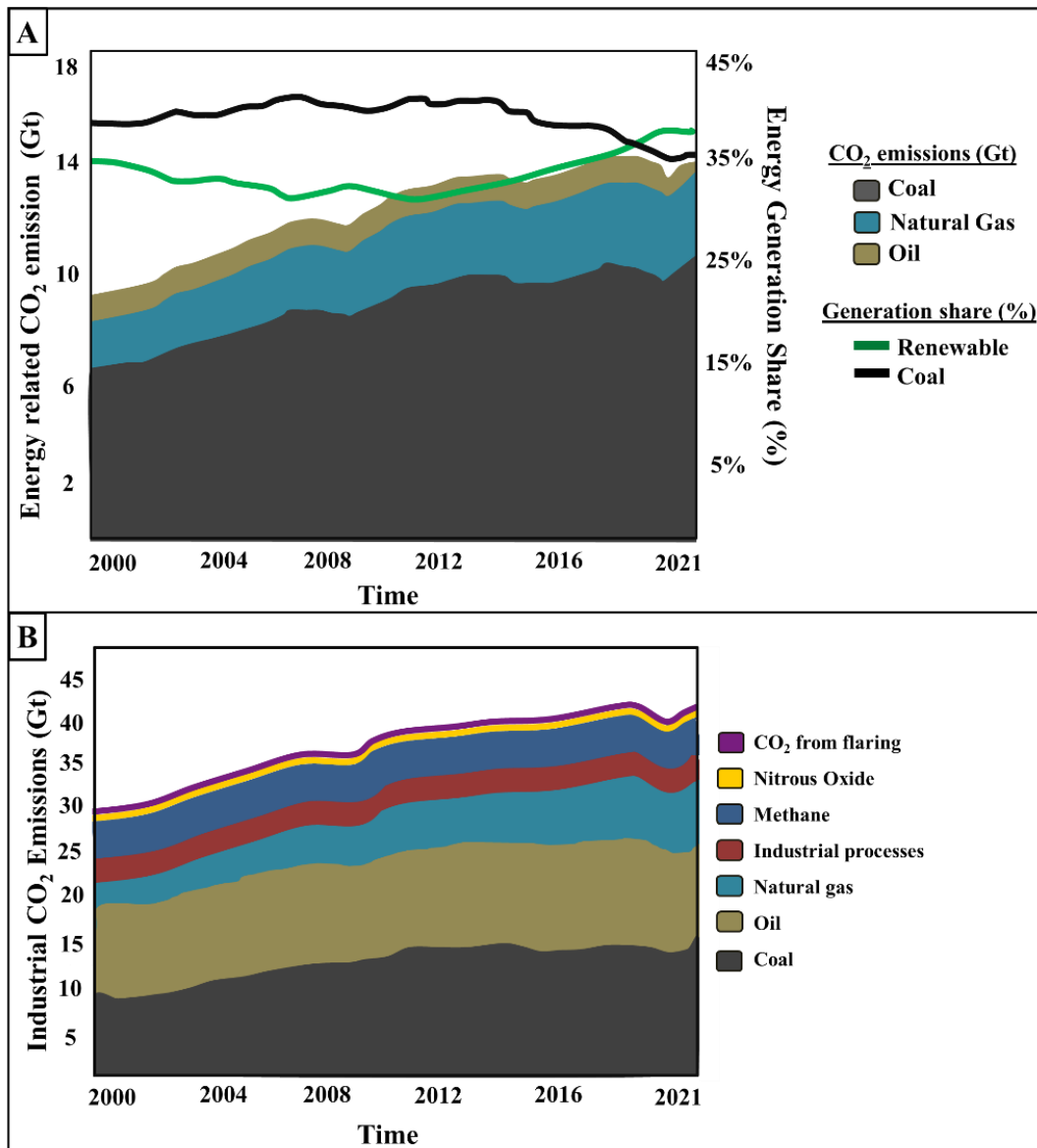


Figure 2.2: Illustration of (A) Percentage of coal usage and low-carbon technologies in energy production and (B) Usage of fossil fuels in the industrial sector and production of other essential products (adapted from IEA 2021 Report [40], [41]).

The hard-to-abate sectors like cement, chemical, iron, and steel industries are trying to adapt new technology for heat production by adapting hydrogen technology. Relying on hydrogen is essential for net-zero emissions. This will reduce the CO₂ emissions into the atmosphere and the reliance on fossil fuels like coal and petroleum. However, this technology is at a nascent stage, and deep research must be carried out for large-scale hydrogen production. Many

industrial and hard-to-abate sectors are looking towards other technologies to decarbonize power generation [41]. Carbon Capture Utilization and Sequestration (CCUS) technology stands as one of the dependable approaches to lower the CO₂ concentration in the Earth's atmosphere[35], [42].

2.3 Carbon Capture Utilization and Sequestration (CCUS)

2.3.1 Carbon Capture and Utilization

After CO₂ is captured from the emission source, mostly from thermal power plants and the metallurgical industry, it is converted into other valuable products using CO₂ utilization technologies. There are technologies like methanation, where the CO₂ is chemically converted into methane through hydrogenation. The production of hydrogen from natural gas, coupled with carbon capture utilization and storage, is denoted as "blue hydrogen," serving as a low-carbon substitute in the hydrogen production process. Utilizing hydrogen as a fuel in the metal industry can contribute to a decrease in fossil fuel consumption and CO₂ emissions. Biofuel production uses artificial photosynthesis, where CO₂ and water are converted into hydrocarbons and oxygen using artificial light or sunlight, and similarly, bioethanol production uses algae and captured CO₂. Recently, other technologies have been combined with Carbon Capture and Storage or Sequestration (CCS) to reduce CO₂ emissions. For example, BECCS (Bio-Energy with Carbon Capture and Storage), where biomass is used for energy production, and CO₂ is emitted from this production process, is captured and sequestered safely [43].

Carbon Capture and Utilization (CCU) is a technology where the captured CO₂ may be utilized as a raw material for many industries to process and manufacture value-added products and materials [44], [45]. CCU has the ability to partially reduce the CO₂ emission footprint from the majority of industrial sectors. Implementation of CCU in the industrial sectors can increase efficiency and reduce their dependence on the products and materials manufactured or

processed by non-renewable resources. This can build another industry sector and develop a market for carbon products [44], [45]. The following are common CO₂ utilization technologies illustrated in **Figure 2.3**.

Methane and methanol fuels are cleaner than traditionally available fossil fuels that are currently being used. The usage of both fuels ranges from domestic to industrial applications. Methane is used for the power generation section of the boiler in manufacturing plants, and in the coldest countries, methane is used for heating homes and cooking. In the industrial sector, methane is required in the chemical production of methanol, hydrogen, and various fertilizers. It is also observed to have a major use in the transportation sector as a fuel in the form of compressed and liquefied natural gas (CNG and LNG) [45], [46]. Methanol is the most versatile chemical for its utilization in chemical Industries. It is a potentially cleaner fuel because of its lower CO₂ emissions than traditional fuels like gasoline and diesel. In the chemical industrial sector, it is utilized as a raw material in the chemical production of dimethyl ether, acetic acid, and formaldehyde. It is also used as a solvent for many industrial processes [47].

The captured CO₂ can be used for the production of fuels like methane and methanol. CO₂ is used as an intermediate chemical in the carbon dioxide reduction process, where synthesis gas is produced. Employing a chemical process like the Sabatier reaction, methane can be produced from captured CO₂. Moreover, syngas may be produced from methanol during the carbon dioxide reduction process. The consumption of methane and methanol in the industrial process and recapturing of CO₂ will create a closed-loop carbon cycle [47], [48]. Nonetheless, still, CO₂ emission into the atmosphere is inevitable. Additionally, for each cycle, the CO₂ has to be captured. It is financially expensive and may require a high-power input [45]–[47].

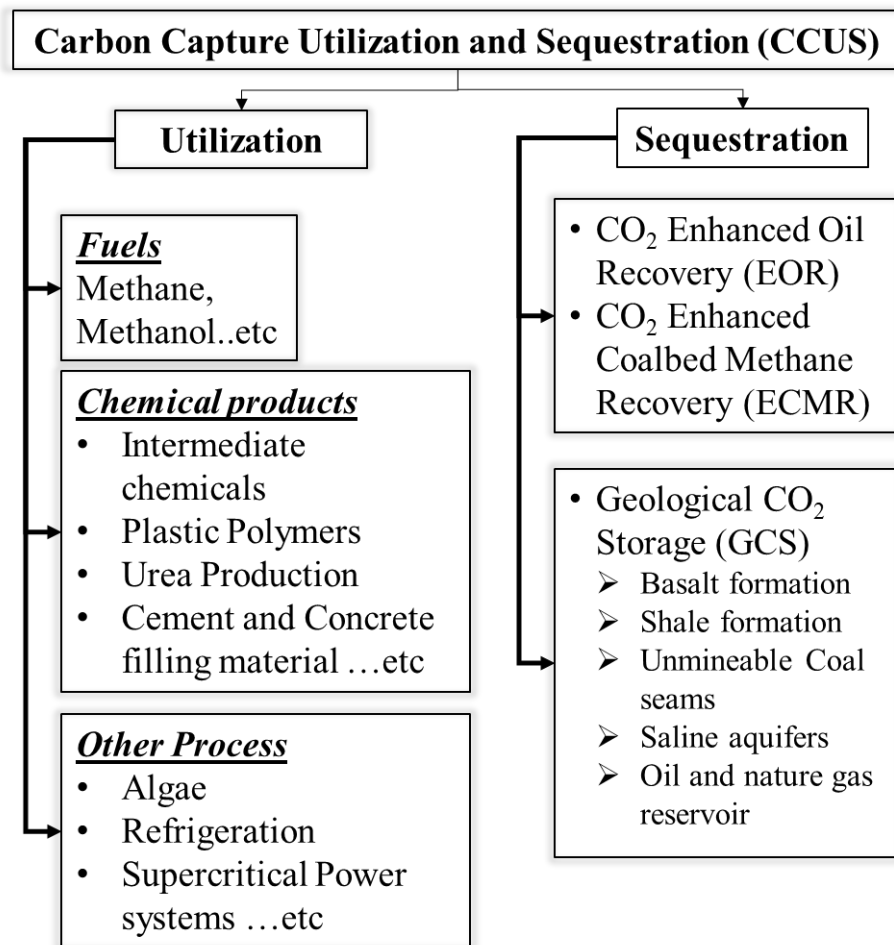


Figure 2.3: Illustrates a flow chart of Carbon Capture Utilization and Sequestration classification.

Only major categories are included in the flow chart.

In some technologies and chemical processes, the captured CO₂ can be used to produce intermediate chemicals that are essential feedstocks and building blocks for manufacturing and production industries. Products like plastic, rubber, resins, etc., are the final goods used in daily life, and their application ranges from household to industrial scale. For the past decade, rigorous research has been done on utilizing captured CO₂ in the manufacturing processes of these intermediate chemicals [45], [49]. Urea production is one such example of an intermediate chemical process that uses CO₂. In the urea manufacturing process, CO₂ reacts with ammonia to form ammonium carbamate, which is then hydrolyzed to generate urea.

Another example is the production of formic acid, a chemical that is utilized in several industrial processes. Through a series of chemical processes involving hydrogen, CO₂ may be converted into formic acid. CO₂ epoxides are used in polymer production by polymerization [45], [49]. In the hard-to-abate sector, Cement manufacturing contributes significantly to CO₂ emissions, accounting for approximately 7% of worldwide greenhouse gas emissions [45], [50]. The CO₂ captured from emission sources such as power plants, metal industries, etc., can be used as raw materials in the cement manufacturing process. In the cement manufacturing process, CO₂ combines with calcium and other minerals to generate solid carbonates, an important cement component. This technology has the potential to minimize CO₂ emissions related to cement manufacturing while also providing a means to store carbon dioxide in solid form [45], [50].

In the refrigeration industry, Chlorofluorocarbons (CFCs), Hydrochlorofluorocarbons (HCFCs), and Hydrofluorocarbons (HFCs) have traditionally been employed as refrigerants. Traditional refrigerants like CFCs have an enormous global warming potential and contribute significantly to greenhouse gas emissions, which contribute to climate change. There has been a considerable rise in interest in using natural refrigerants for refrigeration, such as carbon dioxide (CO₂). Compared to CFCs and HCFCs, CO₂ is a non-toxic, non-flammable, and easily accessible refrigerant with a low global warming potential. CO₂ is also well-suited for use in low- and medium-temperature refrigeration applications and has been used in commercial refrigeration systems for many years [51], [52].

A supercritical power system is a form of power generation technology in which supercritical carbon dioxide (ScCO₂) is used as the working fluid. Supercritical power systems operate at greater temperatures and pressures, increasing thermal efficiency and lowering fuel consumption [53]. Because of its advantages over conventional power plants, supercritical power systems are a viable technology for next-generation power plants.

2.3.2 Carbon Capture and Sequestration (CCS)

Sequestration technologies, such as Enhanced oil recovery (EOR) and Enhanced coalbed methane recovery (ECMR), extract residual oil from depleted oil reservoirs by utilizing chemicals and water. It involves injecting water, gas, or chemicals into the reservoir to increase oil recovery. Enhanced oil recovery can employ captured CO₂ to extract more oil from depleted reservoirs. Capturing industrial CO₂ and injecting it into an oil reservoir enhances oil recovery. The injected CO₂ acts as a solvent, reducing the viscosity of the oil and allowing it to flow more easily. The CO₂ is then stored in the reservoir, where it remains trapped underground, reducing the amount of CO₂ released into the atmosphere. Whereas in CO₂-enhanced coalbed methane recovery (CO₂-ECBM), CO₂ is injected into the coal seam as part of the CO₂-ECBM process in order to displace the coalbed methane and bring it to the surface [35].

CO₂ sequestration and utilization are two approaches for mitigating greenhouse gas emissions and mitigating the impacts of climate change. While both approaches have advantages and disadvantages, some key differences and advantages of CO₂ sequestration are described below.

2.3.2.1 Economic Advantages of CCS

Cost-effectiveness: CO₂ geological sequestration can be a cost-effective option for mitigating greenhouse gas emissions, especially when integrated with other technologies. The cost of injecting and storing CO₂ in subsurface geological formations is relatively low compared to the cost of other mitigation options, such as renewable energy or energy efficiency technologies [54].

Revenue generation: Due to the implementation of CCS technology, employment will mainly increase in the region. This leads to a positive economic impact. CCS technologies provide industries and the electricity sector with opportunities to reduce carbon emissions. Carbon capture and storage (CCS) technology can establish new industries to reduce carbon emissions

and global warming. There will be an increase in investment into CCS technology from other carbon emission companies to reduce carbon emissions and get subsidies from the carbon tax. This can lead to good economic activity among the companies [54]. In some cases, CO₂ geological sequestration can generate revenue by utilizing the captured CO₂ to be sequestered for use in enhanced oil recovery (EOR) operations, which can help offset the cost of CO₂ sequestration [54].

2.3.2.2 Financial benefits over other alternative technologies

Investment potential: CO₂ geological sequestration projects can attract both public and private sector investment, providing funding for developing and deploying the technology. According to the Intergovernmental Panel on Climate Change (IPCC) report, the action toward a clean climate may be more expensive, up to 138%, without considering the CCS technology [54]. The cost for CCS can be reduced as the plant scale of implementation increases and attends the commercial scale approach. Many of the cost-benefit analyses of CCS have stated that the medium and sizeable commercial-scale plant is the best fit in terms of financial aspects [54].

Long-term benefits: CO₂ geological sequestration provides a long-term solution for mitigating greenhouse gas emissions, which can attract investment from entities that prioritize long-term sustainability and mitigation of climate change [54].

2.3.2.3 Safety Assessment of CCS

Long-term impact: CO₂ geological sequestration has the potential to reduce greenhouse gas emissions for hundreds or thousands of years, making it a long-term solution for mitigating climate change. Indirectly, it will improve the health index of the population. This approach leads to positive vibrant in the establishment of a new organization in the country [54].

Safe storage: Geological formations have been safely storing natural CO₂ and other gases for millions of years, making them an appropriate and safe option for the storage of captured CO₂. CO₂ geological sequestration projects typically include monitoring and verification systems to ensure the safety and security of the stored CO₂ [10].

Large storage capacity: There is a large capacity for CO₂ storage in subsurface geological formations, making CO₂ geological sequestration a feasible option for mitigating large amounts of greenhouse gas emissions [10].

There is always a hindrance to any technology, and CCS technology is no exception. In order to inject the supercritical CO₂ into the domain, an injection grid must be built at the injection point [55]. The injection grid is equipped with monitoring units and seismic sensors to monitor and study the integrity of the reservoir domain after injection. The site's monitoring operations must be carried out for at least ten years for safety monitoring analysis. The cost for the construction of an injection grid and monitoring unit is high, and it would be a financial burden in the case of some commercial-scale unit operations. In sizeable commercial-scale operations, the price of injection per ton of CO₂ decreases as more storage resources are available [56], [57].

In carbon utilization, the captured CO₂ has been a feedstock or raw material for the manufacturing or production of value-added products. During the production of value-added products like methane, methanol, cement, etc., greenhouse gas is emitted, and the energy utilization and reliability of this process increase the CO₂ emissions into the atmosphere. This is the continuous close-loop carbon cycle. This way, the utilization and reliance on electricity will increase the burden on the energy sector, ultimately increasing the usage of fossil fuels. Moreover, the CCU techniques are still in the development phase. Integrating carbon capture

technology and handling storage of captured CO₂ will be more expensive in CCU than in CCS [45], [49].

2.3.2.4 Summary

Carbon Capture and Sequestration (CCS) is a viable technology that has the ability to decrease industrial CO₂ emissions into the atmosphere. There are three main types of sequestration: ocean sequestration, terrestrial sequestration, and geological sequestration. In ocean sequestration, the captured CO₂ will be injected into deep ocean floors. But it will increase the ocean's pH, further leading to ocean acidification. Whereas in terrestrial sequestration, the captured CO₂ is released in the terrestrial site. This technology has minimal capacity for CO₂ sequestration compared to other types of sequestration. The captured CO₂ is injected and stored in deep geological formations in geological sequestration. CO₂ is stored in various geological formations like basalt, unmineable coal seams, shale formations, oil and natural gas reservoirs, and saline aquifers [58], [59].

2.4 CO₂ Geological Sequestration (CGS)

In this technology, the CO₂ emitted into the atmosphere is captured and transported into the injection grid, where the CO₂ is injected into the geological subsurface formation domain for safe storage; see **Figure 2.4**. In CO₂ geological sequestration, the captured CO₂ is sequestered in the supercritical state. The purpose of injecting in a supercritical state is to increase the storage quantity of CO₂ with less volume [30]. The first commercial-scale CCS technology, famously known as the Sleipner project, was implemented in Norway [60], [61].

Once the CO₂ is injected into the geological domain, several trapping mechanisms confine the CO₂ within the geological formation and restrict it from escaping into the Earth's surface. The four major trapping mechanisms that occur in the formation domain are structural trapping, residual trapping, solubility trapping, and mineral trapping. The injection of CO₂ is generally

carried out at 800 m below the Earth's surface. In most cases, the CO₂ is injected in the supercritical phase, and in a few cases, CO₂ is injected after dissolution in water [30], [58], [62], [63].

The choice between injecting CO₂ in a supercritical phase or dissolving in water for CO₂ geological sequestration depends on various factors, including the geological characteristics of the storage formation, the availability of injection and storage infrastructure, and the specific project requirements. Both injection methods have their advantages and disadvantages, and a thorough evaluation of the storage formation and project constraints is necessary to determine the optimal injection strategy [4], [6], [64]–[69].

Supercritical CO₂ injection is preferred in cases where the storage formation has the capacity to retain supercritical CO₂ without any significant leakage, and the injection infrastructure and operational costs are feasible. Supercritical CO₂ has a high density and low viscosity, which enables it to fill the pore space of the storage formation efficiently. Moreover, the phase behavior of supercritical CO₂ is predictable, and it exhibits high diffusion rates, allowing for rapid dissolution and mineral carbonation reactions [4], [67]–[69].

On the other hand, injecting CO₂ dissolved in water, also known as a CO₂ aqueous solution, is preferred in cases where the storage formation has low permeability and can retain CO₂ only in the dissolved phase. CO₂ aqueous solution has a lower density than supercritical CO₂, making it less effective in filling the pore space. However, it can reduce the risk of buoyancy-driven CO₂ migration and ensure a more uniform CO₂ distribution within the storage formation. Moreover, the injection of CO₂ dissolved in water can facilitate the transport of CO₂ to reactive minerals in the storage formation, enhancing mineral carbonation reactions [6], [64]–[66].

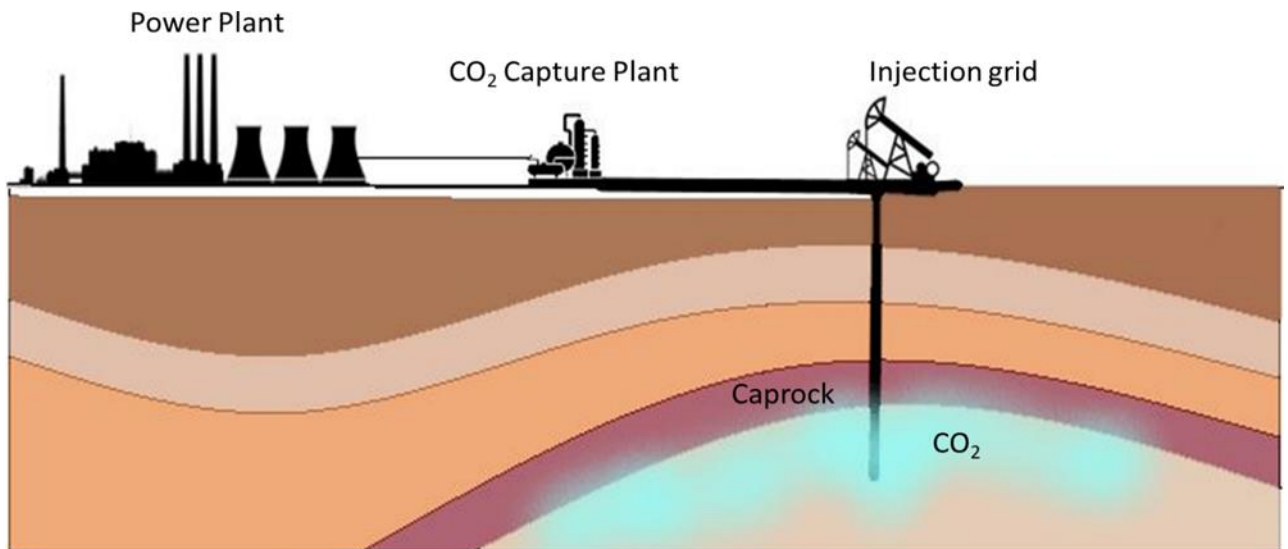


Figure 2.4: Schematic of Carbon Capture Storage (CCS), Illustrating the CO₂ capture point and geological injection grid.

2.5 Trapping Mechanisms

The captured CO₂ is converted into a supercritical state and injected into a selected geological formation as part of the geological sequestration process. After supercritical CO₂ (ScCO₂) injection, the formation zone experiences hydrodynamic and geochemical phenomena. Due to these phenomena, the majority of injected CO₂ is seized by various trapping mechanisms. They are structural, residual, solubility, and mineral trapping, as illustrated in **Figure 1.1**. These mechanisms cause the injected CO₂ to dissolve in the formation liquid and become permanently trapped in the geological subsurface region [30], [58], [62], [63], [70].

Most naturally formed formation layers have impermeable layers with associated geological features embedded within them. The geological features are often in the form of domes, and in general, these are referred to as anticline and syncline sequences in the geology terminology [63], [71], [72]. These perturbations of anticline and syncline are the primary factors that influence the migration and movement of the CO₂ plume in the subsurface region during the CO₂ geological sequestration process [63], [71], [72]. These sequences of geological features of the anticline and syncline of a geological domain function like a trap, restraining carbon

dioxide migration within the observable domain [73]–[75]. This way, structural trapping takes place in the subsurface geological domain. While migrating through porous media, some amount of CO₂ will get confined in the porous rock structure; this way, the residual trapping takes place. Solubility trapping takes place within a few days due to the dissolution of CO₂ into the resident reservoir liquid. Due to the availability of the minerals in the subsurface rock formation, geochemical reactions occur; this way, the mineral trapping occurs in the subsurface region [8], [76]–[78]. A detailed description and literature review of each trapping mechanism are given in the subsequent sub-sections.

2.5.1 Structural Trapping

After the injection of CO₂ in the geological formation, the CO₂ plume tends to move and percolate upwards due to the buoyancy effect until the impermeable layer, or caprock structure, restricts it. This phenomenon of CO₂ getting restricted or trapped under an impenetrable geological structure is known as a structural trapping mechanism. The quantity of CO₂ obstructed by the impermeable layer is categorized under structurally trapped CO₂ [30], [72], [79], [80]; see **Figure 1.1**.

The perturbations of anticline and syncline are the primary factors that influence the migration and movement of the CO₂ plume when the injected CO₂ has a tendency to migrate in a collateral direction with the top surface. These sequences of geological features of the anticline and syncline geological domain function like a trap, limiting carbon dioxide migration within the domain [73]–[75].

Hydrodynamic or structural trapping simulations can be utilized to estimate the quantity of CO₂ that can be safely confined in a formation. This is achieved through the simulation carried out on the synthetic geological three-dimensional grid domain of a realistic structure based on the available data. Through these simulations, the lateral spreading distance of injected CO₂ beneath caprock can be assessed. This lateral spreading assessment can be utilized to

calculate the stressed caprock region and will aid in identifying the crucial area of the caprock. The structural trapping simulation can also be used to determine the influence of caprock shape on trapping and the effectiveness or capacity of considered subsurface structures.

The fate of injected CO₂ during the structural and residual trapping phases determines the effectiveness of CCS [81]. It is crucial to comprehend the movement and distribution of CO₂ in its many forms for a particular geological formation. As more CO₂ is trapped in the rigid porous formation, a significantly higher amount of CO₂ will undergo solubility-trapping, resulting in an increase in the formation of carbonic acid, which in turn increases the mineral reaction and mineral trapping in the rock formation region [25], [58], [82].

Deep geological formations' in-situ pressures and temperatures are favorable for operating the geological sequestration process in the supercritical state. Because of the in-situ pressure and temperature of the subsurface formation domain, CO₂ injected at the deepest geological depth will remain supercritical [23]–[25]. The buoyancy force causes CO₂ as a plume to travel upwards when injected deep beneath geological formations. In this process, as injected CO₂ percolates through the subsurface formation layer, it encounters porous channels and traps [83], [84]. The traps are generated as a result of tectonic forces within the more conspicuous geological structure, which serves as a storage place or mini reservoir [85].

The subsurface caprock topography of the formation region is one of the crucial geological parameters that can impact the structural integrity and safe storage of sequestered CO₂ [25], [30], [86]. The study by H. Lee et al., [71] described the effect of anticline structure on the selection of injection rate for CO₂ sequestration. At a higher injection rate, it was noticed that the CO₂ plume is directed towards the anticline structure. In contrast, at a lower injection rate, it was observed that the CO₂ is immobilized in the migration pathway towards the anticline structure [30]. Prior research and analyses concentrated on the analysis of topographical parameters on the topography, explicitly pertaining to top-surface perturbations and

morphological structures that feature two distinct types of folds, namely asymmetrical and chevron folds. The influence of the folds on the top surface was observed with regard to their impact on structural entrapment and residual trapping [80]. Numerous academics and researchers have developed numerical tools to elucidate and explain the influences of various topographical surfaces on the geological sequestration of carbon dioxide [19], [74].

2.5.2 Residual Trapping

Due to the low density of injected CO₂ than the connate reservoir water, the CO₂ plume moves upwards and infiltrates the pore network structure. While percolating upwards, tiny droplets of CO₂ will get confined in the porous media migration pathway. This quantity of CO₂ is categorized under residual trapping; see **Figure 1.1** [30], [58], [80], [87]–[92].

The fate of injected CO₂ during structural and residual trapping phases determines the CGS's effectiveness [81]. It is crucial to comprehend the movement and distribution of CO₂ in its many forms for a particular geological formation. As more CO₂ is trapped in the rigid porous formation, a greater amount of CO₂ will undergo solubility trapping, resulting in an increase in the creation of carbonic acid, which in turn increases the mineral reaction and mineral trapping in the domain of the formation [25], [58], [82].

Most of the research on the residual trapping mechanism takes the aspect of CO₂ saturation to estimate the residual trapping efficiency in the geological domain [74], [93]–[95]. In most of the previous literature, the studies are mainly focused on studying the influence of parameters like pore aspect ratio [96], [97], rock type [88], capillary pressure [92], [98], [99], saturation [79], [83], interfacial tension forces [100], flow rate [101], [102], porosity [22], overburden pressure [89], [103], etc., on residual trapping mechanism. Most of this research was conducted using numerical simulations and experimentation by considering the smaller domain and controlled parameters [74], [104]. Most researchers employ experimental approaches, including core-flooding techniques and X-ray micro-tomography, to study the residual trapping

capacity at the lab scale [83], [89], [101], [105]. In the simulation approach, the residual CO₂ saturation in the geological domain and at the boundaries is considered to estimate the residual CO₂ percentage [75], [95].

Simulation analysis of the flow dynamics of the CO₂ plume along the migration pathway and the contact area of the CO₂ plume with water largely depends on domain heterogeneity, which determines the residual- and solubility trapping percentage [71]. A similar conclusion was reached by A. Raza et al., [106]; it was found that aquifer heterogeneity influences the injection rate selection [106]. Z. Rasheed et al., [107] investigated the degree of acceptable heterogeneity for conducting safe CO₂ sequestration using the petroleum Lorenz coefficient [107].

The effectiveness of the solubility trapping mechanism is primarily dependent on residual trapping. The greater the amount of CO₂ trapped by residual trapping, the greater the amount of CO₂ subjected to solubility trapping. If there is a greater amount of residual trapping, the caprock will have less burden. This is ensured due to the fact that the amount of CO₂ that is able to reach the caprock will decrease as the extent of force that is exerted by the CO₂ plume on the caprock. Most of the remaining trapping percentage is found in the formation domain with a narrower permeable range. A safe range of petrophysical data for injecting into the Indian geological domain can be evaluated by running the simulation for CO₂ sequestration [30], [80].

2.5.3 Solubility Trapping

The CO₂ trapped under structural features and confined in the migration pathway will dissolve in the resident water and undergo geochemical reactions. The CO₂ dissolved water gets denser and tends to move downwards, forcing the freshwater upwards, further interacting with the undissolved CO₂. The movement of denser CO₂ dissolved water moving downwards and freshwater moving upwards create fingering patterns, which are known as the solubility

fingering phenomena or simply fingering phenomena see **Figure 1.1** [63], [71], [91], [108]–[111].

In a numerical simulation performed by Khudaida & Das. [112] to study the influence of heterogeneity on CO₂ geological sequestration. It was noticed that most of the injected CO₂ is stored in the homogeneous domain through solubility trapping. The CO₂ plume moved in the lateral directions and spread efficiently, increasing the contact area with reservoir water and enhancing solubility trapping. In contrast to the homogeneous domain, the residual trapping percentage increases in the heterogeneous domain due to the restriction on the flow of CO₂ plume in the migration pathway [112].

In the past decade, researchers' investigations have focused on parametric analyses to determine the geological and sequestration characteristics that influence the solubility trapping efficiency of a domain. Y. Zapata et al., [113] performed simulation analysis to investigate the effects of heterogeneity caused by petrophysical characteristics and the uncertainty present in the subsurface region, such as lithofacies. During the sequestration phase, the horizontal permeability, porosity, and injection rate were observed to affect the lateral spreading of injected CO₂. The effect of petrophysical characteristics, irreducible water saturation, and capillary pressure on the solubility trapping was significant. Substantial amounts of CO₂ injected into the domain were under the category of free mobile [113]. The availability of the reservoir's water table also affects the efficiency of the solubility trapping [113].

According to the experimental investigation by M. K. Abba et al., [108], a higher water table promotes solubility trapping in the geological subsurface region. In the CO₂ sequestration process, the increase in solubility trapping would raise the overall trapping percentage. In addition, the author described solubility trapping as a secondary trapping process following structural and residual trapping. The solubility trapping efficiency can impact the long-term

security of CO₂ entrapment; if CO₂ dissolution increases, so will the percentage of CO₂ trapped by mineral trapping increase [108].

The solubility trapping simulation, by considering the Indian-origin geological petrophysical data of the Deccan Volcanic Province, can give an idea about the feasibility of implementation and establishment of Carbon Capture and Sequestration (CCS) in India. By doing this simulation, the trapping efficiency of the solubility trapping mechanism can be estimated. An adequate time for the solubility trapping can be known, which is vital for post-sequestration analysis.

2.5.4 Mineral Trapping

The injected CO₂, after undergoing solubility trapping, forms weak carbonate acids, and further reactions will decrease the pH of the domain. This decrease in the pH of the formation domain will trigger mineral reactions; see **Figure 1.1**. In this way, the deleterious CO₂ is permanently eliminated. The order of dissolution and precipitation of minerals in the domain depends on the minerals available in the surface formation domain [8], [77], [78], [114]–[118].

Numerous research has been performed to determine the parameters that influence the mineral trapping mechanism [8], [74], [113], [116], [119]–[124]. From the literature, it was determined that the reservoir temperature [74], reservoir pressure [74], the composition of the host rock, composition of reservoir water [74], pH in the subsurface region [74], water table, etc., had the most significant influence on mineral entrapment. The efficiency and effectiveness of mineral trapping mainly depend on the sequestration site and composition of mineral rock.

According to prior research, the mineral trapping period varies based on the availability of rock minerals [8], [74], [113], [116], [119]–[124]. Mineral trapping mechanisms typically activate after a few hundred years. However, in a few experiments on basalt formation rock, mineral reactions were observed within a few months of injections [8], [11], [66], [78], [117], [118],

[125]–[128]. Certain investigations also observed that the experimental and simulation results disagreed, indicating the complexity of numerical mineral trapping studies [118].

Deccan Basalt is a type of rock that originated in India due to the cooling and solidification of molten lava produced as a byproduct of a volcanic eruption that occurred approximately 65 million years ago. Almost 11 varieties of basalt rock formations are known in India, with new forms of basalt rock expected to be discovered. The core basalt formation in India is similar to the basalt formation in Iceland. The mineral groups Pyroxene, Plagioclase, and Olivine dominate the mineral composition of Deccan basalts [1], [64], [129].

Minerals such as Calcite, Dolomite, Aragonite, Magnesite, and Siderite are abundant in the Indian Deccan Traps formation. The basalt rock formation is mostly composed of divalent cations such as Ca^{2+} , Mg^{2+} , and Fe^{2+} , which aid in the formation of secondary minerals [66]. Mineral precipitation reactions occur when these divalent cations react with a bicarbonate solution, and minerals such as calcite, magnesite, and siderite are formed. These divalent cations occur as a result of the dissolution of ultramafic basaltic rocks rich in calcium, magnesium, and iron silicates prior to the injection of CO_2 into the formation area. These minerals form when CO_2 is injected back into the domain by interacting with CO_2 -saturated water or carbonic solutions. The hazardous injected CO_2 is thus permanently consumed from the region [3], [78], [118].

In basalt formation, secondary minerals are usually found in the rock's cavities, and these secondary minerals include amygdales, carbonates, aluminosilicates, and silica minerals. The Indian basalt rock formation is beneficial because around 25% of the mineral weight consists of calcium, magnesium, and iron oxides [78]. Basalt is an acceptable candidate for CO_2 sequestration due to the presence of these minerals. Compared to other sedimentary rocks, basalt rock may be more reactive to injected CO_2 [78].

The research by P. S. R. Prasad et al., [11] provides experimental observations regarding the likelihood of CO₂ sequestration in the Picritic basalt formation collected from the Igatpuri basalt formation in India. Three samples of Picritic basalt formation IGP-29, 36, and 40 have been gathered for experimentation analysis. In the control experiment, supercritical CO₂ is injected into a sealed container containing Picritic basalt. Throughout the experiment, 100 degrees Celsius and 60 bars of pressure are maintained [11]. After five months, a secondary carbonate was observed to be formed. The formation of this secondary carbonate is analyzed using Fourier Transform Infrared (FTIR) spectroscopy; the resulting characteristic is comparable to that of the Ankerite (Fe-carbonate) mineral, and a release of SiO₂ is observed from the three IGP-29,36,40 samples. In the experiment, it was also noticed that the reaction rate for the formation of secondary carbonates tends to rise when water is added [11].

Mineral Trapping provides a permanent solution for eradicating CO₂. The efficiency of the mineral trapping is essential for the CGS, and to determine the expected mineral entrapment, numerical simulation is necessary. By doing the simulation, one will know the crucial minerals for the reaction with carbonic acids. The dissolution and precipitation reactions change the porosity and permeability of the formation domain. So, the relative change in porosity and permeability data can be calculated by doing a simulation. This simulation on mineral trapping is much needed during the post-injection period.

2.5.5 Caprock Structural Integrity

In carbon dioxide (CO₂) geological sequestration, the caprock refers to a rock layer positioned above the CO₂ storage reservoir, serving as an impermeable barrier against the upward migration of CO₂ and other fluids [56], [57]. A caprock with high structural integrity is defined by several parameters, which encompass:

Thickness: An advantageous characteristic of an effective caprock is its substantial thickness. A thicker caprock layer provides a more formidable obstruction against CO₂ leakage, enhancing containment [57].

Porosity and Permeability: Desirable caprocks possess low porosity and permeability to impede the upward movement of CO₂ and other fluids, reinforcing containment within the reservoir [56].

Mechanical Strength: The mechanical strength of a caprock is crucial to withstand the pressure resulting from CO₂ injection and the burden of the overlying rocks. High mechanical strength ensures stability and integrity [130], [131].

Geochemical Stability: A caprock must exhibit geochemical stability to avoid any potential reactions or alterations that could compromise its integrity. This stability prevents degradation over time, ensuring the long-term containment of CO₂. A chemically stable caprock, resistant to interactions with CO₂ or other fluids, is preferred to prevent dissolution and weakening [4], [7], [62].

Geomechanical Properties: Geomechanical properties, such as stress state, brittleness, and fracture density, impact the mechanical stability and long-term integrity of the caprock.

Fracture Density: A caprock characterized by low fracture density is desirable, as it minimizes pathways for CO₂ migration. Fewer fractures reduce the risk of leakage and improve the effectiveness of CO₂ containment [130], [131].

Geological and Lithological Characteristics: The geological and lithological properties, including rock type and mineral composition, play a role in a caprock's structural integrity. Some rock types, such as dense and massive formations (like basalt or shale), exhibit a higher structural integrity. However, susceptibility to dissolution or alteration in the presence of CO₂ must also be considered [4], [57], [62].

These parameters collectively contribute to the high structural integrity of a caprock, serving as a reliable seal for the CO₂ storage reservoir and minimizing the potential for CO₂ leakage into the surrounding formations or the atmosphere. It is important to note that specific parameters and characteristics of a caprock can vary based on geological context and project requirements [4], [7], [57], [62], [130], [131]. Geotechnical investigations and laboratory testing are typically conducted to evaluate and characterize the caprock's properties for a particular site or project.

2.5.6 Worldwide CGS Projects

The CGS is one of the prominent technologies that is gaining interest among various research and government institutions because of its ability to reduce CO₂ emissions into the atmosphere. Over two dozen CGS plants are currently operating worldwide, ranging from small pilot projects to industrial scale. The crucial part of selecting any region for the CGS establishment depends on the subsurface geological characteristics. Some known subsurface geological storage options are mature natural gas and oil reservoirs, uneconomic organic shale coalbeds rich in oil and gas, deep aquifers, saline caverns, and flooded Basalt formations.

As of 2021, there are 65 commercial-scale CGS projects worldwide; among these, 26 projects are currently under active status. The remaining projects are in various stages, from approval to construction. Furthermore, 34 pilot-scale projects were operational till 2020 [87], [132]; some important projects are illustrated in **Table 2-1**. The current capacity for all the CGS projects is approximately 40 million tons, and the world emissions are nearly 38 billion tons [132].

The Bio-Energy Carbon Capture and Storage facility was commencing in the United Kingdom. This facility is integrated with Drax Power Station. The Drax Power Station has undergone specific changes in power production. The power station will start relying on biomass, moving away from a traditional coal fire. Under this modification, the power station will be equipped

with a BECCS grid [133]. Moreover, it is estimated that around 4 million tons will be captured and stored annually in the North Sea, and this project is expected to commence operation in 2030 [132], [133].

Santos Limited, an energy company in Australia, is constructing a CCS plant in the Moomba gas plant. It is expected to have about 1.7 million tons of capture and geological storage capacity annually [132]. A USA-based Enchant Energy in New Mexico has established integrated CCS and EOR projects. The CO₂ will be captured from the Sa Juan power station and sequestered in the Permian Basin. The estimated capacity is around 6 million tons per year [132]. Colorado-based cement company Lafarge Holcim is partnered with the other enterprises Svante, Oxy Low Carbon Venture, and Total. It has a capacity of 0.7 million tons per year [132].

Table 2-1: Notable CCS projects worldwide for CO₂ geological storage. The asterisk next to the year indicates that the information is current as of that year [134].

Name of site location	Country	Year of Operations	Storage Unit Type	Storage Capacity
<i>Sleipner</i>	Norway	1996-2019*	Saline aquifer	0.9 Mt per year
<i>Weyburn-Midale</i>	Canada	2000-2019*	Oil and gas reservoir	3000-5000 tons per day
<i>Frio Brine Pilot Project</i>	Texas, USA	2004-2006	Saline aquifer	1850 tons in total injected
<i>In Salah</i>	Algeria	2004-2011	Oil and gas reservoir	4000 tons per day
<i>Zama</i>	Canada	2006-2019*	Oil and gas reservoir	13 Mt per year
<i>Snøhvit</i>	Norway	2007-2019*	Saline aquifer	0.7 Mt per year
<i>Otway Basin</i>	Australia	2008-2019*	Oil and gas reservoir	65445 tons per year
<i>Ketzin</i>	Germany	2008-2009	Saline aquifer	67000 tons is the total injected
<i>Cranfield</i>	Mississippi, USA	2009-2019*	Oil and gas reservoir	1.5 Mt per year of CO ₂
<i>Ordos</i>	Inner Mongolia, China	2010-2019*	Saline aquifer	3.6 Mt of CO ₂ per year
<i>Citronelle</i>	Alabama, USA	2011-2019*	Saline aquifer	Average of 0.2 Mt per year
<i>Decatur</i>	Illinois, USA	2011-2019*	Saline aquifer	1100 tons per day
<i>Northern Reef Trend</i>	Michigan, USA	2013-2019*	Oil and gas reservoir	Total injection restricted to 1 Mt
<i>Port Arthur</i>	Texas, USA	2013-2019*	Oil and gas reservoir	220000 Tons of CO ₂ are injected
<i>Boundary Dam</i>	Saskatchewan, Canada	2014-2019*	Saline aquifer	Average of 1 Mt per year
<i>Alberta Carbon Trunk Line</i>	Alberta, Canada	2018-2019*	Oil and gas reservoir	14 Mt of CO ₂ per year
<i>CarbFix, Iceland</i>	Hellisheidi, Iceland	2012-2019*	Basalt	12,000 tons of CO ₂ per year
<i>Wallula Basalt Pilot</i>	Washington State, USA	2010-2015	Basalt	1,000 tons is the total injected

Among the CO₂ storage sites, the Sleipner project is the most famous. It was established in 1996, and it is still active. It might be the first commercial-scale operating plant among the Scandinavian countries. It is operated by Statoil offshore in Norway. The initiative for this project was to overcome the carbon tax that the Norwegian government has imposed to reduce carbon emissions. The CO₂ is sequestered into the Utsira saline formation, which is about 200-250 m thick and at a depth of 800 m. This site is still active for sequestration [60], [135], [136]. The Snøhvit site has also started because of the effects of Norway's carbon tax exemption. It was built and operated by Statoil and allied partners of Statoil. Unlike the Sleipner site, the Snøhvit site doesn't utilize an offshore grid for CO₂ sequestration. The CO₂ is pumped from the onshore grid to the offshore site through the pipeline. It is estimated that 0.7 Mt of CO₂ is injected per year. The CO₂ is injected into the Snøhvit aquifer [130], [137]. Weyburn–Midale is probably the world's largest site for the CCS-EOR in Canada. It started its operation around 2000, and in this project, the captured CO₂ is used for the reservoir's Enhanced Oil Recovery (EOR). The capacity of the injection is between 3000 and 5000 tonnes per day. Initially, it was operated by Cenovus Energy; later, the Petroleum Technology Research Centre (PTRC) was allotted for safe operation after an allegation of leakage in 2011. The EOR is carried out in two subsurface beds known as vuggy and marly beds [138], [139]. The Zama project is also a Canadian project that started its operations in 2006. In this specific project, CO₂ with H₂S is injected into the formation domain. This reduces the cost of the separation of CO₂ and H₂S; it was planned to sequester both at the time. It is operated by the Plains CO₂ Reduction Partnership and Apache Canada. The injection mixture contains 70% CO₂ and 30% H₂S. Approximately 1.3 Mt of CO₂ and about 0.5 Mt of H₂S are estimated to be injected into the domain [140], [141]. The Boundary Dam project, located in Saskatchewan, Canada, has been operational since 2014. It is one of the first commercial-scale plants where the carbon is extracted and captured from the post-combustion process; SaskPower operates the project. The

major source of carbon comes from the Weyburn field plant. The CO₂ is injected about 3.4 km deep from the surface of the Earth in the brine-rich sandstone formation [138]. The Alberta Carbon Truck Line project, located in Alberta, Canada, is another Canadian CCS plant that has been operational since 2018. This CCS project is in virtue of surpassing the Weyburn-Midale site as the world's largest site for the CCS. The Alberta site was commissioned at the year 2018. It is estimated to have an injection capacity of about 14 Mt CO₂ per year. It is operated by Enhance Energy Inc. [134], [142].

Frio Brine is a pilot project in Texas, USA, operated under the guidance of the Texas Bureau of Economic Geology. In 2004, 1600 tonnes of CO₂ were injected at a depth of 1500 m; later, in 2006, an additional 250 tonnes of CO₂ were injected at a depth of 1600 m [143]. This site is used for scientific research purposes [143]. The Cranfield site, located in Mississippi, USA, is operated by the Southeast Regional Carbon Sequestration Partnership (SECARB) and other government organizations of the USA. It has reached the milestone of injecting 3 Mt of CO₂ in the Tuscaloosa formation at a depth of 3000 m [144]–[146]. Another American CCS project in Alabama, USA, is the Citronelle project. This project is also operating under SECARB. The Citronelle project has two operational formations in the subsurface region: Paluxy formation, which is held at a depth of 335 m, and another saline aquifer at a depth of 3000-3400 m; the source of carbon is obtained from the Barry power station [147], [148]. The Decatur storage is the scientific research site for CCS, operated by Archer Daniels Midland, the Midwest Geological Sequestration Consortium, and Richland County College, located in Illinois, USA. The sequestration is done in the Mount Simon sandstone formation. This formation is integrated with the Eau Claire shale. This research will help study the integrated wells with CO₂ storage capabilities over the years [134], [149]. The Port Arthur project is a commercial project located in Texas. This project has one of the operational structures where the distances between the source and sink are very high. It has been functioning since around 2013. It is

operated and maintained by Air Products & Chemicals Inc, Denbury Onshore Inc, Bureau of Economic Geology at the University of Texas at Austin, and Valero Energy Corporation. The source of CO₂ is obtained from the methane reformation plant operated by the Valero refinery. The carbon is injected in the EOR site at Oyster Bayou and the west hasting oilfield, which is 120 km from the source site. It is estimated that more than 220000 Tonnes of CO₂ is injected into the formation [134], [150]. The Northern Reef Trend is a research project operated by Midwest Regional Carbon Sequestration Partnership (MRCSP), DTE Energy, and allies located in Michigan, USA. The project started operations in 2013, with its life span expected to be 3-5 years till 2018. It has injected 1 Mt of CO₂ into the subsurface reservoir [134], [151]. The Salah project in Algeria is operated by British Petroleum (BP) and Statoil. The CO₂ that is obtained from the separation process of the produced natural gas is injected back into the Carboniferous Krechba sandstone formation at a depth of 1900 meters of the depleted gas field of the Salah project. The Sequestration capacity is almost 4000 tonnes of CO₂ per day. Approximately 4 Mt of CO₂ has been injected into the formation site until its decommissioning [102], [152], [153]. Due to the dread of well integrity of CO₂ storage, the site was terminated for CO₂ sequestration in 2011 [102], [152], [153].

Otway Basin is the pilot project operated by the Cooperative Research Centre for Greenhouse Gas Technologies (CO₂CRC) under the observance of the Australian Government. It is located on the southern coast of Australia and started operations in 2008 [154]–[156]. This project might be the largest onshore project in the world. This project aims to conduct adequate research on CCS technology and study the impact of acceptance on the public. The sequestration is conducted at the Waarre Formation; the reservoir is a depleted gas reservoir [154]–[156].

The Ketzin partners and the German Research Centre for Geosciences in Germany started the Ketzin project. This site was operational from 2008-2009 for one year as a pilot project for

research purposes. It is the first on-shore project in the European Union. The CO₂ is sequestered into the saline sandstone aquifer, which is 630 m below the surface. About 67000 tonnes of CO₂ was injected into the formation domain in one year. The source of the CO₂ for injection is obtained from Schwarze Pumpe Power Station. The project is implemented to study the aftermath economics for site maintenance and post-sequestration monitoring for risk analysis [149], [157]. Ordos project is located in Inner Mongolia, China. First, it was established as a pilot-scale project in 2010 and was later upscaled to a full-scale project. It is operated by China's largest coal company, Shenhua Group. This project started in the spirit of reducing CO₂ emissions. To date, it is estimated that about 150000 tonnes of CO₂ were injected into the geological subsurface [158], [159]

2.6 Potentiality of CGS in India

India is a developing nation that is aiming to reach its goal of self-reliance and self-sufficiency and build the one-place hub for manufacturing world supplies. During the pandemic of 2019-2021, most countries relied on a single country to manufacture products and felt vulnerable. Hence, most countries chose or looked towards highly skilled and cost-effective manufacturing countries like Vietnam and India. Many companies enhanced their investments in India in the fiscal year 2020-2021. In the year 2022, it was observed that the surge of coal production was increased by 12 % for power production [10], [39], [160]. This scenario points to relying on the thermal power sector for power production and the increase of demand in India due to the new establishments for the manufacturing sector. [10], [39], [160].

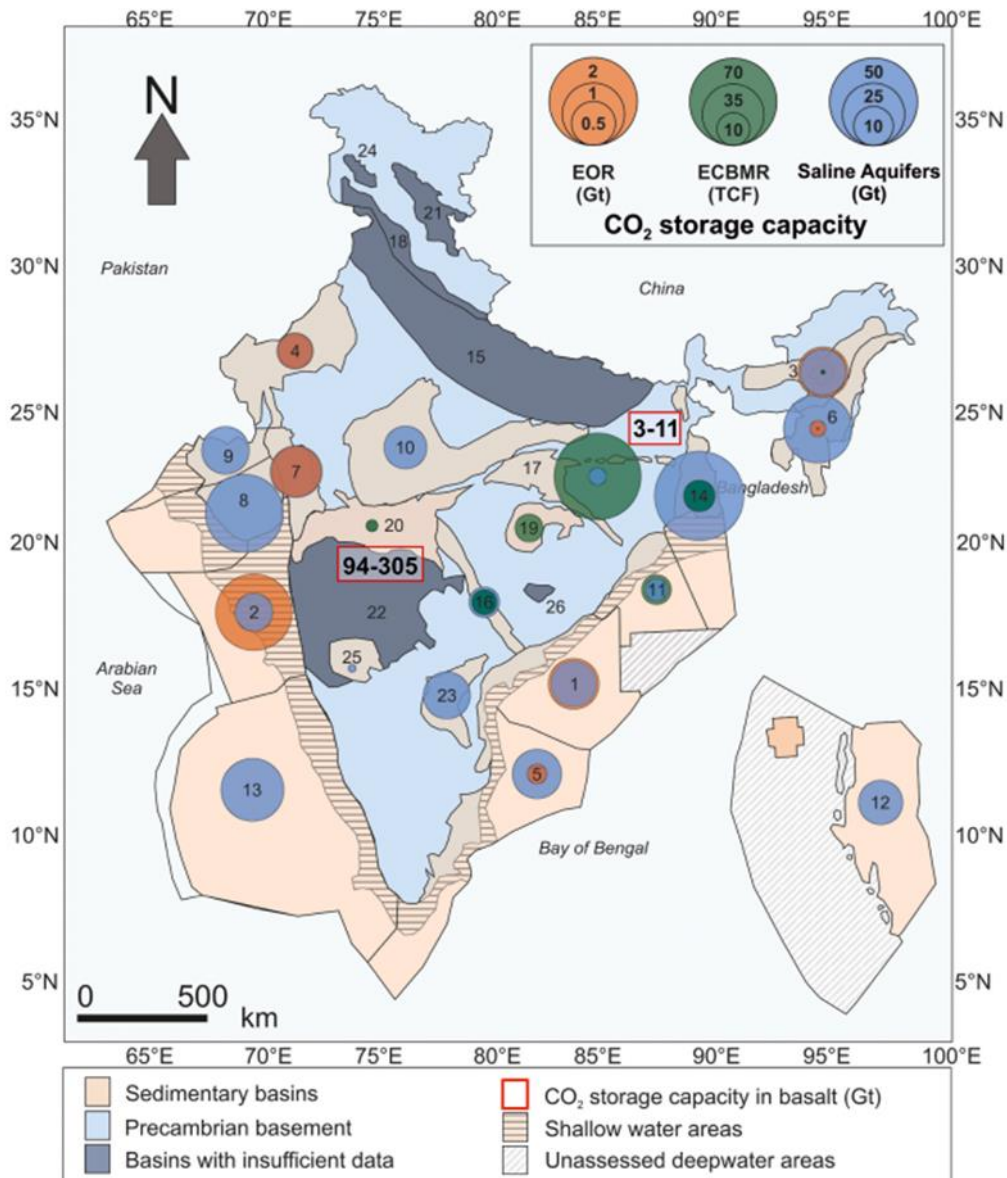


Figure 2.5: Notable locations across India where carbon may be stored [161].

Meeting the Paris Climate Agreement targets while simultaneously accommodating the rising power demand in India poses a significant challenge. The Indian government has the option to rely on CCS technologies for the reduction of CO₂ in the atmosphere. Most Indian researchers aim to develop Carbon Capture and Utilization technologies, where the captured CO₂ can be utilized to produce value-added products. **Figure 2.5** illustrates India's possible sequestration sites with their approximate storage capacity [161]. As the development of reliable and cost-effective CCUS technology is still in the emerging stage, the Indian government has to look

towards other alternative options [10], [39], [162], [163]. As per a survey conducted by R.V. Kapila et al., [39], [164], the top priority of the Indian government is nuclear power plants and solar energy development projects. Alternative technologies for reducing CO₂ emissions are the third priority of the Indian government. However, the Indian government is rolling out specific research projects through its research organizations, where the topics are directed towards developing CCUS technologies with industrial integration [39], [164].

P. Jain et al., [165] researched the source and sink for CO₂ emission in Eastern India. The author has found three geological sites in eastern India for the geological sequestration that is Talcher Coalfield, IB River Coalfield, and Krishna-Godavari basin [165]. The research by A. Shukla et al., [126] addresses the potential CO₂ sequestration on the Indian Peninsula. The author explains CO₂ sequestration in the Cretaceous volcanic zone in this research. The Deccan Volcanic Province represents a minor portion of the Cretaceous area. The Deccan and Cretaceous regions possess essentially identical petrophysical characteristics. This area of the Cretaceous is generated by volcanic eruptions. Rajeshwari field (Barmer), Ingoli and Padhra fields (Cambay), and Razol formation in the KG basin are Cretaceous locations where CO₂ sequestration and hydrocarbon development are possible. For identifying hydrocarbons in the subsurface, techniques such as Pre-stacking and Depth Migration (PSDM) and Pre-stacking and Time Migration (PSTM) are utilized, and CO₂ sequestration can be employed for exploration [126].

Author R. Chatterjee [166] and others did a geological assessment and concluded that the Jharia coalfield in India was the best location for CO₂ sequestration. There is a lot of methane in this coalfield. CO₂ is released into the atmosphere during the extraction of methane from coal. Enhanced CBM Recovery is the name given to this method (Enhanced Coal Bed Methane Recovery). Coal from the Jharia coalfield has a high concentration of vitrinite macerals, which makes it a good candidate for Enhanced Coal Bed Methane Recovery [166].

Research on the Indian geological formations suitable for CO₂ geological storage is currently limited, with little progress made in the field of geological sequestration. This can be attributed to the scarcity of adequate geological data regarding the aquifer and suitable formation domains, which represent a significant challenge to the advancement of this technology. Even in the available data, uncertainty arises on important parameters like thickness, rock density, petrophysical properties, surface layer fracture network, etc. These parameters play a crucial role in the safe storage of CO₂ for an extensive period of time without any implications on the structural integrity of the formation layer. The current study primarily focuses on CO₂ geological sequestration in the Deccan Volcanic Province, where Basalt rock is predominant.

2.6.1 Basalt Geological Formations

Basalt formation is considered a good sink for the captured CO₂. It can be confirmed by observing two pilot-scale CCS projects on the Basalt formations. BigSky partnership CCS project and CarbFix Iceland projects are pilot-scale projects established considering the continental flooded basalt as a CO₂ sink. The BigSky partnership CCS project is under the observation of the Department of Energy of the United States, located in Southern Washington. The US's first CCS project considered continental flooded basalt as a carbon sink. The injection bore drill was initiated in 2009, and the drill was of a precise depth of 1253 meters [2], [5], [6], [11]. The interflow zones of the subsurface basalt formation layers are considered the sequestration region. The CarbFix project is another project situated in Hellisheiði, Iceland. In this project, rather than injecting CO₂ in the supercritical state, the CO₂ dissolved water is injected into the geological domain. This way, the concern of CO₂ leakage can be eliminated [2], [5], [6], [11].

These basalt formations are formed due to sequences of volcanic eruption and cooling of lava. In basalt, depending on the cooling rate and release of gases during the cooling period during

a volcanic eruption, different types of basalt formations are formed. The Basalt, which contains vesicles, is ideal for the CCS. However, there is still uncertainty concerning petrophysical properties and subsurface fracture networks. The Columbia River basalt is estimated to have a carbon sink capacity of 10 to 50 GT [2], [5], [6], [11]. Many researchers and geologists believe that the subsurface basalt deposits are still to be explored. The basalt formations are available both onshore and offshore; the offshore basalt formation has additional security features with the presence of ocean water as a blank layer if sequestered CO₂ escapes from the surface region. The availability of reactivity based on the mineral compositions of basalt can be advantageous. Mineral trapping generally takes hundreds of years to take place, but in some research studies, it was found that the injected CO₂ reacts with mineral rocks within 100 years. This ability of mineral reactivity can be advantageous as it will permanently eradicate the harmful CO₂ in the domain [2], [5], [6], [11].

2.6.2 Deccan Volcanic Province

The Deccan Plateau, a vast elevated region in India, spans over 1.9 million square kilometers. Positioned between the Western and Eastern Ghats, the plateau is characterized by its higher elevation compared to surrounding coastal plains. The Godavari and Krishna rivers, among others, traverse this expanse, contributing to its hydrology. The Deccan Plateau does not have a distinct maritime boundary, but it transitions into coastal areas such as the Konkan coast along the Arabian Sea and the Coromandel Coast along the Bay of Bengal. This geographical concept encompasses both land and the adjacent coastal regions, forming a significant part of India's central and southern landscape [167]–[170]. Notably, the Deccan region is renowned for the Deccan Traps, a vast volcanic plateau formed by extensive lava flows. The Deccan Traps cover a substantial part of the plateau in the states of Maharashtra, Gujarat, Madhya Pradesh, Karnataka, and Telangana. They represent a significant geological feature in the

region's history. This geological phenomenon is a crucial aspect of the Deccan Plateau's landscape, adding to its complexity and historical significance [161], [171], [172].

As illustrated in **Figure 2.5** and **Figure 1.2**, it can be observed that India has very good potential for the implementation of the CCS project. **Figure 1.2** shows that in the Western Ghats region of India, a good portion is highlighted for the possible sink for the capture of CO₂. This region is called the Deccan Volcanic Province; the basalt layers are found in the subsurface region. This Basalt formation is mainly observed in the Deccan Traps, which are spread around 5,00,000 km² [3], [173]. Basalt rocks are good for mineral trapping because they are highly reactive and contain high concentrations of calcium and magnesium ions that chemically react with CO₂ to form stable carbonate minerals. Basaltic rocks are often fractured and porous, containing storage space for the mineralized CO₂. Basalts contain high concentrations of calcium and magnesium ions that chemically react with CO₂ to make calcite, dolomite, and magnesite. The presence of these chemical species will increase the mineral reactions, which accounts for mineral trapping. Basalt exhibits promising potential as a viable carbon sink site in India, owing to its capacity for secure subsurface geological storage and injection of CO₂ relative to other available options [2], [5], [177], [8], [10], [11], [32], [164], [174]–[176].

Some researchers have carried out a study on the Basalt obtained from different places in the Deccan Volcanic Province. Experiments involving CO₂ sequestration in the Picritic basalt formation from the Igatpuri basalt formation, India, were described in a report published by P. S. R. Prasad et al., [8], [11]. Three samples of Picritic basalt formation IGP-29, 36, and 40 have been gathered for experimental testing. The experiment is conducted at a temperature of 100 °C and a pressure of 60 bar [8], [11]. The Picritic basalt is placed in a sealed reactor, and supercritical CO₂ is injected in a controlled manner. After five months, a secondary carbonate has formed. A release of SiO₂ from the three samples of IGP-29,36,40 is noticed using Fourier-transformed infrared spectroscopy (FTIR), similar to the Ankerite (Fe-carbonate) mineral's

characteristic. When water was added to the experiment, it was found that the reaction rate for secondary carbonates would increase [8], [11].

In the research conducted by O.P. Pandey et al., [31], the author expresses support for the concept that Deccan Volcanic Province is an excellent location for CO₂ sequestration. The author used Killari bore (KLR-1) as an illustration. The bore well was drilled up to 617 meters from the Earth's surface. Alternate structured layers of massive basalt and vesicular basalt (amygdaloidal basalt) were seen in this exploration. This is moulded due to successive volcanic eruptions and rapid cooling of the lava that occurred 65 million ago [3], [173]. These emerging phenomena from the volcanic eruption led to the formation of Basalt rock layers. The Mesozoic volcanic layer is succeeded by a layer of Mesozoic sediments in successive Basalt layers. According to the author, the sequestration of CO₂ in Mesozoic sediments is optimal because of the massive and vesicular basalt on top and the Mesozoic volcanic strata at the bottom [31].

2.7 Numerical Study of Reactive Transport Modelling (RTM)

Reactive transport modeling is essential for evaluating the feasibility of CO₂ geological sequestration to mitigate greenhouse gas emissions. Reactive transport modeling is a computational approach to simulate the interactions between fluid flow, mass transport, and chemical reactions in porous media. In the context of CO₂ geological sequestration, it is used to understand the behavior of CO₂ as it is injected into deep geological formations. The objective is to assess the fate of the CO₂, including its migration and chemical reactions with the surrounding rock and fluid, to predict the long-term storage stability of the CO₂. Reactive transport models are based on mathematical equations that describe the relevant physical and chemical processes and are solved using numerical methods. The models can assess the potential storage capacity of various geological formations and identify the most suitable sites for CO₂ storage. Additionally, reactive transport models can help predict the performance of

CO₂ storage projects over time and identify potential challenges or issues that may arise in the future [14].

Modeling of reactive transport can also aid in understanding the intricate interactions between the injected CO₂ and the subsurface environment. The models can provide intuition on the possible concerns connected with CO₂ storage, such as the chance of leakage and the likelihood of chemical reactions (that could affect CO₂'s stability during storage). By modeling the behavior of CO₂ in the subsurface, reactive transport models may also be used to improve CO₂ injection tactics and develop and evaluate monitoring programs for long-term CO₂ storage [14], [16], [18], [178], [179]. Following is a glimpse of the associated benefits of utilizing reactive transport modeling for evaluating CO₂ geological sequestration study:

Understanding the complex process: Reactive transport models can give a complete understanding of the complex interactions between fluid flow, mass transport, and chemical reactions in the subsurface, hence aiding in the prediction of CO₂'s behavior in the subsurface over time [14].

Critical implementation study: Reactive transport models may be used to examine various CO₂ injection scenarios and optimize CO₂ storage project design and execution. Typically, the investigations entail comparing the findings of reactive transport simulations to field data or laboratory investigations and assessing the model's ability to represent essential physical and chemical processes. These studies ensure that the results of reactive transport simulations may be used to guide the design and execution of CO₂ storage projects, as well as to anticipate the long-term performance of these projects over time by evaluating the reliability and dependability of the models [14], [16], [18], [22], [178], [179].

Long-term evaluation: Reactive transport models may be used to evaluate the long-term stability of CO₂ storage and to identify possible dangers, such as leakage or chemical reactions, that could affect the storage stability of CO₂ [14], [16], [18], [22], [178], [179].

Predictive monitoring: Reactive transport models may be used to build and evaluate monitoring strategies for the long-term assessment of CO₂ storage and identify the most crucial parameters to monitor to assess the effectiveness of CO₂ storage projects over time [14], [16], [18], [22], [178], [179].

Cost-effectiveness: Reactive transport models may assist in reducing the costs of CO₂ storage by improving injection tactics, minimizing the need for costly field experiments, and giving a complete knowledge of the subsurface environment to influence project design and execution [14], [16], [18], [22], [178], [179].

Overall, reactive transport modeling is essential for comprehending and controlling the risks associated with CO₂ geological sequestration and assuring its safe and successful application as a climate change mitigation technique. Various geological and sequestration characteristics can be evaluated using reactive transport modeling before practical implementation with a low financial expense.

2.8 Geological and Sequestration parametric studies

The trapping mechanisms are affected by various geological and sequestration parameters during various stages. Numerous research has been carried out by performing experimental and numerical simulations to explore the dependence of these parameters on the trapping mechanisms. Despite this large quantity of research and assessments on various geological subsurface formations, some research gaps still exist in the assessments regarding the implementation of CCS. Following are some of the literature and research studies that are carried out on various geological and sequestration parameters

Various geological and sequestration characteristic parameters influence trapping mechanism efficiency during the CO₂ geological sequestration process. The parameters such as petrophysical heterogeneity, well injection configuration, wettability, salinity, top subsurface perturbation, etc., are some of the crucial characteristic parameters that can influence and impact the entrapment percentage and structural integrity of the subsurface domain. E. A. Al-Khdheawi et al., [180]–[183] investigated wettability influences in the heterogeneous (variation in petrophysical parameters) domain. The purpose of this analysis is to investigate the impact of wettability during CO₂ sequestration.

Within the subsurface reservoir of the natural geological regions, the wettability can range from strongly water wet to strongly CO₂ wet. The wettability primarily affects variables such as relative permeability, capillary pressure, CO₂ residual saturation, and CO₂ mass transfer into the connate reservoir water. However, because wettability mostly depends on the rock's surface chemistry, the water's composition in the connate reservoir, and the temperature of the reservoir, the extent of these influences may be unpredictable [180]–[184].

Another simulation analysis considers five distinct ranges of reservoir parameters of relative permeability-saturation and capillary pressure-saturation. They are strongly water-saturated, strongly CO₂-saturated, intermediately saturated, weakly water-saturated, and weakly CO₂-saturated. According to the results of this numerical investigation, the vertical migration of injected CO₂ was faster in the strongly CO₂ wet domain than in the strongly water wet domain. However, lateral spreading was lower in the strongly CO₂ wet domain than in the strongly water wet domain. As a result, residual CO₂ entrapment was minimal in the strongly CO₂ wet domain. In contrast, the solubility trapping and free mobile CO₂ quantity were more significant in the strongly CO₂ wet domain than in any other domain analyzed. The author suggests a strongly water-wet region is ideal and feasible for CO₂ geological sequestration (CGS). This is because the CO₂ plume takes longer to reach the caprock in the strongly water-wet domain than

in all other wetted domains [180]–[183]. The wettability simulation study is highly computationally intensive due to the requirement for an accurate mesh. Because of this, the wettability analysis was excluded from the current study since it is preferable to conduct by utilizing the mesoscale modeling technique and software [21].

E. A. Al-Khdheawi et al., [185]–[187] have undertaken simulation analyses on injection well configuration [185] and salinity [186], [187] in addition to wettability. According to the injection well configuration analysis, horizontal injections are preferred to vertical injections. The lateral distribution of CO₂ in the domain was increased during the horizontal well injection. Furthermore, it increases the contact area between the injected CO₂ and the reservoir water. As a result, the residual and solubility entrapment in the domain increased. However, implementing and monitoring horizontal wells in the reservoir would be more difficult during operations [185]. The effect of salinity is investigated using four sets of simulated analyses considering four different salinity values. It was discovered that when the reservoir water salinity increased, so did the mobility and vertical migration distances of injected CO₂. As a result, lesser salinity resulted in increased residual and solubility entrapment. The salinity greatly influences the domain's relative permeability and capillary pressure. As a result, less salinity is preferred for CO₂ geological sequestration [186], [187].

A. Afanasyev et al., [188] investigated CO₂ movement in a sloping aquifer in the undip direction. This is done by constructing governing equations for immiscible flow equations. The empirical equation's output is validated utilizing numerical simulations. The link between dip angle, porosity, permeability, and saturation function was analyzed. This methodology is utilized for leakage detection, risk assessment, and uncertainty quantification [188].

M. J. Rahman et al., [131] performed a research analysis on the caprock seal integrity. The investigation concentrated on the geomechanical features of shale caprock. The field-scale

analysis was performed on the overlaying Drake formation shales of the Early Jurassic Cook and Johansen formations situated offshore of Norway at the Horda Platform area. The field-scale investigation used fifty exploration wells with 3D and 2D seismic lines. The Aurora injection location of the Drake formation was used for CO₂ leakage investigation and risk assessment. It was discovered that the stress caused by CO₂ injection was distributed by shale caprock. The risk assessment showed that the formation's top seal prevented CO₂ leakage. The author also suggested that numerical simulations be used to assess risk factors with different macroscale parametric modifications [131].

2.9 Utilization of Machine Learning in CO₂ Geological Sequestration Analysis

Simulation analysis can be carried out using numerical techniques such as reactive transport modeling [21], [22]. Simulating such a complicated system with intricate relationships will be computationally expensive and will take more time [16, 74]. To address these issues, researchers began building Artificial Neural Network (ANN) models to predict the future value of the dependent variable based on historical input and output from experiments and simulation findings [189]–[192].

The employment of artificial neural networks (ANNs) within reservoir engineering has experienced a notable increase over the past ten years. The neural network is becoming more popular in fields ranging from finance to engineering. The use of neural networks will cut processing time while increasing accuracy. The use of neural networks has lowered the overall processing overheads required in simulation analysis. G.L.A.F.Arce et al., [192] employed a time series neural network to estimate CO₂ storage in various sequestration approaches such as ocean, terrestrial, and geological sequestration [192]. D. Ma et al., [190] performed CO₂ leakage experiments and used time series neural networks NAR (Nonlinear Autoregressive Network) and NARX (Nonlinear Autoregressive Network with Exogenous Inputs) to forecast future CO₂

leakage percentages based on experiment results. Wind speed, wind direction, and air temperature in the NARX are used as input factors in this analysis, with leaking CO₂ concentration as the target variable. The NARX model is found to be marginally more accurate than the NAR model in estimating CO₂ concentration. Both neural network models performed admirably in terms of predicting a target variable. The author also said that the prediction accuracy depends on the type of NARX input variable data [190].

Y. Kim et al.[189] used the GEM-Computational Modeling to simulate CO₂ sequestration. The numerical simulation data is used as input variable data in the Multilayer Perceptron (MLP) neural network. In this study, the Structural Trapping Index (STI), Residual Trapping Index (RTI), and Total Trapping Efficiency Index (TTEI) were predicted using three training algorithms: Levenberg-Marquardt, Scaled Conjugate Gradient, and Bayesian Regularization. The author noticed that Multilayer Perceptron - Levenberg-Marquardt (MLP-LM) produced good results with respectable R² and RMSE values. This trained neural network was then utilized to predict a real-world case study of the Gorae V Structure in the South-Eastern Sea, Korea [189]. Y. Song et al., [193] created an Artificial Neural Network Geological CO₂ Sequestration (ANN-GCS); software like Python and Keras was used to create the ANN-GCS. The modeled synthetic domain of Pohang Basin, Coast of Pohang, South Korea, is used for the conventional numerical modeling of CO₂ sequestration. GEM-CMG was used to simulate and analyze the Residual Trapping Index (RTI), Solubility Trapping Index (STI), and Total Trapping Efficiency Index (TTEI). The numerical simulation data is used for ANN-GCS analysis, and the author claims that ANN-GCS results have over 98% accuracy [193]. The research analysis carried out by G. Wen et al., [194] employed a deep neural network to predict the migration of CO₂ plumes in the domain. The petrophysical parameters of a geological domain are fed into the neural network for CO₂ plume forecasting. According to the author,

the created neural network has learned the significance of gravity, capillary force, viscous force, and buoyant force acting on CO₂ plume movement [194].

2.10 Chapter Summary

The chapter provides a comprehensive literature review on CO₂ geological sequestration, covering various aspects related to the topic. Below are several key bullet points from the chapter, presented in an illustrated format.

- The CGS technology is the need of the hour; for developing countries, this option is viable to reach Net Zero Emission goals.
- For the financial year 2022, India has seen a surge in coal demand by 12%. This surge is due to an increase in manufacturing plants due to local and foreign investors seeing India as a safe manufacturing hub [10], [39], [160].
- Low carbon emission technology can't satisfy the countries' energy demands alone. The CCS has to be integrated into the goal of net zero emissions.
- Reliable CCS fields in India: Jharia coalfield (ECBM), Rajeshwari field (Barmer), Ingoli - Padhra fields (Cambay), Razol formation in the KG basin, and Deccan basalt formation [39], [161], [175], [176].
- In India, the basalt formation is mainly observed in the Deccan Traps, which are spread around 5,00,000 km² [173].
- Basalt can be considered a potential candidate for the carbon sink due to the presence of a good quantity of silica minerals and a commendable range of Calcium, Iron, and Magnesium.
- Due to the availability of vast basalt formations and commendable mineral reactivity, Deccan Volcanic Province is a good candidate for the implementation of CGS in India.
- The availability of the mineral compositions of basalt can be advantageous.

- In certain research experiments on basalt, injected CO₂ interacts with mineral rocks within 100 years. Mineral entrapment usually takes hundreds of years.
- The mineral reactivity published by some researchers brings a sense of confidence for selecting Basalt formations as the Sequestration region.
- CO₂ geological sequestration research in India is limited to small-scale lab experiments.
- There is minimal research on the geological morphology of the Deccan Volcanic Province. No research has determined the exact Deccan trap's CO₂ storage range. The appropriate percentage of efficiency of different trapping mechanisms of the Deccan Volcanic Province needs to be analyzed.
- The unique characteristics of the Deccan Traps and the potential of basalt formations for CO₂ geological sequestration are explored. The mineral reactivity and geological morphology of the Deccan Volcanic Province are discussed in the context of CO₂ sequestration. Many academics believe the Deccan trap is ideal for sequestration.
- The mineral trapping mechanism occurs in the formation, takes nearly hundreds of years, and the experiment setup can't be maintained for such long. The simulation analysis has the advantage of considering all the trapping mechanisms for analysis over a geological time scale.
- The importance of simulation analysis in considering all trapping mechanisms and analyzing caprock leakage is emphasized.
- The location of the Deccan Volcanic Province in an area with significant CO₂ emissions makes it crucial for mitigating the effects of climate change in India.

The literature review has provided an extensive analysis of various aspects related to carbon capture and storage (CCS), ranging from the current state of CO₂ emissions and the technology being used to mitigate them to the different CCS projects being implemented across the globe. The review also delves into the numerical modeling used to optimize and simulate the different

CGS methods. In the next chapter, the focus shifts to reactive transport modeling, a critical component in understanding the behavior of CO₂ when injected into geological formations for storage. Reactive transport modeling involves simulating the complex interactions between CO₂, the host rock, and any fluids present in the subsurface. This modeling approach enables researchers to predict how CO₂ will behave over time and assess the potential risks associated with its storage. The next chapter aims to provide a more in-depth understanding of this crucial study area by discussing reactive transport modelling for CGS.

**CHAPTER 3: Multiphase and Reactive
Transport Modelling of CO₂
Geological Sequestration**

3 Multiphase and Reactive Transport Modelling for CO₂ Geological Sequestration

3.1 Introduction

This chapter emphasizes the utilization of multiphase reactive transport modeling in the context of carbon dioxide (CO₂) geological sequestration. The multiphase flow equations are used to elucidate the intricate fluid dynamics and transport phenomena that occur during CO₂ injection and storage in subsurface formations. The Brooks-Corey relation, which characterizes the capillary pressure, saturation, and relative permeability relationship, is used to model the behavior of multiphase fluids in porous media. This chapter explains the reactive transport modeling that facilitates the multiphase interactions between CO₂, water, and rock formations, including mineral dissolution, precipitation, and geochemical reactions. The chapter also discusses the estimation of trapping percentage, quantifying the amount of CO₂ trapped due to major trapping mechanisms happening in the subsurface formations. In the end, the modeling approach of the synthetic computational domain is explained, which is used in the subsequent chapters for the modeling and simulation analysis of different geological morphological domains.

3.2 Reactive Transport Modeling for CGS

The present research analysis employs multiphase and multicomponent reactive transport modeling techniques to conduct this simulation analysis. CGS technology is a prominent topic because of its potential to reduce atmospheric CO₂ levels due to its widespread interest in it and the need to model its effects and analyze various parameters that have gained significant interest among the research community. It plays a crucial role in examining the intricate interactions between geochemical reactions and fluid flow in porous media. Scientific institutions have collaborated to create numerical tools for simulating the effects of CO₂

sequestration. Consequently, numerous software products have been developed to analyze geochemical and geomechanical factors. CrunchFlow [16], [195], TOUGH2 [16], [196], PSU-COALCOMP [197], TOUGHREACT [16], [198], and PFLOTRAN [16], [21], [22], [199] are some of the popular examples of reactive transport software [16].

CrunchFlow, also known as CrunchTope, was developed by Carl I. Steefel at Lawrence Berkeley National Laboratory in 1988 [16], [195]. This open-source software package enables the simulation of reactive flow and transport in the Earth and environmental sciences. Its versatility lies in its capacity to incorporate a wide range of reactions, including mineral dissolution/precipitation, ion exchange, surface complexation, and microbial-mediated reactions. Based on the CrunchFlow reactive transport modeling framework, additional software repositories such as Chombo-Crunch have been developed in recent years [16], [195].

TOUGHREACT, another open-source software, was developed by Nic Spycher, Eric Sonnenthal, and Liange Zheng at Lawrence Berkeley National Laboratory [16], [198]. It is a numerical simulator specifically designed for chemically reactive non-isothermal flows of multiphase fluids in porous and fractured media [16], [198]. The reactive chemistry for multiphase flow was incorporated into its predecessor, TOUGH2 [16], [196]. PSU-COALCOMP, developed by Manik and Ertekin in 1999 at Pennsylvania State University, is a simulator specifically built for CO₂ sequestration in coal seams [197].

PFLOTRAN has been collaboratively developed by experts from renowned institutions such as Lawrence Berkeley National Laboratory, Pacific Northwest National Laboratory, Oak Ridge National Laboratory, Sandia National Laboratories, Argonne National Laboratory, and other prominent research organizations [16], [21], [199]. It stands out as an open-source, state-of-the-art, massively parallel subsurface flow and reactive transport code. PFLOTRAN is specifically designed to address the complexities of multiphase, multicomponent, and

multiscale reactive flow and transport in porous materials. The software provides efficient solutions for solving the reactive transport equations using either a fully implicit Newton-Raphson algorithm or the operator splitting method [16], [21], [199].

A significant application area of PFLOTRAN lies in the field of CO₂ geological sequestration. Previous scientific publications from the core developers have demonstrated PFLOTRAN's capabilities in simulating the coupled system of mass and energy conservation equations for the two-phase system consisting of supercritical CO₂ and H₂O [21], [22]. The software enables researchers to assess the impact of injected CO₂ on various parameters, including pH, CO₂ concentration within the aqueous phase, and mineral stability [21], [22]. The utilization of the PETSc parallel library package, based on MPI, enables effective parallelization, facilitating the efficient utilization of computational resources for large-scale field applications involving multi-component chemistry [16], [21], [199]. The extensive repositories, active community support, and preceding research on CO₂ sequestration on PFLOTRAN made it the preferred choice for the current research study.

To effectively assess CO₂ storage in geological formations, it is necessary to consider a range of crucial characteristics of the CO₂ sequestration process. Multiphase flow and Reactive transport modeling are key methods for analyzing the fate of CO₂ following injection into a geological formation. It can analyze the system's behavior with coupled chemical, physical, and biological processes. The application of reactive transport modeling is sufficient for evaluating the fate of CO₂ after its injection into a geological formation and examining the behavior and performance of injected CO₂ during geological time. The reactive transport simulation can provide answers to numerous sequestration concerns about geological site selection and post-injection analysis [18], [20].

3.3 Multiphase Flow Equations

The following illustrated mass and energy conservation equations are solved for a multiphase system. These equations, characterized by their partial differential nature, serve as the basis for computational analysis and modeling within this context. The interactions between the water and CO₂ plume are investigated using multiphase and multicomponent mass and energy balance equations. The conservation equations describe the interactions between the water and the CO₂ plume. In the illustrated conservation equations, see *Eq. (3.1)* and *Eq. (3.2)*; the first term is affiliated with accumulation, the second is affiliated with net flux, and the third is affiliated with the source and sink terms. In the mass conservation equation, the first term states the accumulation of mass in the considered control volume, the second term states net flux in the control volume, and the third term states the injection of CO₂ into the domain for current simulation analysis [16], [20], [21], [199]. In the following sub-sequential equations, the subscripts and superscripts *l* and *g* represent liquid and gas phases, respectively. Subscript *w* and *c* represents water and CO₂, respectively.

$$\frac{\partial}{\partial t} [\phi(S_l \rho_l X_w^l + S_g \rho_g X_w^g)] + \nabla \cdot [q_l \rho_l X_w^l + q_g \rho_g X_w^g - \phi(S_l D_l \rho_l \nabla \cdot X_w^l + S_g D_g \rho_g \nabla \cdot X_w^g)] = Q_w$$

Eq. (3.1)

$$\frac{\partial}{\partial t} [\phi(S_l \rho_l X_c^l + S_g \rho_g X_c^g)] + \nabla \cdot [q_l \rho_l X_c^l + q_g \rho_g X_c^g - \phi(S_l D_l \rho_l \nabla \cdot X_c^l + S_g D_g \rho_g \nabla \cdot X_c^g)] = Q_c$$

Eq. (3.2)

Porosity is symbolically denoted by ϕ . The terms saturations, density, and molecular density are represented by $S_{l \text{ or } g}$, $\rho_{l \text{ or } g}$, and $D_{l \text{ or } g}$ in the mass conservation equations. The mole fraction of water and CO₂ for both phases are represented by $X_w^{l \text{ or } g}$ and $X_c^{l \text{ or } g}$, respectively. The source or sink terms are denoted by Q_w and Q_c , representing the injection and extraction of CO₂

or water from the domain. The subscript p in the subsequent represents the phases. The Darcy velocity for both phases is obtained from the following **Eq. (3.3)**.

$$\mathbf{q}_p = \frac{-kk_{rp}}{\mu_p} \nabla \cdot (\mathbf{P}_p - \rho_p \mathbf{g}z) \quad \text{Eq. (3.3)}$$

From the above **Eq. (3.3)**, the variables permeability, pressure, mass density, and fluid viscosity are symbolized by k_{rp} , P_p , ρ_p , and μ_p , respectively. Absolute permeability, acceleration due to gravity, and vertical height are represented by k , g , and z , respectively.

3.4 Brooks-Corey Relation

The current simulation analysis utilized the Brooks Corey function to characterize the relations between saturation and capillary pressure. Furthermore, the Brooks Corey Burdine function is utilized to establish the relations between saturation and relative permeability for reservoir simulations [22], [200]. The following **Eq. (3.4)** describes the relationship between saturation and capillary pressure.

$$S^{eff} = (\alpha P_c)^{-\lambda} \quad \text{Eq. (3.4)}$$

The effective saturation for both phases is shown in **Eq. (3.5)** and **Eq. (3.6)**. The terms S_l , S_l^r and S_g^r represent liquid saturation, residual liquid saturation, and residual gas saturation, respectively.

$$S_l^{eff} = \frac{S_l - S_l^r}{1 - S_l^r} \quad \text{Eq. (3.5)}$$

$$S_g^{eff} = \frac{S_l - S_l^r}{1 - S_l^r - S_g^r} \quad \text{Eq. (3.6)}$$

The effective saturation can be used to evaluate the relative permeability of both phases using the following illustrated formulae. The α and λ are empirical constants. The relative

permeability of both phases, the liquid phase “ k_{rl} ” and gas phase “ k_{rg} ”, are formulated as *Eq. (3.7)* and *Eq. (3.8)*.

$$k_{rl} = (S_l^{eff})^{3+2/\lambda} \quad \text{Eq. (3.7)}$$

$$k_{rg} = (1 - S_l^{eff})^2 \left[1 - (S_g^{eff})^{3+2/\lambda} \right] \quad \text{Eq. (3.8)}$$

The capillary pressure is evaluated from the pressure extended by wetting and non-wetting fluids, illustrated in the following *Eq. (3.9)*. The relationship between phase saturation and mole fraction for both phases is described as follows *Eq. (3.10)* and *Eq. (3.11)*.

$$P_c = P_{nw} - P_w \quad \text{Eq. (3.9)}$$

$$S_l + S_g = 1 \quad \text{Eq. (3.10)}$$

$$x_g + x_l = 1 \quad \text{Eq. (3.11)}$$

The following, illustrated in *Eq. (3.12)*, is the energy balance equation that has been used in the simulation analysis.

$$\frac{\partial}{\partial t} [\phi(S_l \rho_l U_l + S_g \rho_g U_g) + (1 - \phi) \rho_r C_r T] + \nabla \cdot (q_l \rho_l H_l + q_g \rho_g H_g - \kappa \nabla T) = Q_e \quad \text{Eq. (3.12)}$$

The terms $U_{l \text{ or } g}$ and $H_{l \text{ or } g}$ are represented by internal energy and enthalpy, respectively, for both phases. The rock density and heat capacity of the porous rock formation are denoted by ρ_r and C_r , respectively. The terms κ and T represents thermal conductivity and temperature, respectively. The source or sink terms is represented by Q_e ; it indicates the thermal changes at the injection point in the formation domain.

3.5 Reactive Transport Modelling

The multicomponent reactive transport equation (see *Eq. (3.13)*) is coupled with the conservation equations to incorporate the geochemical reaction in the simulation analysis [20],

[21], [199], [200]. In the subsequent text, subscript j indicates the primary species, subscript i the secondary species, and m denotes the minerals.

$$\frac{\partial}{\partial t} [\phi (S_l \psi_j^l + S_g \psi_j^g)] + \nabla \cdot (\varpi_j^l + \varpi_j^g) = -\sum_m \nu_{jm} I_m \quad \text{Eq. (3.13)}$$

The terms ψ , ϖ , ν_{jm} , and I represents species concentration, flux, stoichiometric coefficients, and dynamic rate of reaction. The concentration of primary species j at their respective phase p is illustrated as follows; see *Eq. (3.14)*.

$$\psi_j^p = \delta_i^p C_j^p + \sum_i \nu_{ji} C_i^p \quad \text{Eq. (3.14)}$$

The net flux of primary species j at their respective phase p is illustrated as follows; see *Eq. (3.15)*. The term phase diffusivity coefficient is represented by D_p .

$$\varpi_j^p = (-\tau \phi S_p D_p + q_p) \psi_j^p \quad \text{Eq. (3.15)}$$

The following equation, *Eq. (3.16)*, illustrates the dynamic rate of reaction I_m formula, whereas terms kinetic rate constant of a mineral, surface area of the minerals, and activity of the i^{th} species symbolic denotes as K_m , $A_m \phi$ and a_i .

$$I_m = -K_m A_m \phi [\prod_i a_i^{n_i}] (1 - K_m Q_m) \quad \text{Eq. (3.16)}$$

The ion activity product, Q_m , is evaluated using the following formula, see *Eq. (3.17)*.

$$Q_m = \prod_j (\gamma_j^p C_j^p)^{\nu_{jm}} \quad \text{Eq. (3.17)}$$

PFLOTTRAN possesses the capability to simulate thermal-hydrological-chemical (THC) coupled processes in three-dimensional spatial dimensions, encompassing non-isothermal conditions and variable saturation for flow in the porous media. In the present simulation analysis, a multiphase fluid flow system is modeled, incorporating multicomponent reactive transport of gaseous, aqueous, and mineral species for a CO₂ geological sequestration

simulation study [21], [22]. PFLOTRAN consists of two modules, namely PFLOW and PTRAN. The PFLOW module is responsible for handling fluid flow within the system, while the PTRAN module manages the multicomponent geochemical reactive transport for the simulation system. Within the PFLOW module, mass and energy conservation equations are solved, whereas the PTRAN module focuses on solving the multicomponent reactive transport equation [16], [19]–[22], [200].

The multicomponent geochemical reactive transport module considers homogeneous aqueous and heterogeneous gaseous speciation reactions, along with mineral dissolution, precipitation, ion exchange, and surface sorption reactions. The fluid flow module (PFLOW) and reactive transport module (PTRAN) are sequentially coupled to perform the current transient model simulation of CO₂ geological sequestration [21], [22]. To model the flow behavior of multiphase fluids in porous media, the Brooks-Corey relation is used to evaluate the domain's capillary pressure, saturation, and relative permeability. In the PFLOW module, flow velocities, saturation, pressure, and temperature are evaluated at each time step and submitted to the PTRAN module [21], [22]. Based on the submitted values, the multicomponent reactive transport equation is solved, resulting in corresponding changes in mineral volume fraction within each grid cell. The mineral volume fraction values are then utilized to update the porosity and permeability of the grid cells, which, in turn, influence the migration pathway of CO₂ within the domain [21], [22].

In the PTRAN module, the aqueous speciation reactions are typically considered homogeneous in the reactive transport module, assuming local chemical equilibrium due to their fast reaction rates. However, when the solid phase of minerals is involved, heterogeneous reactions occur, and the rates of mineral reactions are governed by factors such as mineral surface area, initial mineral volume fraction, and kinetic rate constants of the reactions [16], [19]–[22], [200].

In the structural and residual trapping mechanism simulation study, only the PFLOW module is utilized to model dual-phase fluid flow in the porous media [21], [22], [30], [80]. However, both the PFLOW and PTRAN modules are employed in the simulation of the solubility trapping mechanism. The PTRAN module specifically considers gaseous and aqueous reactions while excluding mineral components and their associated dissolution and precipitation reactions [21], [22], [63], [111]. The complete routine of PFLOW and PTRAN, which involves multiphase multicomponent reactive transport, is employed to comprehensively evaluate the mineral trapping mechanism [21], [22].

PFLOTTRAN utilizes the PETSc (Portable, Extensible Toolkit for Scientific Computation) to solve the system of equations. The PFLOW module employs Scalable Nonlinear Equation Solvers (SNES) from PETSc for solving the nonlinear system of equations, while the PTRAN module utilizes the Krylov Subspace iterative method (KSP) algorithm [21], [22]. As PFLOW and PTRAN are sequentially coupled, both modules' routines are executed sequentially. However, the PTRAN module requires considerably smaller time steps compared to the PFLOW module. Consequently, the interpolated calculated field variables from PFLOW are submitted to PTRAN at its smaller time step [21], [22].

3.6 Estimation of trapping percentage

Using conservation of mass, a modified version of Darcy's law, relative permeability is utilized to quantify the flow in the reservoir domain. The porosity, pore volume, and CO₂ saturation of the grid cells are taken into consideration in the process of performing calculations for the entrapment percentage. The quantity of CO₂ that remains after structural and residual trapping is referred to as the movable plume [30], [80]. The term n_f denotes the total number of cells in the grid arrangement. CO₂ saturation and residual CO₂ saturation are represented by S_{CO_2} and S_{rCO_2} , respectively. V_s and V_r represent the cell volumes of structural traps and residual traps,

respectively. The top surface perturbation cell vertex heights are evaluated and analyzed for structural traps. Following *Eq. (3.18)* and *Eq. (3.19)* are the formulas for calculating the structural and residual trapping.

$$\mathbf{Structural\ trapping} = \sum_{n=1}^{nf} (\phi V_s \rho_{co_2}) \times \mathbf{min} (S_{co_2}, S_{rc_{o_2}}) \quad \mathbf{Eq. (3.18)}$$

$$\mathbf{Residual\ trapping} = \sum_{n=1}^{nf} (\phi V_r \rho_{co_2}) \times \mathbf{min} (S_{co_2}, S_{rc_{o_2}}) \quad \mathbf{Eq. (3.19)}$$

The top caprock perturbations are integrated on the mesh surface by utilizing MATLAB Gaussian noise function. The height differences between each mesh surface cell are determined. The structural traps are then recognized, and the sequential cells are saved and evaluated as structural trapping cells during simulations. The active cells for residual trapping computation are the remaining cells of a domain other than the structural trapping cells. For the calculation of entrapment, only immobile CO₂ saturation cells are included. The remaining cell saturations are considered in the calculations for the mobile plume. The analysis of solubility trapping involves an investigation of both the aqueous CO₂ and gaseous CO₂ within the geological simulation domain. The analysis of mineral volume fraction is conducted in conjunction with the assessment of domain saturation and aqueous CO₂ concentration to estimate mineral trapping. This analysis involves various numerical simulations incorporating diverse geological and sequestration parameters [30], [63], [80], [111]. The following **Table 3-1** presents a concise overview of vital equations in Multiphase flow and Reactive Transport, and auxiliary equations, aiming to offer readers a quick reference.

Table 3-1: Multiphase flow and reactive transport model equations for CO₂ geological sequestration [22].

Multiphase Flow and Reactive Transport Modelling Equations		
Name of the Equation	Equation	Eq. No
Multiphase flow equations		
Water phase, mass balance equation	$\frac{\partial}{\partial t} [\phi(S_i \rho_l X_w^l + S_g \rho_g X_w^g)] + \nabla \cdot [q_l \rho_l X_w^l + q_g \rho_g X_w^g - \phi(S_i D_l \rho_l \nabla X_w^l + S_g D_g \rho_g \nabla X_w^g)] = Q_w$	3.1
	Darcy velocity of the water phase $q_l = \frac{-kk_{rl}}{\mu_l} \nabla(p_l - \rho_l g z)$	3.1a
ScCO ₂ phase, mass balance equation	$\frac{\partial}{\partial t} [\phi(S_i \rho_l X_c^l + S_g \rho_g X_c^g)] + \nabla \cdot [q_l \rho_l X_c^l + q_g \rho_g X_c^g - \phi(S_i D_l \rho_l \nabla X_c^l + S_g D_g \rho_g \nabla X_c^g)] = Q_c$	3.2
	Darcy velocity of gas phase $q_g = \frac{-kk_{rg}}{\mu_g} \nabla(p_g - \rho_g g z)$	3.2a
Energy balances equation	$\frac{\partial}{\partial t} [\phi(S_i \rho_l U_l + S_g \rho_g U_g) + (1 - \phi) \rho_r C_r T] + \nabla \cdot (q_l \rho_l H_l + q_g \rho_g H_g - k \nabla T) = Q_e$	3.12
Axillary Equations		
Saturation relation for all phases for a singular component	$\sum S_p = 1$	3.10
Brooks–Corey–Mualem model: the relationship between relative permeability to effective saturation	$k_{rl} = (S_l^{eff})^{3+\frac{2}{\lambda}}$	3.7
	$k_{rg} = (1 - S_l^{eff})^2 [1 - (S_g^{eff})^{3+2/\lambda}]$	3.8
Brooks-Corey relationship between the effective saturation and capillary pressure	$S_l^{eff} = \frac{S_l - S_l^r}{1 - S_l^r}$	3.5
	$S_g^{eff} = \frac{S_l - S_l^r}{1 - S_l^r - S_g^r}$	3.6
Capillary pressure	$P_c (= (\rho_l - \rho_g) g h = \Delta \rho g h)$	3.9
Reactive Transport Equations		
Multicomponent reactive transport equation	$\frac{\partial}{\partial t} \left(\phi \left(\sum_l S_l \psi_j^l \right) \right) + \nabla \cdot \sum_p \Omega_j^p = - \sum_m v_{jm} I_m$ Where, $- \sum_m v_{jm} I_m$ is the Rate of reaction equation, j refers to the primary species	3.13
Total concentration	$\psi_j^p = \delta_l^p C_j^p + \sum_i v_{ji} C_i^p$	3.14
Total flux	$\bar{\omega}_j^p = \left(-\tau \phi S_l D_l \nabla + \left(\frac{kk_l}{\mu_l} \nabla (W_l \eta_l - \rho_l g z) \right) \right) \psi_j^l$	3.15
Trapping estimation		
Structurally trapped CO ₂ quantity	$structural - trapping = \sum_{n=1}^{nf} (\emptyset V_s \rho_{CO_2}) \times \min(S_{CO_2}, S_{rCO_2})$	3.18
Residually trapped CO ₂ quantity	$Residual - trapping = \sum_{n=1}^{nf} (\emptyset V_r \rho_{CO_2}) \times \min(S_{CO_2}, S_{rCO_2})$	3.19

3.7 Modeling of Synthetic Domain: Methodology and Approaches

The Deccan Volcanic Province is known for its vast volcanic rock formations, making it a potential site for CO₂ geological sequestration (CGS). The multiphase flow and reactive transport modeling equations are comprehensively presented in **Table 3-1**. The geological domain considered in the chapter is based on the Deccan Volcanic Province in the Saurashtra region of India. The geological data was obtained from D. N. Murthy et al. [201]. Modeling of the synthetic domain from Deccan Volcanic province data is presented in subsequent subsections. For the structural- and residual-trapping simulations, **Section 3.7.1** presents the procedure of computation domain modeling, and the procedure for solubility- and mineral-trapping is presented in **Section 3.7.2**. The next chapter focuses on various factors that can influence trapping efficiency in the Deccan Volcanic Province.

3.7.1 Synthetic geological domain for Structural- and Residual-trapping

The Deccan Volcanic Province of India is spread across a total area of 500,000 km² [173]. Because of its petrophysical and geochemical characteristics, it is one of the greatest sinks in India for the geological sequestration of CO₂. In 1970, the Indian government proposed to store nuclear waste in these traps; however, the concept was scrapped because of environmental concerns and the possibility that it might contaminate the underground water. According to the results of a prior investigation that the Indian government carried out in conjunction with the Pacific Northwest National Laboratory (PNNL), it was estimated that approximately Deccan Volcanic Province might store 150 Gt of captured CO₂ through the implementation of strategic CO₂ sequestration [10].

These basalt rock formations resemble the basalt formations that can be seen in Iceland and the Columbia River basalts found in the northwestern United States. Because of this factor, the

Deccan traps have the ability to be evaluated as a possible option for the sequestration of carbon dioxide [2], [6], [66], [103], [116], [126], [177], [202], [203]. The geological data for modeling a synthetic domain that was considered in this research was of Saurashtra Peninsula, with the precise position being between 21.50° N and 23° N latitude and between 69.75 ° E and 71.50° E longitude, see **Figure 3.1A**. It is anticipated that the Deccan traps would cover the majority of the Saurashtra Peninsula. The geological data of the region was obtained from D. N. Murthy et al., [201].

In order to model structural and residual trapping, the synthetic domain is modeled. To begin, the top surface of the domain is modeled initially for a synthetic domain. The elevation of the structure can be reconstructed with the use of a contour map obtained from the relevant research by applying a MATLAB image processing technique. The top surface of the domain is then modeled in MATLAB by superimposing a visualization of the mesh grid on top of elevation data, see **Figure 3.1B** and **Figure 3.1C**. In addition to that, the whole structure of the grid is modeled. The geological fractures and cracks that occur naturally in the domain were not included in the modeled domain since their presence would have increased the complexity of the simulation and made it more challenging to complete. The territory covers an area that is 160 kilometers wide, 160 kilometers deep, and 1.8 kilometers high. Each of the 2,56,000 grid cells of the modeled synthetic domain is discretized into $160 \times 160 \times 10$, and the physical dimension itself is divided into these cells; see **Figure 3.1B, C, and D** [30], [63], [80], [111].

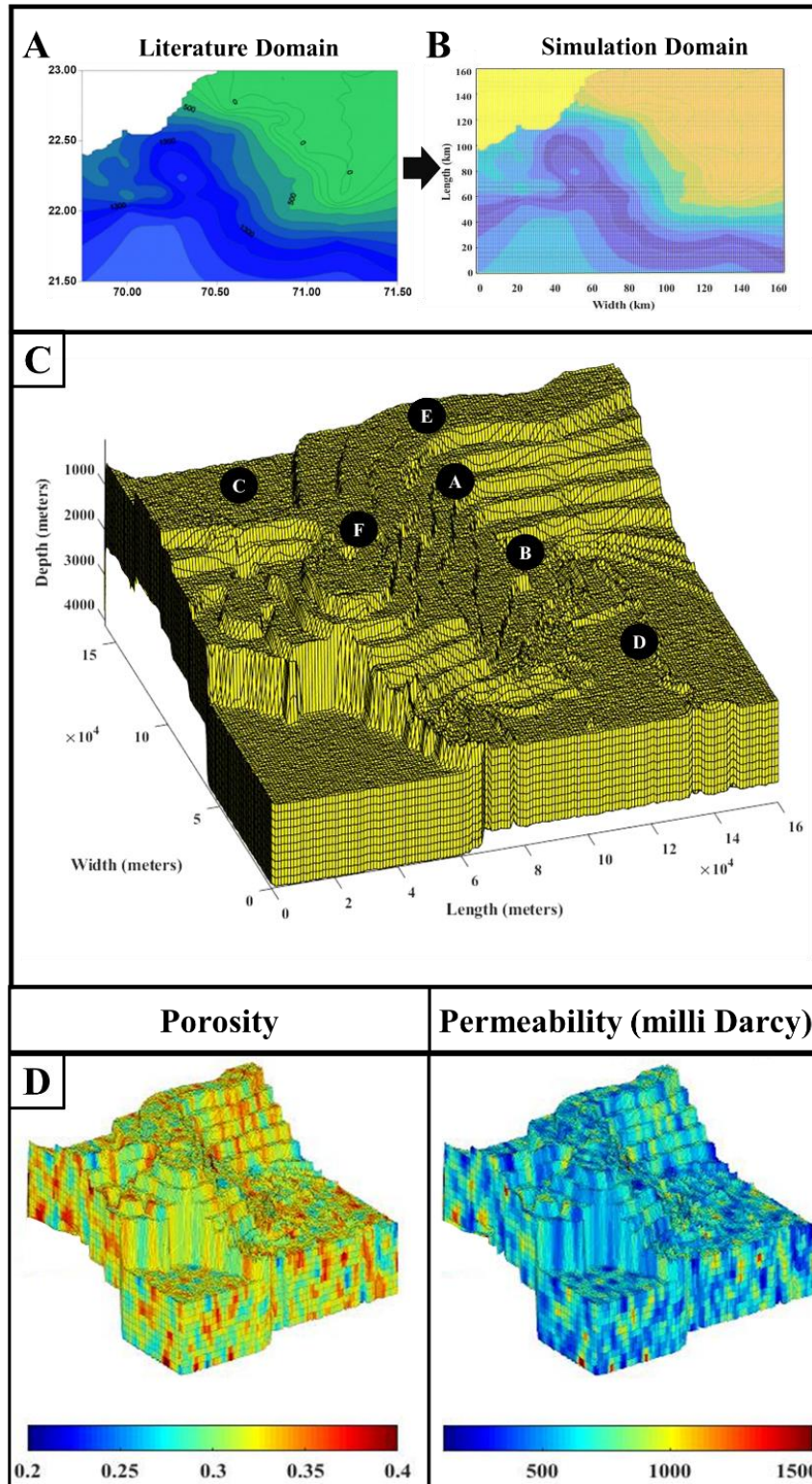


Figure 3.1: The figure illustrates different components: (A) Contour plots sourced from literature D. N. Murthy et al., [201], (B) Contour plot of the modeled geological domain, (C) Three-dimensional grid structure, and (D) The distribution of porosity and permeability within the domain, used for simulating Structural and Residual trapping [30], [111]

The top surface topography of the modeled synthetic domain is about as described. An effort was made to create a model of the domain that provided an appropriate representation of the real-world scenario. The range of porosity that is considered is with respect to the Deccan basalt. The porosity range that is kept between 0.2 and 0.4 is maintained for the modeled synthetic geological domain, and this value is obtained from the literature [173], [203]. The Gaussian function arbitrarily assigns porosity values to each grid cell in the matrix. Utilizing the Carmen-Kozeny relation allows for the evaluation of the permeability to its respective porosity range. In the modeled domain, the permeability values range from 10 to 1500 mD; see **Figure 3.1D** [30], [63], [80], [111].

3.7.2 Synthetic geological domain for Solubility- and Mineral-trapping

The simulation of solubility and mineral trapping was conducted in a specific geographical region, defined by the coordinates 21.50° N, 22.40° N, 69.75° E, and 71.50° E. The simulation's data and inputs were obtained from D. N. Murthy et al., [201], as represented in **Figure 3.2A** and **Figure 3.2B**. The considered simulation region is highlighted with the red rectangle box in **Figure 3.2A**, and for the same region, the top surface is modeled as shown in **Figure 3.2B**. Detailed visualizations of the discretized domain can be found in **Figure 3.2B**, **Figure 3.2C** and **Figure 3.2D**, offering a comprehensive view of the region's characteristics. To carry out the simulation effectively, the region was discretized into a grid with dimensions of 80 kilometers in width, 160 kilometers in length, and 1.8 kilometers in depth. The resulting grid comprised $80 \times 160 \times 10$ cells, totaling 128,000 individual cells [30], [63], [80], [111]. The reactions illustrated in **Table 3-2** are the possible reactions that tend to happen in the subsurface basalt rock formation. The K_{eq} term in the following table denotes the equilibrium constant [66], [78], [118].

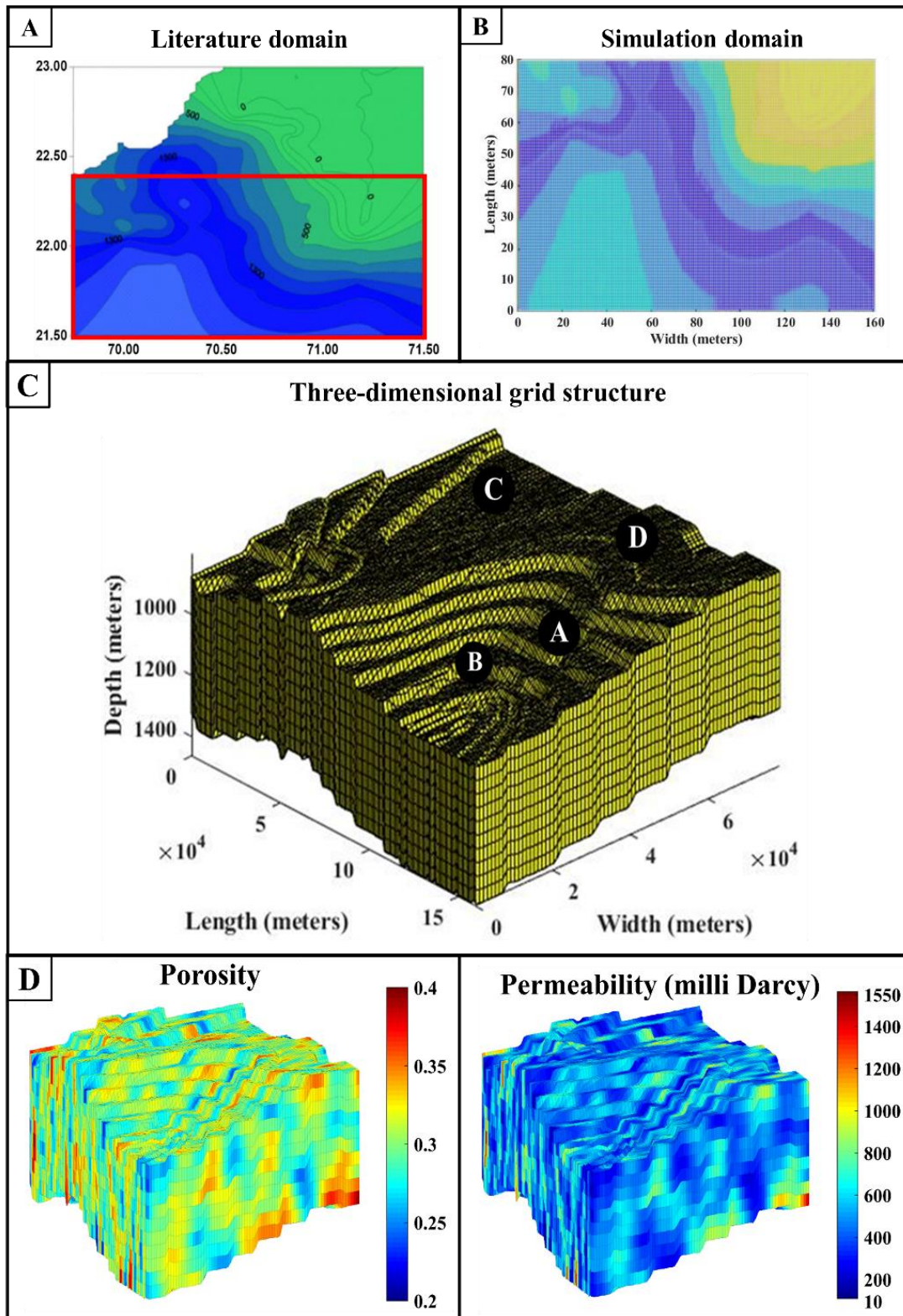


Figure 3.2: Figure shows (A) contour plots extracted from literature, D. N. Murthy et al., [201], (B) contour plot of the geological domain modeled, (C) three-dimensional grid structure, and (D) distribution of porosity and permeability in the domain used for the Solubility trapping simulation.

Table 3-2: Subsurface geochemical reactions of solubility and mineral trapping mechanisms [204].

Mineral trapping reactions	Minerals/ Dissolution	Reaction	Keq (mol/m ² . sec)	Mineral vol. fraction	
	Solubility trapping reactions		$H_2O \leftrightarrow H^+ + OH^-$	1×10^{-4}	
			$CO_2 - 2H^+ + H_2O \leftrightarrow HCO_3^-$	2×10^{-4}	
			$CO_2 - 2H^+ + H_2O \leftrightarrow CO_3^{2-}$	2×10^{-4}	
			$CO_2 + H_2O \leftrightarrow H_2CO_3 \leftrightarrow H^+ + HCO_3^-$	2×10^{-4}	
			$CO_2 + OH^- \leftrightarrow HCO_3^-$	2.7×10^{-3}	
Albite	$NaAlSi_3O_8 + 4H^+ \rightleftharpoons Al^{3+} + Na^+ + 2H_2O + 3SiO_{2(aq)}$	1×10^{-12}	0.09		
Anorthite	$CaAl_2Si_2O_8 + 8H^+ \rightleftharpoons 2Al^{3+} + Ca^{2+} + 4H_2O + 2SiO_{2(aq)}$	1×10^{-11}	0.09		
Aragonite	$CaCO_3 + H^+ \rightleftharpoons Ca^{2+} + HCO_3^-$	1×10^{-6}	0.01		
Calcite	$CaCO_3 + H^+ \rightleftharpoons Ca^{2+} + HCO_3^-$	1×10^{-6}	0.09		
Clinochlore-14A	$(Mg_5Al(AlSi_3O_{10})(OH)_8) + 16H^+ \rightleftharpoons 2Al^{3+} + 5Mg^{2+} + 12H_2O + 3SiO_{2(aq)}$	1×10^{-12}	0.01		
Diopside	$MgCaSi_2O_6 + 4H^+ \rightleftharpoons Mg^{2+} + Ca^{2+} + 2H_2O + SiO_{2(aq)}$	1×10^{-11}	0.01		
Dolomite	$CaMg(CO_3)_2 + 2H^+ \rightleftharpoons Ca^{2+} + Mg^{2+} + 2HCO_3^-$	1×10^{-6}	0.01		
Saponite-Ca	$Ca_{0.25}(Mg, Fe)_3((Si, Al)_4O_{10})(OH)_2 \cdot H_2O + 7H^+ \rightleftharpoons 0.38Al^{3+} + 3Mg^{2+} + 0.16Ca^{3+} + 4.6H_2O + 3SiO_{2(aq)}$	1×10^{-26}	0.05		
Quartz	$SiO_2 \rightleftharpoons SiO_{2(aq)}$	1×10^{-15}	0.5		

3.8 Simulation Methodology

The chapter focused on the application of multiphase flow and reactive transport modeling of CO₂ geological sequestration in the Deccan Volcanic Province. The comprehensive overview

of simulation methodology adapted to elucidate the geological sequestration phenomena is explained as follows.

In **Chapter 4**, simulations were conducted on Deccan traps to understand and analyze the four trapping mechanisms and their relative contributions to overall CO₂ storage. To explain primary trapping mechanisms, in **Section 4.2**, simulations are conducted using the multiphase flow equations, **Table 3-1: Eq. 3.1, 3.2, and 3.12** with auxiliary equations for the relationship between porosity, permeability, capillary pressures, and phase saturations, **Table 3-1: Eq. 3.6, 3.8, 3.9, and 3.10**. To explain the solubility trapping of primarily trapped CO₂, simulations are performed, see **Section 4.3**, the equations **Eq. 3.1-3.20 (Table 3-1)** are utilized for the simulation by incorporating only the reaction mechanisms of CO₂ dissolution in water. Finally, mineral trapping mechanism simulations are presented in **Section 4.4**, using equations **Eq. 3.1-3.20 (Table 3-1)** by incorporating the solubility trapping reactions and the mineral speciation reactions as mentioned in **Table 3-2**.

In **Chapters 5 and 6**, additional synthetic domains are arbitrarily modeled to conduct the parametric studies; these synthetic domains are modeled in a similar way as mentioned in **Section 3.7**. In **Chapter 5**, the study was focused on investigating the influence of caprock morphology and crack on the CO₂ plume migration and CO₂ entrapment due to solubility trapping in the domain by excluding the mineral trapping mechanism. In **Chapter 6**, the primary trapping mechanism simulations were conducted in a synthetic domain with anticline and syncline geological features. The data obtained from these simulations are used to train and test machine learning models to predict future forecasts.

In the simulations, the injection of CO₂ into each synthetic domain occurs at depths below 800 meters from the Earth's surface. Beyond this depth, the natural temperature and fluid pressures surpass the critical point of CO₂ in most locations on Earth. Consequently, CO₂ injected at this

depth or deeper will maintain a supercritical state due to the prevailing temperatures and pressures. Supercritical CO₂, being denser and exhibiting more liquid-like behavior than gas, offers the potential for efficient storage.

As the simulation domain is sloping and has staircase features, an initial reservoir pressure uniform for the whole simulation domain cannot be assumed. The terrain modeled for this study is sloping in nature. Hence, the initial pressure of the reservoir varies in relation to the depth parameter '*h*' associated with each grid cell. The formula ρgh is utilized to determine the initial reservoir pressure. The initial reservoir pressure is derived using the formula ρgh . Due to the constant density of water throughout the geological domain, the pressure only depends on the depth factor, *h*. No flow conditions are applied at the top surface as the caprock is impermeable. Neumann boundary conditions are considered for the remaining surfaces of the synthetic computation domains.

Additionally, in all the numerical simulations conducted in this thesis, the initial thermal conductivity of formation rock is considered as 2.5 W/mK [205]–[207], with a rock density of 2.7×10^3 Kg/m³ [206], [208], and a heat capacity of rock is assumed as 1×10^3 J/Kg K [209], [210]. These properties remain consistent across simulation time, while structural and residual trapping simulation analysis is due to neglecting geochemical reactions. Whereas in mineral trapping simulation, the previously mentioned parameters are subjected to change due to geochemical reaction consideration in the simulations.

**CHAPTER 4: Investigation of Trapping
Mechanisms in Deccan
Volcanic Province**

4 Investigation of Trapping Mechanisms in Deccan Volcanic Province

4.1 Introduction

The definition of various trapping mechanisms -structural, residual, solubility, and mineral trappings are explained in previous chapters. From the literature, it is understood that each mechanism follows the geological time scale. The order of occurrence is first, the structural and residual trapping of injected CO₂; second, the solubility trapping of structural and residual trapped CO₂; and finally, the mineral trapping of solubility trapped aqueous CO₂. Therefore, for a better understanding of the fate of CO₂ by each trapping mechanism, simulations are conducted for the aforementioned order.

First, the structural and residual trapping simulations for injected CO₂ are presented in **Section 4.2**. In the parametric simulation study, the numerical simulation investigation is initially performed by considering primary trapping mechanisms (Structural- and Residual Trapping mechanisms, **Section 4.2**). For this, first, the base case scenario on primary trapping mechanisms is explored in **Section 4.2.1**. Next, the investigation delves into how the heterogeneity of petrophysical properties, such as porosity and permeability, can impact primary trapping mechanisms in the Deccan Volcanic Province (**Section 4.2.2**). Furthermore, the influences of injection point selection (**Section 4.2.3**) and injection rate (**Section 4.2.4**) on primary trapping mechanisms of the Deccan Volcanic Province are examined. These factors can significantly affect the distribution and movement of CO₂ within the rock formations, thus influencing trapping efficiency.

Second, the solubility trapping mechanism is investigated (**Section 4.3**), which involves the dissolution of CO₂ in water and subsequent migration through the rock formation. The primary and solubility trapping mechanisms are compared to understand their relative contributions to long-term CO₂ storage in the Deccan Volcanic Province (**Section 4.3.1**). Additionally, the

analysis includes how the heterogeneity of petrophysical properties (**Section 4.3.2**) and injection point selection (**Section 4.3.3**) can influence solubility trapping efficiency in the Deccan Volcanic Province.

Finally, the investigation delves into the mineral trapping mechanism (**Section 4.4**), which involves the geochemical reaction between CO₂ and minerals in the rock formation, as another crucial and potential mechanism for safe CO₂ storage in the Deccan Volcanic Province. By thoroughly investigating these trapping mechanisms in the Deccan Volcanic Province, this chapter aims to provide valuable insights into the factors that can influence trapping efficiency, thus contributing to the development of effective CGS strategies in Deccan Volcanic Province formations.

4.2 Investigation of Structural- and Residual Trapping Mechanisms in CGS

The geological formations, particularly anticline and syncline sequences depicted in **Figure 4.1**, are crucial for understanding structural- and residual-trapping phenomena affecting CO₂ migration. These formations act as traps, hindering CO₂ movement within the anticline dome during sequestration. Initially, the injected CO₂ will form a plume and have a movement in the domain, and it is referred to as a movable plume, see **Figure 4.1B**. This CO₂ plume, while migrating through porous media, will displace water in the pores. During injection, structural and residual trapping mechanisms become significant factors in CO₂ migration, see **Figure 4.1A-E**. The injected CO₂, after reaching the caprock, moves laterally, see **Figure 4.1C**, and once the injection is ceased, it gets structurally trapped under anticline domes, see **Figure 4.1E**. Residual trapping occurs as some CO₂ remains confined in the porous structure, favoring mineralization over time, see **Figure 4.1D** and **Figure 4.1E**. The fate of CO₂ injection during the post-injection period is depicted in **Figure 4.1E**, transforming from a movable plume to structural- and residual trapping [30], [76].

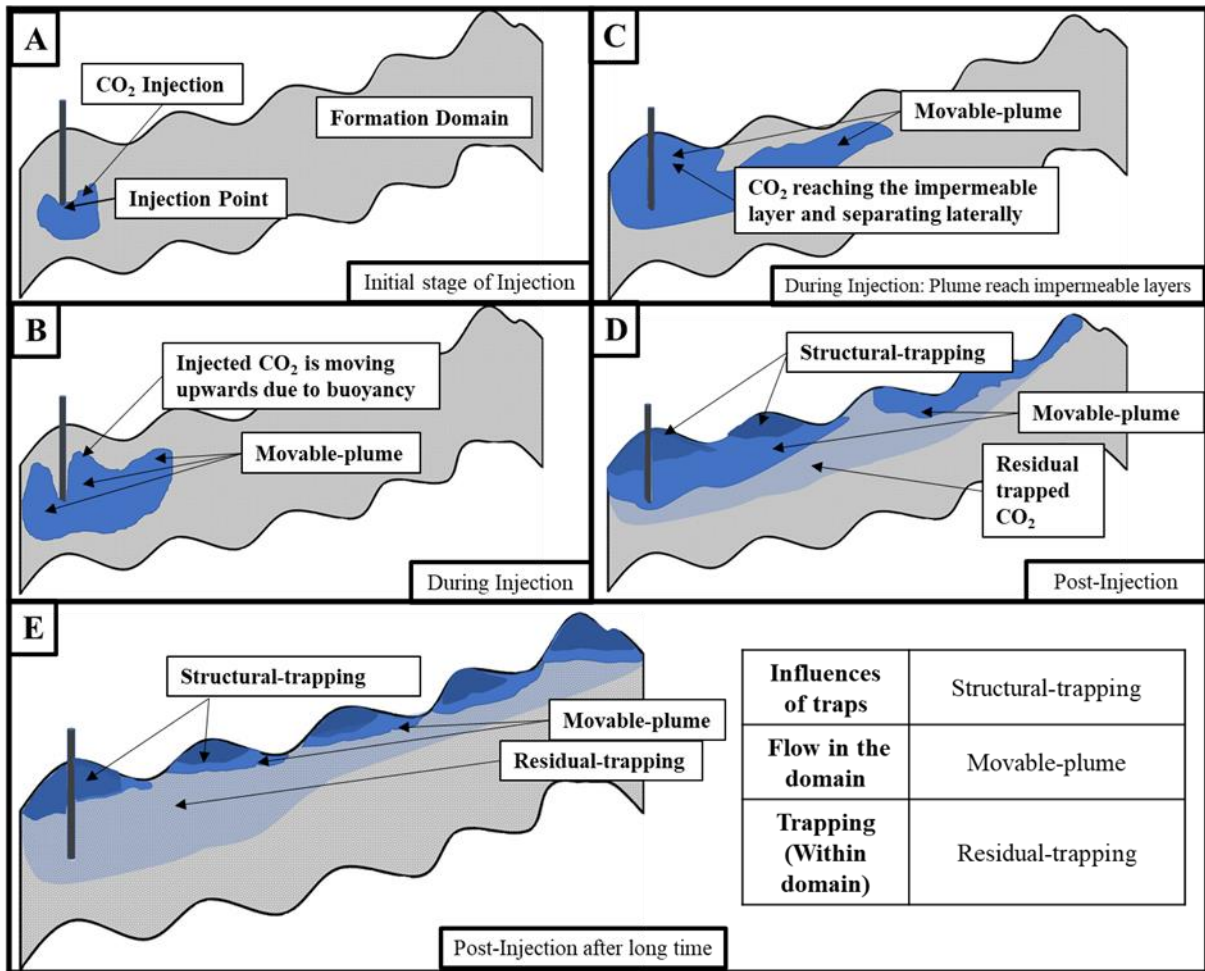


Figure 4.1: Illustration of the categorization of structural trapping, residual trapping mechanisms, and movable plume in geological sequestration: (A-E) depicting the fate of CO₂ during and after injection into the geological formation [30].

The behavior of CO₂ plume during the initial stages can influence the structural and residual entrapment, which further affects the effectiveness of CO₂ geological sequestration (CGS). As a result, having solid insight into the movement of CO₂ plumes and their diffusion in various forms is essential for a particular geological formation. As a greater quantity of carbon dioxide is sequestered in the rigid porous formation, a more significant portion of carbon dioxide will undergo solubility trapping, which will lead to an increase in the production of carbonic acid. This will eventually lead to an increase in mineral reaction and mineral trapping within the formation domain. The estimated structural and residual trapping percentage data can provide

a robust interpretation of the solubility and mineral trapping data. Therefore, this section aims to understand the structural- and residual trapping mechanisms for CO₂ storage in the subsurface formation area. The investigation of structural and residual trapping alone will help us understand what happens to CO₂ in the geological formation domain and will assist in additional studies on the use of field-scale technology [30], [76].

4.2.1 Base Case Scenario

This section describes a numerical simulation for the base case scenario of CO₂ injection at injection point B of the synthetic computation domain. Continuous CO₂ injection is performed for the initial 20 years at a volumetric flow rate of 99×10^5 m³/day. Three thousand years of simulations were performed to observe the structural and residual trapping phenomena in the considered synthetic domain. The geological domain consists of a distinct range of perturbations corresponding to a peak known as an anticline dome. A comprehensive assessment and illustration of the fate of CO₂ due to structural- and residual trapping in the geological domain is depicted in **Figure 4.2**, which comprises two congener outcomes. The first column indicates the CO₂ saturation in the transparent three-dimensional domain, which may be used to analyze the dispersion and displacement of CO₂ plume in the geological domain. The second column illustrates the height of saturated CO₂ in the domain. During the initial stage of a project for commercially viable CO₂ sequestration, the lateral spreading should be high in order to cover a significant volume of the geological domain. This substantial spreading can positively affect the economics of CO₂ sequestration by reducing the need for the number of injection points.

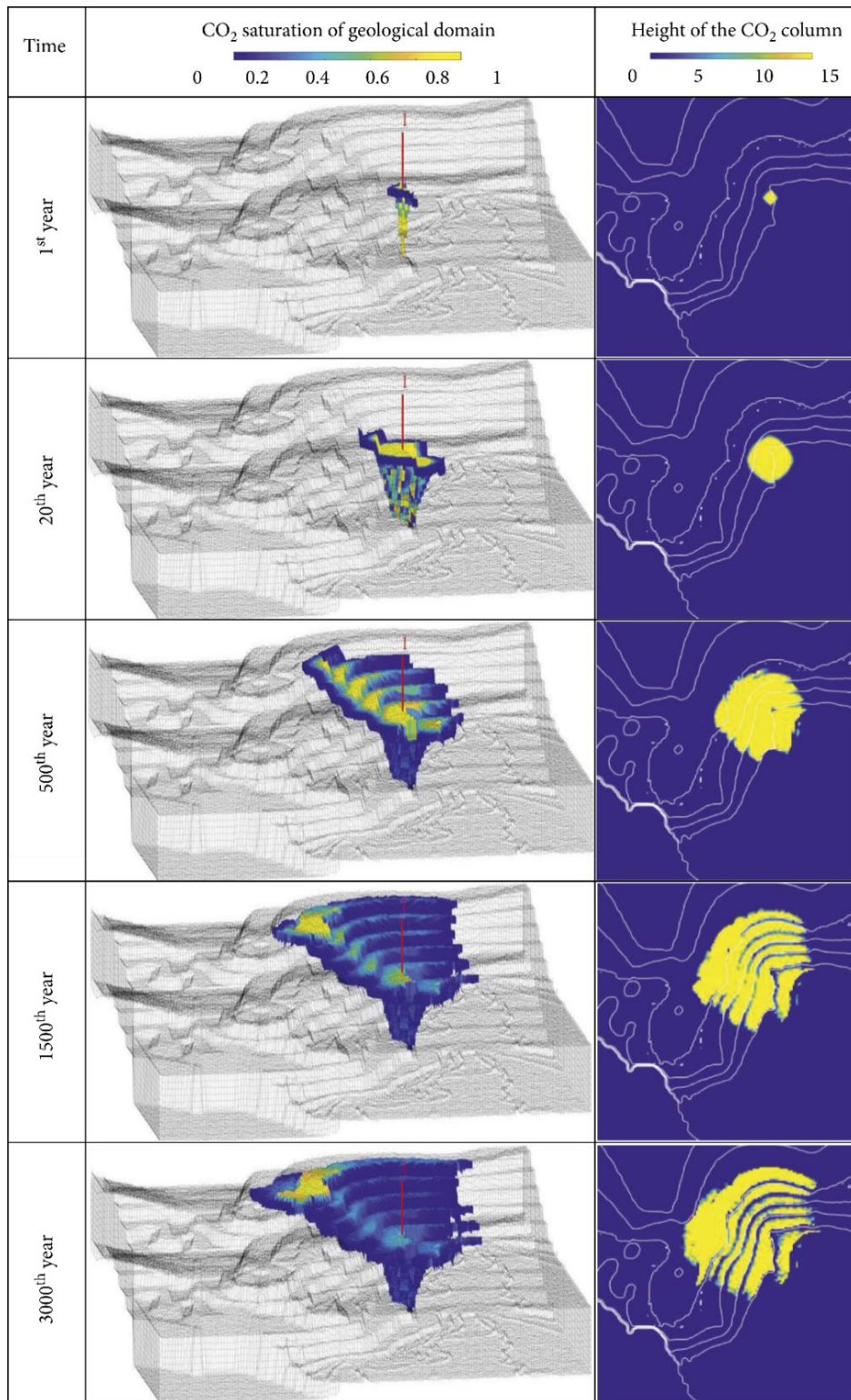


Figure 4.2: *The fate of CO₂ through structural- and residual trapping phenomena across geological time is represented by the height of saturated CO₂ from the surface; the injection point is displayed by the letter I and (ii) CO₂ saturation in the 3D domain. A total of $7.227 \times 10^{10} \text{ m}^3$ of CO₂ was injected for the first 20 years [30].*

The histogram, see **Figure 4.3**, displays the proportions of structural trapping, residual trapping, and mobile plume on a geological time scale. In this particular outcome, the CO₂ plume produced by CO₂ injection has travelled towards the highest elevation zone of an anticline dome. Because the injection force, in addition to the buoyancy forces, operates on the CO₂ plume, the movement was rapid up to the injection period (till the initial 20 years), see **Figure 4.2**. It was observed that within 500 years, the CO₂ plume reached the peak of the anticline dome. Still, it takes around 2500 years for the CO₂ plume to spread across the anticline's top surface. This observation suggests that the injection force plays a crucial role in the lateral spread of the CO₂ plume during the initial stage of CO₂ injection. During the post-injection period, when the injection force gradually decreases, the movement of CO₂ significantly slows down in the synthetic domain. Due to this, the CO₂ plume tends to get trapped in the structural traps or in the porous migration pathway. So, from **Figure 4.3**, one can observe the moveable plume's transition into structural trapping and residual trapping. Further, there could be a transition from structural to residual trapping after an extended period of time. **Figure 4.3** illustrates this occurrence of percentage growth in structural trapping and residual trapping across a geological time span. Particularly, an increase in the percentage of residual CO₂ will promote the coexistence of CO₂ and water in the form of an emulsion, hence promoting the dissolution of CO₂ and triggering solubility trapping phenomena.

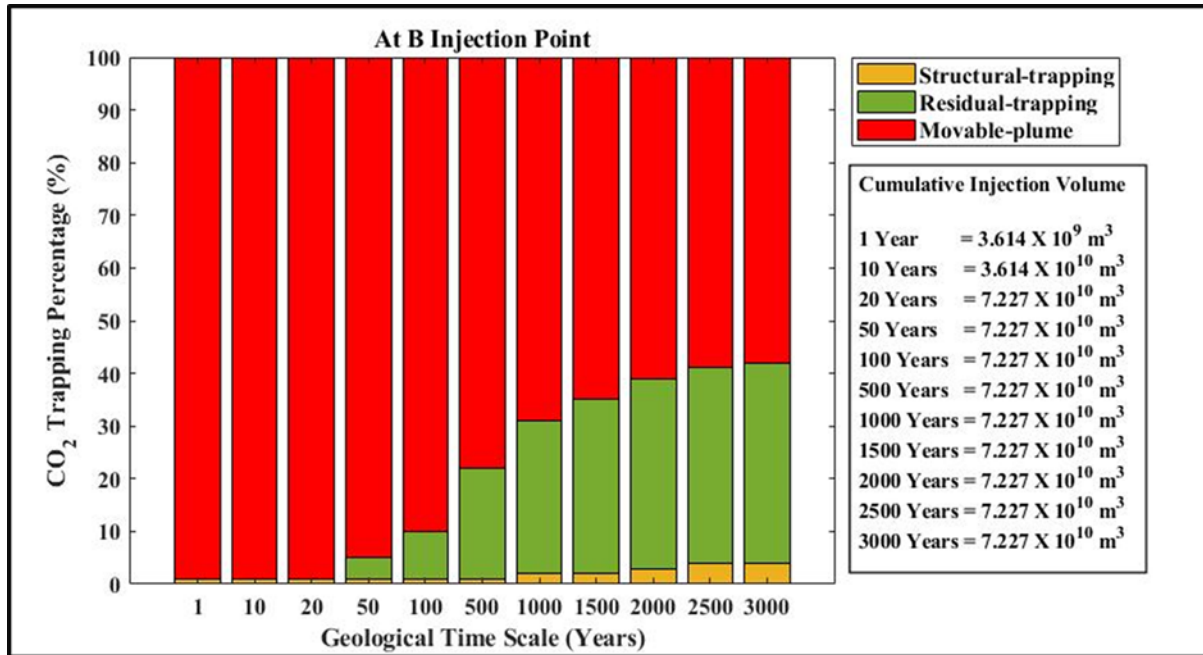


Figure 4.3: The percentage of CO₂ trapped in structural trapping, residual trapping, and movable plume is represented by a histogram. It was reported that the structural trapping and residual trapping contributions increased after injection [30].

4.2.2 Influence of Heterogeneity –Petrophysical properties

This simulation studied the impacts of petrophysical properties such as porosity and permeability on the sweeping efficiency in the geological domain. For these simulations, two sets of porosity and permeability ranges are considered. These simulations are conducted at injection site B with an injection rate of $99 \times 10^5 \text{ m}^3/\text{day}$ for the first 20 years, with the next 2980 years set aside for post-injection analysis. The porosity ranges for simulation set-1 are 0.05 to 0.1, while the permeability range is 1 to 10 mD. For simulation set-2, the range of porosity and permeability are 0.2 to 0.4 and 10 to 1500 mD, respectively. The selection of porosity ranges for both simulation sets was made arbitrarily based on insights from existing literature studies [203], [206], [211], [212]. The objective was to investigate the variations in CO₂ migration, sweeping, and corresponding entrapment when injecting CO₂ into formations

with low-range petrophysical properties compared to those with normal-range petrophysical properties.

The sweeping efficiency is termed as the space covered by the non-wetting or injection fluid that spreads laterally throughout the geological region. As lateral spreading increases, so does the CO₂ sweeping efficiency, reducing the number of injection points necessary for the expansion of CGS. This will eventually have a positive impact on the financial aspects of the implementation of the CO₂ sequestration project. **Figure 4.4A** demonstrates that simulation set-1 has a lower sweeping efficiency than simulation set-2 for the same injection rate of $99 \times 10^5 \text{ m}^3/\text{day}$ at injection site B. This difference in sweeping efficiency results from the different range of petrophysical parameters considered in the two simulation sets. Due to the incorporation of a low range of petrophysical properties in simulation set-1, the injected CO₂ will encounter considerable restriction while percolating through the porous domain, hence reducing the lateral spread of CO₂ in the geological domain. As lateral spreading and plume displacement are minimal, the percentage of CO₂ trapped by structural and residual trapping will decrease over geological time. Due to the slow movement of the CO₂ plume, it will take time to explore the traps in the geological domain. This behavior is evident in **Figure 4.4B's** histogram plots, which depict the structural- and residual trapping percentage for a geological time at the end of the 3000th year.

The sweeping efficiency directly influences the percentage of entrapment recorded for structural and residual trapping, as represented in **Figure 4.4**. The CO₂ lateral movement (Sweeping efficiency) in simulation set-2 is observed to be higher than that of simulation set-1 because more CO₂ will percolate and explore more traps in the domain. As a result, the structural- and residual entrapment percentages are higher in simulation set-2 than in simulation set-1; these results are clearly illustrated in **Figure 4.4B**. Because of the low range of petrophysical properties in simulation set-2, the lateral movement of injected CO₂ is low in

the simulation domain, resulting in the movable plume dominating in the lateral years compared to simulation set-1. The minimal lateral movement of CO₂ in the geological sequestration process might affect the structural integrity of the geological domain due to the low range of petrophysical properties. Even if the geological storage of structural arrangement remains unaffected, the CO₂ will undergo solubility and mineral reaction in the region. If the dissolution reaction dominates the mineral reactions, it may weaken the injection well point and the surrounding region. If precipitation reactions dominate, decreasing porosity may have an impact on storage capacity.

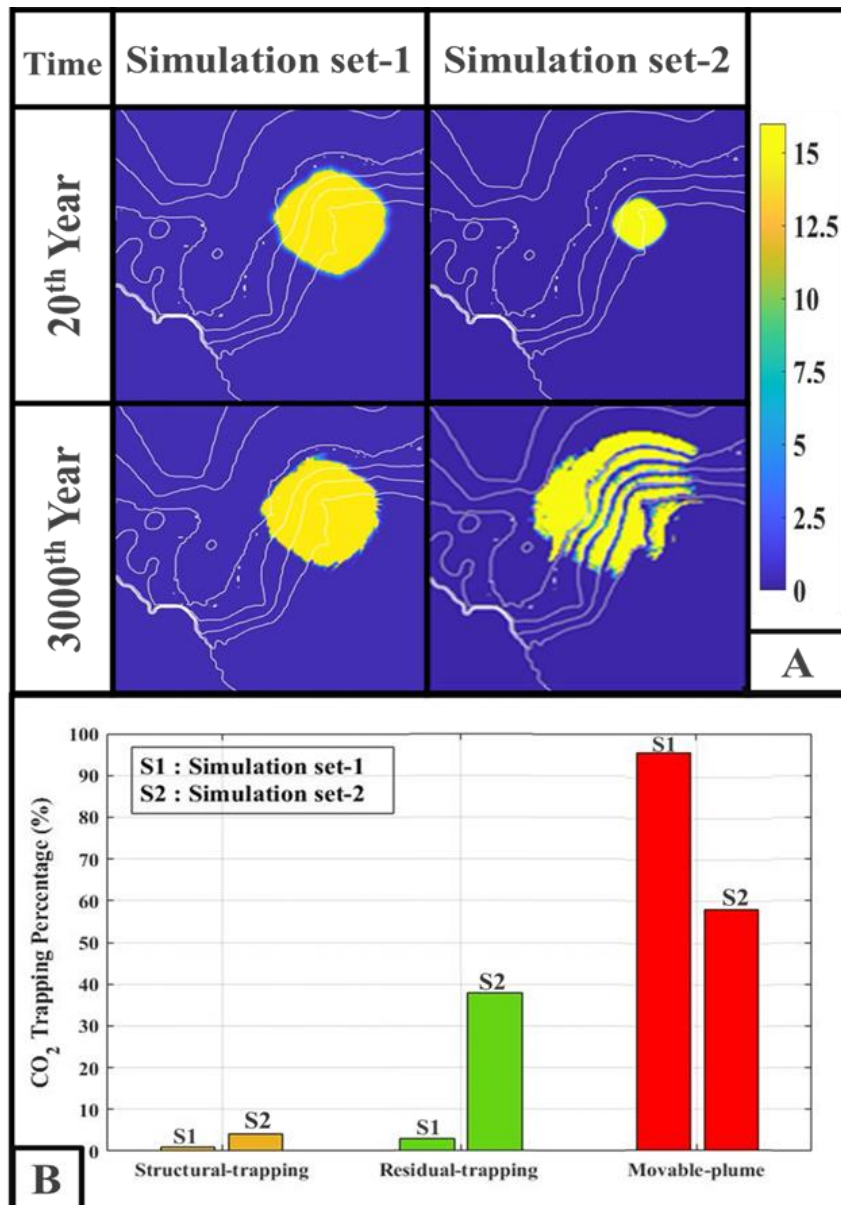


*Figure 4.4: A) Comparison of Sweeping efficiency for two distinct porosity and permeability ranges
 B) Comparison of Structural trapping, Residual trapping, and movable-plume percentages between the two petrophysical ranges [30].*

4.2.3 Influences of Injection Point Selection

The injection location significantly influences CO₂ sequestration in a geological domain. **Figure 4.5** illustrates the dynamic evolution of the entrapment of CO₂ during pre-injection and post-injection periods at each injection point. **Figure 4.5** reveals two insightful observations,

namely that the movable plume gradually decreases over geological time. In addition, structural and residual trapping are increasing over geological time. At each injection point, the progression of structural and residual trapping is in a different order. This distinction is a result of the topographical variation and injection site location [30].

To explain the effects of topographical variation, the modeled domain is divided into three parts: the flat bottom of the domain is the first part, the sloping traps are the second part, and the highest elevation of the structural domain is the third part. When CO₂ is injected at C, E, and F injection points at the highest elevation point, as shown in **Figure 4.6**, the trapping percentage is low due to the limited availability of migration pathways and traps, as shown in **Figure 4.5** [30].

To investigate the effects of the sloping traps, two injection points are chosen: one at the lowest point of the sloping traps (Injection point B) and another at the top section of the sloping traps (Injection point A). According to the results, the entrapment percentage recorded at injection point B is the highest of all injection points. When CO₂ is injected at the lowest point, it takes more time to migrate upwards, and the plume encounters a greater number of structural and residual traps than when the injection is carried out in injection point A. As a result, despite injecting on the sloping trap region, injection point A has a lower entrapment percentage than injection point B. When CO₂ is injected at the flat bottom (at injection point D), it does not migrate as far as it does at injection point B. The injection force has an enormous influence on the lateral spread of the CO₂ plume at injection point D. However, in addition to the injection force, the slope of the domain aids in achieving more migration and lateral spreading at injection point B [30].

By the end of the post-injection phase, the total entrapment percentage for A, B, C, and D injection points is also significantly higher than for E and F injection points. This is due to the

location of injection points and CO₂ plume migration in the synthetic domain. The injection point far from the anticline dome takes much longer in the migration, and as a result, the movable plume decreases over time. This significant observation implies that positioning the injection points near the sloping traps region results in a higher amount of trapping due to higher CO₂ migration. However, when CO₂ is injected at the top of the anticline, the lateral movement of the CO₂ plume decreases, resulting in a lower percentage of entrapment. From the preceding explanation, it is clear that topographical variation and injection point selection play a significant role in the implementation of CO₂ geological sequestration [30].

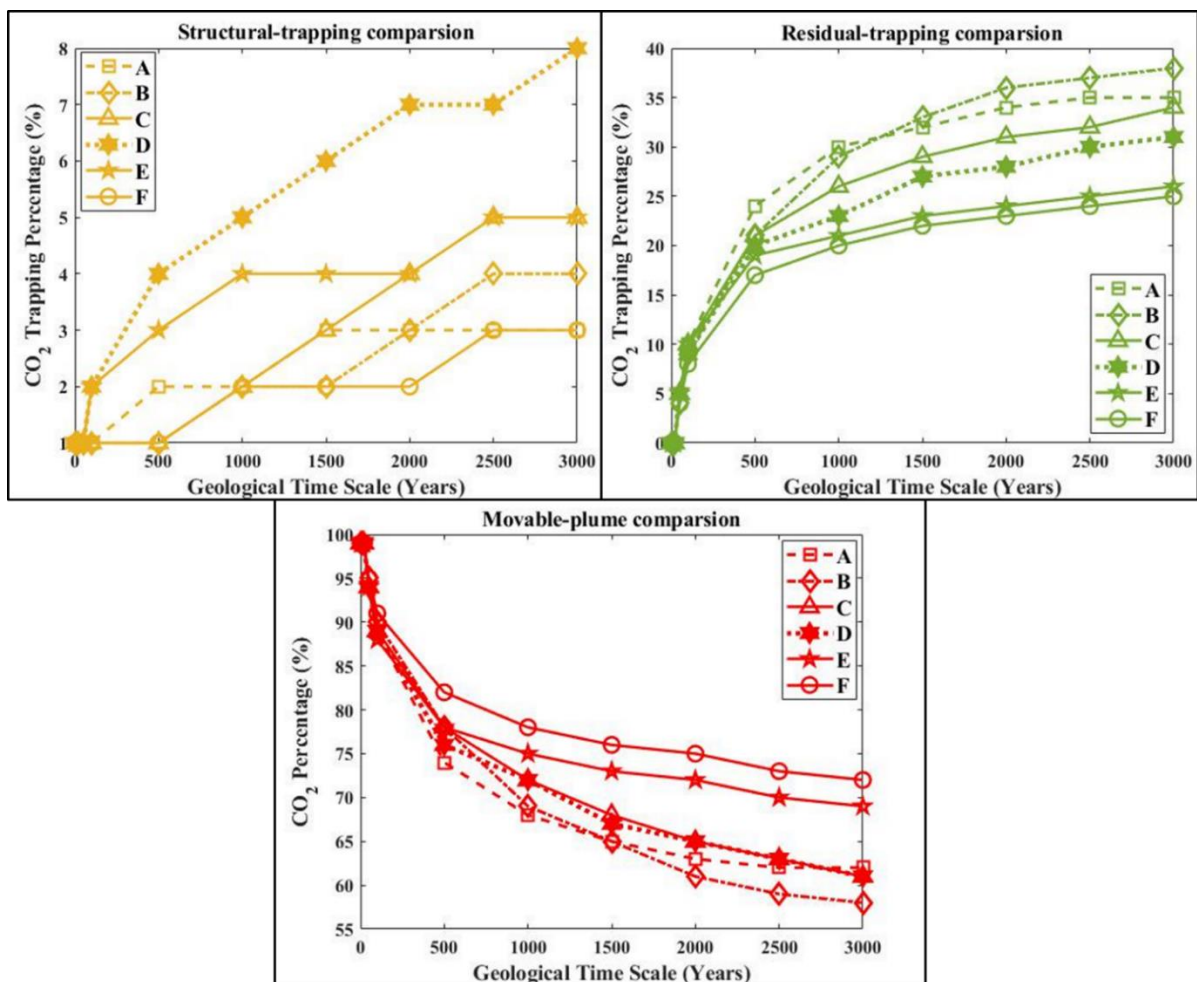


Figure 4.5: Dynamic evolution of Structural trapping, Residual trapping, and Movable plume when CO₂ is injected at A, B, C, D, E, and F injection points of the synthetic geological domain

[30].

The vast majority of the naturally accessible geological domains in the Deccan Volcanic Province are made up of geological stripes, also known as geological steps or traps. In the current synthetic computation domain, these stripes (all surface traps have been highlighted in white in **Figure 4.6**) are elevated in the direction of an enormous anticline dome, which also influences the sloping geological domain. Some CO₂ will be trapped in the geological steps during these CO₂ movements through the geological domain. The simulation outcomes of various injection points, as shown in **Figure 4.6**, illustrate that the CO₂ plume is travelling away from the injection site and towards the highest elevation point (highlighted dark red point); this suggests that the height of the anticline dome dominates the movement of the injected CO₂ through the sloping traps. When CO₂ passes through these sloping traps, a greater amount of CO₂ is expected to be trapped, ultimately benefiting the solubility- and mineral trapping mechanisms. These observations lead to the conclusion that topographic features such as slope and geological domain perturbation substantially affect the structural- and residual trapping mechanisms and CO₂ storage in the geological formation. These observations illustrate the significance of selecting a geological site based on geological configurations and topography [30].

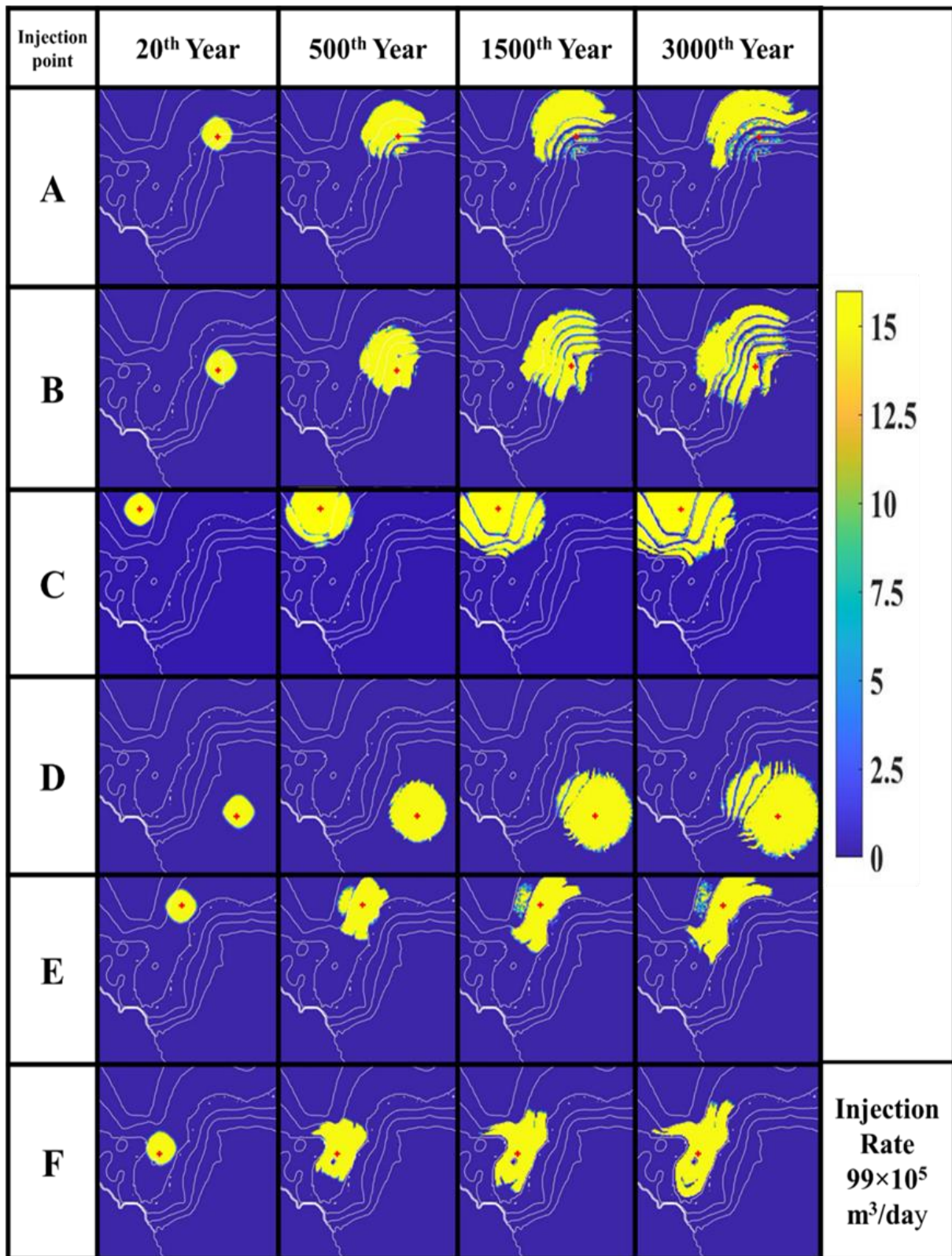


Figure 4.6: Geological topography has an impact on structural and residual entrapment. The diagram depicts the migration of CO₂ when it is introduced at various spots in the computation domain [30].

4.2.4 Influences of Injection Rate

Figure 4.7 depicts a histogram of the trapping percentage to comprehend the impact of injection rates on the geological domain. The results indicate that as the injection rate decreases, the percentage of entrapment does not change across all injection rates. In contrast, the residual trapping contribution increases while the movable-plume contribution is drastically reduced. Because the geological domain contains a finite number of traps, increasing the injection rate results in a greater quantity of CO₂ being injected into the domain. However, the geological domain can only trap a finite amount of CO₂ plume. The remaining portion of the plume will move freely within the domain. As a result, as the injection rate decreases, a slight upward trend in the trapping percentage is observed, whereas the movable plume declines [30].

The structural- and residual trapping mechanisms play an essential role in facilitating the interaction with the aqueous phase for solubility- and mineral trapping mechanisms in CO₂ sequestration. As a result, more structural- and residual trapping than movable-plume at any time for any point of injection represents favorable CO₂ sequestration, see **Figure 4.5** and **Figure 4.7** [30].

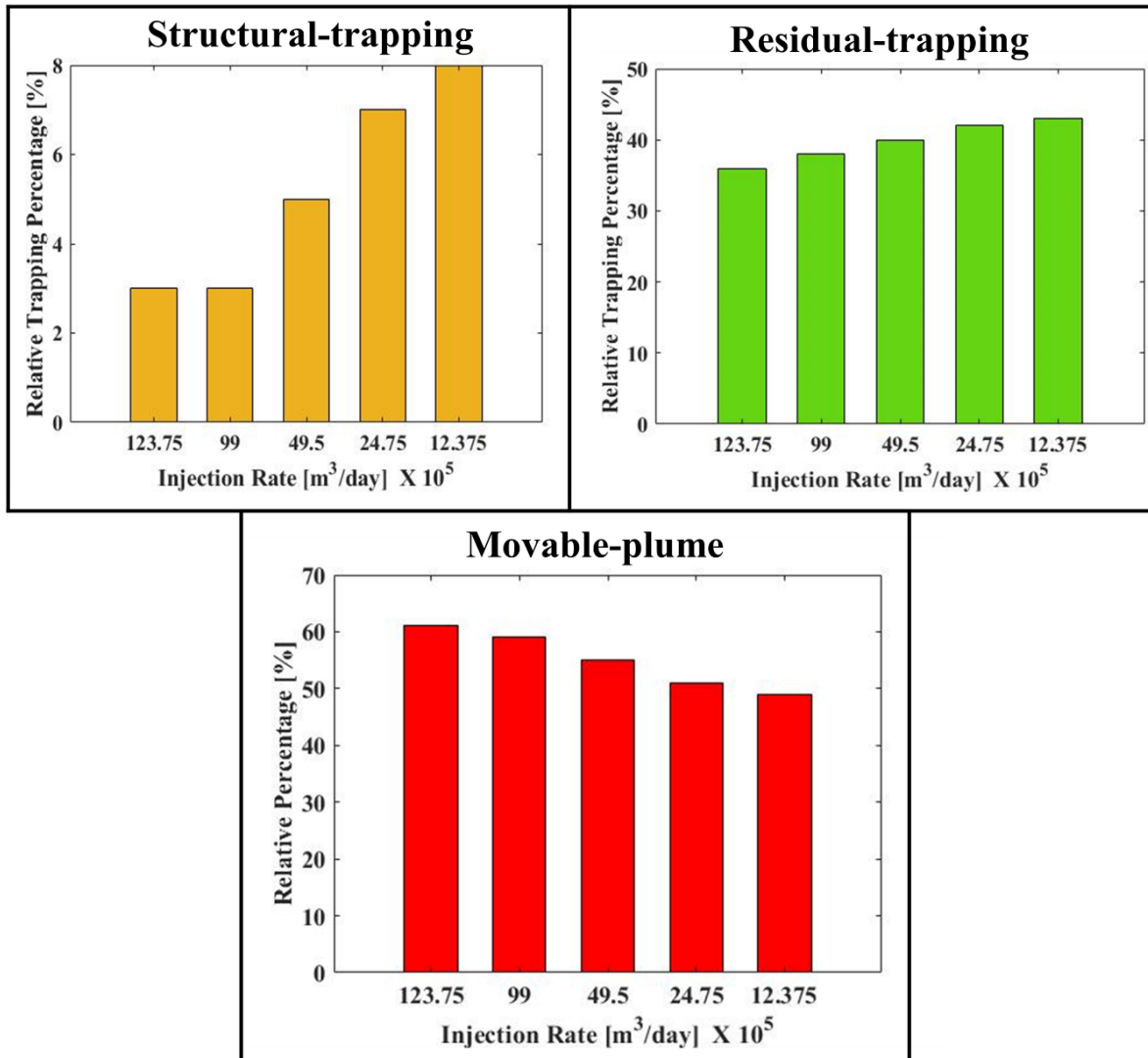


Figure 4.7: Illustration of Structural trapping, Residual trapping, and Movable-plume at injection points B and C for varying injection rates $123.75 \times 10^5 m^3/day$, $99 \times 10^5 m^3/day$, $49.5 \times 10^5 m^3/day$, $24.75 \times 10^5 m^3/day$, and $12.375 \times 10^5 m^3/day$ [30].

4.3 Investigation of Solubility Trapping Mechanism in CGS

The solubility-trapping mechanism is a crucial aspect of CO₂ geological sequestration, contributing significantly to the safe disposal of injected CO₂. When CO₂ is injected, it forms a stable plume under the injection pressure and migrates upwards, spreading laterally beneath the impermeable caprock. During this process, a thin interface layer gradually develops between the CO₂ plume and the reservoir water as CO₂ dissolves into the water. Once this

interface layer reaches a certain thickness, fluid channelling occurs. These channelling effects arise due to density differences between the CO₂-dissolved water and reservoir water, leading to diffusive convection within the pore space [213], [214].

This convective movement gives rise to a geological anastomosing pattern called the solubility fingering phenomenon. Here, dissolved CO₂ fluid moves downwards due to gravitational forces acting on the higher-density fluid, causing the CO₂ plume to come into contact with fresh water. Consequently, more CO₂ dissolves into the subsurface domain. This convective process continues to enhance solubility-trapping until the pH and density of the formation domain reach equilibrium [213], [214].

After dissolving in the reservoir water, the CO₂ readily engages in CO₂-Water-Rock interactions with the surrounding rock. This interaction sets off a sequence of geochemical reactions that ultimately lead to the trapping of CO₂ in the subsurface through a mineral-trapping mechanism [198, 199]. In the mineral-trapping process, the formation rock undergoes several geochemical reactions with the neighbouring CO₂ and reservoir water. Detailed coverage of this mineral trapping phenomenon can be found in the subsequent section of the present chapter.

The percentage of solubility trapping directly impacts the efficiency of mineral trapping, thereby influencing the overall effectiveness of Carbon sequestration technology. Hence, the phenomena of solubility trapping play a significant role in enhancing CO₂ geological storage. Continued research and investigation into these mechanisms are essential to further advance the field of CO₂ sequestration and ensure its successful implementation.

In this simulation analysis, it is assumed that no mineral reactions occur within the domain. The focus is solely on the dissolution of injected ScCO₂ and the resulting pH fluctuations. To achieve this, all the multiphase flow equations (**Table 3-1: Eq. 3.1, 3.2, and 3.12**), along with

the Auxiliary equation (**Table 3-1: Eq. 3.6, 3.8, 3.9, and 3.10**), are solved. In the context of multicomponent reaction transport equations (**Table 3-1: Eq. 3.13, 3.14, and 3.15**), the mineral reaction terms are considered inert, indicating that no mineral reactions take place. Consequently, petrophysical parameters such as porosity and permeability remain static across geological time due to the absence of the mineral trapping process.

The effects of geological and sequestration parameters, such as petrophysical properties and caprock morphology, on the solubility trapping mechanism were investigated in this current section of simulation analysis. Two synthetic domains with two distinct ranges of petrophysical properties were considered to assess the influences of petrophysical properties. Four injection points were chosen at distinct parts of the synthetic geological domain to explore the impact of caprock shape on CO₂ plume migration and sweeping efficiency at these injection locations of the synthetic geological domain, see **Figure 3.2C**. This simulation study also gives insight into the selection of injection locations with a suitable range of petrophysical parameters to perform CGS safely, considering solubility trapping [111].

It should be noted that no flow boundary conditions are applied to the top and bottom faces of the domain, which effectively act as impermeable layers. This setup ensures that the injected CO₂ is prevented from escaping the domain during vertical migration. In the simulations, the Neumann boundary conditions are applied. For simulation purposes, the density and viscosity of water considered are 975.86 kg/m³ and 0.3086 × 10⁻³ Pa.s, respectively, whereas those of CO₂ considered are 686.54 kg/m³ and 0.0566 × 10⁻³ Pa.s, respectively.

4.3.1 Comparison between Primary and Solubility trapping mechanisms

Two simulation sets are considered in the base case scenario. Only primary trapping mechanisms, such as structural and residual trapping, are considered in the first simulation set. The solubility trapping mechanism, in addition to the structural- and residual trapping

processes, is considered in the second simulation set. The CO₂ injection was performed at injection point B, as shown in **Figure 3.1C** and **Figure 4.8A**. At the same time, the variation of petrophysical properties, which was illustrated in **Figure 3.2D**, is considered for both simulation sets. With a volumetric injection rate of $77.2 \times 10^3 \text{ m}^3/\text{day}$, with a cyclic injection manner. The injection was carried out over the first 80 years, with a one-year interval between injections, while the remaining 2920 years were set aside for post-injection analysis.

The simulation's injection rate was determined by considering the tensile and compressive strength of the Deccan basalt. If the injection rate is too high, pressure may build up in the targeted location, resulting in structural integrity failure. The strength of Deccan basalt varies depending on location; tensile strength ranges from 12 to 20 MPa [215], and uniaxial compressive strength is roughly 80 MPa [215], [216].

After the injection of CO₂ into the domain, it has been found that the CO₂ plume tends to rise due to the buoyancy effect. Due to the presence of structural elevation, the CO₂ plume migrates in the direction of the elevation of the domain. As soon as the CO₂ plume reaches the top caprock, its upward motion will be impeded since the surface is impermeable. Then, it spreads in a lateral direction parallel to the impermeable layer.

During the injection period, the injection force acts on the CO₂ plume, increasing CO₂ plume movement in the migration pathway while decreasing residual trapping in the synthetic domain. When the injection into the domain stopped, the injection force on the CO₂ plume gradually faded away, resulting in CO₂ confinement in the migratory pathway and structural traps. Furthermore, structurally trapped CO₂ and CO₂ contained in the migration pathway would dissolve in the surrounding reservoir water, contributing to solubility trapping. **Figure 4.8A** depicts the top view of the synthetic domain, where the CO₂ saturation on the domain's top can be observed. **Figure 4.8A** and **Figure 4.9** show that following the injection, CO₂ moved

towards the highest elevation zone from the injection location. The saturation profile results reveal that the direction of CO₂ migration in the domain is comparable in both simulation sets. However, due to the addition of solubility trapping in simulation set-2, the saturation of CO₂ on top of the domain is lower than in simulation set-1. **Figure 4.8B** shows that the structural trapping observed was low compared to residual trapping over the geological time scale. Because the injected CO₂ spends a significant portion of its time migrating towards the elevation formed by the stairsteps trap, and only a small portion of the CO₂ is trapped in the stratigraphic traps. Even at the end of the simulation time, the CO₂ plume is still migrating through the domain's stairsteps traps. The residual trapping percentage may grow even after the injection is stopped in the domain.

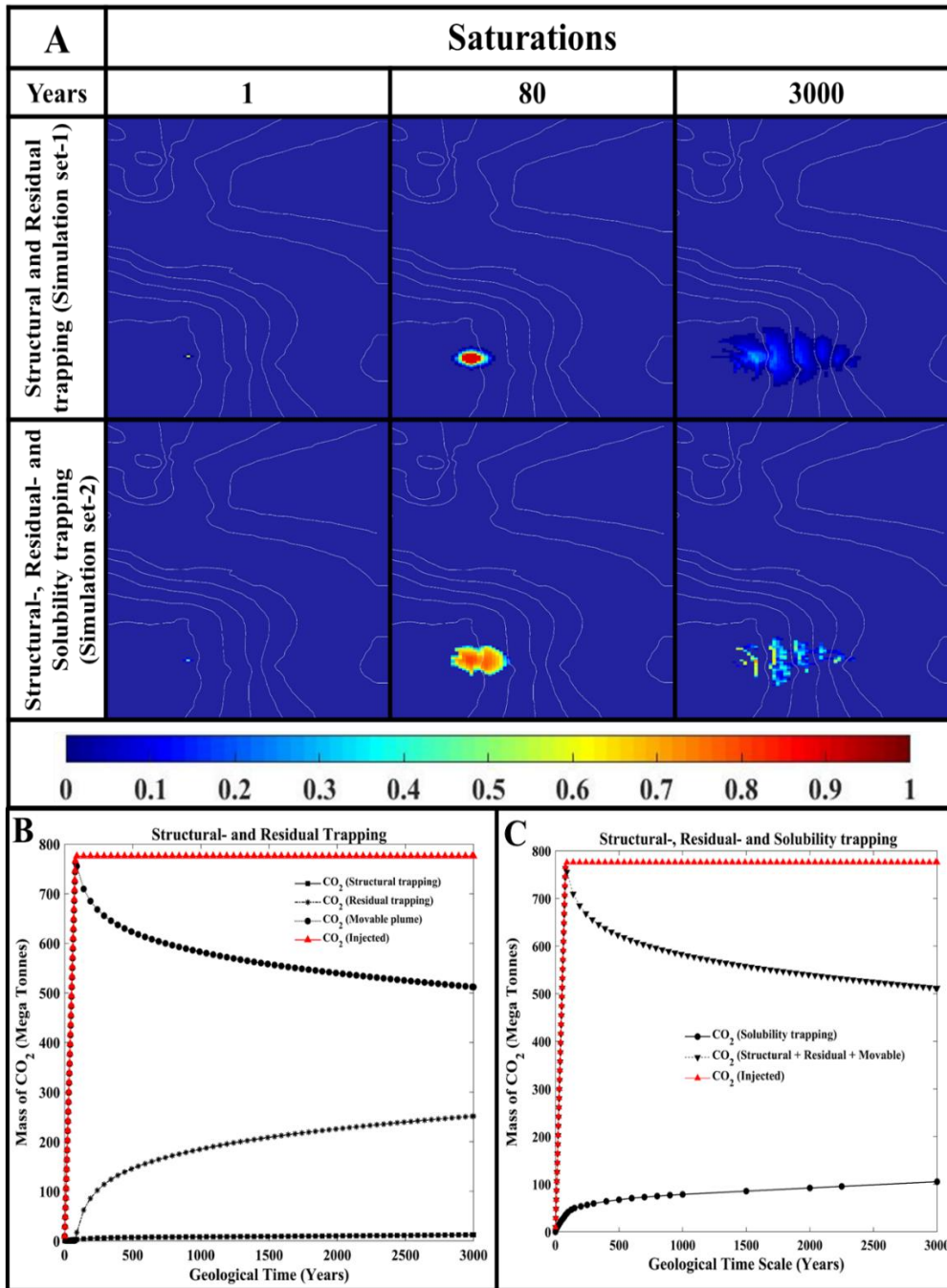


Figure 4.8: (A) Comparison of CO₂ saturation for two simulation sets, (B) Structural-, Residual trapping and Movable plume percentage variation, and (C) Structural-, Residual-, Solubility trapping and Movable plume percentage variation over geological time scale [111].

Figure 4.9 depicts the variation in liquid CO₂ mole fraction in the domain for both simulation sets. The injected CO₂ plume can be noticed traveling towards the domain's highest elevation region in both simulation sets. The solubility fingering phenomenon can be observed in

simulation set-2 due to the consideration of geochemical reactions, as illustrated in **Figure 4.9**. Due to the exclusion of the geochemical reactions, no solubility fingering phenomena are visible in simulation set-1. The instability between the fluid densities caused the solubility fingering phenomenon, which resulted in convection mixing in the domain. During the post-injection phase, CO₂ migration to higher elevations improved sweeping efficiency. In addition, the gradual decrease in the momentum of the CO₂ plume increases the contact duration between CO₂ and water, leading to an increase in CO₂ dissolution and solubility trapping in the domain; see **Figure 4.8C** and **Figure 4.9**. The first appearance of solubility fingering in simulation set-2 was detected at the 1500th year, and solubility fingering increased in the domain by the end of the simulation duration (3000th year).

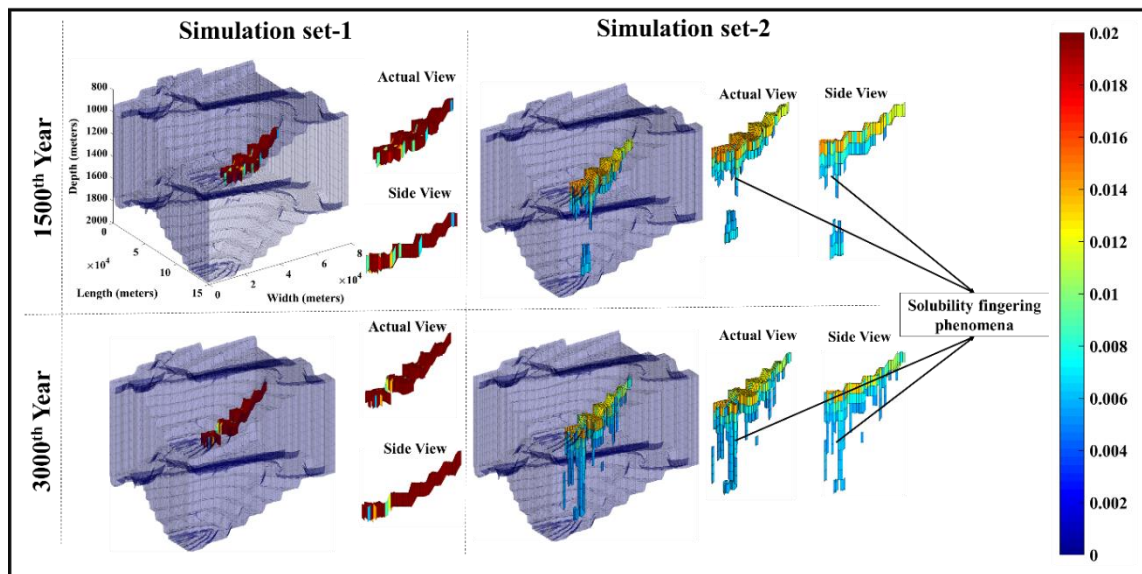


Figure 4.9: Comparison of CO₂ mole fraction in both simulation sets at 1500th and 3000th year.

This result illustrates the solubility fingering phenomena observed in simulation set-2. In the 1500th year, the first sight of solubility fingers was observed in simulation set-2 [111].

4.3.2 Influence of Heterogeneity –Petrophysical properties

This section investigated the influence of geological domain heterogeneity resulting from variations in petrophysical properties. The influence of two distinct ranges of petrophysical

properties on the solubility trapping for the same caprock morphology and structural features was investigated. This simulated research will better understand the CO₂ plume movement, sweeping efficiency, and structural integrity of the geological domain during CO₂ sequestration. In this investigation, two synthetic domains with distinct petrophysical properties are considered. As depicted in **Figure 3.2D**, one synthetic model has a porosity ranging from 0.2 to 0.4, while the permeability ranges from 10 to 1500 mD. The simulation on this synthetic domain will be referred to as Simulation set-1. In another model, the range of porosity and permeability are 0.05 to 0.1 and 1 to 10 mD, and the simulation on this synthetic domain will be referred to as Simulation set-2. In both simulation sets, the mechanism of solubility trapping is considered. Using the Gaussian function in MATLAB, arbitrary petrophysical properties are assigned to the synthetic domain grid cells. The remaining simulation parameters are identical to the previous section.

Figure 4.10A depicts the CO₂ mole fraction variation and pH variation findings in the simulated domain for both simulation sets across a geological time scale. The CO₂ plume in simulation set-2 was more resistant to CO₂ spreading in the synthetic simulation domain than the CO₂ plume in simulation set-1. This resistance to CO₂ movement in the domain is attributable to the simulation set-2's inherent low range of porosity and permeability. Because of the slow migration of CO₂ in the reservoir, the contact time for CO₂-water interaction was quite long. The synthetic domain's reservoir pressure has also increased due to the CO₂ injection in the lower porosity domain. This increase in contact duration and reservoir pressure would eventually favor faster CO₂ dissolving into the reservoir water. As a result, solubility in simulation set-2 has revealed a more significant amount of CO₂ to dissolve in the in-situ reservoir water than in simulation set-1. The CO₂ solubility trapping results in **Figure 4.10B** support these findings. Although the solubility trapping reported in simulation set-2 is greater than that recorded in simulation set-1, it is assumed that simulation set-1 contains the requisite

range of petrophysical parameters. Because the average reservoir pressure recorded in simulation set-1 is lower than that recorded in simulation set-2, this may be helpful in terms of structural integrity and safe CO₂ storage.

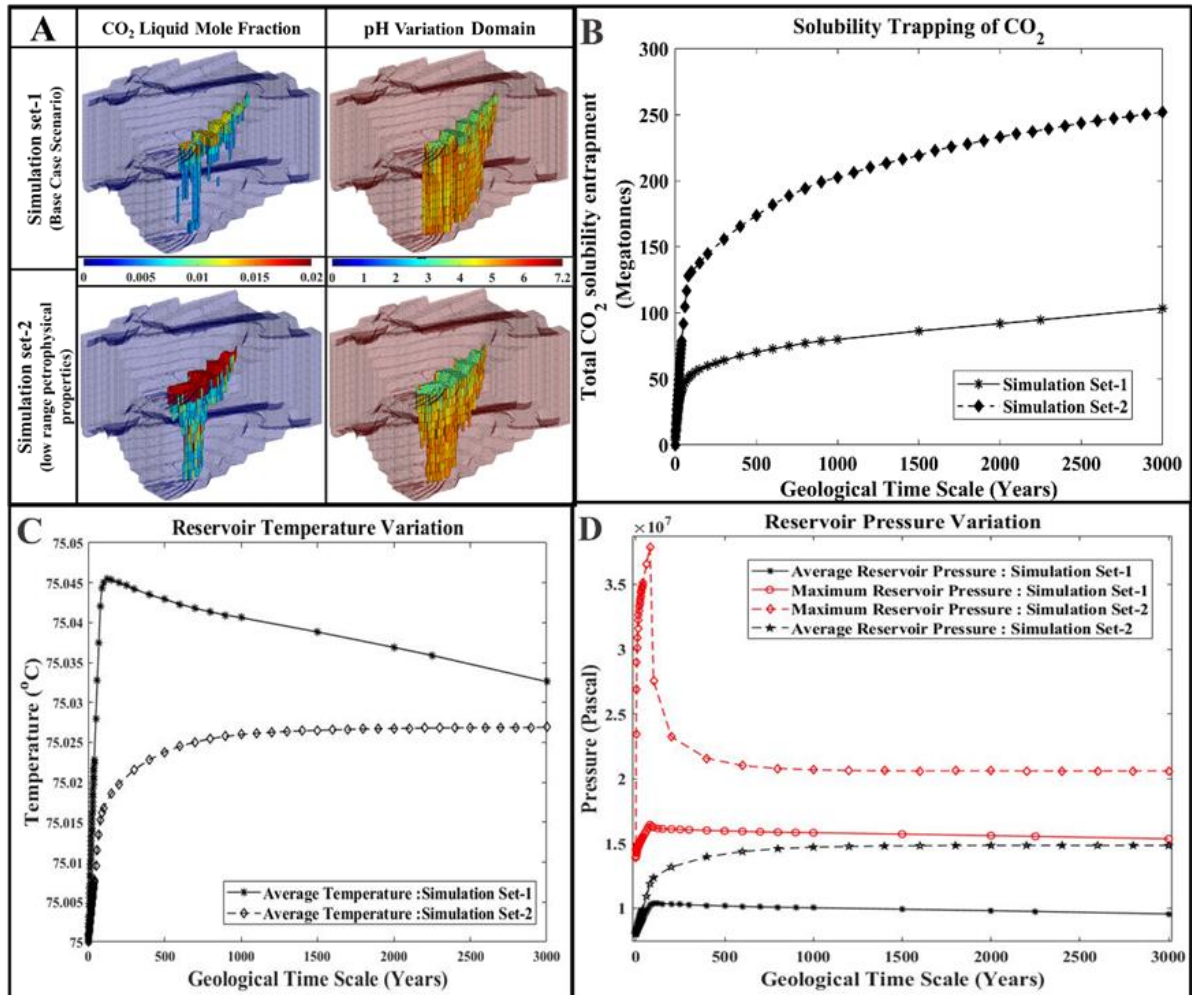


Figure 4.10: (A) Illustration of the CO₂ liquid mole fraction migration and pH variation at the end of simulation time (3000th year), (B) Total CO₂ solubility trapping, (C) Reservoir pressure variation, and (D) Reservoir temperature variation for two simulation sets over geological time scale [111].

As shown in **Figure 4.10D**, the average reservoir pressure obtained in simulation set-2 is approximately 33% higher than what was observed in simulation set-1. As a result of the CO₂ injection, the average pressure in the reservoir shoots up during the injection time in both simulations. However, in simulation set-2, because of the low porosity and permeability range, the pore pressure of the reservoir will be high. This, in turn, adds to the normal reservoir

pressure being higher than it would have been without the injection pressure. Because of this, it is clear that the average pressure in the reservoir during simulation set-2 was significantly higher than the pressure during simulation set-1 (see **Figure 4.10A**). On the other hand, there was hardly any difference in the average temperature of the reservoir between the two different simulation sets (see **Figure 4.10C**).

Figure 4.10A depicts the effects of petrophysical properties on the synthetic domain. In the findings of both simulation sets, a certain domain volume was covered by a low pH range. This drop in the simulation domain's pH range indicates both solubility trapping and solubility fingering. The pH range observed was between 3 and 6, considered optimum for triggering mineral dissolution, and at lateral, once the alkaline pH range returns, the mineral precipitation reaction takes place within the domain and contributes directly to the mineral trapping mechanism [69]. In simulation set-1, a more significant proportion of the simulated domain was covered by a lower pH range than in simulation set-2. As the low pH zone increases, more aqueous CO₂ produced during the solubility trapping phase will be consumed during the mineral trapping period, minimizing the danger of CO₂ injection.

4.3.3 Influences of Injection Point Selection

In order to investigate the impact of the selection of injection points on the solubility trapping mechanism on the various sections of considered caprock morphology, four injection points located in different parts of the synthetic domain are taken into consideration. These injection points are spread out across the synthetic domain. These specific injection point locations were chosen in order to provide intuition into various positions and sections of the synthetic geological domain that was being considered. **Figure 3.2C** shows that injection point A can be found on the stairsteps traps, injection point B can be found on the bottom of the stairsteps traps, injection point C can be found on the top surface of the synthetic domain, and injection

point D can be found on the top of the stairsteps trap. Injection point A has a coordinate of (38273, 127914, 1584), Injection point B's coordinates are (22158, 126907, 1452), Injection point C's coordinates are (51367, 35252, 1474), and Injection point D's coordinates are (69496, 92662, 1166). It is assumed that the parameters for the CO₂ injection will be the same as those for the previous section. These simulation results have highlighted the critical role of selecting an injection point site in CO₂ geological sequestration (CGS). When the appropriate injection points are chosen at a specific section of the domain, it is possible to enhance the amount of CO₂ that can be stored within the domain, and it is also possible to lessen the worries regarding the structural integrity that will occur during the process of CO₂ sequestration.

Figure 4.11 depicts the domain's CO₂ mole fraction and pH fluctuation for all injection locations. The sweeping efficiency for injection point B was found to be high in this simulation analysis. Because the increased sweeping efficiency makes the contact area between CO₂ and water more prominent, this results in more CO₂ dissolving into the domain. As a result, the CO₂ solubility trapping for the B injection point was more pronounced when compared to the other injection points; see **Figure 4.12A**. **Figure 4.11** depicts the sweeping efficiency and migration of the CO₂ plume in the domain for all injection points. The effects of CO₂ dissolution at all injection points are shown in the pH fluctuation in the domain (see **Figure 4.11**). Injection point B covers most of the domain volume with a low pH range, followed by injection points A and C. The low pH will enhance the dissolution of CO₂ in the domain. Subsequently, when the pH returns to an alkaline level, mineral reactions occur, leading to the precipitation of carbonate minerals. The dissolution and precipitation of minerals, following solubility trapping, can impact the porosity and permeability of the formation domain, thereby influencing the flow path of the CO₂ plume.

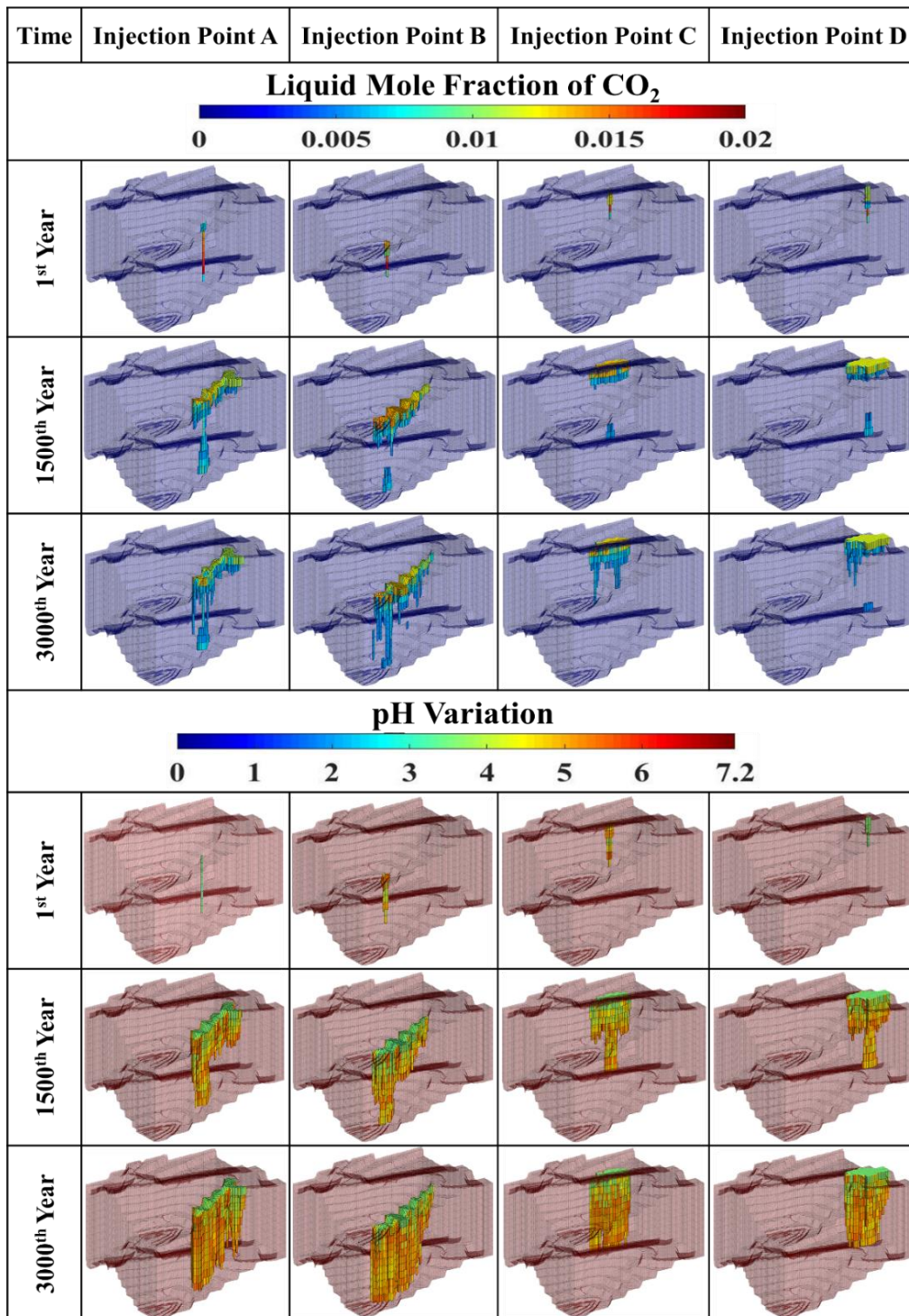


Figure 4.11: Illustration of the CO₂ liquid mole fraction migration and pH variation at 1st, 1500th, and 3000th year. In the 1500th-year result, most of the injection points displayed solubility fingering

[111].

Figure 4.12A depicts the outcomes of CO₂ solubility entrapment, which indicates that at the end of the simulation duration (3000 years), the B injection point recorded a larger CO₂

solubility entrapment. By picking the injection point in the bottom portion of the traps, the injected CO₂ will tend to rise due to the elevation of the stairsteps traps. Due to the injection force, this motion would be rapid during the injection period. Consequently, the contact time between CO₂ and water during the injection phase would be limited. After ceasing injection, however, CO₂ migration would gradually decrease, promoting CO₂ sequestration. This is why CO₂ solubility trapping was lower during the first injection phase and higher during the post-injection period. **Figure 4.12A** demonstrates that during the post-injection period, the dissolution of CO₂ at injection point B was greater than at other injection points due to decreasing momentum, rapid sweeping, and longer contact time.

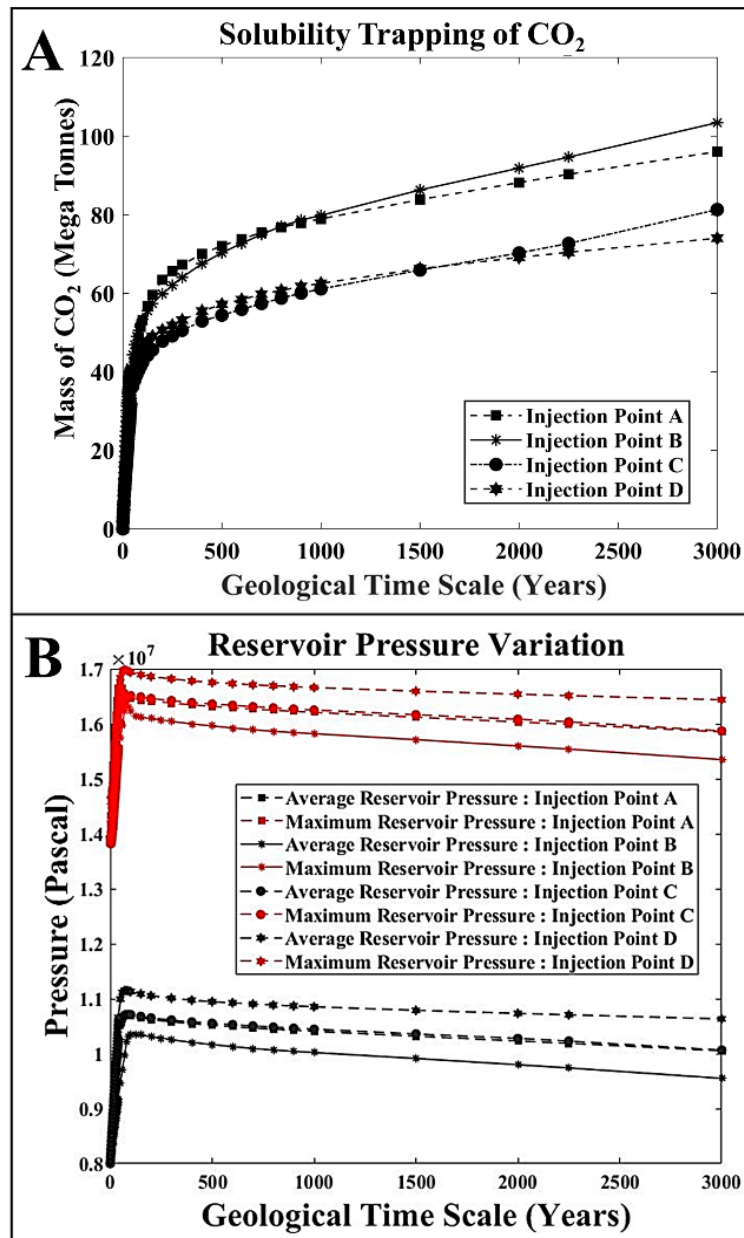


Figure 4.12: (A) Total CO₂ solubility trapping and (B) Reservoir pressure variation for all injection points over a geological time scale [111].

By studying the results depicted in **Figure 4.12B** for reservoir pressure, injection point B at the bottom of the stairsteps traps proved to be the superior injection point. Maximum and average reservoir pressure results for injection site B were within the reasonable limit. The pressure in the natural reservoir increases with depth. Even if injections were performed in the lower region of stairsteps traps, the pressure did not rise by more than 5% compared to other injection points.

This may be the result of the quick upward migration of the injected CO₂ plume and increased CO₂ plume spreading, which results in the rapid equilibration of injection pressure with normal reservoir pressure. **Figure 4.12B** demonstrates that the pressure increases until the end of the injection time; following the injection period, the pressure stabilizes at the reservoir pressure and declines gradually. All injection points exhibit the same trend, as observed.

In this simulation study, a multicomponent reactive transport equation integrated with a multiphase flow equation is used to model the solubility trapping process. This is accomplished by incorporating only CO₂ dissolving in resident water in the simulation analysis. In the subsequent step, a simulation of combined structural, residual, solubility and mineral trapping processes is carried out by including both the solubility reactions and the mineral speciation reactions for the simulation analysis.

4.4 Investigation of Mineral Trapping Mechanism in CGS

A simulation model is established by taking major flooded basalt minerals into the domain. It is necessary to thoroughly study and analyze the mineral volume fraction over the geological time scale in order to conduct an analysis of the mineral reactions that occur during the process of CO₂ sequestration in the domain. The minerals considered in this simulation analysis are obtained from Kumar & Shrivastava [118]. A total of nine minerals are considered in this simulation: Albite, Anorthite, Aragonite, Calcite, Clinocllore-14A, Diopside, Dolomite, Quartz, and Saponite. The modeled synthetic domain consists of irregularity and heterogeneity, which resemble the naturally available sub-surface domain. The temperature and pressure of the domain are maintained at 75°C and 85 bars. The total amount of injected CO₂ is 774.6 metric megatons at the rate of 38.7 metric megatons at every one-year relaxation for every one year of injection for up to 40 years. The simulation results were analyzed for up to 2000 years. The petrophysical properties considered for formation domains are in the range of 20-40 %

porosity and 10 - 1500 mD of permeability, see **Figure 3.2D**. The pH was initiated at 5 before the simulation started; after initiation, the pH increased to around 6. The mean pH of the domain was maintained at about 6.2 pH.

Figure 4.13 results show that the migration and momentum of the CO₂ plume along the caprock are slow due to the top surface topography and petrophysical property variation. This heterogeneity helps the CO₂ plume to have low momentum, which will increase the reactive time and further increase the consumption of injected CO₂ through mineral reaction held during the mineral trapping period (see **Figure 4.13**).

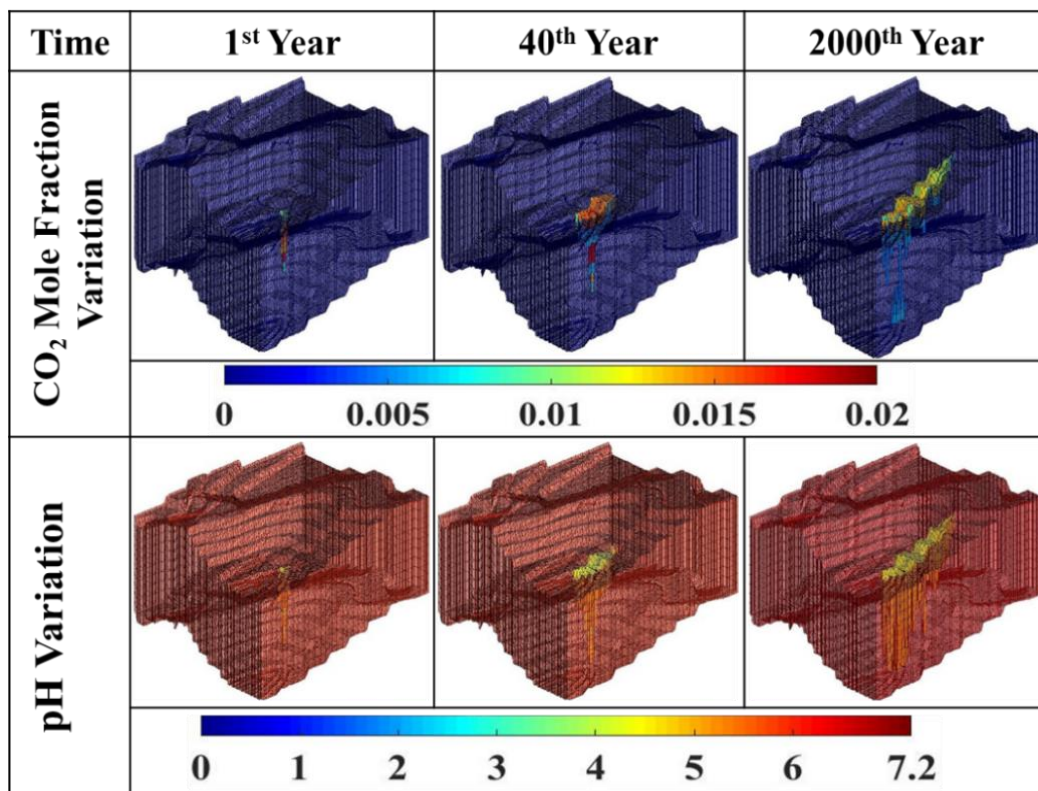


Figure 4.13: Illustration of the CO₂ liquid mole fraction migration and pH variation in the 1st, 40th, and 2000th year.

At the migration pathway, where the CO₂ plume moves in bulk in the pure supercritical state, the pH is reduced to 5.4 from 6.2 (see **Figure 4.13**). The change in the mineral volume fraction was observed in this migration pathway; it means that mineral reactions are happening in the

migration pathway (see **Figure 4.13**). This indicates that the weak carbonic acid formed during the initial interaction of the CO₂ plume with water contributes to the mineral reactions. **Figure 4.14** shows that the calcite mineral precipitates at a higher rate in the synthetic domain, followed by the dolomite. In contrast, Aragonite dissolves at a greater pace compared to other minerals in the synthetic domain. Chinochlore-14A and diopside minerals have minimal volume fraction variation; quartz and saponite-Ca are negligibly reactive. The porosity change in the domain is calculated by considering the volume fraction of the minerals; the porosity change results have not shown much variation. The obtained simulation results show that the change in mineral volume fraction is observed at a more commendable rate during the higher pH range of the domain. This conclusion from the simulation analysis has gained substantiated support from experimental research conducted by some researchers acquired from the literature study. N. Rani et al., [217] led the experimental research on the basalt samples collected from the Mandla lobe of the Eastern Deccan Volcanic Province. The experiments were conducted at the initial conditions of 5 and 10 bar CO₂ pressure and 100 °C and 200 °C temperatures. It was observed that the secondary minerals were formed for the sample treated at 5 bar and 100 °C for the duration of 70 and 80 hours. The secondary minerals observed were Calcite, Magnesite, Siderite, and Aragonite. This basalt alteration and secondary mineral formation were detected by using X-ray powder diffractograms (XRD). A similar kind of study was referred to by N. Rani et al., [217] and carried out by A. P. Gysi et al.,[218]. This study was conducted on the basalt samples collected at the Stapafell and Vellankatla of Iceland. The experiments were conducted for the three different temperatures with varying initial dissolved CO₂ concentrations. The considered temperatures were 75 °C, 150 °C, and 250 °C. This research stated that a temperature below 100 °C and an alkaline pH range for basalt rocks is suitable for implementing the CGS [218]. From this simulation analysis and literature study, it is

understood that an initial alkaline range pH range and temperature below 100°C are preferable conditions to attain good mineral trapping in basalt rock.

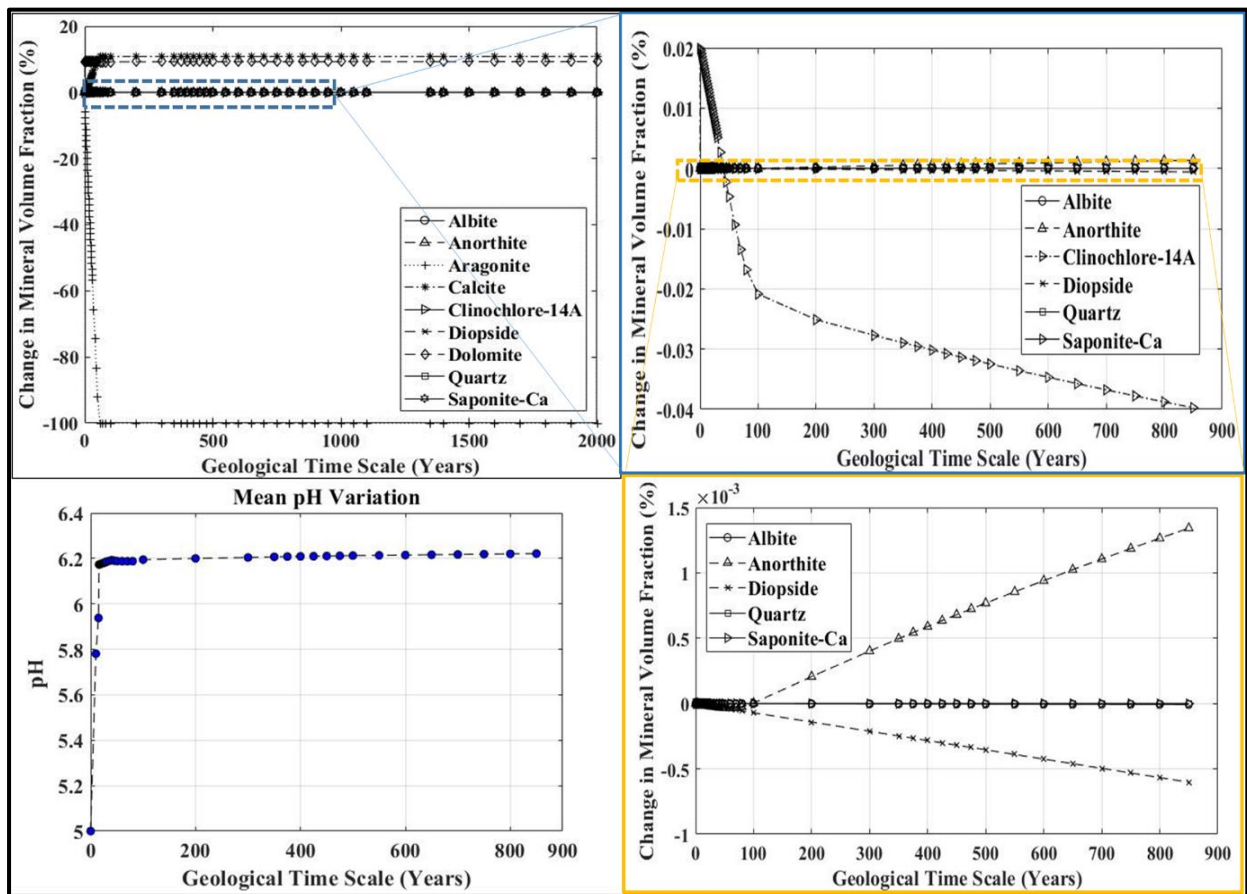


Figure 4.14: The figure illustrates the results of dynamic mineral volume fraction evolutions

4.5 Summary

The chapter investigates factors influencing trapping efficiency in the Deccan Volcanic Province for CO₂ geological Sequestration. CO₂ sequestration simulations are conducted on Deccan traps of the Saurashtra region in India. The investigation is carried out by modeling the synthetic domain of Deccan traps obtained from the literature [201]. In **Section 4.2**, Primary trapping mechanisms, i.e., structural and residual trappings, are investigated to elucidate the multiphase flow patterns of CO₂ and water. The base case scenario is initially presented by injecting CO₂ with an appropriate injection rate at a predetermined injection point. Based on the simulation findings, the structural- and residual trapping percentages are analyzed and

studied for the different parametric variations such as injection point, injection rate, and petrophysical parameters. The analysis presented in this research primarily concerns the effects of geological characteristics such as topography, petrophysical properties, and injection point selectivity on improving structural- and residual trapping mechanisms. This research will provide an understanding of events throughout geological time scales influenced by subsurface topography and the lateral flow of injected CO₂ in a sizeable geological area with top surface perturbations and anticline structure. This simulation investigation has provided insight into the structural- and residual trapping dependence on the geological and sequestration parameters.

In **Section 4.3**, The solubility trapping mechanism, involving CO₂ dissolution in water and migration through the rock formation, is investigated and compared to primary trapping mechanisms. Solubility trapping entrapment depends on sweeping efficiency and primary trapping mechanisms, while petrophysical property variations affect reservoir pressure distribution and structural integrity. Petrophysical property heterogeneity and injection point selection are analyzed for their effects on solubility trapping efficiency.

In **Section 4.4**, the mineral trapping mechanism involving geochemical reactions between CO₂ and minerals in the rock formation is explored as another potential mechanism for safe CO₂ storage. The investigation of the mineral trapping mechanism needs further investigation that includes i) the comprehensive mineralogy of Deccan traps and ii) high computation times to understand the CO₂ and mineral interactions over an expanded geological time scale.

Key results show that natural reservoir perturbations and top surface morphology affect CO₂ movement and entrapment percentages in structural and residual trapping. The presence of stairsteps landscape in Deccan traps provides advantages for safe CO₂ trapping over an extended period. Injection point selection near the stairsteps exhibits higher integrity compared

to other points. Increasing injection rates decrease structural and residual trapping entrapment due to finite trap availability. Petrophysical properties significantly impact sweeping efficiency. Mineral trapping reveals slight changes in porosity, lower pressure build-up compared to solubility trapping, and different precipitation and dissolution rates for various minerals. Chinoclone-14A and Diopside show minimal variations in volume fractions, while Quartz and saponite-Ca exhibit negligible reactivity.

This chapter investigated different trapping mechanisms in the Deccan Volcanic Province, including structural, residual, solubility, and mineral trapping mechanisms. It provided valuable insights into trapping mechanisms and their influencing factors, contributing to the development of effective CGS strategies in Deccan volcanic basalt formations. The following chapter examines the role of caprock morphology and structural integrity in the solubility trapping mechanism.

**CHAPTER 5: Investigating the Role of Caprock
Morphology and Structural
Integrity on the Solubility
Trapping Process**

5 Investigating the Role of Caprock Morphology and Structural Integrity on the Solubility Trapping Mechanism

5.1 Introduction

In the preceding chapter, a comprehensive understanding of solubility trapping was presented. The visualization of CO₂ entrapment within the domain has given insight into the significance of solubility fingering phenomena in enhancing overall CO₂ entrapment. Moving on to the present chapter, the focus is shifted to examining the impact of caprock morphology and its integrity on CO₂ plume sweeping and migration beneath it. The analysis and investigation of caprock morphology help understand its role in influencing CO₂ movement and distribution and further influencing the entrapment of CO₂ in the domain, especially during the presence of cracks in the caprock. This in-depth analysis of caprock morphology and its influence on CO₂ movement and entrapment contributes valuable insights to the broader understanding of effective CO₂ sequestration strategies linked to the selection of injection sites and structural integrity of caprock.

The comprehensive analysis begins with the modeling of synthetic domains, allowing the examination of different scenarios and facilitating an investigation into the impact of caprock morphology on solubility trapping efficiency (**Section 5.2**). Next, a comparison between primary trapping and solubility trapping mechanisms is conducted in the base case scenario to understand their relative contributions to long-term CO₂ storage (**Section 5.2.2**). Solubility fingering phenomena involving the dissolution of CO₂ in water and its migration through the pore spaces of the rock formation are also examined (**Section 5.2.2.1**).

Furthermore, a comparison study is conducted between two different caprock morphologies to analyze their impacts on CO₂ migration and solubility trapping (**Section 5.2.3**). The influence of structural integrity on solubility trapping is also analyzed, as the presence of structural

defects in the caprock can create preferential pathways for CO₂ leakage (**Section 5.3**). Finally, the impacts of caprock morphology on CO₂ leakage in the stairsteps domain (**Sections 5.3.2 and 5.3.3**), a hypothetical CO₂ storage site, are explored. By thoroughly investigating these aspects, this chapter aims to provide valuable insights into the role of caprock morphology and structural integrity in the solubility trapping process, contributing to the development of effective CGS strategies for long-term CO₂ storage.

5.2 Influence of caprock morphology on the solubility trapping

5.2.1 Modeling of synthetic geological domains

In this simulation analysis, two synthetically modeled geological domains are examined for the numerical geochemical analysis in order to comprehend the impact of caprock shape on the interaction between the CO₂ plume and connate reservoir water for the solubility trapping mechanism. **Figure 5.1** depicts the three-dimensional domains and distributions of petrophysical characteristics used for the simulations. The two synthetic geological domains with a disguised feature are considered in this simulation investigation. One domain possesses a caprock anticline structure, while the other domain has no structural features. These synthetic domains include the same amount of perturbations and a similar distribution of porosity and permeability petrophysical properties. This simulation analysis will aid in assessing the domains' injected CO₂ storage and entrapment potential through solubility and structural entrapment. The injection point coordinates considered in these simulations are (4000, 4000, 950), depicted in **Figure 5.1** in dark red with the letter I.

The synthetic domains have physical dimensions of around 10 km × 10 km × 0.15 km and are discretized into 50 × 50 × 10 grid cells (25,000 grid cells). For the distribution of petrophysical parameters, the porosity ranges from 20 to 40%, and the permeability ranges from 10 to 1500 mD [30], [63], [111]. **Figure 5.1** depicts the distribution of porosity and permeability for both

synthetic domains. In the current numerical analysis, the essential assumptions are set such that only the solubility reactions and not the mineral reactions are considered. Before beginning the injection of ScCO₂, the initial concentrations of CO₂ and H₂O for the entire domain are 4.610-12 M and 55.508 M, respectively. The initial pH of the whole domain is preserved at 5.6.

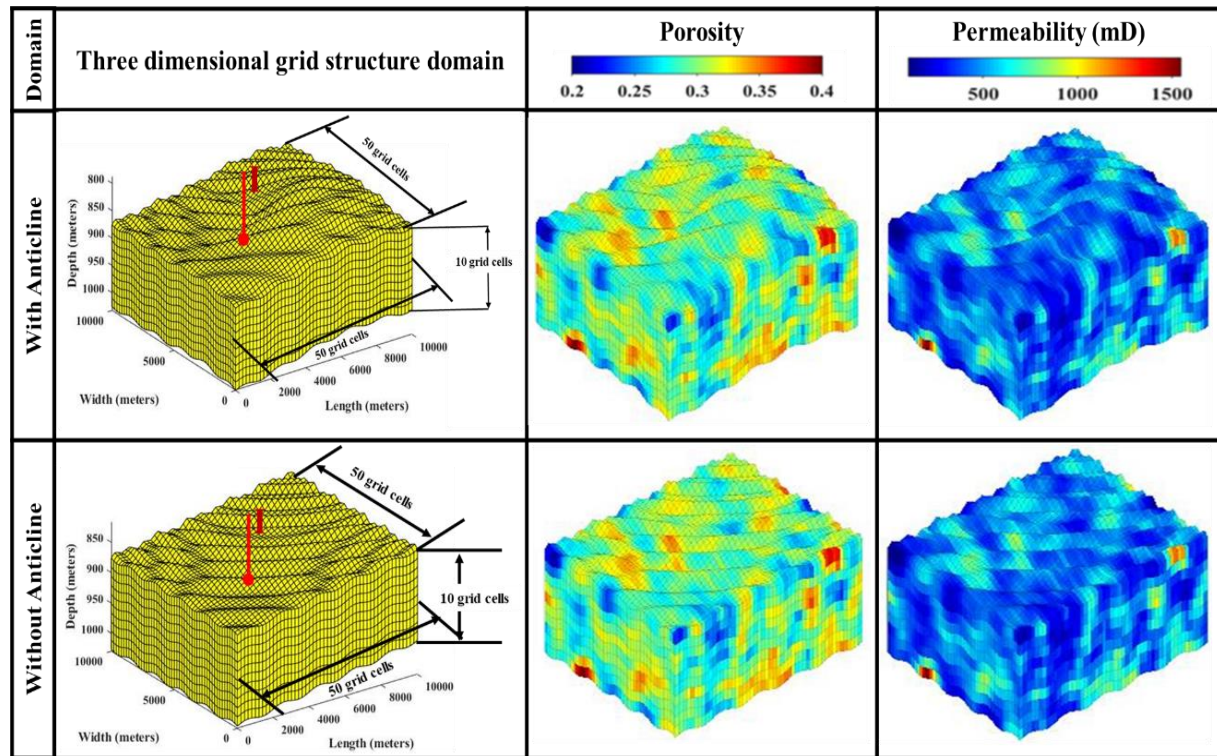


Figure 5.1: Illustration of a schematic diagram of the three-dimensional grid structure of both the domains and petrophysical properties distribution [63].

5.2.2 Base Case Scenario

The CO₂ entrapment in the formation zone can be visualized by analyzing the simulation results of the CO₂ mole fraction and pH fluctuations. Here, CO₂ mole fraction distributions for the entire domain illustrate the migration of CO₂. The pH variation within the domain facilitated the visualization of solubility fingering phenomena and solubility trapping within the domain. In addition, the average reservoir pressure, average reservoir temperature, and CO₂ trapped in the various stages have provided sufficient insight into the effect of caprock morphology. This

simulation analysis studies and shows the impact of caprock morphology on the amount of CO₂ captured by the solubility trapping mechanism in the domain. Continuous CO₂ injection is performed for the first 30 years at a mass flow rate of 0.31 Mt/year. In the simulations, the viscosity and fluid density of water are 0.3086×10^{-3} Pa.s and 975.86 kg/m^3 , respectively, while those of CO₂ are 0.0566×10^{-3} Pa.s and 686.54 kg/m^3 , respectively [39]. The initial temperature of the reservoir is fixed at 75 degrees Celsius. As noticed in **Figure 5.1**, the reservoir depth begins at 800 m, indicating that CO₂ sequestration in the simulated region happens 800 m below the Earth's surface. In this research investigation, the synthetic domain considered is a sloping landscape. Hence, the depth value 'h' for each grid cell varies. The initial reservoir pressure is derived using the formula $\rho_w gh$. Assuming that the density of water (ρ_w) in the geological domain is constant, the pressure only depends on depth (h). The reservoir pressure in the geological domain ranges from 77 to 84.6 bars. The tortuosity values of the rock formation are assumed to be 1, and the rock density is assumed to be 2900 kg/m^3 [208]. For the simulation examination of solubility trapping, the starting pH of the domain is kept at 5.6.

A synthetic anticline domain (**Figure 5.1**) was used as a base case scenario to explore solubility trapping phenomena. Two sets of simulation analyses were performed, one considering primary trapping mechanisms and the other considering solubility trapping in addition to primary trapping mechanisms. The simulation set that considers only primary trapping mechanisms (does not include geochemical reactions) will be referred to as simulation set-1 in the following paragraphs. In the simulation setup, the solubility trapping, in addition to structural and residual trapping (geochemical reactions are evaluated), will be referred to as simulation set-2. These simulations are performed at the same injection rate and injection point. In **Figure 5.2A**, the third row shows the saturation values of simulation set-1, whereas the fourth row depicts the CO₂ saturation distribution of simulation set-2.

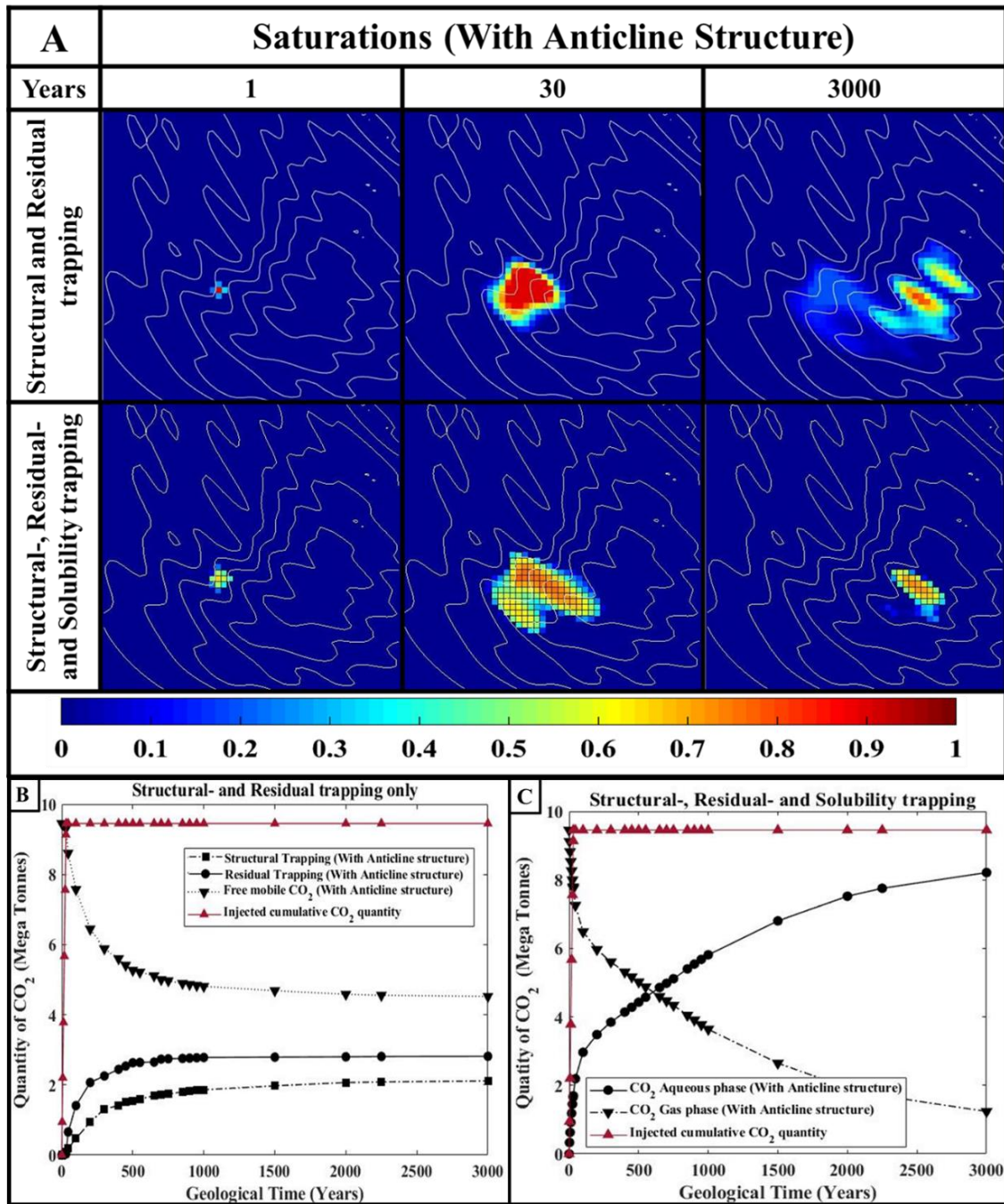


Figure 5.2: (A) Comparison of top view saturation of Structural- and Residual trapping only (Simulation set-1) and Structural-, Residual-, and Solubility trapping (simulation set-2) at 1st, 30th, and 3000th year (B) Structural- and Residual trapping variation (Without geochemical reactions), and (C) Structural-, Residual- and Solubility trapping (With geochemical reaction) variation over geological time scale [63].

Due to the absence of geochemical reactions in simulation set-1, the injected CO₂ percolates through the domain and becomes structurally and residually trapped. At the 3000th year of simulation set-1, it is observed in **Figure 5.2A** that the CO₂ plume is left behind on the top surface of the domain along the migration pathway. In simulation set-2, the ScCO₂ dissolves into the resident reservoir water and undergoes solubility trapping, in addition to structural and residual trapping. Consequently, the saturation of CO₂ on the top surface of the domain is more apparent in simulation set-1 compared to simulation set-2 (see **Figure 5.2A**). **Figure 5.2B** depicts the variance in structural and residual trapping, whereas **Figure 5.2C** depicts the fluctuation in aqueous CO₂ concentration across geological time. **Figure 5.2B** illustrates the structural and residual trapping that have been nearly consistent for 1000 years. Once the injected CO₂ plume completely reaches the anticline dome and becomes stagnant, the CO₂ plume is prevented from moving laterally. This limiting of the CO₂ plume inside the domain will reduce the residual entrapment. In contrast, when the CO₂ plume has stagnated beneath the anticline dome, there will eventually be the dissolution of CO₂ into the resident water. From **Figure 5.2C**, it is evident that the aqueous CO₂ concentration in the region increased during geological time.

5.2.2.1 Solubility fingering phenomena

The fingering phenomenon happens due to the dissolution diffusion convection (DDC) process during the solubility trapping mechanism. The solubility fingers that form during solubility trapping enhance the solubility trapping efficiency. More CO₂ comes in contact with fresh formation water as a result of the fingering phenomenon. **Figure 5.3** depicts the illustrative outcomes of the fingering phenomena. During the injection period, the CO₂ concentration is greater near the injection well, and dissolution does not dominate in the domain for 30 years; see **Figure 5.3**. During the post-injection period, the plume's sweeping over a geological timescale generates a greater CO₂-water contact, which facilitates the CO₂ dissolution

phenomenon. The fingering phenomenon is observed beneath the anticline dome, where the CO₂ maximum plume migration is observed. **Figure 5.3** illustrates the 200- and 3000-year observations for the progression of the number of fingers over the geological time scale. This phenomenon of the solubility trapping effect is illustrated in **Figure 5.2** for the comparison of CO₂ saturation in residual trapping-only and residual- and solubility trapping.

Figure 5.3 and **Figure 5.4** depict the fate of CO₂ at discrete geological times as a CO₂ mole fraction over the domain based on simulation findings. After reaching the impervious caprock, the plume expands laterally beneath it. During this time, the CO₂ mole fraction was found to be steadily decreasing. This is due to residual and solubility trapping, which operate in unison to improve CO₂ trapping in the domain. Within one year, the plume reaches the caprock, and towards the completion of the injection period, it begins to move gently towards the anticline dome. Assuming that the domain's top layer is impermeable, it will prevent CO₂ from flowing through it and enable it to move towards the anticline. Throughout the migration process, the momentum of the CO₂ plume decreases due to insufficient injection force and perturbation on the caprock. This leads to an increase in the duration of contact between CO₂ and water, as well as the quantity of CO₂ that becomes trapped within the domain. After the injection phase, a gradual drop in the mole fraction of CO₂ and a rise in the total amount of CO₂ in the aqueous phase indicate that the solubility trapping mechanism traps CO₂.

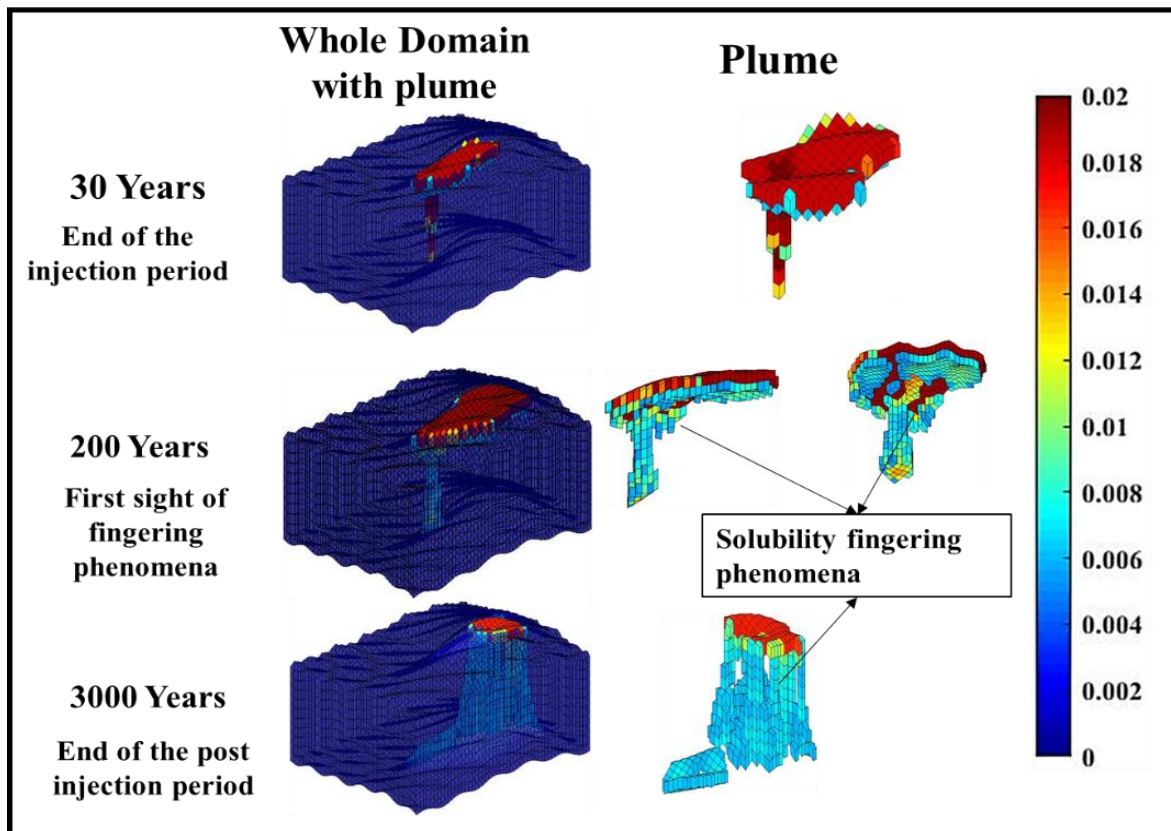


Figure 5.3: Solubility fingering phenomenon during CO₂ geological sequestration and their evolution over geological time scale [63].

Figure 5.4 displays the CO₂ mole fraction and pH change results. The entire domain is initially assigned a pH of 5.6. As CO₂ flows upstream and percolates through the porous formation layer, it begins to dissolve in connate reservoir water, decreasing pH inside the domain. **Figure 5.4** shows that a considerable portion of the synthetic domain is occupied with a low pH. This occurs owing to lateral spreading and the solubility fingering phenomena of the CO₂ plume inside the domain. The pH decreases to 3.5, suggesting solubility trapping events with safe entrapment of injected CO₂ within the domain. The pH of the domain plays a crucial role during the mineral trapping mechanism. For example, a low pH range with a high concentration of H⁺ ions on the reactant side is desired to facilitate the dissolution of silicate minerals. In order for precipitation to occur, a slightly higher pH is preferred. It is preferable to have an appropriate pH range for efficient sequestration trapping.

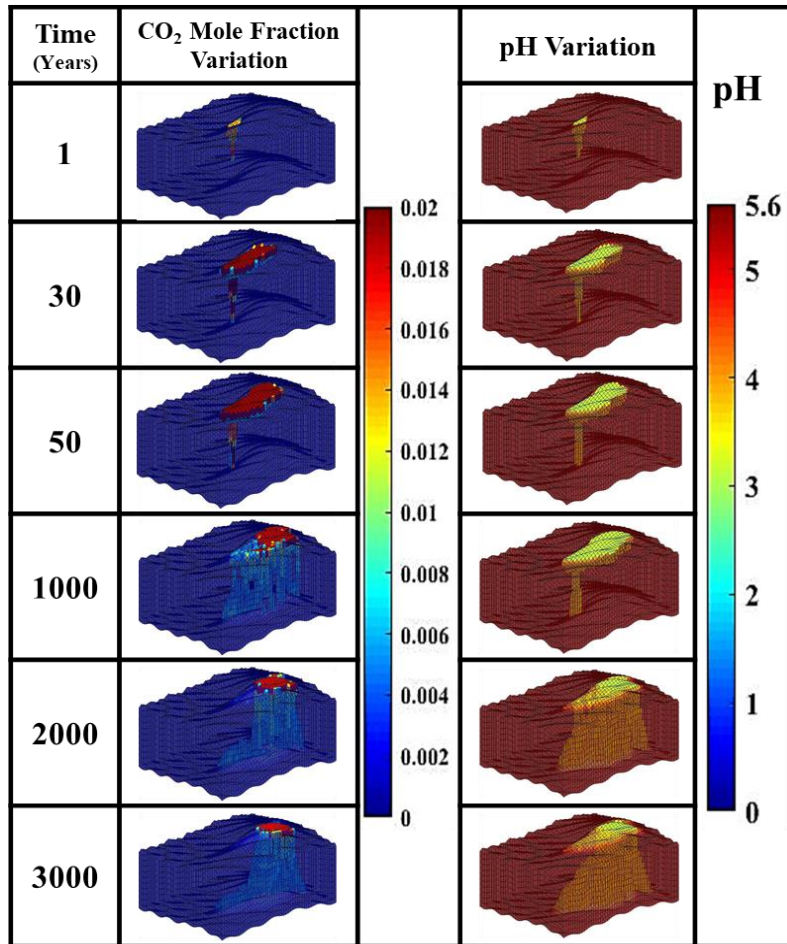


Figure 5.4: Illustration of CO₂ Mole Fraction and pH variation over geological time scale during CO₂ geological sequestration [63].

5.2.3 Comparison study between two distinct caprock morphology

The simulation research is carried out in this section to investigate the effect of caprock structure on CO₂ geological sequestration. The first set of simulations was performed on the synthetic domain, which has an anticline dome incorporated into it; this modeled synthetic domain will be referred to as synthetic domain-1 in the following text. The second set of simulations considers a synthetic domain without containing any caprock morphological features, such as an anticline dome; this will be referred to as synthetic domain-2. The CO₂ mole fraction distribution for both synthetic domains is depicted in **Figure 5.5**. According to **Figure 5.5A**, towards the end of the simulation time, the CO₂ mole fraction distribution in

synthetic domain-2 is lesser than in synthetic domain-1. It might be attributable to synthetic domain-2's great lateral spreading and displacement efficiency. Because of the significant lateral spreading, a considerable amount of CO₂ came into contact with connate water, triggering a dissolution reaction and initiating the fingering phenomena. As a result, the total aqueous phase CO₂ amount detected in the synthetic domain-2 was more prominent, whereas the free mobile CO₂ quantity was lower, as shown in **Figure 5.6C**.

Figure 5.5A and **Figure 5.5B** illustrate the enhanced solubility of injected CO₂ in synthetic domain-2 compared to synthetic domain-1. In **Figure 5.5B**, the simulation results for pH change reveal that a greater proportion of synthetic domain-2 is enveloped with lower pH than synthetic domain-1. In synthetic domain-1, the volume covered and displacement efficiency of the injected CO₂ plume are lesser than in synthetic domain-2. Because the CO₂ plume's migration path towards the center of the anticline is congested and narrowed. Due to the absence of an anticline dome in synthetic domain-2, the injected CO₂ plume causes more sweeping in the lateral direction, resulting in more CO₂ dissolution. In addition, it contributes to the fingering phenomena, which accelerates CO₂ dissolution along the depth axis and leads to vertical spreading.

Figure 5.6A illustrates the average reservoir pressure of both synthetic domains. It is observed that the average pressure recorded in synthetic domain-1 is greater than in synthetic domain-2 at the end of the simulation. Because of the constrained flow channel and the accumulation of CO₂ in the center of the dome, the normal reservoir pressure will be maintained in synthetic domain-1. During the course of the CGS simulations, it was noticed that the average temperature of the reservoir did not demonstrate any significant fluctuations. The temperature impacts and variation observed over the course of geological time are minimal (see **Figure 5.6B**).

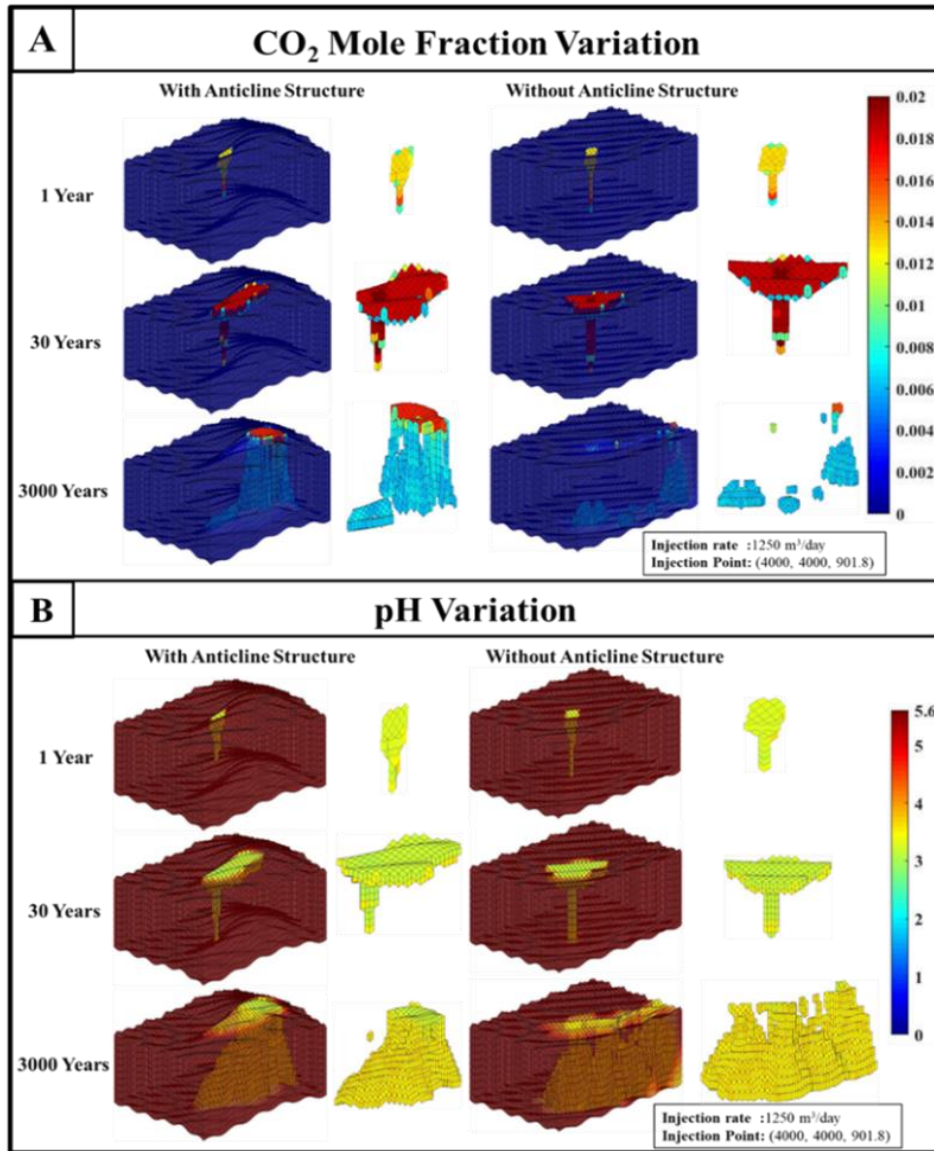


Figure 5.5: Influence of caprock morphology on (A) CO₂ Mole Fraction and (B) pH variation over a geological time scale [63].

The solubility trapping data, displayed from the aqueous CO₂ results and shown in **Figure 5.6C**, show that over a geological time scale, a greater quantity of aqueous CO₂ was recorded in synthetic domain-2 compared to synthetic domain-1. This is because the synthetic domain-2 has a high lateral spreading, further resulting in increased trapping along the migration path. Due to the presence of anticline structure in synthetic domain-1, the lateral spreading of the CO₂ plume was lower in synthetic domain-1 than in synthetic domain-2. This, in turn, resulted in a reduction in the amount of residual and solubility entrapment that occurred.

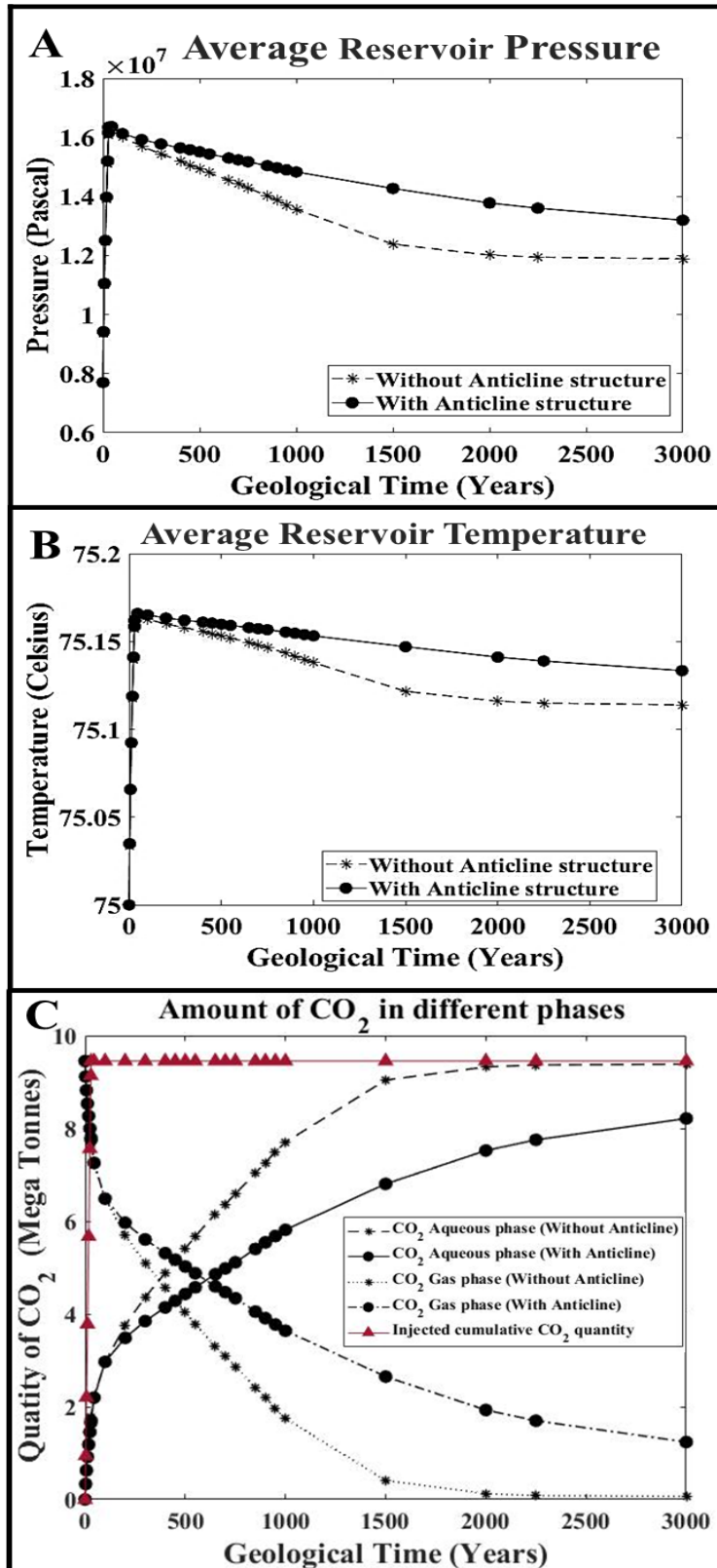


Figure 5.6: Influence of caprock morphology on (A) Average reservoir pressure, (B) Average reservoir temperature, and (C) Aqueous and gaseous phase CO₂ quantity variation over geological time scale [63].

When compared to synthetic domain-1, the overall quantity of free mobile CO₂ is significantly lower in synthetic domain-2 (see **Figure 5.6C**). However, when the injection rate was increased, synthetic domain-2 demonstrated that a significant amount of CO₂ was moving out from the observable domain. Suppose the injected CO₂ is to be contained within the bounds of the accessible domain (to contain the CO₂ plume from exploring geological fractures, faults, and other features), synthetic domain-2 caprock morphology would be the better option. The risk factor and the financial aspects of the operation of CGS in synthetic domain-2 can rise due to the poor availability of storage volume and the low injection rate.

5.3 Influence of Structural Integrity Analysis on the Solubility Trapping

Studies on the structural stability of geological formations are essential prior to the initial deployment of carbon capture and storage. The comprehensive risk assessment with parametric analysis needs to be considered before CGS can be accepted or implemented in any region. The risk assessment involves the study of numerical simulation to analyze CO₂ migration in the subsurface formation domain to determine structural integrity and the probability of leakage in the domain. The subsurface formation is a complex structure for simulating the influence of various reservoir parameters, such as CO₂ migration and entrapment, in order to evaluate the structural integrity and safety of CGS. One of the significant disadvantages of numerical simulation is the lack of geological subsurface data for simulations.

The numerical analysis of caprock morphology in the previous section demonstrates its influences on the primary and solubility trapping processes. The presence of geological features such as anticline and syncline altered the migration pathway and demonstrated that geological structures with varying caprock morphologies affect sweeping efficiency. The sweeping efficiency has been observed to influence the solubility entrapment; when the sweeping is high, more CO₂ plume will come into contact with the connate water, increasing the solubility

trapping. The CO₂ plume was safely confined under an anticline dome, which caused the contact area between CO₂ and water to be low, which led to slower solubility entrapment in the domain. But, when the CO₂ plume is stored inside specific geological boundaries, it would cut monitoring costs.

In the current section, the simulation study aimed to investigate the effects of caprock leakage on CO₂ entrapment and study the influence of caprock morphology on the leakage analysis of CGS. Additionally, the research aimed to investigate the influence of caprock morphology on the leakage analysis of CGS. In order to accomplish this, an investigation into the effect of geological structures and features on entrapment and structural integrity is conducted using three synthetic geological domains. Each of these geological domains has a distinct caprock morphology from the others. By monitoring the CO₂ mole fraction and pH distribution throughout the domain, CO₂ migration and sweeping efficiency can be analyzed. The investigation into the structural integrity was carried out by monitoring the CO₂ mole fraction and the entrapment of solubility trapping. Evaluation of the reservoir pressure distribution throughout the domain was an essential part of the structural integrity study that was carried out.

5.3.1 Modeling of synthetic geological domains

In the current research analysis, the first two synthetic domains taken into consideration are partially adapted from the previous study and partially similar to the previous section's synthetic domain [63]. In the current section, the synthetic domains are incorporated with the fault caprock. **Figure 5.7** shows the synthetic domain-1 incorporated with anticline structure, whereas synthetic domain-2 does not incorporate any geological features apart from the perturbation. The synthetic domain-3 has been modeled based on the data that is currently available for the Deccan basalt region. Based on the available geological data, the stairsteps

morphology was incorporated in modeling the synthetic domain [30], [111], [201]. For modeling the first two synthetic domains, the 50×50×20 grid, which is comprised of 50,000 grid cells, has been used; see **Figure 5.7**. The synthetic domains 1 and 2 each have a physical dimension of 10 km ×10 km × 350 m. Both synthetic domain-1 and -2 have injection points situated in nearly identical locations. The physical dimension of the synthetic domain-3 is 10 km ×10 km × 800 m, see **Figure 5.7**. The sloping nature of the anticline dome can be found within the synthetic domain-3, along with the stairsteps traps that are embedded within it. Geological features similar to these can be found in the Deccan Volcanic Province [30], [111], [201].

The CO₂ was injected at the rate of 0.63 Mt/year into the synthetic domain-1 and -2. The injection was conducted for an initial 30-year period, while the subsequent 2970 years of the simulation were kept for post-injection observations. In synthetic domain-3, a fixed injection rate of 0.36 Mt/year was maintained for a period of 60 years. The subsequent simulation time of 2940 years was allocated for the purpose of post-injection analysis. Approximately 18.9 Mt of ScCO₂ was injected into the synthetic domain-1 and -2, while in the synthetic domain-3, the total injection was around 21.6 Mt. The initial reservoir pressure and temperature conditions considered for the current section simulation study are the same as mentioned in **Section 5.2.2**.

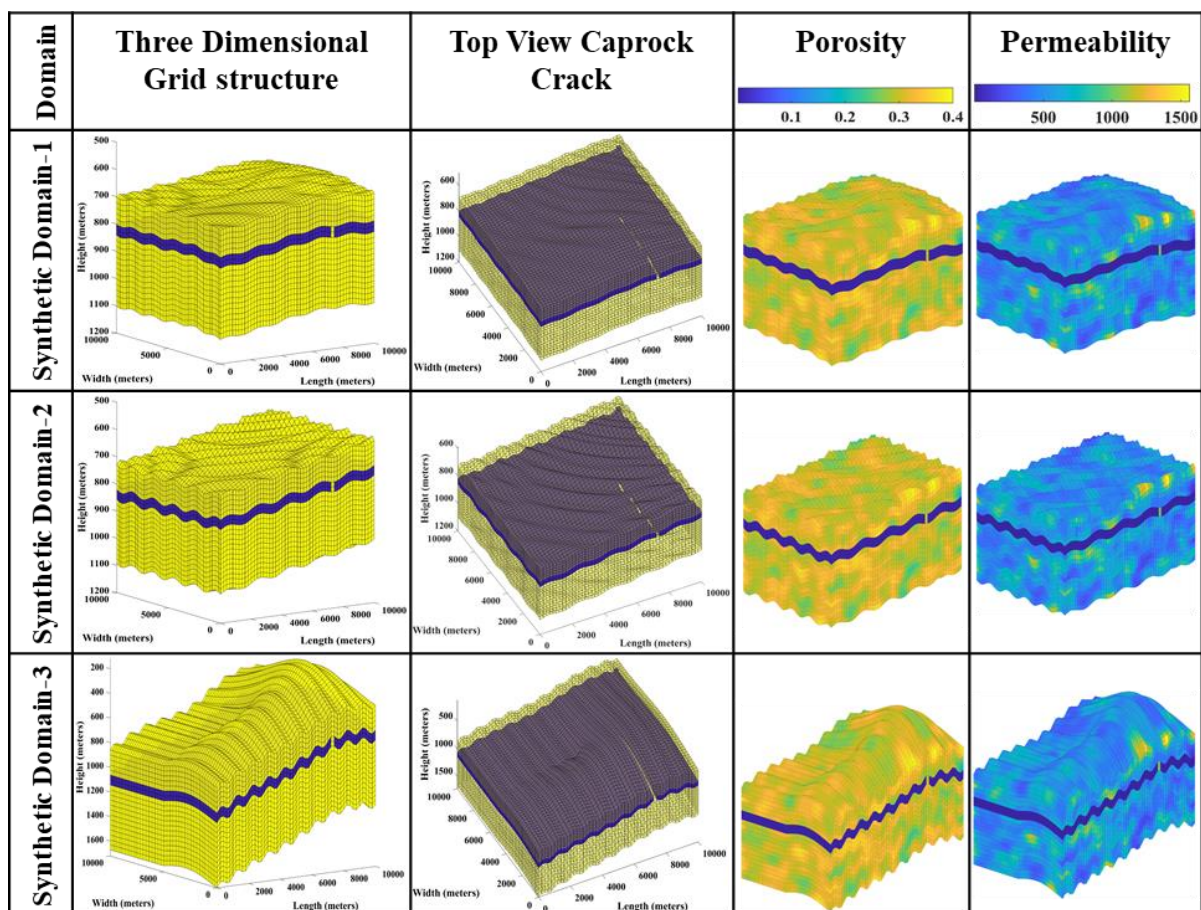


Figure 5.7: Illustrates a schematic diagram of the three-dimensional grid structure, the top view of the domain, and the distribution of petrophysical properties of three considered synthetic domains. In column two, the three-dimensional domain is made transparent in order to view the crack on the caprock from the top view.

Figure 5.7 illustrates the three-dimensional grid structure and petrophysical variation in all three considered synthetic domains. The first column of **Figure 5.7** depicts the three-dimensional grid structure of synthetic domains. The synthetic domain-1 and 2 begin at a depth of approximately 600 meters, while the caprock is positioned at approximately 800 meters. In synthetic domain-3, the domains begin at 200 meters, and similar to synthetic domain-1 and -2, the caprock is located at approximately 800 meters. The slope of synthetic domain-3 resembles the Deccan traps of the Deccan Volcanic Province. The second column illustrates the top view of the domain's transparent grid structure by highlighting the caprock crack. The

third and fourth columns display the synthetic domains' porosity and permeability distribution. The values for porosity and permeability are arbitrarily assigned to each grid cell of the synthetic domain. All synthetic domains share the same range of petrophysical properties, with porosities ranging from 0.2 to 0.4 and permeability between 10 and 1500 mD, see **Figure 5.7**.

5.3.2 Impacts of caprock morphology on leaky caprock and CO₂ entrapment

This simulation analysis investigates the impact of caprock morphology on CO₂ plume migration, sweeping efficiency, and CO₂ leakage. In simulation 1, the synthetic domain-1 is used, while in simulation 2, the synthetic domain-2 is utilized. The caprock cracks are located at the same location for both domains. In simulation 1, the anticline dome in the synthetic domain is positioned near the crack in order to assess its effect on CO₂ leakage. The injection site, rate, and other simulation parameters are identical in both simulations. The sole variation between the two synthetic domains is the top caprock morphology.

Figure 5.8 depicts the simulation outcomes of the first two synthetic domains. Following CO₂ injection, the CO₂ plume moves towards the elevated region. In simulation 1, due to the presence of an anticline dome, most of the plume moves along a confined path and stagnates in the anticline dome. In simulation 2, the synthetic domain-2 lacks geological structures, and the injected CO₂ has spread in the lateral direction beneath the caprock.

While comparing two sets of simulations, **Figure 5.8** results reveal that the CO₂ leakage is greater in simulation 1 than in simulation 2. Due to high sweeping efficiency in synthetic domain 2 (simulation 2), only a small amount of CO₂ reached the crack. In contrast, due to the CO₂ accumulating in the close vicinity of the anticline in simulation 1, where the crack was present, a greater quantity of CO₂ leaked from simulation 1. This revealed the disadvantage of having cracks and leakage faults near geological features with elevation, such as anticline

domes. The leakage rate may also be high if the crack is located along the CO₂ plume migration path.

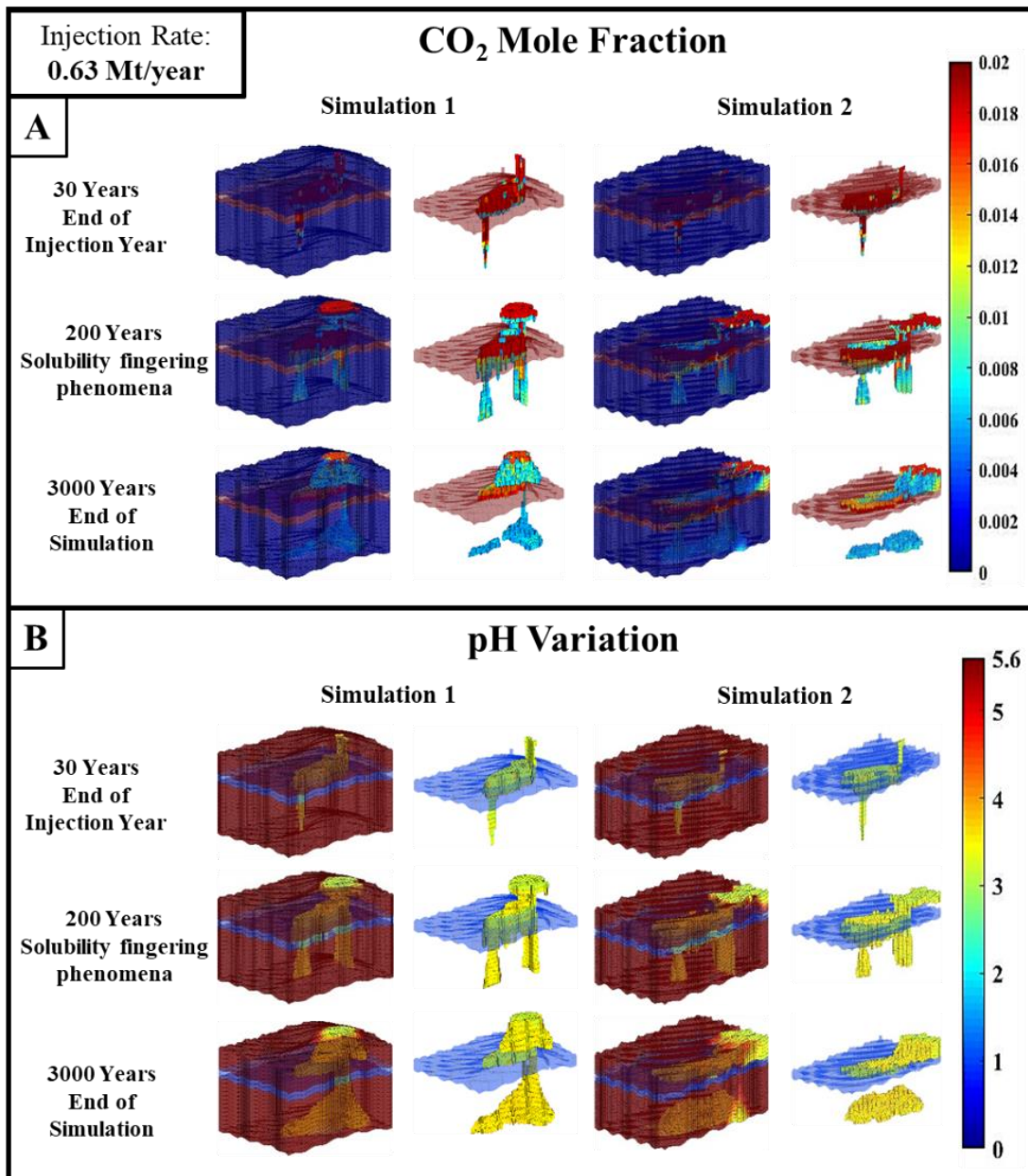


Figure 5.8: Illustration of (A) CO₂ Mole Fraction and (B) pH variation over geological time scale during CO₂ geological sequestration.

The CO₂ leakage can be visualized from the CO₂ mole fraction and pH variation results in **Figure 5.8A** and **Figure 5.8B**, which depict the incorporation of leaky caprock into the

domains. The line crack is placed near the anticline dome of the synthetic domain, which acts as a systematic geological fracture crack. The CO₂ liquid mole fraction results at 30 years indicate that after CO₂ migrates into the bottom caprock anticline dome, it rapidly escapes to the top section of the synthetic domain due to the presence of a caprock fracture. The top caprock is free of cracks and will prevent injected CO₂ from escaping to the Earth's surface. In order to study the structural integrity of the domain during CO₂ sequestration in the presence of leaky caprock, parameters such as reservoir pressure, sweeping efficiency, and solubility entrapment are analyzed. For example, the solubility fingering phenomenon at the bottom caprock is effective from around the 500th year, while at the top caprock, it is triggered around the 1000th year (see **Figure 5.8**). This could be a result of the height of the CO₂ plume stagnating in the dome and the reservoir pressure distribution with respect to reservoir depth. The solubility trapping close to the caprock crack is essential because it may result in mineral precipitation, which may lessen the intensity of caprock leakage.

As shown in **Figure 5.8B**, synthetic domain-2 has a more significant portion of the domain covered by low pH in the bottom section of the domain than synthetic domain-1. When comparing synthetic domains 1 and 2, synthetic domain-1 has a smaller volume covered and a lower displacement efficiency in the bottom section of the domain than synthetic domain-2. It's because the CO₂ plume's migration path became narrower as it approached the anticline's center. The injected CO₂ plume has enhanced spreading in the lateral direction under the caprock in the bottom section of the synthetic domain-2, which increases CO₂ dissolution because the absence of an anticline dome in synthetic domain-2 increases the contact area between the CO₂ plume and reservoir resident water, due to which the solubility trapping will be high. The fingering phenomenon helps to improve the vertical spreading in the depth axis by contributing to convection mixing. Assume the pH range of the domain is within acceptable limits. In that case, the low pH region created during the solubility trapping phase may result

in a mineral reaction for the mineral trapping mechanism. After CO₂ leaked to the top section of the synthetic domain-1, the CO₂ plume stagnated in the top section's anticline dome. After a while, it was clear that solubility trapping and a low pH region predominated in the area. Once the pH range returns to the alkaline level, it could be advantageous if the mineral reaction near the crack of the bottom section caprock can contribute to crack healing.

Figure 5.9 depicts the average reservoir pressure, temperature, and percentage of solubility entrapment over a geological time scale. The pressure variation in the average reservoir pressure results in both synthetic domains following a similar trend. However, the average pressure in simulation 1 for the synthetic domain-1 decreased slightly at the end of the simulation time. This could be because of a crack in the anticline dome. If there is no crack near the anticline dome, the pressure would be similar to or greater than that of the synthetic domain-2. Because the CO₂ plume's flow will be constrained in a narrow pathway, the CO₂ will eventually accumulate in the dome's center. This confined CO₂ plume would increase pressure at that point, but the pressure would be released if a crack was present, see **Figure 5.9A**. In simulation 1, a high amount of CO₂ solubility entrapment was recorded in the top section of the domain compared to simulation 2 because more CO₂ escaped to the top section of the domain. In simulation 2, in the absence of geological features, a large amount of CO₂ was spread in all directions, resulting in only a small amount of CO₂ reaching the crack and leaking into the top section of the domain, see **Figure 5.9C**. In the domain, the temperature variation was minimal and considered nearly negligible, see **Figure 5.9B**.

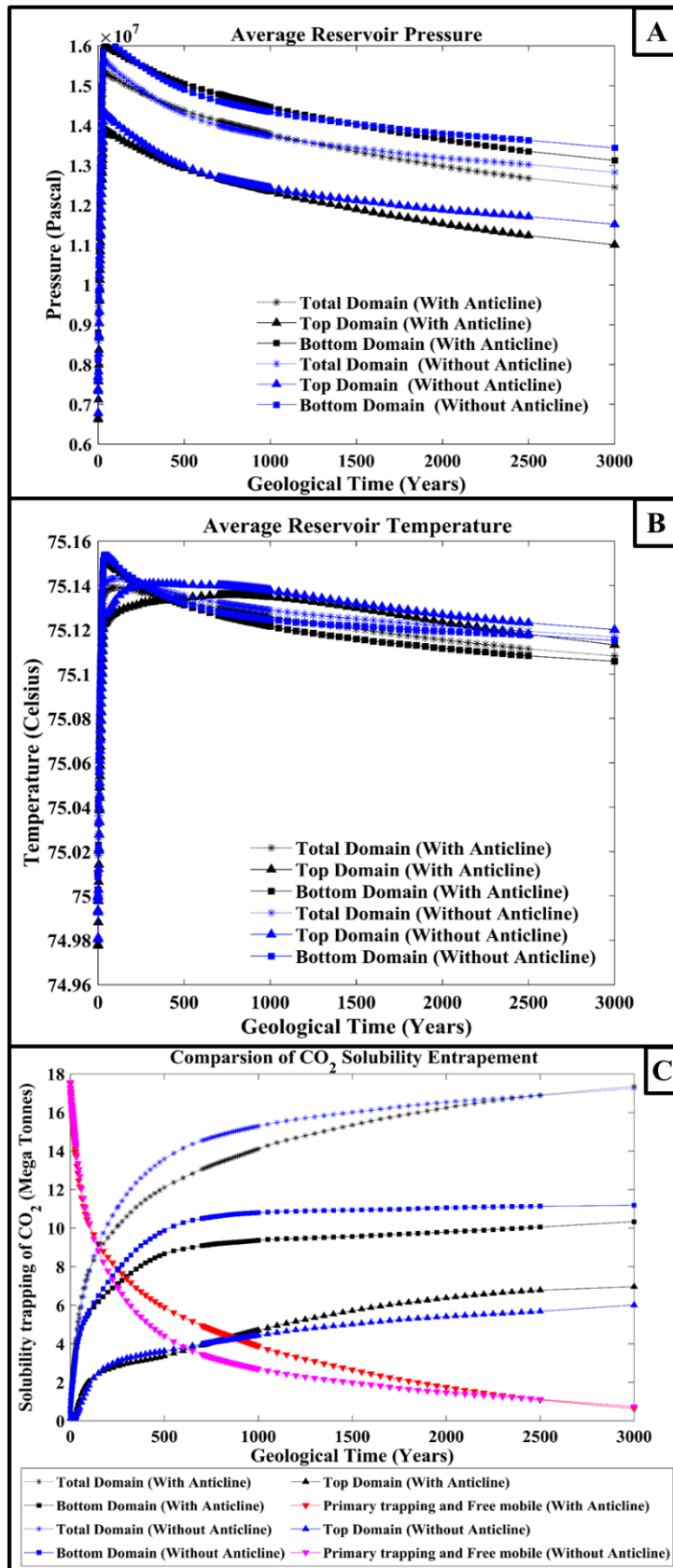


Figure 5.9: Influence of caprock morphology on (A) Average reservoir pressure, (B) Average reservoir temperature, and (C) Solubility trapping of CO₂ variation over geological time scale.

5.3.3 CO₂ leakage in the stairsteps domain

In this section, an analysis of CO₂ leakage was conducted in the synthetic domain-3. CO₂ leakage analysis in this synthetic domain-3 will provide insight into plume migration, solubility trapping, and leakage prediction in a domain with stairsteps geological features. The synthetic domain-3 contains anticlines, stairsteps, and a sloping orientation. Once the ScCO₂ is injected into the domain, due to the influence of the stairsteps feature, the CO₂ tends to spread laterally; when this plume comes under the influence of the anticline structure, the plume tends to rise toward the high elevated region. During CO₂ migration, it encounters the crack near the anticline dome, through this, the CO₂ plume escapes to the top section of the synthetic domain.

Figure 5.10B depicts the pH variation in the subsurface formation. It can be noticed that the pH of the domain was low in the migration pathway, indicating solubility trapping in the migration pathway. A substantial portion of the bottom section of the domain is covered with low pH. Comparing **Figure 5.8A**, **Figure 5.8B**, **Figure 5.10A**, and **Figure 5.10B**, it is clear that the solubility trapping was more rapid in the bottom section than in the top. It could be because of the pressure distribution in the simulation domain. As it is well known that reservoir pressure increases with reservoir depth, solubility trapping will occur more rapidly at greater reservoir depth.

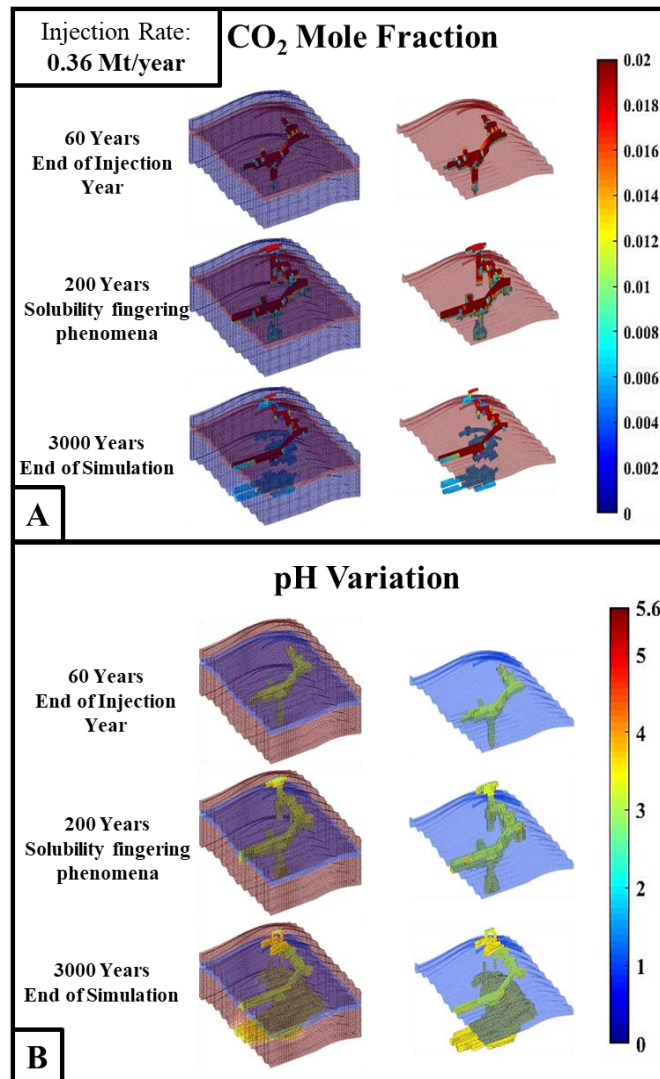


Figure 5.10: Illustration of (A) CO₂ Mole Fraction and (B) pH variation over geological time scale during CO₂ geological sequestration.

The average reservoir pressure for the top section, bottom section, and entire domain is depicted in **Figure 5.11A**. As illustrated by the results of the average reservoir pressure, it is observed that the reservoir pressure increases with depth. The top section's average reservoir pressure is low compared to the bottom section's average reservoir pressure, and the entire domain's average reservoir pressure is in between the pressure variations of the top and bottom sections. The injection was conducted approximately 1100 meters below the Earth's surface; this is the reason for the increase in average reservoir pressure compared to simulations 1 and 2. **Figure 5.11B** illustrates that the domain's temperature has not changed significantly.

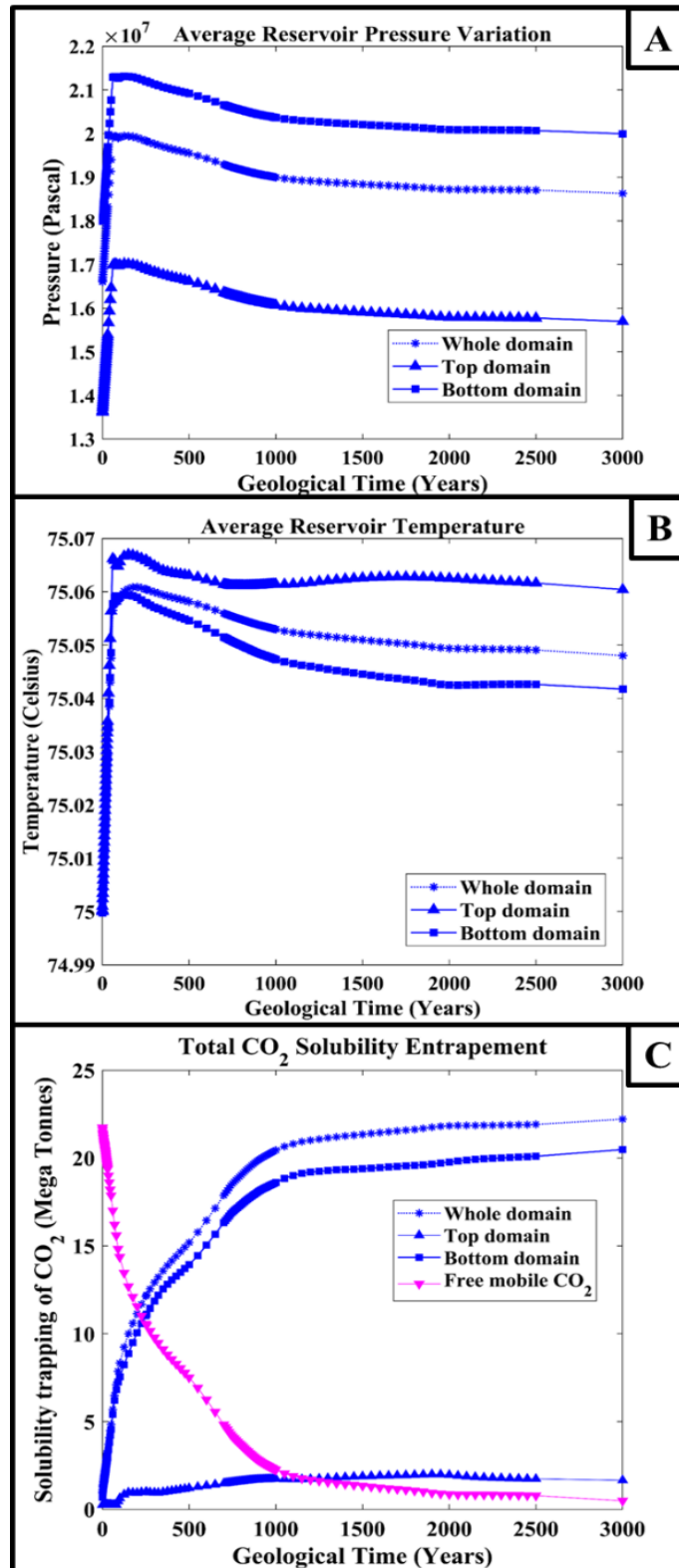


Figure 5.11: Influence of caprock morphology on (A) Average reservoir pressure, (B) Average reservoir temperature, and (C) Solubility trapping of CO₂ variation over geological time scale.

Figure 5.11C depicts the solubility trapping recorded on a geological scale. This observation suggests that solubility trapping is greater in the bottom section than in the top section. As shown in **Figure 5.10A** and **Figure 5.10B**, the majority of the CO₂ plume spread in a lateral direction and underwent solubility trapping, which may explain these observations. In addition, the reservoir pressure in the bottom section was elevated, which increased solubility entrapment in the bottom section. Comparing the results of synthetic domain-1 and -2 from **Section 5.2.3**, it can be noticed from the solubility trapping results that the top domain solubility of synthetic domain-1 and -2 was greater than that of synthetic domain-3 in terms of total injection quantity. This analysis also provides insight into the selection of injection location relative to the location of a crack, taking geological features and slope into account to analyze CO₂ plume migration in the domain. The migration of the CO₂ plume is one of the most critical parameters that must be analyzed to assess the structural integrity and CO₂ leakage from the injected formation domain.

5.4 Summary

The objective of this chapter was to investigate the impact of caprock leakage on CO₂ sequestration as well as the influence of top surface morphology on CGS leakage analysis. Three synthetic geological domains with different caprock morphologies are used to assess the impact of geological features and fault characteristics on entrapment and structural integrity. The CO₂ mole fraction and pH distribution in the domain are used to investigate CO₂ migration and sweeping efficiency. Monitoring the CO₂ mole fraction and entrapment of solubility traps was used to conduct the structural integrity assessment and leakage analysis. The reservoir pressure distribution in the domain was evaluated as part of structural integrity research.

During the analysis of caprock morphology's effects on the solubility trapping mechanisms, the presence of geological features, such as anticline structures, has influenced the migration

path of the CO₂ plume. It demonstrated that geological features with varying caprock morphologies impact sweeping efficiency, further effecting the CO₂ entrapment in the domain. When the sweeping efficiency is high, a greater quantity of the CO₂ plume will be in contact with the connate water, which will increase the solubility entrapment [63], [111].

The top subsurface caprock morphology has the potential to influence the migration of CO₂ plumes and the percentage of entrapment of CO₂ in the domain. The selection of the desired top surface and the appropriate injection point plays a significant role in the secure and cost-effective implementation of the CGS. For instance, the crack was incorporated into the ongoing simulation analysis somewhere in close proximity to the anticline domain. Because of this, the rate at which CO₂ leakage from the bottom formation layer will be rapid. If the same crack were located away from the migration pathway and the anticline dome, the percentage of leakage would be significantly reduced. The chapter broadly analyzed the influence of caprock morphology and structural integrity on the solubility trapping mechanism and its impact on leaky caprock and entrapment. The next chapter investigates the use of machine learning in analyzing CO₂ geological sequestration.

**CHAPTER 6: Utilization of Machine Learning
in the CO₂ Geological
Sequestration Analysis**

6 Utilization of Machine Learning in the CO₂ Geological Sequestration Analysis

6.1 Introduction

CO₂ Geological Sequestration (CGS) is a potential technology, but carrying out the research on this technology by means of experiments would be extremely unfeasible from both a financial and a scientific point of view. When dealing with simulation analysis of a complicated geometrical model, using traditional numerical approaches proved to be both time-consuming and resource-intensive for research. Therefore, the incorporation of machine learning into the simulation study offers a promising avenue to minimize computational load and time, making CGS research more viable and efficient.

The study unfolds through the integration of traditional numerical approaches with machine learning. The outcomes of numerical simulations serve as input data for machine learning, enabling an assessment of future trends of the targeted parameters. Initially, conventional multiphase flow simulations are carried out over the geological time span, and the results of these simulations become the input for the time series neural network, anticipating the post-injection trends of the target variable. The validity of the findings is ensured through validation against previously generated numerical simulation results of output parameters at the same temporal range. The current investigation aims to explore the effects of heterogeneous caprock morphology on forecasting future structural and residual trapping percentages. Furthermore, the present research delves into exploring how caprock morphological heterogeneity influences the forecasting capabilities of the time series neural network, introducing an intriguing dimension to this study.

This chapter begins with modeling the computational domain to create synthetic scenarios for studying CO₂ sequestration (**Section 6.2**). The numerical simulation results obtained serve as

data for training and testing machine learning algorithms (**Section 6.3**). Subsequently, the focus shifts to utilizing machine learning, particularly time series neural network analysis, to examine the simulation results and extract valuable insights (**Section 6.4**). Time series neural networks possess a remarkable ability to capture temporal dependencies in the data, enabling the identification of patterns and trends present in traditional numerical simulations in significantly less time. For this, the NARX and NAR models are preferred as the initial choice due to their straightforward implementation and relatively low prediction requirements compared to other models. This makes them ideal for preliminary stage analysis and data exploration. [190], [219].

6.2 Modeling of synthetic geological domains

In this study, the CO₂ geological sequestration was analyzed with the help of PFLOTRAN. The amount of CO₂ trapped beneath the top surface structural topography is referred to as structural trapping. The amount of CO₂ trapped in the migration pathway is evaluated as residual trapping. The moveable plume is the excess CO₂ that is not structurally or residually trapped. For assessing the structural trapping, residual trapping, and moveable plume, the saturation and the amount of CO₂ plume that is present are considered [30], [219].

A synthetic domain was modeled to be utilized in the numerical simulations. The modeled synthetic domain has a physical dimension of 10 km × 10 km × 150 m and is discretized into 25,000 cells. The top surface of the simulated domain is characterized by heterogeneous irregular perturbation morphology. The considered domain's porosity and permeability ranges are 0.2 to 0.4 and 10 to 1500 mD, respectively [30], [80]. The domain pressure is initiated by establishing the datum at 801 m deep for 70 bars with hydrostatic pressure conditions, and the temperature was initiated at 75°C in the whole domain. In the simulations, the water and CO₂ densities are considered as 975 kg/m³ and 686.54 kg/m³, respectively, and their viscosities as

0.308×10^{-3} Pa.s and 0.056×10^{-3} Pa.s, respectively [30], [80]. **Figure 6.1A** depicts the three-dimensional grid structure with perturbations and heterogeneous morphology, whereas **Figure 6.1B** depicts the distribution of corresponding petrophysical properties in the domain grid structure. As shown in **Figure 6.1A**, CO₂ was injected in the center of the domain at the coordinates (5000, 5000, 816), highlighted by the letter “I”. The injection rate is fixed at 3,600 m³/day for a duration of 30 years, whereas 370 years was kept for post-injection analysis [219].

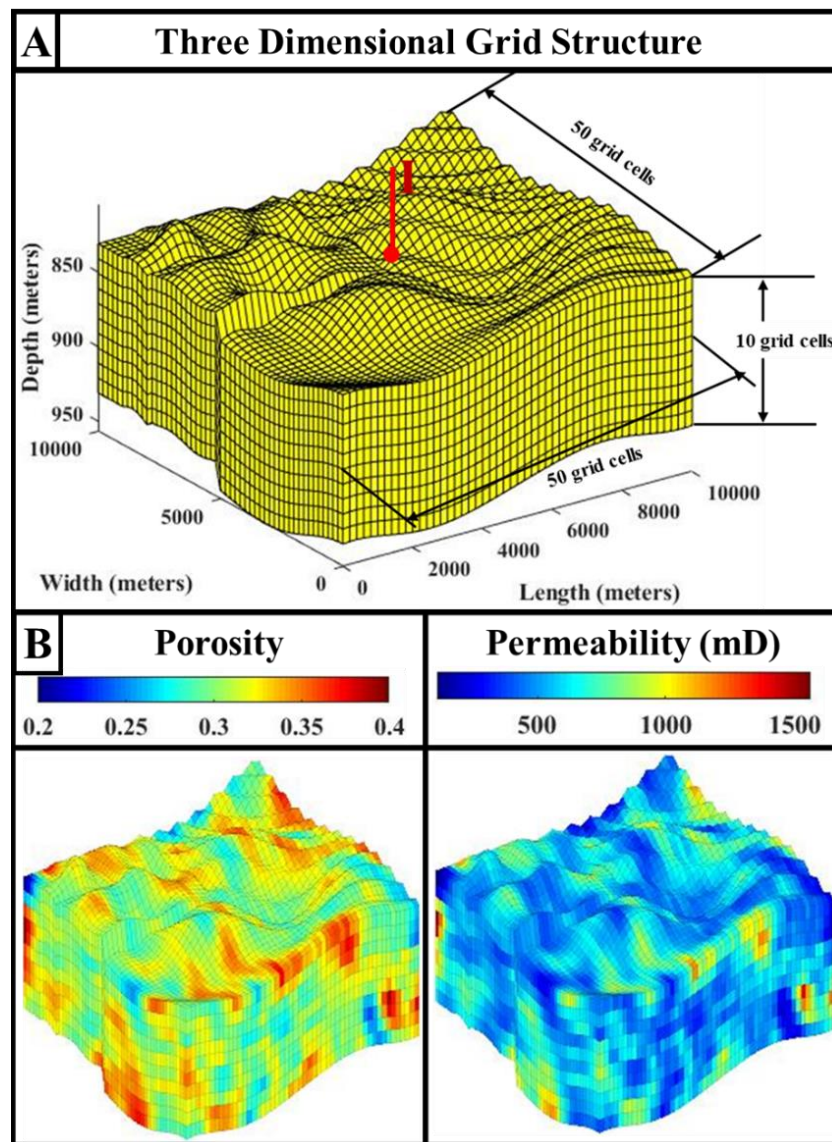


Figure 6.1: (A) Three-dimensional grid structure with physical dimensions and computational cells; (B) Petrophysical properties distributions. The bold red letter I in the current figure is the injection point [219].

6.3 Numerical Simulation Results

The injection force and the elevation of the surrounding anticline dome both have an impact on the movement of the CO₂ plume as it travels through the domain. In **Figure 6.2A**, one can see an illustration of the saturation profile of CO₂ as it enters the domain. According to the saturation profile, the CO₂ plume gradually makes its way into the adjacent anticline domes. **Figure 6.2B** depicts the number of partially or entirely CO₂-saturated cells on a geological time scale. **Figure 6.2B** illustrates the number of CO₂-saturated cells across geological time. Between 200 and 400 years, an inconsistency in the number of CO₂-saturated cells can be noticed. During CO₂ migration, the CO₂ spreads laterally in many cells. After the injection is ceased, the injection force decreases, and the CO₂ plume in the plunging syncline zone will travel under the effect of elevation to stagnate under the anticline dome. The CO₂ saturation of the cells will drop in the syncline plunging zone, whereas it will increase in the anticline region. This suggests that the CO₂ plume in the vicinity of the syncline plunge is migrating and stagnating under the anticline dome. **Figure 6.2B** shows that the number of saturated cells decreases after 200 years, primarily due to perturbations in the caprock shape [219].

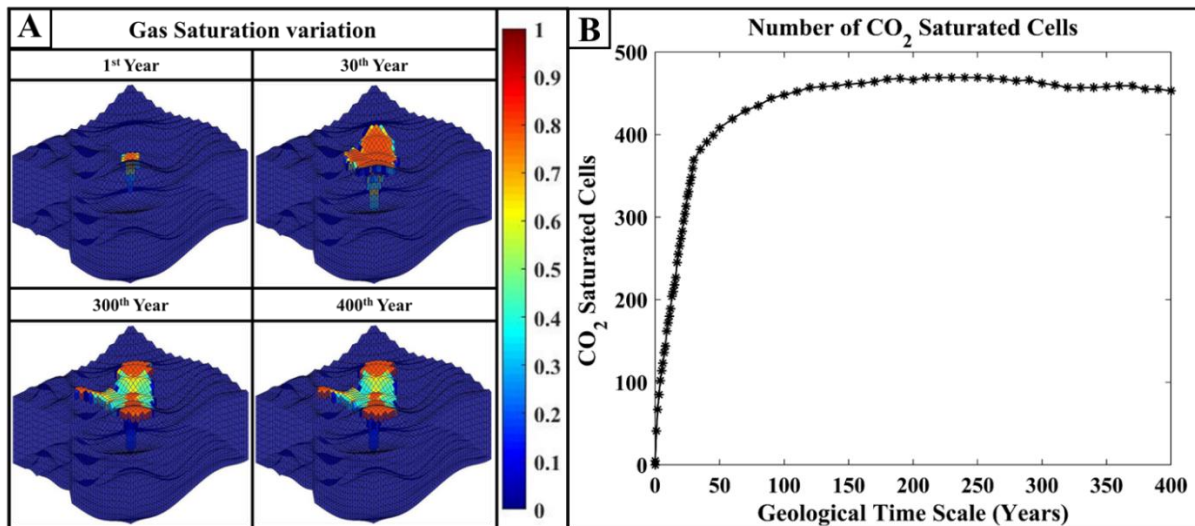


Figure 6.2: (A) CO₂ plume migration in the geological domain, the results illustrated for 1, 30, 300, and 400 years, and (B) the number of CO₂ saturated cells variation over geological time scale

[219].

The average reservoir pressure during geological time is shown in **Figure 6.3A**. During the injection period, the average reservoir pressure rises by approximately 30 MPa. The average reservoir pressure gradually drops and stabilizes in the domain following injection. The average reservoir temperature has increased by approximately 0.45 °C from the baseline temperature (see **Figure 6.3A**). The structural and residual trapping data, shown in **Figure 6.3B**, show that CO₂ structural trapping has increased from the initial years. When there are heterogeneous perturbations on the top surface (**Figure 6.2A**), the CO₂ plume flows, spreads laterally, and becomes trapped in the structural perturbations. The CO₂ is confined in the migration pathway in the case of residual trapping. The effects of injection force on the CO₂ plume and the residual entrapment percentage were marginally visible during the injection time, as shown in **Figure 6.3B**. The injection force's impact on the CO₂ plume will progressively decrease after the injection phase. After 30 years, the residual entrapment percentage seems to be increasing (see **Figure 6.3B**), as the capillary effects will trap CO₂ in the migration pathway during this period. The percentage of mobile plumes decreases throughout geological time, as observed in **Figure**

6.3B. This decline in moveable plume suggests that structural- and residual trapping has increased in the domain over the geological time during post-injection [219].

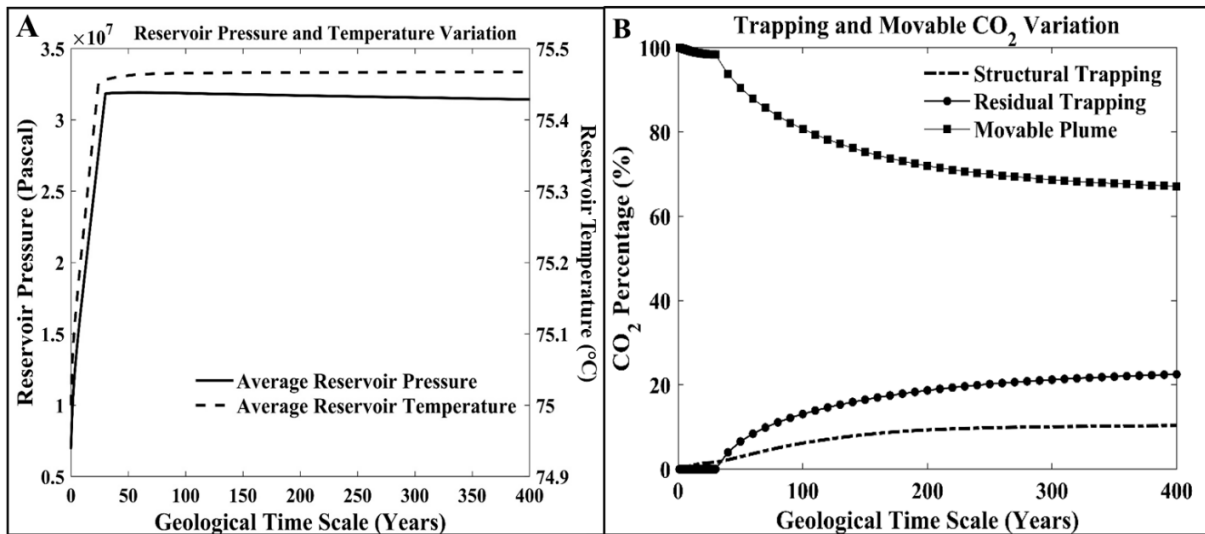


Figure 6.3: (A) Average reservoir pressure and temperature variation; and (B) structural and residual trapping and movable plume variation over geological time scale [219].

6.4 Utilization of Machine Learning: Time Series Neural Network Analysis

In order to make a reasonable forecast of the target variables, NARX and NAR algorithms were implemented using the neural network toolbox in MATLAB. The NARX and NAR models are the preferred choices owing to their simplicity in implementation and their ability to provide accurate forecasts with minimal data requirements. These models are particularly well-suited for initial stage analysis. The input parameters required for these models are acquired using traditional techniques by solving the multiphase flow equations, as described in the previous section. The percentages of CO₂ trapped structurally and residually are considered target variables. The NARX and NAR architecture are shown in **Figure 6.4A** and **Figure 6.4B**, using the structural entrapment percentage as the target variable [219].

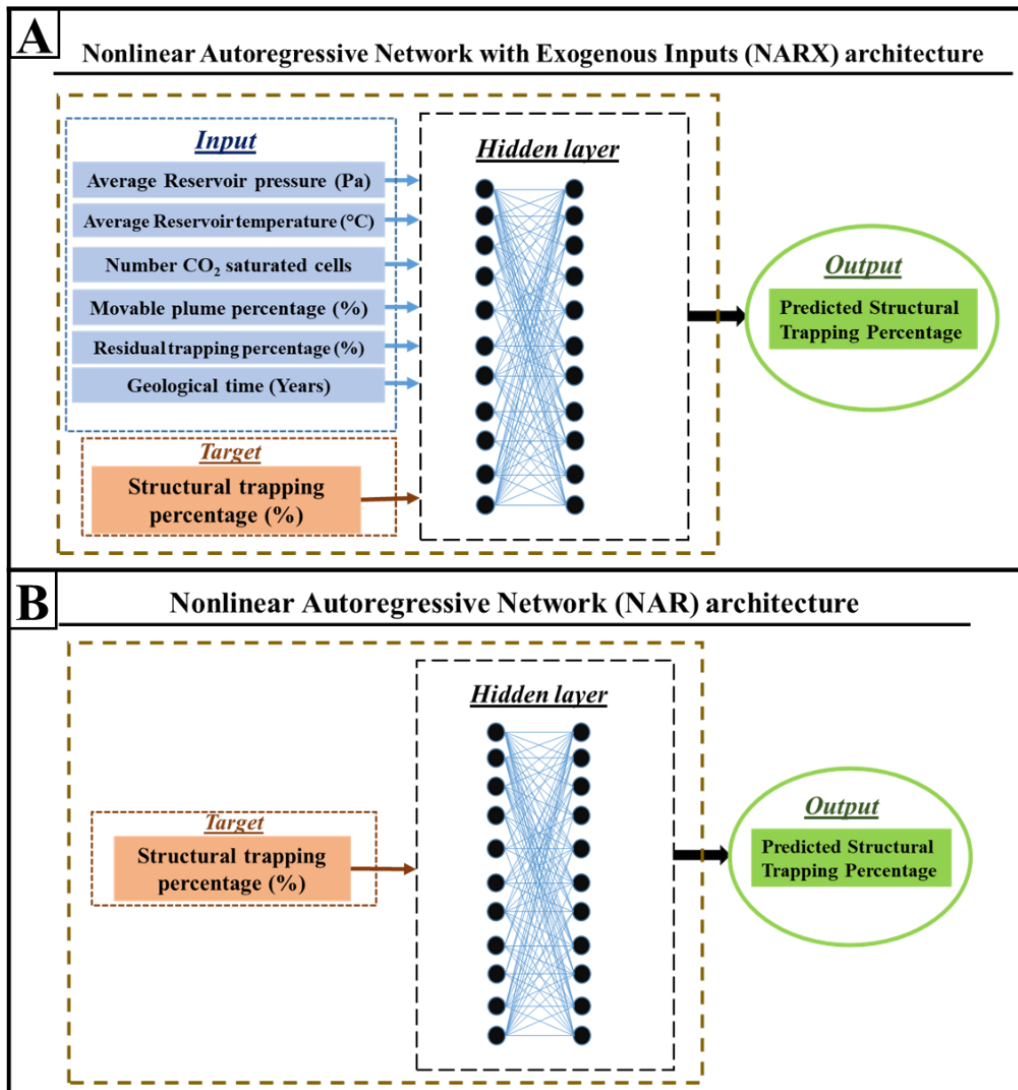


Figure 6.4: (A) Nonlinear Autoregressive Network with Exogenous Inputs (NARX) architecture; (B) Nonlinear Autoregressive Network (NAR) architecture. The figure illustrated the structural trapping as the target variable. In the case of NARX, if the residual trapping is selected as the target variable, then the structural trapping will be considered under the input variable [219].

The NARX model considers average reservoir pressure, average reservoir temperature, number of CO₂ saturated cells, a geological time in years, moveable plume percentage, and structural or residual trapping percentage as input parameters. Structural trapping and residual trapping are used interchangeably. If structural trapping is the target variable, residual trapping is considered for the input variable, as shown in **Figure 6.4**. Meanwhile, in the NAR neural network architecture, only a target variable is employed, and no input variables are considered,

as shown in **Figure 6.4B**. For example, suppose structural trapping is the parameter of interest. In that case, future values of the target variable are projected based on previous values of the target variable, as shown in **Figure 6.4B**. The design of both neural networks includes two hidden layers and ten neurons. Initially, the network is trained in an open-loop environment, and then it is changed to a closed-loop environment to predict the future values of the target variable. Multistep prediction is only possible in a closed-loop network in NAR and NARX. This research investigates twelve training function algorithms to determine the best method for predictive trapping percentage analysis (see **Figure 6.5**) [219].

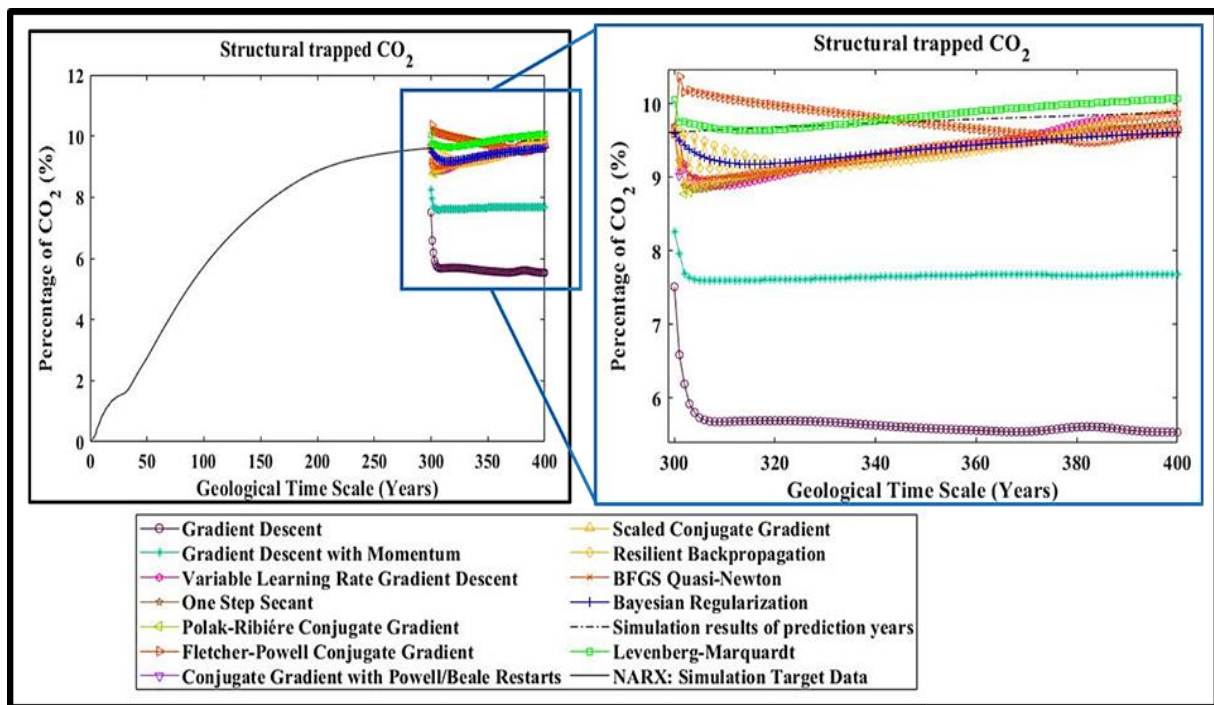


Figure 6.5: Comparison of different training function algorithms used with the NARX neural network. Levenberg-Marquardt has shown low deviation from simulation target data [219].

Levenberg-Marquardt (LM) has performed well among all training models (see **Figure 6.5**). As shown in **Figure 6.6A** and **Table 6-1**, the Nonlinear Autoregressive Network with Exogenous Inputs-Levenberg-Marquardt (NAR-LM) has a smaller deviation for structural trapping simulation results than the Nonlinear Autoregressive Network with Exogenous Inputs-

Levenberg-Marquardt (NARX-LM). **Table 6-1** presents the R^2 value and root mean square deviation (RMSE) obtained for NARX-LM and NAR-LM. The R^2 value for NARX-LM is 0.9001, while the RMSE is 0.0582. On the other hand, the R^2 value and RMSE for NAR-LM are 0.9801 and 0.0515, respectively. Because structural trapping and residual trapping are comparable data types, the NAR-LM and NARX-LM are utilized to anticipate residual trapping percentages in the future forecast (see **Figure 6.6B**).

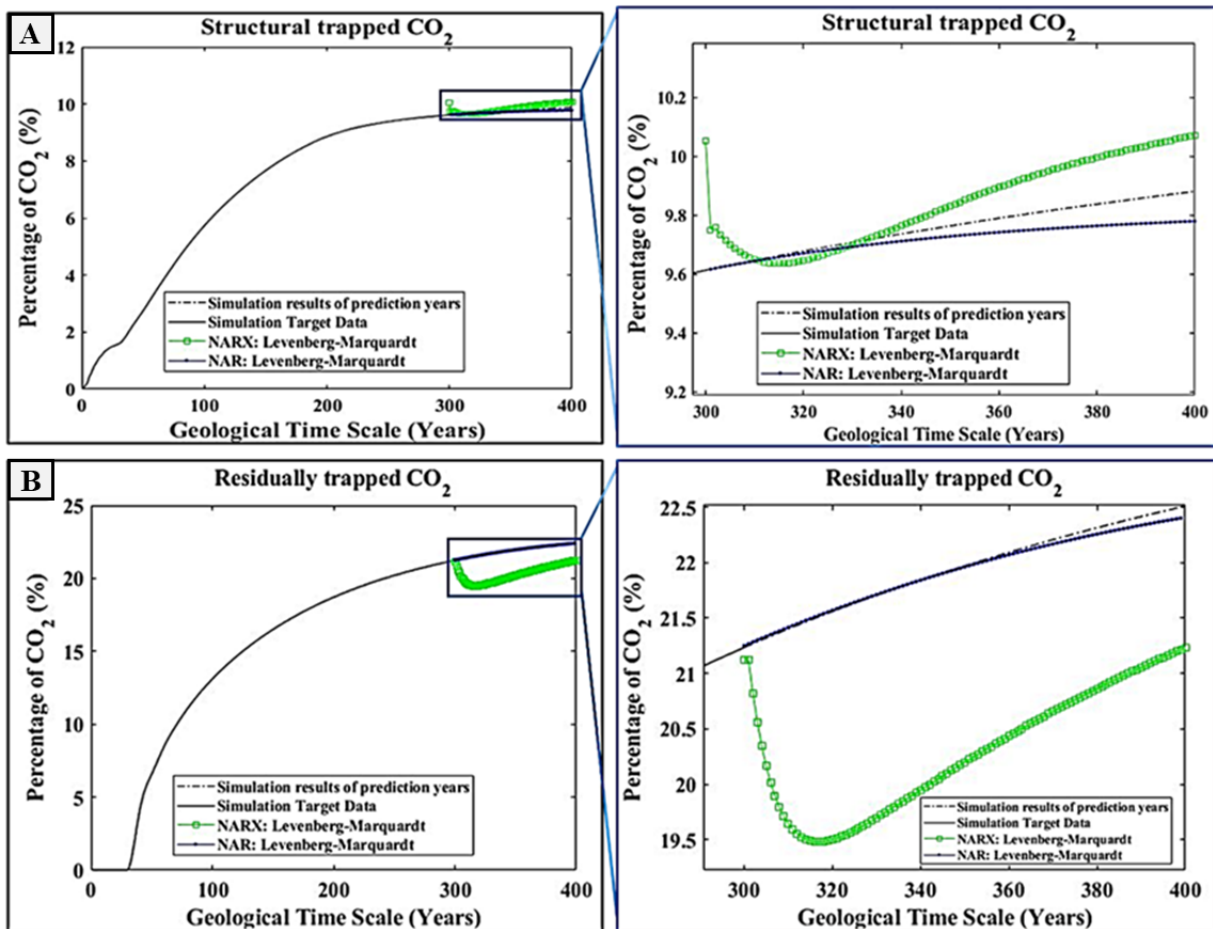


Figure 6.6: Comparisons of NAR-LM and NARX-LM with numerical results for (A) Structural trapping percentage variation and (B) Residual trapping percentage variation. NAR-LM has a very low deviation from target data at the same geological time scale [219].

In general, the NARX forecast should have better prediction compared to the NAR forecast [19]. But, in the present scenario, NAR has a somewhat better performance than NARX.

Because NARX depends on the input variables, there was an irregularity in the data for the number of saturation cells (see **Figure 6.2B**). This inconsistency may have impacted the structural- and residual entrapment percentage forecasts, as observed in **Figure 6.6**. While NARX relies on the target variable's prior values to forecast future values, NAR has produced more dependable findings. **Figure 6.6** compares the predictive forecast of NAR-LM and NARX-LM with convectional numerical simulated data. This investigation shed light on the sensitivity of neural networks in the perturbed and diverse domain's future forecast [219].

Table 6-1: Comparison of R-squared and RMSE values of different training function algorithms for structural trapping [219].

	Algorithm Name	R-Squared	Root-mean-square deviation
Nonlinear Autoregressive Network with Exogenous Inputs (NARX)	Levenberg-Marquardt	0.9001	0.0582
	Bayesian Regularization	0.7045	0.3763
	BFGS Quasi-Newton	0.7434	0.4386
	Resilient Backpropagation	0.5781	0.4130
	Scaled Conjugate Gradient	0.8741	0.4440
	Conjugate Gradient with Powell/Beale Restarts	0.8900	0.4402
	Fletcher-Powell Conjugate Gradient	0.8189	0.2604
	Polak-Ribière Conjugate Gradient	0.8052	0.4621
	One Step Secant	0.8784	0.4680
	Variable Learning Rate Gradient Descent	0.8804	0.4534
	Gradient Descent with Momentum	0.0111	2.1304
	Gradient Descent	0.2620	4.1181
Nonlinear Autoregressive (NAR): Levenberg-Marquardt		0.9801	0.0515

The results of this study provide valuable insights into the impact of heterogeneous caprock morphology on future structural and residual trapping percentage forecasting. The use of numerical simulation and time series neural network analysis has proven to be effective in

predicting the behavior of the target variables on the synthetic domain. The two architectures, NARX and NAR, have demonstrated their capability to capture the underlying dynamics and trends of the system. Overall, this research contributes to a better understanding of the complexity involved in CO₂ sequestration for forecasting the primary trapping mechanisms. Further studies can build upon this work to explore other aspects of the system and enhance the accuracy of the predictions.

6.5 Summary

This chapter focuses on integrating traditional numerical approaches with ANN to investigate the future trend of primary trapping mechanisms in CO₂ geological sequestration (CGS). Traditional numerical simulations are time-consuming and resource-intensive, so machine learning is a potential alternative to analyze simulation results and extract valuable insights. Numerical multiphase flow simulation results are performed to generate data for training and testing of time series neural network models. Time series neural network models, NARX and NAR, were used to forecast the structural and residual trapping percentage using input and target variables. Twelve training algorithms were used for both NARX and NAR models. Among all algorithms, the Levenberg-Marquardt algorithm has shown superior prediction for the provided data type. The impact of input data on the NARX prediction is observed as the change in saturation profile influences the forecast of trapping percentages, whereas this influence was excluded in the NAR model. Both models have obtained an adequate range of R² and RMS values for the Levenberg-Marquardt algorithm. Overall, the NAR has recorded higher accuracy compared to NARX.

- NARX-Levenberg-Marquardt: R² = 0.9001 and RMS = 0.0582
- NAR-Levenberg-Marquardt: R² = 0.9801 and RMS = 0.0515

CHAPTER 7: Conclusions

7 Conclusions

7.1 Realistic geological subsurface domain- Saurashtra, Gujarat, India

Geological formations at depths ranging from several hundred meters to a few thousand meters below the surface are generally considered suitable for CO₂ sequestration. This range of depth provides assurance that the CO₂ would be stored securely and, hence, effectively isolated from the atmosphere. [220], [221]. The target geological formations should possess the necessary porosity and permeability to accommodate the injected CO₂. The location of the storage formation should be suitable in terms of proximity to CO₂ sources, transportation infrastructure, and other factors that could affect the viability and cost-effectiveness of the CGS project [32], [39], [162], [165]. It is important to note that the specific conditions for CO₂ geological sequestration can vary depending on the characteristics of the target storage formation and the specific project requirements. Thorough site characterization, including geophysical surveys, well drilling, and monitoring, is typically conducted to assess the suitability and safety of a potential CO₂ storage site [32], [39], [162], [165].

The Basalt formation's petrophysical properties considered in this research have displayed great potential in the long-term storage of CO₂. The basaltic formation available in Deccan Volcanic Province, India, has characteristics similar to the Columbia River Basalt region for the implementation of CO₂ sequestration [3], [11], [222], [223].

Due to the lack of subsurface geological data on the entirety of the Deccan Volcanic Province, ongoing research and interest were limited to the Saurashtra Peninsula. Detailed mapping of the potential subsurface layers for CO₂ sequestration can give a little more insight into the implementation of CO₂ sequestration in the Deccan Volcanic Province. A more accurate analysis of the mineralogy of the subsurface could potentially lead to a better estimation for the overall implementation of CGS in the Deccan Volcanic Province.

7.2 Structural- and Residual Trapping

A comprehensive study is conducted to relate the dependence of structural- and residual trapping on certain sequestration parameters like the petrophysical properties, injection rate, and injection point. Maximum storage for a longer period of time may be achieved without affecting the integrity of the caprock, provided CO₂ is injected at the optimal injection rate and at the ideal injection site. During the research study, the following were prominent observations:

- Structural- and residual trapping contribute considerably to store CO₂ for a significant period. In this primary trapping simulation analysis, it was observed that the percentage of structural- and residual trapping of the structure decreased upon an increase in the injection rates. This trend would be consistent across all injection locations due to the finite amount of trap capacity.
- Residual trapping is further impacted by the proximity of formation traps to the respective injection sites. This is due to the fact that formation traps often operate as mini-reservoirs and greatly contribute to the overall trapping phenomenon.
- It was also observed that the range of both porosity and permeability values significantly impacts the sweeping efficiency. Simulation results indicated that a geologically modeled domain's lower petrophysical characteristic range exerted a greater constraint on CO₂ flow. Thus, this result demonstrated that the structural- and residual trapping depended on the petrophysical properties.
- This simulation analysis also provided a few insights into the selection of optimal injection points based on the percentage of structural- and residual trapping occurring within the formation region. The closer the structural traps are to a specific injection point, the higher the chances of structural- and residual trapping specifically.

7.3 Solubility Trapping

In addition to primary trapping mechanisms, solubility trapping and its associated geochemical reactions were also considered in these simulation studies to better understand the effect of injection site and petrophysical characteristics upon the solubility trapping mechanism. It was evident that the choice of injection location significantly impacts the subsequent migration and sweeping of CO₂. The major observations from the simulation study on Solubility trapping analysis are as follows:

- Simulation studies involving the selection of injection points provided valuable insights into the migration and sweeping of CO₂ after injection. These results revealed an assessment of the structural integrity and storage capacity.
- Among all the considered injection points, injection point B exhibited the best solubility trapping. Furthermore, the average reservoir pressure at point B was found to be within an acceptable range.
- An apparent pressure increase was observed in the modeled domain in a study on the influences of petrophysical properties that incorporated a low range of petrophysical properties. As a result of this high pressure, CO₂ was also observed to dissolve into the connate water at a greater amount throughout the domain.
- The rise in the pressure in the reservoir, due to the low range of petrophysical properties, would cause a buildup of stress on the formation domain, which would ultimately have an effect on the structural integrity of the entire subsurface structure.
- During the mineral trapping mechanism, the reservoir pressure and domain pH, both of which are influenced by the solubility trapping mechanism, could have an effect on the processes of mineral dissolution and precipitation [68], [116], [117].

A comparative simulation study was conducted to investigate the impact of caprock morphology on solubility trapping, and the study was performed by considering two synthetic simulation domains, one with incorporating an anticline dome and another without incorporating any geological structural features. During the research study, the following were prominent observations:

- It was observed that the presence of the anticline dome decreases the solubility trapping efficiency but increases the injection rate range.
- From the simulation study, it has been observed that the solubility fingering phenomena greatly influence the injected CO₂ trapping in the domain.
- The average reservoir pressure observations have provided insight for two comparison simulation model sets, which assisted in analyzing the effective storage of CO₂ injected into the formation domain.
- The CO₂ plume migration was observed to have safely stagnated in the anticline dome, but the solubility entrapment observed was moderate compared to another simulation set.
- In any case, the CO₂ plume that is stored within certain geological features like anticline domes will cut down on the expenses associated with monitoring during the post-injection period.
- The current study provided insight into the use of naturally occurring geological subsurface features for CGS for safely storing captured CO₂ [63], [111].

7.4 Mineral Trapping

In basalt rocks, mostly secondary minerals like carbonates, aluminosilicate, and silica are found in the rock's cavities and amygdales [78]. The Indian basalt rock formation is considered advantageous as it contains about 25% of the mineral weight of Calcium, Magnesium, and Iron

oxides. Consisting of these minerals makes basalt a suitable candidate for CO₂ sequestration. Basalt rock can react more to the injected CO₂ than other sedimentary rocks [78]. When the ScCO₂ is injected into the formation domain, the domain's pH will decrease due to the solubility trapping of CO₂ into the reservoir fluid. Once the pH gradually returns to an alkaline level, it triggers the mineral reaction with divalent cations. These cations react with carbonate solution and form secondary minerals due to precipitation reactions [66], [224].

The multiphase and multicomponent reactive transport modeling is used in the current research analysis to study the influence of mineral trapping on the CGS. Mineralogy plays a significant role in the determination of effective mineral trapping in the geological subsurface. In naturally available basalt formation, numerous minerals are found [2], [4], [6], [8], [66], [73], [117], [126], [127], [225]. However, the study considered nine minerals due to the unavailability and limitation of mineral repositories. During simulations in the modeled synthetic domain, the pH of the domain was observed to increase except in the migration pathway. This is due to the formation of weak carbonic acid, which further leads to mineral dissolution and precipitation at this migration pathway. The dissolution and precipitation of minerals in the domain depends mainly on the other minerals present in the domain. The mineral trapping simulation results reveal that Calcite mineral precipitation occurs at a faster rate in the synthetic domain, with Dolomite following closely.

On the other hand, Aragonite dissolves at a significantly higher pace than other minerals in the synthetic domain. Chinochlore-14A and Diopside minerals exhibit minimal volume fraction variation, while Quartz and Saponite-Ca show negligible reactivity. The porosity changes in the domain have not shown much variation. This all depends on the mineral composition present in the subsurface domain. From literature and current numerical simulation analysis, it is observed that mineral trapping is optimal at temperatures around 100 °C and at an alkaline range of pH for the basalt rock [116], [117].

7.5 Structural Integrity

The structural integrity simulations were carried out to investigate the influence of caprock morphology and caprock crack, with its subsequent impact on CO₂ entrapment and CO₂ leakage during CGS. The presence of a crack in the migration pathway affects critical attributes such as entrapment percentage, structural integrity, and safe storage, all of which are critical for the safe implementation of CGS [56], [57], [226]. Three synthetic geological domains with different caprock morphologies are considered in this analysis to investigate the influence of geological structures and features on entrapment and structural integrity. These simulations provided insight into CO₂ leakage for various morphological features. This study has explained the influence of geological structures and blended geological morphology features on plume migration in the presence of a crack, as well as its implications on entrapment percentage and structural integrity. Following are some of the major observations of this study

Compared to synthetic domain-1 and -2, the presence of anticline structure in the domain reduces the sweeping efficiency of the injected CO₂ plume, further influencing solubility trapping. Because of the higher lateral sweeping in synthetic domain-2 compared to synthetic domain-1, significantly less CO₂ plume reached the fault in synthetic domain-2, and the leakage recorded was lower. However, this study would also highlight the significance of geological features; if the crack were not located near the anticline dome, synthetic domain-1 might be a safer option for sequestration.

The investigation of the synthetic domain-3, which was constructed using existing geological data of the Deccan Volcanic Province, offers insights into the migration of CO₂ plumes and the impact of geological features, such as an anticline dome. A crack in close proximity to the anticline structure may result in CO₂ leakage. During the first few years, the stairstep structure influenced CO₂ movement; during this period, the CO₂ plume mainly spread horizontally in a

single stripe of the trap. When the CO₂ plume comes under the influence of the anticline dome elevation, the CO₂ plume tends to move up-dip direction, passing through stairsteps traps. This observation shows that geological structure dominates in influencing CO₂ plume movement in the subsurface geological domain.

When comparing CO₂ leakage into the top section of a domain in all of the synthetic modeled domains, it can be observed that the leakage of CO₂ into the top section was most significant in synthetic domain-1 and -2 when compared to synthetic domain-3. Because the CO₂ plume migrated and percolated through stairsteps, traps were subjected to primary trapping, and only a small amount leaked into the domain's top section. This provides insight into CO₂ migration and leakage in a domain that is embedded with geological features and structures.

7.6 Machine Learning Technique in CGS

The financial and scientific impracticality of performing CGS analysis through experiments is enormous. Complex geometric models have been found to be computationally costly and slow when utilizing traditional numerical methodologies [16], [227]. In this work, conventional numerical simulation results are integrated with machine learning methodologies to forecast the future trend of target parameters. A time series neural network is used to anticipate the trend of target parameters throughout the post-injection period, with the CO₂ sequestration parameter values serving as both the input and the target for the network. Validation is accomplished using target parameter simulation data that already exists. This study evaluates the influence of heterogeneity on top subsurface morphology on the neural network time series forecast [219].

Amongst the twelve employed algorithms, the Levenberg-Marquardt algorithm has exhibited superior predictive performance for the given data type. Both the NARX and NAR architecture models have achieved a satisfactory range of R² and RMS values when utilizing the Levenberg-Marquardt algorithm. The forecasting outcomes of the NARX model underscore its

dependence on input data; irregularities in the saturation profile have led to deviations in the projections for the predicted years. In aggregate, the NAR architecture has demonstrated higher accuracy in comparison to NARX. Here are the specific metrics for both cases:

- NARX-Levenberg-Marquardt: $R^2 = 0.9001$, $RMS = 0.0582$
- NAR-Levenberg-Marquardt: $R^2 = 0.9801$, $RMS = 0.0515$

This study offers a concise summary of the use of ANN with convectional simulation data. Many aspects, including the training function technique, the number of neurons, the number of hidden layers, and so on, can influence the accuracy of a time series analysis. The forecast in this study is impacted by the input and target variable data [219].

7.7 Overall conclusions

Structural and residual trapping processes considerably contribute to the storage of CO₂ for a very prolonged duration. The performed simulation study reveals that reducing injection rates increases the percentage of structural and residual trapping. Due to the limited capacity of the traps, this tendency was constant across all injection locations. The dominance of residual trapping is determined by the proximity of formation traps to injection locations, as formation traps function as mini-reservoirs and significantly contribute to the overall trapping phenomenon. Utilizing the optimal injection rate at the ideal injection position can result in maximum storage for extended periods without jeopardizing the caprock's structural integrity.

The essential insight garnered from the caprock morphological study is that it can influence the migration pathway of the injected ScCO₂ in the geological domain, ultimately influencing the solubility trapping. The current research analysis has shed light on the influence of the caprock's sweeping efficiency and caprock morphology on the solubility trapping over a

geological time. The solubility fingering during lateral migration in the stairsteps traps provides insight into the effect of geological features on the solubility trapping mechanism.

Petrophysical heterogeneity in geological formations has significantly impacted the CO₂ trapping mechanisms during CO₂ geological sequestration (CGS). Heterogeneity refers to variations in the distribution of porosity and permeability within the storage formation [63], [80], [111]. It affects the overall storage capacity and the distribution of CO₂ within the formation. Heterogeneity can influence the occurrence and relative contributions of trapping mechanisms, such as structural, residual, and solubility trapping mechanisms [63], [80], [111], [228], [229]. Highly heterogeneous formations may exhibit variations in the dominance of these trapping mechanisms, impacting the long-term storage capacity and the potential for CO₂ leakage [63], [80], [111], [228], [229].

The mineralogy of the target storage formation plays a significant role in ensuring the long-term stability and effectiveness of the storage site. Suitable mineralogy for CO₂ geological sequestration typically includes minerals that can chemically react with CO₂ and undergo mineral carbonation [4], [114], [120], [230], [231]. Minerals such as Olivine, Serpentine, basalt, and certain types of ultramafic rocks are considered favorable due to their high magnesium, calcium, and iron content [4], [6], [8], [73], [78], [117], [126], [225]. These minerals can react with CO₂, forming stable carbonate minerals through mineral carbonation. The mineral carbonation of CO₂ helps to immobilize and store the carbon dioxide in a solid form, reducing the risk of CO₂ leakage and providing long-term storage. Additionally, silica-rich minerals, such as quartzite, can contribute to the sealing capacity of the storage formation, enhancing the containment of CO₂. It is essential to consider the mineralogical composition of the storage formation to ensure favorable conditions for successful and secure CO₂ geological sequestration [4], [6], [8], [73], [78], [117], [126], [225].

Numerous minerals are discovered in naturally occurring basalt formation. Due to limitations and the unavailability of mineral repositories for simulations, only a small number of minerals are used in this study. The pH was observed to rise in the three-dimensional domain except in the migration pathway. In addition, weak carbonic acid formation causes minerals to dissolve and precipitate along this path. The dissolution and precipitation of minerals in a domain are largely determined by the presence of other minerals in the domain. When H^+ predominates within a domain, calcite is observed to precipitate. Changes in the domain's porosity have exhibited little variation. This is contingent upon the mineral composition of the subsurface domain.

The geological formation must exhibit stability to avoid the risk of structural failure or displacement of the stored CO_2 . Stability is assessed by evaluating factors such as geological history, tectonic activity, and the absence of active faults or fractures that could compromise the integrity of the storage reservoir [57], [85]. The presence of a crack in the migration pathway affects critical attributes such as entrapment percentage, structural integrity, and safe storage, all of which are essential for the successful implementation of CGS risk-free. This analysis offered some valuable insights into leakage analysis for a number of different morphological features. This research has explained the role that geological structures and aspects of geological morphology play in plume migration when there is a crack present in the area. Additionally, this analysis has provided a description of the implications that this has for the percentage of further entrapment and structural integrity.

Table 7-1 presented below provides an illustration of the principal governing parameters that exert an influence on their respective trapping mechanisms. These major governing parameters have been considered based on the authors' preliminary understanding while acknowledging that additional parameters may also impact trapping. It is important to note that each formation

layer possesses distinct characteristics; therefore, its influence on trapping may vary accordingly.

Table 7-1: Illustration of major governing parameters influencing the corresponding trapping mechanisms [56], [58], [184]–[187], [204], [232], [63], [80], [109], [111], [180]–[183].

Trapping Mechanisms	Major Governing Parameters
Structural Trapping	<ul style="list-style-type: none"> • Porosity and permeability distribution within the storage formation • Caprock morphology and subsurface caprock features • Presence of faults, fractures, and sealing mechanisms • Selection of injection location for CO₂ sequestration • Geological structure and stratigraphy characteristic
Residual Trapping	<ul style="list-style-type: none"> • Porosity and permeability distribution within the storage formation. • Pore aspect ratio and pore network connectivity of the subsurface formation layer. • The water table of the subsurface domain • Selection of injection location for CO₂ sequestration • Injection scheme for CO₂ injection • Caprock morphology and sweeping distance of CO₂ plume • Reservoir fluid density and average reservoir pressure
Solubility Trapping	<ul style="list-style-type: none"> • Capillary pressure and interfacial tension between CO₂ and the reservoir fluid • Entrapment percentage of primary trapping mechanisms • pH variation of the subsurface formation • The availability of water and salinity of the domain • Pore size and pore network connectivity • Wettability characteristics of the rock surfaces • The presence of low-permeability barriers or trapping layers
Mineral Trapping	<ul style="list-style-type: none"> • Availability and reactivity of minerals capable of carbonation Surface area and accessibility of reactive minerals • Entrapment percentage of primary and solubility mechanisms • pH variation of the subsurface formation • Reaction kinetics influenced by temperature and pressure conditions • The presence of dissolved CO₂ in water facilitates mineral reactions

The utilization of Machine Learning models was explored to streamline the analysis process in CO₂ geological sequestration. This involved investigating the reduction of time and computational intensity required for analysis. The study focused on modeling and analyzing intricate geometric models, which traditionally necessitate costly and rigorous numerical

methods. Consequently, an attempt was made to integrate machine learning and numerical simulation to forecast significant parameter trends. The results obtained from the numerical simulation were considered to validate the findings. While the time series results closely resembled the simulated numerical outcomes, it was observed that input variables such as petrophysical heterogeneity and top subsurface morphology impacted the neural network's ability to forecast accurately [219].

7.8 Limitations of the Research

The modeled simulation domain does not depict the naturally available structure. The simulation domain must include the geological faults, cracks, and minor geomorphological structures to identify the structure's durability for CO₂ sequestration. The realistic modeling of the synthetic domain incorporating various geological features like lenses, laminates, faults, cracks, etc., can lead to the analysis of various other phenomena and their influences on the CO₂ trapping and integrity of the subsurface geological structure.

The current simulation analysis is limited in its ability to analyze and simulate microscale phenomena. This is particularly relevant in a realistic case, where cracks in the subsurface region can create secondary porosity and have a significant impact on fluid flow in the porous domain. Unfortunately, due to a lack of geological data, the simulation analysis cannot incorporate the influence of these cracks. Additionally, the unavailability of data about the mineral composite of the resident rock results in less accurate predictions. Several crucial pieces of data are also unavailable, including information about the geological subsurface water table, the stretch of the underground water network, and the rock strength around the network. More data is needed to gain a better insight into the different top surface caprock morphologies and their impacts, such as elevation, slope angle, and types of folds. Without access to this

important data, the simulation analysis is limited in its ability to accurately model and predict real-world behavior.

7.9 Future Research scope

The Basalt formation petrophysical properties considered in this research, for its good porous structure, have displayed great potential in the long-term storage of CO₂. The Basaltic formation available in Deccan Volcanic Province, India, has similar favorable characteristic properties to the Columbia River Basalt region for the implementation of CO₂ sequestration [3], [5], [222], [223]. The results of trapping mechanisms are promising to conduct future theoretical studies on the feasibility of implementing CGS by considering more minerals in the Deccan Volcanic Province. The following illustrates some potential future areas of work in CO₂ sequestration, including the Deccan Volcanic Province and other studies on sequestration parameters.

- The scope of future work should be on carrying out the development of multiphase reactive transport simulations for CO₂ sequestration simulation incorporating more minerals of Deccan basalts [8], [11], [162], [203]. These simulations can provide a more accurate estimation of a reservoir's storage capacity and feasibility for the implementation of CO₂ sequestration.
- The research on Enhanced Oil Recovery simulations in the Indian subsurface regions has to be studied to estimate the carbon sink capacity.
- The influences of subsurface water tables on the CGS and mostly on the entrapment mechanisms, especially on the solubility trapping, will be crucial studies to conduct. The influence of microbial surface formation on the CGS has to be performed.

- Investigate the effects of geological heterogeneities such as faults, fractures, and discontinuities on CO₂ storage capacity, injection rates, and pressure accumulation. This can give useful information for risk evaluation of CO₂ storage activities.
- Study the long-term fate of stored CO₂ under various environmental circumstances such as temperature, pressure, and geochemistry. This can help to improve knowledge of long-term storage integrity and potential leakage.
- Investigate the possibility of integrating CGS with other energy technologies such as enhanced oil recovery (EOR), geothermal energy generation, or hydrogen production. This has the potential to bring significant economic benefits while also increasing the overall efficiency of the CGS system.

This thesis is a thorough and comprehensive analysis of CO₂ geological sequestration that delves into multiple aspects, including reactive transport modeling, caprock morphology, and machine learning techniques. The literature review provides a panoramic view of existing technologies and worldwide CGS projects, highlighting the immense potential of CGS in India. The investigation of trapping mechanisms in the Deccan Volcanic Province explored various crucial factors that influence successful CO₂ sequestration, such as injection point selection, heterogeneity-petrophysical properties, and injection rate. The chapter on caprock morphology and structural integrity provided an insightful analysis of the solubility trapping mechanism and CO₂ leakage, giving significant consideration to the Stairsteps domain. Finally, the utilization of machine learning techniques provided valuable insights into time series neural network analysis in CO₂ geological sequestration. In conclusion, this thesis is a significant contribution to scientific research and lays the groundwork for future studies in CO₂ emissions reduction.

References

- [1] O. de Q. F. Araújo and J. L. de Medeiros, “Carbon capture and storage technologies: present scenario and drivers of innovation,” *Current Opinion in Chemical Engineering*, vol. 17. Elsevier Ltd, pp. 22–34, 2017. doi: 10.1016/j.coche.2017.05.004.
- [2] S. R. Gislason and E. H. Oelkers, “Carbon storage in basalt,” *Science (80-.)*, vol. 344, no. 6182, pp. 373–374, 2014, doi: 10.1126/science.1250828.
- [3] B. P. McGrail, H. T. Schaef, A. M. Ho, Y.-J. J. Chien, J. J. Dooley, and C. L. Davidson, “Potential for carbon dioxide sequestration in flood basalts,” *J. Geophys. Res. Solid Earth*, vol. 111, no. 12, pp. 1–13, Dec. 2006, doi: 10.1029/2005JB004169.
- [4] Y. Takaya, K. Nakamura, and Y. Kato, “Geological, geochemical and social-scientific assessment of basaltic aquifers as potential storage sites for CO₂,” *Geochem. J.*, vol. 47, no. 4, pp. 385–396, Aug. 2013, doi: 10.2343/geochemj.2.0255.
- [5] L. Rycroft and J. Craig, “IEAGHG, Review of CO₂ Storage in Basalts,” 2017. [Online]. Available: <https://ieaghg.org/publications/technical-reports>
- [6] L. Basava-Reddi, “Geological Storage of CO₂ in Basalt,” 2011.
- [7] R. J. Rosenbauer, B. Thomas, J. L. Bischoff, and J. Palandri, “Carbon sequestration via reaction with basaltic rocks: Geochemical modeling and experimental results,” *Geochim. Cosmochim. Acta*, vol. 89, pp. 116–133, 2012, doi: 10.1016/j.gca.2012.04.042.
- [8] P. S. R. Prasad, D. S. Sarma, and S. N. Charan, “Mineral trapping and sequestration of carbon-dioxide in Deccan basalts: SEM, FTIR and Raman spectroscopic studies on secondary carbonates,” *J. Geol. Soc. India*, vol. 80, no. 4, pp. 546–552, Oct. 2012, doi: 10.1007/s12594-012-0175-z.
- [9] D. Liu, R. Agarwal, F. Liu, S. Yang, and Y. Li, “Modeling and assessment of CO₂ geological storage in the Eastern Deccan Basalt of India,” *Environ. Sci. Pollut. Res.*, vol. 29, no. 56, pp. 85465–85481, Dec. 2022, doi: 10.1007/s11356-022-21757-y.
- [10] P. Viebahn, S. Höller, D. Vallentin, H. Liptow, and A. Villar, “Future CCS implementation in India: A systemic and long-term analysis,” in *Energy Procedia*, Elsevier, Jan. 2011, pp. 2708–2715. doi: 10.1016/j.egypro.2011.02.172.

- [11] P. S. R. Prasad *et al.*, “Geological sequestration of carbon dioxide in Deccan basalts: preliminary laboratory study,” *Curr. Sci.*, vol. 96, no. 2, pp. 288–291, 2009, [Online]. Available: <https://www.jstor.org/stable/24105195>
- [12] Luigi Marini, *Geological Sequestration of Carbon Dioxide Thermodynamics, Kinetics, and Reaction Path Modeling*. Elsevier Developements in Geochemistry, 2006.
- [13] B. Metz, O. Davidson, H. de Coninck, M. Loos, and L. Meyer, *IPCC special report on carbon dioxide capture and storage*. United States: Cambridge University Press, New York, NY (United States), 2005. [Online]. Available: <https://www.osti.gov/biblio/20740954>
- [14] C. I. Steefel, D. J. DePaolo, and P. C. Lichtner, “Reactive transport modeling: An essential tool and a new research approach for the Earth sciences,” *Earth Planet. Sci. Lett.*, vol. 240, no. 3–4, pp. 539–558, Dec. 2005, doi: 10.1016/j.epsl.2005.09.017.
- [15] T. Xu, L. Zheng, and H. Tian, “Reactive transport modeling for CO₂ geological sequestration,” *J. Pet. Sci. Eng.*, vol. 78, no. 3–4, pp. 765–777, Sep. 2011, doi: 10.1016/j.petrol.2011.09.005.
- [16] C. I. Steefel *et al.*, “Reactive transport codes for subsurface environmental simulation,” *Comput. Geosci.*, vol. 19, no. 3, pp. 445–478, Sep. 2015, doi: 10.1007/s10596-014-9443-x.
- [17] C. H. V Lagneau Pipart A. and C. H. V Lagneau Pipart A., “Reactive Transport Modelling of CO₂ Sequestration in Deep Saline Aquifers,” *Oil Gas Sci. Technol.*, vol. 60, no. March 2005, pp. 231–247, 2005.
- [18] Y. Xiao, F. Whitaker, T. Xu, and C. Steefel, *Reactive transport modeling: Applications in subsurface energy and environmental problems*. wiley, 2018. doi: 10.1002/9781119060031.
- [19] G. E. Hammond, S. N. Laboratories, and P. Lichtner, “PFLOTRAN: Reactive Flow & Transport Code for Use on Laptops to Leadership-Class Supercomputers,” *Groundw. React. Transp. Model.*, no. January, pp. 141–159, 2012, doi: 10.2174/978160805306311201010141.
- [20] R. T. Mills, C. Lu, P. C. Lichtner, and G. E. Hammond, “Simulating subsurface flow and transport on ultrascale computers using PFLOTRAN,” *J. Phys. Conf. Ser.*, vol. 78,

- no. 1, p. 012051, Jul. 2007, doi: 10.1088/1742-6596/78/1/012051.
- [21] G. E. Hammond, P. C. Lichtner, and R. T. Mills, “Evaluating the performance of parallel subsurface simulators: An illustrative example with PFLOTRAN,” *Water Resour. Res.*, vol. 50, no. 1, pp. 208–228, 2014, doi: 10.1002/2012WR013483.
- [22] C. Lu and P. C. Lichtner, “PFLOTRAN: Massively Parallel 3D Simulator for CO₂ Sequestration in Geologic Media,” in *Fourth annual conference on carbon capture and sequestration DOE/NETL conference proceedings*, 2005.
- [23] S. Bachu and J. J. Adams, “Sequestration of CO₂ in geological media in response to climate change: Capacity of deep saline aquifers to sequester CO₂ in solution,” *Energy Convers. Manag.*, vol. 44, no. 20, pp. 3151–3175, 2003, doi: 10.1016/S0196-8904(03)00101-8.
- [24] S. Bachu, “Sequestration of CO₂ in geological media: Criteria and approach for site selection in response to climate change,” *Energy Convers. Manag.*, vol. 41, no. 9, pp. 953–970, Jun. 2000, doi: 10.1016/S0196-8904(99)00149-1.
- [25] S. Bachu, “CO₂ storage in geological media: Role, means, status and barriers to deployment,” *Prog. Energy Combust. Sci.*, vol. 34, no. 2, pp. 254–273, Apr. 2008, doi: 10.1016/j.pecs.2007.10.001.
- [26] R. Gholami, A. Raza, and S. Iglauer, “Leakage risk assessment of a CO₂ storage site: A review,” *Earth-Science Rev.*, vol. 223, p. 103849, Dec. 2021, doi: 10.1016/j.earscirev.2021.103849.
- [27] F. Basirat, *Process Models for CO₂ Migration and Leakage*. 2017. Accessed: May 07, 2019. [Online]. Available: <http://urn.kb.se/resolve?urn=urn:nbn:se:uu:diva-315490>
- [28] J. Foroozesh, M. A. Dier, and M. G. Rezk, “A simulation study on CO₂ sequestration in saline aquifers: Trapping mechanisms and risk of CO₂ leakage,” *MATEC Web Conf.*, vol. 225, p. 03004, Nov. 2018, doi: 10.1051/mateconf/201822503004.
- [29] H. Deng, P. H. Stauffer, Z. Dai, Z. Jiao, and R. C. Surdam, “Simulation of industrial-scale CO₂ storage: Multi-scale heterogeneity and its impacts on storage capacity, injectivity and leakage,” *Int. J. Greenh. Gas Control*, vol. 10, pp. 397–418, 2012, doi: 10.1016/j.ijggc.2012.07.003.
- [30] P. R. Punnam, B. Krishnamurthy, and V. K. Surasani, “Investigations of Structural and

- Residual Trapping Phenomena during CO₂ Sequestration in Deccan Volcanic Province of the Saurashtra Region, Gujarat,” *Int. J. Chem. Eng.*, vol. 2021, pp. 1–16, Jul. 2021, doi: 10.1155/2021/7762127.
- [31] O. P. Pandey, N. Vedanti, and S. S. . S. Ganguli, “Some Insights into Possible CO₂ Sequestration in Subsurface Formations beneath Deccan Volcanic Province of India,” *J. Indian Geophys. Union*, vol. 1, pp. 20–25, 2016.
- [32] P. Viebahn, D. Vallentin, and S. Höller, “Prospects of carbon capture and storage (CCS) in India’s power sector – An integrated assessment,” *Appl. Energy*, vol. 117, pp. 62–75, Mar. 2014, doi: 10.1016/J.APENERGY.2013.11.054.
- [33] B. Samant and D. M. Mohabey, “Deccan volcanic eruptions and their impact on flora: Palynological evidence,” *Spec. Pap. Geol. Soc. Am.*, vol. 505, pp. 171–191, 2014, doi: 10.1130/2014.2505(08).
- [34] P. K. Nagar, M. Sharma, S. Gupta, and D. Singh, “A framework for developing and projecting GHG emission inventory and preparing mitigation plan: A case study of Delhi City, India,” *Urban Clim.*, vol. 28, no. June 2018, p. 100462, 2019, doi: 10.1016/j.uclim.2019.100462.
- [35] C. M. White, B. R. Strazisar, E. J. Granite, J. S. Hoffman, H. W. Pennline, and Air & Waste Management Association, “Separation and capture of CO₂ from large stationary sources and sequestration in geological formations—coalbeds and deep saline aquifers,” *J. Air Waste Manag. Assoc.*, vol. 53, no. 6, pp. 645–715, Jun. 2003, doi: 10.1080/10473289.2003.10466206.
- [36] C. Brown, P. Alexander, A. Arneeth, I. Holman, and M. Rounsevell, “Achievement of Paris climate goals unlikely due to time lags in the land system,” *Nat. Clim. Chang.*, vol. 9, no. 3, pp. 203–208, 2019, doi: 10.1038/s41558-019-0400-5.
- [37] D. W. J. Thompson, J. J. Kennedy, J. M. Wallace, and P. D. Jones, “A large discontinuity in the mid-twentieth century in observed global-mean surface temperature,” *Nature*, vol. 453, no. 7195, pp. 646–649, May 2008, doi: 10.1038/nature06982.
- [38] Bithunshal U and V. K. Surasani, “Mathematical Modeling of CO₂ Sequestration in Deccan Volcanic Province,” in *Heat and Mass Transfer Conference (IHMT-2017)*, BITS Pilani, Hyderabad, India., 2017.

- [39] R. V. Kapila, H. Chalmers, S. Haszeldine, and M. Leach, "CCS prospects in India: Results from an expert stakeholder survey," *Energy Procedia*, vol. 4, no. June 2009, pp. 6280–6287, 2011, doi: 10.1016/j.egypro.2011.02.642.
- [40] "Global Energy Review: CO₂ Emissions in 2021," 2021. [Online]. Available: <https://www.iea.org/reports/global-energy-review-co2-emissions-in-2021-2>
- [41] "Global Energy Review 2021: Assessing the effects of economic recoveries on global energy demand and CO₂ emissions in 2021," 2021.
- [42] M. T. Craig, H. Zhai, P. Jaramillo, and K. Klima, "Trade-offs in cost and emission reductions between flexible and normal carbon capture and sequestration under carbon dioxide emission constraints," *Int. J. Greenh. Gas Control*, vol. 66, pp. 25–34, Nov. 2017, doi: 10.1016/j.ijggc.2017.09.003.
- [43] A. Mishra, M. Kumar, K. Medhi, and I. S. Thakur, "Biomass energy with carbon capture and storage (BECCS)," in *Current Developments in Biotechnology and Bioengineering*, Elsevier, 2020, pp. 399–427. doi: 10.1016/b978-0-444-64309-4.00017-9.
- [44] N. Von Der Assen, J. Jung, and A. Bardow, "Life-cycle assessment of carbon dioxide capture and utilization: avoiding the pitfalls," *Energy Environ. Sci.*, vol. 6, no. 9, pp. 2721–2734, Aug. 2013, doi: 10.1039/C3EE41151F.
- [45] A. Gulzar, A. Gulzar, M. B. Ansari, F. He, S. Gai, and P. Yang, "Carbon dioxide utilization: A paradigm shift with CO₂ economy," *Chem. Eng. J. Adv.*, vol. 3, p. 100013, Nov. 2020, doi: 10.1016/J.CEJA.2020.100013.
- [46] Z. Zhang *et al.*, "Advances in carbon capture, utilization and storage," *Applied Energy*, vol. 278. Elsevier, p. 115627, Nov. 15, 2020. doi: 10.1016/j.apenergy.2020.115627.
- [47] C. Shi, M. Elgarni, and N. Mahinpey, "Process design and simulation study: CO₂ utilization through mixed reforming of methane for methanol synthesis," *Chem. Eng. Sci.*, vol. 233, p. 116364, Apr. 2021, doi: 10.1016/j.ces.2020.116364.
- [48] P. R. Yaashikaa, P. Senthil Kumar, S. J. Varjani, and A. Saravanan, "A review on photochemical, biochemical and electrochemical transformation of CO₂ into value-added products," *J. CO₂ Util.*, vol. 33, pp. 131–147, Oct. 2019, doi: 10.1016/j.jcou.2019.05.017.
- [49] Q. Zhu, "Developments on CO₂-utilization technologies," *Clean Energy*, vol. 3, no. 2,

- pp. 85–100, May 2019, doi: 10.1093/ce/zkz008.
- [50] D. Ravikumar, D. Zhang, G. Keoleian, S. Miller, V. Sick, and V. Li, “Carbon dioxide utilization in concrete curing or mixing might not produce a net climate benefit,” *Nat. Commun.*, vol. 12, no. 1, pp. 1–13, Feb. 2021, doi: 10.1038/s41467-021-21148-w.
- [51] G. Lorentzen, “Revival of carbon dioxide as a refrigerant,” *Int. J. Refrig.*, vol. 17, no. 5, pp. 292–301, Jan. 1994, doi: 10.1016/0140-7007(94)90059-0.
- [52] F. Bruno, M. Belusko, and E. Halawa, “CO₂ refrigeration and heat pump systems - A comprehensive review,” *Energies*, vol. 12, no. 15. Multidisciplinary Digital Publishing Institute, p. 2959, Aug. 01, 2019. doi: 10.3390/en12152959.
- [53] M. T. White, G. Bianchi, L. Chai, S. A. Tassou, and A. I. Sayma, “Review of supercritical CO₂ technologies and systems for power generation,” *Appl. Therm. Eng.*, vol. 185, p. 116447, Feb. 2021, doi: 10.1016/J.APPLTHERMALENG.2020.116447.
- [54] M. K. Gadogbe, “Cost-Effectiveness Analysis (Cea) of Projected Impact of Carbon Capture and Storage (Ccs) Technologies in Anthropogenic Climate Change Mitigation,” no. June, 2014.
- [55] P. R. Punnam, D. P. Sourya, V. K. Surasani, E. F. Médiçi, and A. D. Otero, “Caprock Topography and Injection Position Influence on the Solubility Trapping Phenomena during CO₂ Geological Sequestration,” in *Album of Porous Media*, Cham: Springer, Cham, 2023, pp. 134–134. doi: 10.1007/978-3-031-23800-0_111.
- [56] D. N. Espinoza and J. C. Santamarina, “CO₂ breakthrough—Caprock sealing efficiency and integrity for carbon geological storage,” *Int. J. Greenh. Gas Control*, vol. 66, pp. 218–229, Nov. 2017, doi: 10.1016/j.ijggc.2017.09.019.
- [57] J. Kaldi *et al.*, “Containment of CO₂ in CCS: Role of caprocks and faults,” in *Energy Procedia*, Elsevier, Jan. 2013, pp. 5403–5410. doi: 10.1016/j.egypro.2013.06.458.
- [58] D. Zhang and J. Song, “Mechanisms for geological carbon sequestration,” in *Procedia International Union of Theoretical and Applied Mechanics IUTAM*, Elsevier, Jan. 2013, pp. 319–327. doi: 10.1016/j.piutam.2014.01.027.
- [59] J. Bradshaw *et al.*, “CO₂ storage capacity estimation: Issues and development of standards,” *Int. J. Greenh. Gas Control*, vol. 1, no. 1, pp. 62–68, Apr. 2007, doi: 10.1016/S1750-5836(07)00027-8.

- [60] U. Gregersen, O. Michelsen, and J. C. Sørensen, “Stratigraphy and facies distribution of the Utsira formation and the Pliocene sequences in the northern North Sea,” *Mar. Pet. Geol.*, vol. 14, no. 7–8, pp. 893–914, Nov. 1997, doi: 10.1016/S0264-8172(97)00036-6.
- [61] A. K. Furre, O. Eiken, H. Alnes, J. N. Vevatne, and A. F. Kiær, “20 Years of Monitoring CO₂-injection at Sleipner,” in *Energy Procedia*, Elsevier, Jul. 2017, pp. 3916–3926. doi: 10.1016/j.egypro.2017.03.1523.
- [62] R. Shukla, P. Ranjith, A. Haque, and X. Choi, “A review of studies on CO₂ sequestration and caprock integrity,” *Fuel*, vol. 89, no. 10, pp. 2651–2664, 2010, doi: 10.1016/j.fuel.2010.05.012.
- [63] P. R. Punnam, B. Krishnamurthy, and V. K. Surasani, “Influence of Caprock Morphology on Solubility Trapping during CO₂ Geological Sequestration,” *Geofluids*, vol. 2022, pp. 1–15, Jun. 2022, doi: 10.1155/2022/8016575.
- [64] I. Gunnarsson *et al.*, “The rapid and cost-effective capture and subsurface mineral storage of carbon and sulfur at the CarbFix2 site,” *Int. J. Greenh. Gas Control*, vol. 79, no. August, pp. 117–126, 2018, doi: 10.1016/j.ijggc.2018.08.014.
- [65] B. Callow, I. Falcon-Suarez, S. Ahmed, and J. Matter, “Assessing the carbon sequestration potential of basalt using X-ray micro-CT and rock mechanics,” *Int. J. Greenh. Gas Control*, vol. 70, no. February, pp. 146–156, 2018, doi: 10.1016/j.ijggc.2017.12.008.
- [66] S. Snæbjörnsdóttir, F. Wiese, T. Fridriksson, H. Ármansson, G. M. Einarsson, and S. R. Gislason, “CO₂ storage potential of basaltic rocks in Iceland and the oceanic Ridges,” *Energy Procedia*, vol. 63, pp. 4585–4600, 2014, doi: 10.1016/j.egypro.2014.11.491.
- [67] M. Mohajeri and S. Shariatipour, “Evaluation of enhancing CO₂ sequestration by post-brine injection under different scenarios using the E300 compositional simulator,” *Pet. Res.*, vol. 4, no. 4, pp. 314–333, Dec. 2019, doi: 10.1016/j.ptlrs.2019.08.001.
- [68] S. Iglauer, “Dissolution Trapping of Carbon Dioxide in Reservoir Formation Brine – A Carbon Storage Mechanism,” in *Mass Transfer - Advanced Aspects*, 2012. doi: 10.5772/20206.
- [69] D. N. Espinoza, S. H. Kim, and J. C. Santamarina, “CO₂ geological storage - Geotechnical implications,” *KSCE J. Civ. Eng.*, vol. 15, no. 4, pp. 707–719, Apr. 2011,

doi: 10.1007/s12205-011-0011-9.

- [70] R. S. Potdar and V. Vishal, “Trapping mechanism of CO₂ storage in deep saline aquifers: Brief review,” in *Geologic Carbon Sequestration: Understanding Reservoir Behavior*, Springer International Publishing, 2016, pp. 47–58. doi: 10.1007/978-3-319-27019-7_3.
- [71] H. Lee, J. Seo, Y. Lee, W. Jung, and W. Sung, “Regional CO₂ solubility trapping potential of a deep saline aquifer in Pohang basin, Korea,” *Geosci. J.*, vol. 20, no. 4, pp. 561–568, 2016, doi: 10.1007/s12303-015-0068-4.
- [72] S. M. Shariatipour, G. E. Pickup, and E. J. Mackay, “The effect of aquifer/caprock interface on geological storage of CO₂,” in *Energy Procedia*, Elsevier, Jan. 2014, pp. 5544–5555. doi: 10.1016/j.egypro.2014.11.588.
- [73] J. E. Beane, C. A. Turner, P. R. Hooper, K. V. Subbarao, and J. N. Walsh, “Stratigraphy, composition and form of the Deccan Basalts, Western Ghats, India,” *Bull. Volcanol.*, vol. 48, no. 1, pp. 61–83, Feb. 1986, doi: 10.1007/BF01073513.
- [74] K.-A. A. Lie, H. M. Nilsen, O. Andersen, and O. Møyner, “A simulation workflow for large-scale CO₂ storage in the Norwegian North Sea,” *Comput. Geosci.*, vol. 20, no. 3, pp. 607–622, Jun. 2016, doi: 10.1007/s10596-015-9487-6.
- [75] O. A. Andersen, H. M. Nilsen, and K. A. Lie, “Reexamining CO₂ storage capacity and utilization of the Utsira Formation,” in *14th European Conference on the Mathematics of Oil Recovery 2014, ECMOR 2014*, European Association of Geoscientists and Engineers, EAGE, 2014. doi: 10.3997/2214-4609.20141809.
- [76] S. Bachu, W. D. Gunter, and E. H. Perkins, “Aquifer disposal of CO₂: Hydrodynamic and mineral trapping,” *Energy Convers. Manag.*, vol. 35, no. 4, pp. 269–279, 1994, doi: 10.1016/0196-8904(94)90060-4.
- [77] S. Ding, Y. Xi, H. Jiang, and G. Liu, “CO₂ storage capacity estimation in oil reservoirs by solubility and mineral trapping,” *Appl. Geochemistry*, vol. 89, pp. 121–128, Feb. 2018, doi: 10.1016/j.apgeochem.2017.12.002.
- [78] A. Kumar, J. P. Shrivastava, and V. Pathak, “Mineral carbonation reactions under water-saturated, hydrothermal-like conditions and numerical simulations of CO₂ sequestration in tholeiitic basalt of the Eastern Deccan Volcanic Province, India,” *Appl. Geochemistry*, vol. 84, no. May, pp. 87–104, 2017, doi: 10.1016/j.apgeochem.2017.05.021.

- [79] C. Lamy, S. Iglauer, C. H. Pentland, M. J. Blunt, and G. Maitland, “Capillary trapping in carbonate rocks,” in *72nd European Association of Geoscientists and Engineers Conference and Exhibition 2010: A New Spring for Geoscience. Incorporating SPE EUROPEC 2010*, Society of Petroleum Engineers, Jan. 2010, pp. 815–823. doi: 10.2118/130720-ms.
- [80] P. R. Punnam, B. Krishnamurthy, and V. K. Surasani, “Influences of Top-Surface Topography on Structural and Residual Trapping During Geological CO₂ Sequestration,” Springer, Singapore, 2022, pp. 113–121. doi: 10.1007/978-981-16-7857-8_9.
- [81] B. Niu, A. Al-Menhali, and S. C. Krevor, “The impact of reservoir conditions on the residual trapping of carbon dioxide in Berea sandstone,” *Water Resour. Res.*, vol. 51, no. 4, pp. 2009–2029, 2015, doi: 10.1002/2014WR016441.
- [82] R. Allen, H. M. Nilsen, O. Andersen, and K. A. Lie, “On obtaining optimal well rates and placement for CO₂ storage,” *Comput. Geosci.*, vol. 21, no. 5–6, pp. 1403–1422, Dec. 2017, doi: 10.1007/s10596-017-9631-6.
- [83] S. Krevor *et al.*, “Capillary trapping for geologic carbon dioxide storage - From pore scale physics to field scale implications,” *Int. J. Greenh. Gas Control*, vol. 40, pp. 221–237, Jan. 2015, doi: 10.1016/j.ijggc.2015.04.006.
- [84] L. K. Abidoye, K. J. Khudaida, and D. B. Das, “Geological carbon sequestration in the context of two-phase flow in porous media: A review,” *Crit. Rev. Environ. Sci. Technol.*, vol. 45, no. 11, pp. 1105–1147, 2015, doi: 10.1080/10643389.2014.924184.
- [85] D. Alexander and D. Boodlal, “Evaluating the effects of CO₂ injection in faulted saline aquifers,” in *Energy Procedia*, Elsevier, Jan. 2014, pp. 3012–3021. doi: 10.1016/j.egypro.2014.11.324.
- [86] H. M. Nilsen, A. R. Syversveen, K. A. Lie, J. Tveranger, and J. M. Nordbotten, “Impact of top-surface morphology on CO₂ storage capacity,” *Int. J. Greenh. Gas Control*, vol. 11, pp. 221–235, Nov. 2012, doi: 10.1016/j.ijggc.2012.08.012.
- [87] IPCC, “IPCC Special Report on CCS,” 2011.
- [88] M. Andrew, B. Bijeljic, and M. J. Blunt, “Pore-scale imaging of trapped supercritical carbon dioxide in sandstones and carbonates,” *Int. J. Greenh. Gas Control*, vol. 22, pp.

- 1–14, Mar. 2014, doi: 10.1016/j.ijggc.2013.12.018.
- [89] A. Saeedi, R. Rezaee, and B. Evans, “Experimental study of the effect of variation in in-situ stress on capillary residual trapping during CO₂ geo-sequestration in sandstone reservoirs,” *Geofluids*, vol. 12, no. 3, pp. 228–235, Aug. 2012, doi: 10.1111/j.1468-8123.2012.00364.x.
- [90] L. Zuo and S. M. Benson, “Process-dependent residual trapping of CO₂ in sandstone,” *Geophys. Res. Lett.*, vol. 41, no. 8, pp. 2820–2826, Apr. 2014, doi: 10.1002/2014GL059653.
- [91] M. Rasmusson, “Residual and Solubility trapping during Geological CO₂ storage : Numerical and Experimental studies,” 2018. [Online]. Available: <http://uu.diva-portal.org/smash/get/diva2:1187364/FULLTEXT01.pdf><http://uu.diva-portal.org/smash/get/diva2:1187364/PREVIEW01.jpg><http://urn.kb.se/resolve?urn=urn:nbn:se:uu:diva-343505>
- [92] M. Soroush, D. Wessel-Berg, O. Torsaeter, and J. Kleppe, “Investigating residual trapping in CO₂ storage in saline aquifers – application of a 2D glass model, and image analysis,” *Energy Sci. Eng.*, vol. 2, no. 3, pp. 149–163, Aug. 2014, doi: 10.1002/ese3.32.
- [93] H. Møll Nilsen, K.-A. Lie, and O. Andersen, “Analysis of CO₂ trapping capacities and long-term migration for geological formations in the Norwegian North Sea using MRST-co2lab,” *Comput. Geosci.*, vol. 79, pp. 15–26, Jun. 2015, doi: 10.1016/j.cageo.2015.03.001.
- [94] H. Ahn, S. O. Kim, M. Lee, and S. Wang, “Migration and Residual Trapping of Immiscible Fluids during Cyclic Injection: Pore-Scale Observation and Quantitative Analysis,” *Geofluids*, vol. 2020, 2020, doi: 10.1155/2020/4569208.
- [95] S. Joodaki, Z. Yang, J. Bensabat, and A. Niemi, “Model analysis of CO₂ residual trapping from single-well push pull test based on hydraulic withdrawal tests – Heletz, residual trapping experiment I,” *Int. J. Greenh. Gas Control*, vol. 97, Jun. 2020, doi: 10.1016/j.ijggc.2020.103058.
- [96] C. H. Pentland, “Measurements of Non-wetting Phase Trapping in Porous Media,” *Dep. Earth Sci. Eng. R. Sch. Mines*, vol. PhD, no. Awarded, p. 154, 2010.
- [97] Y. Tanino and M. J. Blunt, “Capillary trapping in sandstones and carbonates:

- Dependence on pore structure,” *Water Resour. Res.*, vol. 48, no. 8, Aug. 2012, doi: 10.1029/2011WR011712.
- [98] S. Wang and T. K. Tokunaga, “Capillary Pressure-Saturation Relations for Supercritical CO₂ and Brine in Limestone/Dolomite Sands: Implications for Geologic Carbon Sequestration in Carbonate Reservoirs,” *Environ. Sci. Technol.*, vol. 49, no. 12, pp. 7208–7217, Jun. 2015, doi: 10.1021/acs.est.5b00826.
- [99] R. Juanes, E. J. Spiteri, F. M. Orr, and M. J. Blunt, “Impact of relative permeability hysteresis on geological CO₂ storage,” *Water Resour. Res.*, vol. 42, no. 12, pp. 1–13, 2006, doi: 10.1029/2005WR004806.
- [100] F. Jiang and T. Tsuji, “Impact of interfacial tension on residual CO₂ clusters in porous sandstone,” *Water Resour. Res.*, vol. 51, no. 3, pp. 1710–1722, Mar. 2015, doi: 10.1002/2014WR016070.
- [101] A. Raza, R. Gholami, R. Rezaee, C. H. Bing, R. Nagarajan, and M. A. Hamid, “Assessment of CO₂ residual trapping in depleted reservoirs used for geosequestration,” *J. Nat. Gas Sci. Eng.*, vol. 43, pp. 137–155, 2017, doi: 10.1016/j.jngse.2017.04.001.
- [102] Y. Pamukcu, S. Hurter, L. Jammes, D. Vu-Hoang, and L. Pekot, “Characterizing and predicting short term performance for the In Salah Krechba field CCS joint industry project,” *Energy Procedia*, vol. 4, pp. 3371–3378, Jan. 2011, doi: 10.1016/J.EGYPRO.2011.02.259.
- [103] R. S. Jayne, H. Wu, and R. M. Pollyea, “A probabilistic assessment of geomechanical reservoir integrity during CO₂ sequestration in flood basalt formations,” *Greenh. Gases Sci. Technol.*, vol. 9, no. 5, pp. 979–998, 2019, doi: 10.1002/ghg.1914.
- [104] Z. Yang, Y. F. Chen, and A. Niemi, “Gas migration and residual trapping in bimodal heterogeneous media during geological storage of CO₂,” *Adv. Water Resour.*, vol. 142, p. 103608, Aug. 2020, doi: 10.1016/j.advwatres.2020.103608.
- [105] B. Niu, A. Al-Menhali, and S. Krevor, “A study of residual carbon dioxide trapping in sandstone,” in *Energy Procedia*, Elsevier Ltd, Jan. 2014, pp. 5522–5529. doi: 10.1016/j.egypro.2014.11.585.
- [106] A. Raza, R. Rezaee, C. H. Bing, R. Gholami, R. Nagarajan, and M. A. Hamid, “CO₂ storage in heterogeneous aquifer: A study on the effect of injection rate and CaCO₃

- concentration,” in *IOP Conference Series: Materials Science and Engineering*, Institute of Physics Publishing, Apr. 2016, p. 012023. doi: 10.1088/1757-899X/121/1/012023.
- [107] Z. Rasheed, A. Raza, R. Gholami, M. Rabiei, A. Ismail, and V. Rasouli, “A numerical study to assess the effect of heterogeneity on CO₂ storage potential of saline aquifers,” *Energy Geosci.*, vol. 1, no. 1–2, pp. 20–27, Jul. 2020, doi: 10.1016/j.engeos.2020.03.002.
- [108] M. K. Abba *et al.*, “Solubility trapping as a potential secondary mechanism for CO₂ sequestration during enhanced gas recovery by CO₂ injection in conventional natural gas reservoirs: An experimental approach,” *J. Nat. Gas Sci. Eng.*, vol. 71, p. 103002, Nov. 2019, doi: 10.1016/j.jngse.2019.103002.
- [109] L. Jin *et al.*, “Effects of gas relative permeability hysteresis and solubility on associated CO₂ storage performance,” *Int. J. Greenh. Gas Control*, vol. 75, pp. 140–150, Aug. 2018, doi: 10.1016/j.ijggc.2018.06.002.
- [110] J. H. Lee, J. Cho, and K. S. Lee, “Effects of Aqueous Solubility and Geochemistry on CO₂ Injection for Shale Gas Reservoirs,” *Sci. Rep.*, vol. 10, no. 1, p. 2071, Dec. 2020, doi: 10.1038/s41598-020-59131-y.
- [111] P. R. Punnam, B. Krishnamurthy, and V. K. Surasani, “Investigation of solubility trapping mechanism during geologic CO₂ sequestration in Deccan Volcanic Provinces, Saurashtra, Gujarat, India,” *Int. J. Greenh. Gas Control*, vol. 120, p. 103769, Oct. 2022, doi: 10.1016/j.ijggc.2022.103769.
- [112] K. J. Khudaida and D. B. Das, “A Numerical Analysis of the Effects of Supercritical CO₂ Injection on CO₂ Storage Capacities of Geological Formations,” *Clean Technol.*, vol. 2, no. 3, pp. 333–364, Sep. 2020, doi: 10.3390/cleantechnol2030021.
- [113] Y. Zapata, M. R. Kristensen, N. Huerta, C. Brown, C. S. Kabir, and Z. Reza, “CO₂ geological storage: Critical insights on plume dynamics and storage efficiency during long-term injection and post-injection periods,” *J. Nat. Gas Sci. Eng.*, vol. 83, p. 103542, Nov. 2020, doi: 10.1016/j.jngse.2020.103542.
- [114] W. Xiong, R. K. Wells, A. H. Menefee, P. Skemer, B. R. Ellis, and D. E. Giammar, “CO₂ mineral trapping in fractured basalt,” *Int. J. Greenh. Gas Control*, vol. 66, no. June, pp. 204–217, 2017, doi: 10.1016/j.ijggc.2017.10.003.

- [115] S. Kanakiya, L. Adam, L. Esteban, M. C. Rowe, and P. Shane, “Dissolution and secondary mineral precipitation in basalts due to reactions with carbonic acid,” *J. Geophys. Res. Solid Earth*, vol. 122, no. 6, pp. 4312–4327, 2017, doi: 10.1002/2017JB014019.
- [116] N. Rani, V. Pathak, and J. P. Shrivastava, “CO₂ Mineral Trapping: An Experimental Study on the Carbonation of Basalts from the Eastern Deccan Volcanic Province, India,” *Procedia Earth Planet. Sci.*, vol. 7, pp. 806–809, 2013, doi: 10.1016/j.proeps.2013.03.069.
- [117] J. P. Shrivastava, N. Rani, and V. Pathak, “Geochemical Modeling and Experimental Studies on Mineral Carbonation of Primary Silicates for Long-term Immobilization of CO₂ in Basalt from the Eastern Deccan Volcanic Province,” *J. Indian Geophys.*, vol. 1, no. April, pp. 42–58, 2016.
- [118] A. Kumar and J. P. Shrivastava, “Thermodynamic Modelling and Experimental Validation of CO₂ Mineral Sequestration in Mandla Basalt of the Eastern Deccan Volcanic Province, India,” *J. Geol. Soc. India*, vol. 93, no. 3, pp. 269–277, 2019, doi: 10.1007/s12594-019-1173-1.
- [119] T. H. Van Pham, P. Aagaard, and H. Hellevang, “On the potential for CO₂ mineral storage in continental flood basalts-phreeqc batch and 1d diffusion-reaction simulations,” *Carbon Capture Storage CO₂ Manag. Technol.*, pp. 178–202, 2014, doi: 10.1201/b16845.
- [120] T. Xu, J. A. Apps, and K. Pruess, “Mineral sequestration of carbon dioxide in a sandstone-shale system,” *Chem. Geol.*, vol. 217, no. 3-4 SPEC. ISS., pp. 295–318, Apr. 2005, doi: 10.1016/j.chemgeo.2004.12.015.
- [121] T. Xu, J. A. Apps, and K. Pruess, “Numerical simulation of CO₂ disposal by mineral trapping in deep aquifers,” *Appl. Geochemistry*, vol. 19, no. 6, pp. 917–936, 2004, doi: 10.1016/j.apgeochem.2003.11.003.
- [122] Y. Cohen and D. H. Rothman, “Mechanisms for mechanical trapping of geologically sequestered carbon dioxide,” *Proc. R. Soc. A Math. Phys. Eng. Sci.*, vol. 471, no. 2175, 2015, doi: 10.1098/rspa.2014.0853.
- [123] P. Ranganathan, P. Van Hemert, E. S. J. Rudolph, and P. Z. J. J. Zitha, “Numerical

- modeling of CO₂ mineralisation during storage in deep saline aquifers,” in *Energy Procedia*, Elsevier, 2011, pp. 4538–4545. doi: 10.1016/j.egypro.2011.02.411.
- [124] R. Kumar, S. Campbell, E. Sonnenthal, and J. Cunningham, “Effect of brine salinity on the geological sequestration of CO₂ in a deep saline carbonate formation,” *Greenh. Gases Sci. Technol.*, vol. 10, no. 2, pp. 296–312, Apr. 2020, doi: 10.1002/ghg.1960.
- [125] A. P. Gysi and A. Stefánsson, “CO₂-water-basalt interaction. Low temperature experiments and implications for CO₂ sequestration into basalts,” *Geochim. Cosmochim. Acta*, vol. 81, pp. 129–152, 2012, doi: 10.1016/j.gca.2011.12.012.
- [126] A. Shukla, K. S. Misra, A. Shukla, and S. Niyogi, “Possibility of CO₂ Sequestration in Basalt and Sub-Basalt Sediments in and Around Peninsular India,” no. January, pp. 16–19, 2016.
- [127] B. P. McGrail, F. A. Spane, E. C. Sullivan, D. H. Bacon, and G. Hund, “The Wallula basalt sequestration pilot project,” in *Energy Procedia*, Elsevier, Jan. 2011, pp. 5653–5660. doi: 10.1016/j.egypro.2011.02.557.
- [128] H. Abdulalah, A. Al-Yaseri, M. Ali, A. Giwelli, B. M. Negash, and M. Sarmadivaleh, “CO₂/Basalt’s interfacial tension and wettability directly from gas density: Implications for Carbon Geo-sequestration,” *J. Pet. Sci. Eng.*, vol. 204, p. 108683, Sep. 2021, doi: 10.1016/j.petrol.2021.108683.
- [129] K. N. S. S. S. Srinivas, P. P. Kishore, and D. V. S. Rao, “The geological site characterisation of the Mandla region, Eastern Deccan Volcanic Province, Central India,” *J. Earth Syst. Sci.*, vol. 128, no. 5, pp. 1–16, 2019, doi: 10.1007/s12040-019-1131-8.
- [130] L. Chiaramonte, J. A. White, and W. Trainor-Guitton, “Probabilistic geomechanical analysis of compartmentalization at the Snøhvit CO₂ sequestration project,” *J. Geophys. Res. Solid Earth*, vol. 120, no. 2, pp. 1195–1209, Feb. 2015, doi: 10.1002/2014JB011376.
- [131] M. J. Rahman, M. Fawad, J. Jahren, and N. H. Mondol, “Top seal assessment of Drake Formation shales for CO₂ storage in the Horda Platform area, offshore Norway,” *Int. J. Greenh. Gas Control*, vol. 119, p. 103700, Sep. 2022, doi: 10.1016/j.ijggc.2022.103700.
- [132] B. Page, G. Turan, A. Zapantis, J. Burrows, and C. Consoli, “The Global Status of CCS

- 2020: Vital to Achieve Net Zero,” 2020. [Online]. Available: <https://www.h2knowledgecentre.com/content/researchpaper1679>
- [133] “FuelCell Energy in UK carbon capture project at Drax power station,” *Fuel Cells Bull.*, vol. 2019, no. 7, pp. 5–5, Jul. 2019, doi: 10.1016/s1464-2859(19)30274-3.
- [134] MIT, “Carbon Capture and Sequestration Technologies Database.,” MIT. Accessed: Jun. 26, 2019. [Online]. Available: https://sequestration.mit.edu/tools/projects/boundary_dam.html
- [135] M. Angeli, J. I. Faleide, and R. H. Gabrielsen, “Evaluating Seal Quality for Potential Storage Sites in the Norwegian North Sea,” *Energy Procedia*, vol. 37, pp. 4853–4862, Jan. 2013, doi: 10.1016/J.EGYPRO.2013.06.395.
- [136] R. Arts, O. Eiken, A. Chadwick, P. Zweigel, L. van der Meer, and B. Zinszner, “Monitoring of CO₂ injected at Sleipner using time-lapse seismic data,” *Energy*, vol. 29, no. 9–10, pp. 1383–1392, Jul. 2004, doi: 10.1016/j.energy.2004.03.072.
- [137] M. Negrescu, “Economic Modelling of an Oil and Gas Project Involving Carbon Capture and Storage - Snohvit LNG Project (Barents Sea, Norway),” in *EUROPEC/EAGE Conference and Exhibition*, Society of Petroleum Engineers, Apr. 2007. doi: 10.2118/107430-MS.
- [138] K. Worth *et al.*, “Aquistore project measurement, monitoring, and verification: From concept to CO₂ injection,” in *Energy Procedia*, Elsevier, Jan. 2014, pp. 3202–3208. doi: 10.1016/j.egypro.2014.11.345.
- [139] N. Sacuta and K. Anderson, “Creating core CCS messages: Focus Group Testing and Peer Review of Questions and Answers from the IEAGHG Weyburn-midale CO₂ Monitoring and Storage Project,” *Energy Procedia*, vol. 63, pp. 7061–7069, Jan. 2014, doi: 10.1016/J.EGYPRO.2014.11.741.
- [140] J. J. Trivedi, T. Babadagli, R. G. Lavoie, and D. Nimchuk, “Acid Gas Sequestration During Tertiary Oil Recovery: Optimal Injection Strategies and Importance of Operational Parameters,” *J. Can. Pet. Technol.*, vol. 46, no. 03, Mar. 2007, doi: 10.2118/07-03-06.
- [141] D. B. Bennion and S. Bachu, “Drainage and imbibition relative permeability relationships for supercritical CO₂/brine and H₂S/brine systems in intergranular

- sandstone, carbonate, shale, and anhydrite rocks,” *SPE Reserv. Eval. Eng.*, vol. 11, no. 3, pp. 487–496, Jun. 2008, doi: 10.2118/99326-pa.
- [142] S. Cole and S. Itani, “The Alberta Carbon Trunk Line and the Benefits of CO₂,” *Energy Procedia*, vol. 37, pp. 6133–6139, Jan. 2013, doi: 10.1016/J.EGYPRO.2013.06.542.
- [143] S. Hovorka, “Frio brine pilot: The first US sequestration test,” *Southwest Hydrol.*, vol. 8, no. 5, pp. 26–31, 2009, Accessed: Jun. 26, 2019. [Online]. Available: <https://www.scopus.com/record/display.uri?eid=2-s2.0-84857483719&origin=inward>
- [144] Q. Tao, S. L. Bryant, and T. A. Meckel, “Modeling above-zone measurements of pressure and temperature for monitoring CCS sites,” *Int. J. Greenh. Gas Control*, vol. 18, pp. 523–530, Oct. 2013, doi: 10.1016/j.ijggc.2012.08.011.
- [145] T. Meckel and S. Hovorka, “Above-Zone Pressure Monitoring as a Surveillance Tool for Carbon-Sequestration Projects,” in *SPE International Conference on CO₂ Capture, Storage, and Utilization*, Society of Petroleum Engineers, Apr. 2010. doi: 10.2118/139720-MS.
- [146] B. Freifeld *et al.*, “Geothermal Energy Production Coupled with CCS: a Field Demonstration at the SECARB Cranfield Site, Cranfield, Mississippi, USA,” *Energy Procedia*, vol. 37, pp. 6595–6603, Jan. 2013, doi: 10.1016/J.EGYPRO.2013.06.592.
- [147] S.-E. Chen and Y. Liu, “Geophysical Sensing for CO₂ Sequestration and Enhanced Oil Recovery,” in *Contemporary Topics on Testing, Modeling, and Case Studies of Geomaterials, Pavements, and Tunnels*, Reston, VA: American Society of Civil Engineers, May 2011, pp. 41–48. doi: 10.1061/47626(405)6.
- [148] R. Esposito, C. Harvick, R. Shaw, D. Mooneyhan, R. Trautz, and G. Hill, “Integration of Pipeline Operations Sourced with CO₂ Captured at a Coal-fired Power Plant and Injected for Geologic Storage: SECARB Phase III CCS Demonstration,” *Energy Procedia*, vol. 37, pp. 3068–3088, Jan. 2013, doi: 10.1016/J.EGYPRO.2013.06.193.
- [149] M. Streibel, R. J. Finley, S. Martens, S. Greenberg, F. Möller, and A. Liebscher, “From Pilot to Demo Scale – Comparing Ketzin results with the Illinois Basin-decatur Project,” *Energy Procedia*, vol. 63, pp. 6323–6334, Jan. 2014, doi: 10.1016/J.EGYPRO.2014.11.665.
- [150] W. Atkinson, “Carbon capture and sequestration: Real progress taking place,” *Pollut.*

- Eng.*, vol. 46, no. 8, pp. 30–32, 2014, Accessed: Jun. 26, 2019. [Online]. Available: <https://www.scopus.com/record/display.uri?eid=2-s2.0-84905500339&origin=inward>
- [151] M. Kelley *et al.*, “Reservoir Characterization from Pressure Monitoring during CO₂ Injection into a Depleted Pinnacle Reef – MRCSP Commercial-scale CCS Demonstration Project,” *Energy Procedia*, vol. 63, pp. 4937–4964, Jan. 2014, doi: 10.1016/J.EGYPRO.2014.11.524.
- [152] A. Mathieson, I. Wright, D. Roberts, and P. Ringrose, “Satellite imaging to monitor CO₂ movement at Krechba, Algeria,” *Energy Procedia*, vol. 1, no. 1, pp. 2201–2209, Feb. 2009, doi: 10.1016/J.EGYPRO.2009.01.286.
- [153] A. Mathieson, J. Midgely, I. Wright, N. Saoula, and P. Ringrose, “In Salah CO₂ storage JIP: CO₂ sequestration monitoring and verification technologies applied at Krechba, Algeria,” in *Energy Procedia*, Elsevier, Jan. 2011, pp. 3596–3603. doi: 10.1016/j.egypro.2011.02.289.
- [154] A. Hortle, P. de Caritat, C. Stalvies, and C. Jenkins, “Groundwater monitoring at the Otway project site, Australia,” *Energy Procedia*, vol. 4, pp. 5495–5503, Jan. 2011, doi: 10.1016/J.EGYPRO.2011.02.535.
- [155] S. Sharma, P. Cook, C. Jenkins, T. Steeper, M. Lees, and N. Ranasinghe, “The CO₂CRC Otway Project: Leveraging experience and exploiting new opportunities at Australia’s first CCS project site,” *Energy Procedia*, vol. 4, pp. 5447–5454, Jan. 2011, doi: 10.1016/J.EGYPRO.2011.02.530.
- [156] U. Schacht and C. Jenkins, “Soil gas monitoring of the Otway Project demonstration site in SE Victoria, Australia,” *Int. J. Greenh. Gas Control*, vol. 24, pp. 14–29, May 2014, doi: 10.1016/j.ijggc.2014.02.007.
- [157] M. Bock, M. Scheck-Wenderoth, and G. Group, “Research on Utilization of Geo-energy,” *Energy Procedia*, vol. 40, pp. 249–255, Jan. 2013, doi: 10.1016/J.EGYPRO.2013.08.029.
- [158] X. Zhao *et al.*, “The latest monitoring progress for Shenhua CO₂ storage project in China,” *Int. J. Greenh. Gas Control*, vol. 60, pp. 199–206, May 2017, doi: 10.1016/j.ijggc.2017.03.004.
- [159] T. Luo, L. Zhou, Z. Jiao, Y. Bai, and S. Wang, “The Ordos Basin: A Premier Basin for

- Integrating geological CO₂ Storage with Enhanced oil Recovery Projects in China,” *Energy Procedia*, vol. 63, pp. 7772–7779, Jan. 2014, doi: 10.1016/J.EGYPRO.2014.11.811.
- [160] IEA Greenhouse Gas R&D Programme (IEA GHG), “A Regional Assessment of the Potential for CO₂ Storage in the Indian Subcontinent,” 2008. [Online]. Available: http://ieaghg.org/docs/General_Docs/Reports/2008-02.pdf
- [161] V. Vishal, Y. Verma, D. Chandra, and D. Ashok, “A systematic capacity assessment and classification of geologic CO₂ storage systems in India,” *Int. J. Greenh. Gas Control*, vol. 111, p. 103458, Oct. 2021, doi: 10.1016/j.ijggc.2021.103458.
- [162] P. Raj, S. Kumar, B. Mathur, and S. Jhalani, “CCS: Opportunities and Obstacles for India,” in *Canadian Unconventional Resources and International Petroleum Conference*, Society of Petroleum Engineers, Apr. 2010. doi: 10.2118/137717-MS.
- [163] A. Sood, R. Gandhi Proudhyogiki Vishwavidyalaya, M. Pradesh, and I. Savita Vyas, “A Review: Carbon Capture and Sequestration (CCS) in India,” *Int. J. Mech. Eng. Technol.*, vol. 8, no. 2, pp. 1–7, 2017, Accessed: Jul. 03, 2019. [Online]. Available: <http://www.iaeme.com/ijmet/issues.asp?JType=IJMET&VType=8&IType=2>
<http://www.iaeme.com/ijmet/issues.asp?JType=IJMET&VType=8&IType=2>
- [164] R. V Kapila and R. Stuart Haszeldine, “Opportunities in India for Carbon Capture and Storage as a form of climate change mitigation,” in *Energy Procedia*, 2009, pp. 4527–4534. doi: 10.1016/j.egypro.2009.02.271.
- [165] P. Jain, K. Pathak, and S. Tripathy, “Possible source-sink matching for CO₂ sequestration in Eastern India,” *Energy Procedia*, vol. 37, pp. 3233–3241, 2013, doi: 10.1016/j.egypro.2013.06.210.
- [166] R. Chatterjee and S. Paul, “Coal Bed Methane Exploration and Possibility for CO₂ Sequestration in Jharia Coalfield , India,” no. January, pp. 37–41, 2016.
- [167] R. Bastia and M. Radhakrishna, “Subsurface Geology, Depositional History, and Petroleum Systems Along the Western Offshore Basins of India,” in *Developments in Petroleum Science*, vol. 59, Elsevier, 2012, pp. 269–317. doi: 10.1016/B978-0-444-53604-4.00006-5.
- [168] H. C. Tewari, B. Rajendra Prasad, and P. Kumar, “Deccan Volcanic Province Near the

- West Coast,” in *Structure and Tectonics of the Indian Continental Crust and Its Adjoining Region*, Elsevier, 2018, pp. 115–145. doi: 10.1016/b978-0-12-813685-0.00005-4.
- [169] W. D. Huff and L. A. Owen, “Volcanic Landforms and Hazards☆,” in *Reference Module in Earth Systems and Environmental Sciences*, Elsevier, 2015. doi: 10.1016/b978-0-12-409548-9.09512-9.
- [170] S. K. Haldar, “Deposits of Asia,” in *Platinum-Nickel-Chromium Deposits*, Elsevier, 2017, pp. 145–189. doi: 10.1016/b978-0-12-802041-8.00006-7.
- [171] D. K. Pandey, A. Pandey, and S. Rajan, “Offshore Extension of Deccan Traps in Kachchh, Central Western India: Implications for Geological Sequestration Studies,” *Nat. Resour. Res.*, vol. 20, no. 1, pp. 33–43, Mar. 2011, doi: 10.1007/s11053-010-9133-x.
- [172] P. Krishnamurthy, “The Deccan Volcanic Province (DVP), India: A Review: Part 1: Areal extent and distribution, compositional diversity, flow types and sequences, stratigraphic correlations, dyke swarms and sills, petrography and mineralogy,” *J. Geol. Soc. India*, vol. 96, no. 1, pp. 9–35, Jul. 2020, doi: 10.1007/S12594-020-1501-5/METRICS.
- [173] S. B. Deolankar, “The Deccan Basalts of Maharashtra, India —Their Potential as Aquifers,” *Groundwater*, vol. 18, no. 5, pp. 434–437, Sep. 1980, doi: 10.1111/j.1745-6584.1980.tb03416.x.
- [174] K. S. Jayaraman, “India’s carbon dioxide trap,” *Nature*, vol. 445, no. 7126, Nature Publishing Group, p. 350, Jan. 25, 2007. doi: 10.1038/445350a.
- [175] A. Gupta and A. Paul, “Carbon capture and sequestration potential in India: A comprehensive review,” in *Energy Procedia*, Elsevier, Feb. 2019, pp. 848–855. doi: 10.1016/j.egypro.2019.02.148.
- [176] A. Garg, P. R. Shukla, S. Parihar, U. Singh, and B. Kankal, “Cost-effective architecture of carbon capture and storage (CCS) grid in India,” *Int. J. Greenh. Gas Control*, vol. 66, no. September, pp. 129–146, 2017, doi: 10.1016/j.ijggc.2017.09.012.
- [177] D. Guha Roy, V. Vishal, and T. N. Singh, “Effect of carbon dioxide sequestration on the mechanical properties of Deccan basalt,” *Environ. Earth Sci.*, vol. 75, no. 9, pp. 1–13,

- Apr. 2016, doi: 10.1007/s12665-016-5587-4.
- [178] J. JOHNSON and J. NITAO, “Reactive Transport Modeling of Geologic CO₂ Sequestration at Sleipner,” in *Greenhouse Gas Control Technologies - 6th International Conference*, Elsevier, 2007, pp. 327–332. doi: 10.1016/b978-008044276-1/50053-2.
- [179] V. Lagneau, A. Pipart, and H. Catalette, “Reactive transport modelling of CO₂ sequestration in deep saline aquifers,” *Oil Gas Sci. Technol.*, vol. 60, no. 2, pp. 231–247, 2005, doi: 10.2516/ogst:2005014.
- [180] E. A. Al-Khdheawi, S. Vialle, A. Barifcani, M. Sarmadivaleh, and S. Iglauer, “Effect of wettability heterogeneity and reservoir temperature on CO₂ storage efficiency in deep saline aquifers,” *Int. J. Greenh. Gas Control*, vol. 68, pp. 216–229, Jan. 2018, doi: 10.1016/j.ijggc.2017.11.016.
- [181] E. A. Al-Khdheawi, S. Vialle, A. Barifcani, M. Sarmadivaleh, and S. Iglauer, “Influence of CO₂-wettability on CO₂ migration and trapping capacity in deep saline aquifers,” *Greenh. Gases Sci. Technol.*, vol. 7, no. 2, pp. 328–338, Apr. 2017, doi: 10.1002/ghg.1648.
- [182] E. A. Al-Khdheawi, S. Vialle, A. Barifcani, M. Sarmadivaleh, and S. Iglauer, “Impact of reservoir wettability and heterogeneity on CO₂-plume migration and trapping capacity,” *Int. J. Greenh. Gas Control*, vol. 58, pp. 142–158, Mar. 2017, doi: 10.1016/j.ijggc.2017.01.012.
- [183] S. Iglauer, C. H. Pentland, and A. Busch, “CO₂ wettability of seal and reservoir rocks and the implications for carbon geo-sequestration,” *Water Resour. Res.*, vol. 51, no. 1, pp. 729–774, Jan. 2015, doi: 10.1002/2014WR015553.
- [184] E. A. Al-Khdheawi, S. Vialle, A. Barifcani, M. Sarmadivaleh, and S. Iglauer, “Influence of Rock Wettability on CO₂ Migration and Storage Capacity in Deep Saline Aquifers,” in *Energy Procedia*, Elsevier, Jul. 2017, pp. 4357–4365. doi: 10.1016/j.egypro.2017.03.1587.
- [185] E. A. Al-Khdheawi, S. Vialle, A. Barifcani, M. Sarmadivaleh, and S. Iglauer, “Influence of injection well configuration and rock wettability on CO₂ plume behaviour and CO₂ trapping capacity in heterogeneous reservoirs,” *J. Nat. Gas Sci. Eng.*, vol. 43, pp. 190–206, Jul. 2017, doi: 10.1016/j.jngse.2017.03.016.

- [186] E. A. Al-Khdheawi, S. Vialle, A. Barifcani, M. Sarmadivaleh, Y. Zhang, and S. Iglauer, “Impact of salinity on CO₂ containment security in highly heterogeneous reservoirs,” *Greenh. Gases Sci. Technol.*, vol. 8, no. 1, pp. 93–105, Feb. 2018, doi: 10.1002/ghg.1723.
- [187] E. A. Al-Khdheawi, S. Vialle, A. Barifcani, M. Sarmadivaleh, and S. Iglauer, “Impact of injected water salinity on CO₂ storage efficiency in homogenous reservoirs,” *APPEA J.*, vol. 58, no. 1, p. 44, May 2018, doi: 10.1071/aj17041.
- [188] A. Afanasyev, E. Vedeneeva, and S. Grechko, “Scaling analysis for a 3-D CO₂ plume in a sloping aquifer at a late stage of injection,” *J. Nat. Gas Sci. Eng.*, vol. 106, p. 104740, Oct. 2022, doi: 10.1016/j.jngse.2022.104740.
- [189] Y. Kim, H. Jang, J. Kim, and J. Lee, “Prediction of storage efficiency on CO₂ sequestration in deep saline aquifers using artificial neural network,” *Appl. Energy*, vol. 185, pp. 916–928, Jan. 2017, doi: 10.1016/j.apenergy.2016.10.012.
- [190] D. Ma, J. Gao, Z. Gao, H. Jiang, Z. Zhang, and J. Xie, “Gas leakage recognition for CO₂ geological sequestration based on the time series neural network,” *Chinese J. Chem. Eng.*, vol. 28, no. 9, pp. 2343–2357, Sep. 2020, doi: 10.1016/j.cjche.2020.06.014.
- [191] J. You *et al.*, “Machine learning based co-optimization of carbon dioxide sequestration and oil recovery in CO₂-EOR project,” *J. Clean. Prod.*, vol. 260, Jul. 2020, doi: 10.1016/j.jclepro.2020.120866.
- [192] G. L. A. F. Arce, J. A. Carvalho, and L. F. C. Nascimento, “A time series sequestration and storage model of atmospheric carbon dioxide,” *Ecol. Modell.*, vol. 272, pp. 59–67, Jan. 2014, doi: 10.1016/J.ECOLMODEL.2013.09.006.
- [193] Y. Song, W. Sung, Y. Jang, and W. Jung, “Application of an artificial neural network in predicting the effectiveness of trapping mechanisms on CO₂ sequestration in saline aquifers,” *Int. J. Greenh. Gas Control*, vol. 98, p. 103042, Jul. 2020, doi: 10.1016/J.IJGGC.2020.103042.
- [194] G. Wen, M. Tang, and S. M. Benson, “Towards a predictor for CO₂ plume migration using deep neural networks,” *Int. J. Greenh. Gas Control*, vol. 105, p. 103223, Feb. 2021, doi: 10.1016/j.ijggc.2020.103223.
- [195] C. Steefel, “CrunchFlow software for modeling multicomponent reactive flow and

- transport,” 2009.
- [196] K. Pruess, C. M. Oldenburg, and G. J. Moridis, “TOUGH2 User’s Guide Version 2,” United States, 1999. doi: 10.2172/751729.
- [197] J. Manik, T. Ertekin, and T. Kohler, “Development and Validation of a Compositional Coalbed Simulator,” *J. Can. Pet. Technol.*, vol. 41, 2013, doi: 10.2118/2000-044.
- [198] T. Xu, E. Sonnenthal, N. Spycher, and K. Pruess, “TOUGHREACT—A simulation program for non-isothermal multiphase reactive geochemical transport in variably saturated geologic media: Applications to geothermal injectivity and CO₂ geological sequestration,” *Comput. Geosci.*, vol. 32, no. 2, pp. 145–165, Mar. 2006, doi: 10.1016/J.CAGEO.2005.06.014.
- [199] C. Lu and P. C. Lichtner, “High resolution numerical investigation on the effect of convective instability on long term CO₂ storage in saline aquifers,” *J. Phys. Conf. Ser.*, vol. 78, no. 1, 2007, doi: 10.1088/1742-6596/78/1/012042.
- [200] P. C. Lichtner *et al.*, “PFLOTRAN User Manual: A Massively Parallel Reactive Flow and Transport Model for Describing Surface and Subsurface Processes,” 2015. doi: 10.2172/1168703.
- [201] D. N. Murthy, K. Veeraswamy, and T. Harinarayana, “Deep Geoelectric Structure and Its Relation to Seismotectonics of the Saurashtra Region, Western India,” *Open J. Earthq. Res.*, vol. 09, no. 02, pp. 181–200, Mar. 2020, doi: 10.4236/ojer.2020.92011.
- [202] P. Krishnamurthy, “Giant Plagioclase Basalts (GPBs) from the Deccan Volcanic Province (DVP) and the Deccan Volcanic Cycle (DVC), India,” *J. Geol. Soc. India*, vol. 94, no. 3, pp. 223–226, 2019, doi: 10.1007/s12594-019-1300-z.
- [203] K. J. Prasanna Lakshmi, P. Senthil Kumar, K. Vijayakumar, S. Ravinder, T. Seshunarayana, and M. K. Sen, “Petrophysical properties of the Deccan basalts exposed in the Western Ghats escarpment around Mahabaleshwar and Koyna, India,” *J. Asian Earth Sci.*, vol. 84, pp. 176–187, Apr. 2014, doi: 10.1016/j.jseaes.2013.08.028.
- [204] J. L. Palandri and Y. K. Kharaka, “A compilation of rate parameters of water-mineral interaction kinetics for application to geochemical modeling,” Mar. 2004. Accessed: Mar. 03, 2021. [Online]. Available: <https://pubs.usgs.gov/of/2004/1068/>
- [205] D. Halbert and J. Parnell, “Thermal conductivity of basalt between 225 and 290 K.,”

Meteorit. Planet. Sci., vol. 57, no. 8, pp. 1617–1626, 2022.

- [206] L. Ray, R. K. Gupta, N. Chopra, D. Gopinadh, and S. K. Dwivedi, “Thermal and Physical Properties of Deccan Basalt and Neoproterozoic Basement Cores From a Deep Scientific Borehole in the Koyna–Warna Seismogenic Region, Deccan Volcanic Province, Western India: Implications on Thermal Modeling and Seismogenesis,” *Earth Sp. Sci.*, vol. 8, no. 10, p. e2021EA001645, 2021, doi: <https://doi.org/10.1029/2021EA001645>.
- [207] N. Podugu and S. Roy, “Thermal conductivity of Deccan flood basalts,” *J. Earth Syst. Sci.*, vol. 131, no. 2, p. 112, 2022, doi: [10.1007/s12040-022-01868-3](https://doi.org/10.1007/s12040-022-01868-3).
- [208] S. Bhattacharji, R. Sharma, and N. Chatterjee, “Two- and three-dimensional gravity modeling along western continental margin and intraplate Narmada-Tapti rifts: Its relevance to Deccan flood basalt volcanism,” *Proc. Indian Acad. Sci. Earth Planet. Sci.*, vol. 113, no. 4, pp. 771–784, 2004, doi: [10.1007/BF02704036](https://doi.org/10.1007/BF02704036).
- [209] E. C. Robertson, “THERMAL PROPERTIES OF ROCKS,” 1988.
- [210] P. Hartlieb, M. Toifl, F. Kuchar, R. Meisels, and T. Antretter, “Thermo-physical properties of selected hard rocks and their relation to microwave-assisted comminution,” *Miner. Eng.*, vol. 91, pp. 34–41, Jan. 2016, doi: [10.1016/j.mineng.2015.11.008](https://doi.org/10.1016/j.mineng.2015.11.008).
- [211] N. Vedanti, A. Malkoti, O. P. Pandey, and J. P. Shrivastava, “Ultrasonic P- and S-Wave Attenuation and Petrophysical Properties of Deccan Flood Basalts, India, as Revealed by Borehole Studies,” *Pure Appl. Geophys.*, vol. 175, no. 8, pp. 2905–2930, Aug. 2018, doi: [10.1007/s00024-018-1817-x](https://doi.org/10.1007/s00024-018-1817-x).
- [212] N. Vedanti, K. J. P. Lakshmi, S. Dutta, A. Malkoti, and O. P. Pandey, “Investigation of petrophysical properties and ultrasonic P-and S- wave attenuation in Deccan flood Basalts, India,” *SEG Tech. Progr. Expand. Abstr.*, vol. 34, pp. 3274–3278, 2015, doi: [10.1190/SEGAM2015-5858683.1](https://doi.org/10.1190/SEGAM2015-5858683.1).
- [213] C. Chang, Q. Zhou, T. J. Kneafsey, M. Oostrom, and Y. Ju, “Coupled supercritical CO₂ dissolution and water flow in pore-scale micromodels,” *Adv. Water Resour.*, vol. 123, no. July 2018, pp. 54–69, Jan. 2019, doi: [10.1016/j.advwatres.2018.11.004](https://doi.org/10.1016/j.advwatres.2018.11.004).
- [214] Q. Meng and X. Jiang, “Numerical analyses of the solubility trapping of CO₂ storage in geological formations,” *Appl. Energy*, vol. 130, pp. 581–591, 2014, doi: [10.1016/j.apenergy.2014.05.088](https://doi.org/10.1016/j.apenergy.2014.05.088).

- 10.1016/j.apenergy.2014.01.037.
- [215] A. Malik, T. Chakraborty, K. S. Rao, D. Kumar, P. Chandel, and P. Sharma, “Dynamic Response of Deccan Trap Basalt under Hopkinson Bar Test,” in *Procedia Engineering*, Elsevier Ltd, Jan. 2017, pp. 647–654. doi: 10.1016/j.proeng.2016.12.124.
- [216] E. T. Chala, K. Seshagiri Rao, S. Mishra, and A. Kumar, “Geomechanical properties of volcanic rocks from deccan traps, India,” in *ISRM VII Brazilian Symposium on Rock Mechanics, SBMR 2016*, International Society for Rock Mechanics and Rock Engineering, 2016. doi: 10.20906/cps/sbmr-02-0005.
- [217] N. Rani, J. P. Shrivastava, and R. K. Bajpai, “Natural glass from Deccan volcanic province: an analogue for radioactive waste form,” *Int. J. Earth Sci.*, vol. 104, no. 8, pp. 2163–2177, Nov. 2015, doi: 10.1007/s00531-015-1244-5.
- [218] A. P. Gysi and A. Stefánsson, “Experiments and geochemical modeling of CO₂ sequestration during hydrothermal basalt alteration,” *Chem. Geol.*, vol. 306–307, pp. 10–28, May 2012, doi: 10.1016/j.chemgeo.2012.02.016.
- [219] P. R. Punnam, A. Dutta, B. Krishnamurthy, and V. K. Surasani, “Study on utilization of machine learning techniques for geological CO₂ sequestration simulations,” *Mater. Today Proc.*, vol. 72, pp. 378–385, Jan. 2022, doi: 10.1016/j.matpr.2022.08.109.
- [220] D. Y. C. Leung, G. Caramanna, and M. M. Maroto-Valer, “An overview of current status of carbon dioxide capture and storage technologies,” *Renew. Sustain. Energy Rev.*, vol. 39, pp. 426–443, 2014, doi: 10.1016/j.rser.2014.07.093.
- [221] P. Kelemen, S. M. Benson, H. Pilorgé, P. Psarras, and J. Wilcox, “An Overview of the Status and Challenges of CO₂ Storage in Minerals and Geological Formations,” *Front. Clim.*, vol. 1, no. November, pp. 1–20, 2019, doi: 10.3389/fclim.2019.00009.
- [222] W. Xiong, R. K. Wells, J. A. Horner, H. T. Schaef, P. A. Skemer, and D. E. Giammar, “CO₂ Mineral Sequestration in Naturally Porous Basalt,” *Environ. Sci. Technol. Lett.*, vol. 5, no. 3, pp. 142–147, 2018, doi: 10.1021/acs.estlett.8b00047.
- [223] L. Adam, T. Otheim, K. Van Wijk, M. Batzle, T. L. McLing, and R. K. Podgorney, “CO₂ sequestration in basalt: Carbonate mineralization and fluid substitution,” in *Society of Exploration Geophysicists International Exposition and 81st Annual Meeting 2011, SEG 2011*, 2011, pp. 2108–2113. doi: 10.1190/1.3672479.

- [224] P. Krishnamurthy, “Carbonatites of India,” *J. Geol. Soc. India*, vol. 94, no. 2, pp. 117–138, 2019, doi: 10.1007/s12594-019-1281-y.
- [225] J. M. Matter, T. Takahashi, and D. Goldberg, “Experimental evaluation of in situ CO₂-water-rock reactions during CO₂ injection in basaltic rocks: Implications for geological CO₂ sequestration,” *Geochemistry, Geophys. Geosystems*, vol. 8, no. 2, Feb. 2007, doi: 10.1029/2006GC001427.
- [226] J. W. Johnson, J. J. Nitao, and J. P. Morris, “Reactive Transport Modeling of Cap Rock Integrity During Natural and Engineered CO₂ Storage Carbon Dioxide Capture for Storage in Deep Geologic Formations,” pp. 1–52, 2005, Accessed: May 01, 2019. [Online]. Available: <https://www.osti.gov/biblio/15015132-reactive-transport-modeling-cap-rock-integrity-during-natural-engineered-co2-storage>
- [227] H. M. Nilsen *et al.*, “Field-case simulation of CO₂-plume migration using vertical-equilibrium models,” in *Energy Procedia*, Elsevier Ltd, Jan. 2011, pp. 3801–3808. doi: 10.1016/j.egypro.2011.02.315.
- [228] M. Flett, R. Gurton, and G. Weir, “Heterogeneous saline formations for carbon dioxide disposal: Impact of varying heterogeneity on containment and trapping,” *J. Pet. Sci. Eng.*, vol. 57, no. 1–2, pp. 106–118, May 2007, doi: 10.1016/j.petrol.2006.08.016.
- [229] R. Ershadnia *et al.*, “CO₂ geological sequestration in multiscale heterogeneous aquifers: Effects of heterogeneity, connectivity, impurity, and hysteresis,” *Adv. Water Resour.*, vol. 151, May 2021, doi: 10.1016/j.advwatres.2021.103895.
- [230] B. Ottens *et al.*, “Exceptional multi stage mineralization of secondary minerals in cavities of flood basalts from the deccan volcanic province, India,” *Minerals*, vol. 9, no. 6, 2019, doi: 10.3390/min9060351.
- [231] T. K. Flaathen, “Water-rock-interaction during CO₂ sequestration in basalt,” Paul Sabatier University, 2009.
- [232] E. A. Al-Khdheawi, S. Vialle, A. Barifcani, M. Sarmadivaleh, and S. Iglauer, “Enhancement of CO₂ trapping efficiency in heterogeneous reservoirs by water-alternating gas injection,” *Greenh. Gases Sci. Technol.*, vol. 8, no. 5, pp. 920–931, Oct. 2018, doi: 10.1002/ghg.1805.

Research Publications

Journal Paper

- Pradeep Reddy Punnam, Balaji Krishnamurthy, Vikranth Kumar Surasani, Investigation of Solubility trapping mechanism during geologic CO₂ sequestration in Deccan Volcanic Provinces, Saurashtra, Gujarat, India, International Journal of Greenhouse Gas Control, 120(2022) 103769, doi: 10.1016/j.ijggc.2022.103769
- Pradeep Reddy Punnam, Arnab Dutta, Balaji Krishnamurthy, Vikranth Kumar Surasani, Study on utilization of time series neural network for Geological CO₂ Sequestration simulations, Materials Today: Proceedings, 2022, doi: 10.1016/j.matpr.2022.08.109
- Pradeep Reddy Punnam, Balaji Krishnamurthy, Vikranth Kumar Surasani, Influence of caprock morphology on solubility trapping during CO₂ geological sequestration, Geofluids, 2022, doi: 10.1155/2022/8016575
- Pradeep Reddy Punnam, Balaji Krishnamurthy, Vikranth Kumar Surasani, Investigations of structural- and residual-trapping phenomena during CO₂ sequestration in Deccan Volcanic Province of Saurashtra region, Gujarat, International Journal of Chemical Engineering, 2021, 7762127. doi: 10.1155/2021/7762127
- Pradeep Reddy Punnam, Balaji Krishnamurthy, Vikranth Kumar Surasani Investigation of different caprock morphologies on CO₂ leakage and solubility trapping mechanisms, International Journal of Greenhouse Gas Control (Submitted: 24th July 2023)

Book Chapter

- Pradeep Reddy Punnam, Balaji Krishnamurthy, Vikranth Kumar Surasani, Influence of top-surface topography on structural and residual trapping during geological CO₂ sequestration, In: Lecture Notes in Mechanical Engineering, Advances in Computational Modeling and Simulation (Eds.) R. Srinivas et al, 2022, Springer, doi: 10.1007/978-981-16-7857-8_9

Graphical Album

- Pradeep Reddy Punnam, Balaji Krishnamurthy, Vikranth Kumar Surasani, Caprock topography and injection position influence on the solubility trapping phenomena during CO₂ geological sequestration, In: Porous Media Album (Eds.) Medici et al., 2022, Springer. doi: 10.1007/978-3-031-23800-0_111

Conference Talks

- Pradeep Reddy Punnam, Arnab Dutta, Balaji Krishnamurthy, Vikranth Kumar Surasani, Study on utilization of Machine Learning techniques for Geological CO₂ Sequestration simulations NMTEEA-2022 Feb 18-19, 2022.
- Pradeep Reddy Punnam, Lakshmi Devi Voleti, Vikranth Kumar Surasani, Heterogeneity effects on the Solubility-trapping during CO₂ Geological Sequestration. Interpore-2021, May. 31 – June 4. 2021.
- Pradeep Reddy Punnam, Shakti Raj Singh Bawal, Vikranth Kumar Surasani, Parametric study on the residual CO₂ trapping in Deccan Volcanic Basalt. Interpore-2020, Aug. 31 – Sep 4. 2020.
- Pradeep Reddy Punnam, Vikranth Kumar Surasani, Reactive transport modelling and simulation of CO₂ sequestration in geological formation, Carbon Capture, Utilization and storage (CCUS), National Chemical Laboratory, NCL, Pune, 2018.

Biography of Candidate

Mr. Punnam Pradeep Reddy is working on CO₂ geological Sequestration using the reactive transport modelling for the Deccan Volcanic Province. He has published four articles in international journals and one book chapter in this field. Sweden's Blekinge Tekniska Högskola (BTH) granted him a master's degree in mechanical engineering. He received his Bachelor's degree from the Mechanical Engineering Department at Jawaharlal Nehru Technological University in Hyderabad, India.

Biography of Supervisor

Prof. Vikranth Kumar Surasani has expertise in the area of Reactive transport, Lattice Boltzmann Simulations, and Pore Network Modeling. He has applied this expertise in the research fields of Process Engineering, Fluid dynamics, Porous media simulation, Drying phenomena, and Biogeochemical Interaction in the subsurface. His Doctor of Philosophy degree was awarded to him by Otto von Guericke University Magdeburg in 2008. He went on to get a postdoctoral degree from Pennsylvania State University in the United States of America in 2013. During his PhD, he was two times scholarship awardee of Max-Buchner-Dechema and German Research Foundation. Currently, he holds the position of Associate Professor in the Department of Chemical Engineering and Incharge of the Computational Laboratory at BITS-Pilani in Hyderabad. He is also an academic editor of the International Journal of Chemical Engineering. He has thirty articles, and his h-index is 11 while his i10-index is 14. He has nearly 400 citations.

Biography of Co-Supervisor

Prof. Balaji Krishnamurthy has expertise in the area of Electrochemical Energy systems, Batteries, fuel cells, and water treatment. He received his Bachelor of Technology degree from the Central Electrochemical Research Institute in Karaikudi, India. He then went on to receive his Doctor of Philosophy degree from the University of South Carolina in Columbia, South Carolina, in the United States. After this, he held the position of Post-Doctoral Fellow at the Rensselaer Polytechnic Institute in Troy, New York, in the United States of America. Currently, he works as an Associate Professor in the Department of Chemical Engineering at BITS-Pilani in Hyderabad; his research interests include theoretical investigations of fuel cells and batteries, in addition to practical electrochemistry.